



8-2009

"Field Weakening Operation of AC Machines for Traction Drive Applications."

Niranjan Anandrao Patil
University of Tennessee - Knoxville

Follow this and additional works at: https://trace.tennessee.edu/utk_graddiss



Part of the [Electrical and Computer Engineering Commons](#)

Recommended Citation

Patil, Niranjan Anandrao, ""Field Weakening Operation of AC Machines for Traction Drive Applications.". " PhD diss., University of Tennessee, 2009.
https://trace.tennessee.edu/utk_graddiss/78

This Dissertation is brought to you for free and open access by the Graduate School at TRACE: Tennessee Research and Creative Exchange. It has been accepted for inclusion in Doctoral Dissertations by an authorized administrator of TRACE: Tennessee Research and Creative Exchange. For more information, please contact trace@utk.edu.

To the Graduate Council:

I am submitting herewith a dissertation written by Niranjan Anandrao Patil entitled ""Field Weakening Operation of AC Machines for Traction Drive Applications."" I have examined the final electronic copy of this dissertation for form and content and recommend that it be accepted in partial fulfillment of the requirements for the degree of Doctor of Philosophy, with a major in Electrical Engineering.

J. S. Lawler, Major Professor

We have read this dissertation and recommend its acceptance:

L. M. Tolbert, S. M. Djouadi, Suzanne Lenhart

Accepted for the Council:

Carolyn R. Hodges

Vice Provost and Dean of the Graduate School

(Original signatures are on file with official student records.)

To the Graduate Council:

I am submitting herewith a dissertation written by Niranjan Anandrao Patil entitled "Field Weakening Operation of AC Machines for Traction Drive Applications." I have examined the final electronic copy of this dissertation for form and content and recommend that it be accepted in partial fulfillment of the requirements for the degree of Doctor of Philosophy, with a major in Electrical Engineering.

J. S. Lawler

Major Professor

We have read this dissertation
and recommend its acceptance:

L. M. Tolbert

S. M. Djouadi

Suzanne Lenhart

Accepted for the Council:

Carolyn R. Hodges

Vice Provost and Dean of the Graduate
School

(Original Signatures are on file with official student records)

Field Weakening Operation of AC Machines for Traction Drive Applications

A Dissertation
Presented for the
Doctor of Philosophy Degree
The University of Tennessee, Knoxville

Niranjan Anandrao Patil
August 2009

Dedication

This dissertation is dedicated to my parents, Anandrao and Padma; my sister, Swarada; and my wife, Neha, for always believing in me, inspiring and encouraging me to reach higher in order to achieve my goals.

Acknowledgements

I want to thank Dr. Jack Lawler for continuously providing me with invaluable knowledge and guidance, Drs. John McKeever and Leon Tolbert for providing me a research assistantship at Oak Ridge National Laboratory, my department for providing a teaching assistantship, Pedro Otaduy for sharing SRM data with me which was necessary for the nonlinear analysis of SRM motor. I would also like to thank Cliff White, Matthew Scudiere and Chester Coomer for their help at the National Transportation Research Center and I would like to thank Dr. S. M. Djouadi and Dr. Suzanne Lenhart for serving on my committee. Finally, I would like to thank my parents; my sister; my wife; my in-laws, Medha, Arvind and Abhay; and my friends, Rahul, Pushkar, Asim, Anindyo and Weston, for their unending support and encouragement.

Abstract

The rising cost of gasoline and environmental concerns have heightened the interest in electric/hybrid-electric vehicles. In passenger vehicles an electric traction motor drive must achieve a constant power speed range (CPSR) of about 4 to 1. This modest requirement can generally be met by using most of the common types of electric motors. Heavy electric vehicles, such as tanks, buses and off-road equipment can require a CPSR of 10 to 1 and sometimes much more. Meeting the CPSR requirement for heavy electric vehicles is a significant challenge. This research addresses the CPSR capability and control requirements of two candidates for high CPSR traction drives: the permanent magnet synchronous motor (PMSM) and the switched reluctance motor (SRM).

It is shown that a PMSM with sufficiently large winding inductance has an infinite CPSR capability, and can be controlled using a simple speed control loop that does not require measurement of motor phase currents. Analytical and experimental results confirm that the conventional phase advancement method charges motor winding with required current to produce the rated power for the speed range where the back-EMF normally prevents the generation of the rated power. A key result is that for the PMSM, the motor current at high speed approaches the machine rating independent of the power produced. This results in poor partial load efficiency.

The SRM is also shown to have infinite CPSR capability when continuous conduction is permitted during high speed operation. Traditional high speed control is of discontinuous type. It has been shown that this discontinuous conduction itself is the limiter of CPSR. Mathematical formulas have been developed relating the average current, average power, and peak current required producing the desired (rated) power to machine design parameters and control variables. Control of the SRM in the continuous conduction mode is shown to be simple; however, it does require measurement of motor current. For the SRM the motor current at high speed is proportional to the power produced which maintains drive efficiency even at light load conditions.

TABLE OF CONTENTS

1	INTRODUCTION	1
1.1	ELECTRICAL OR HYBRID ELECTRICAL TRANSPORTATION VEHICLES	1
1.2	INTRODUCTION TO FIELD WEAKENING	3
1.3	VIABLE CANDIDATES FOR FIELD WEAKENING OPERATION	6
1.4	DISSERTATION OBJECTIVES AND OUTLINE	8
2	LITERATURE REVIEW: PERMANENT MAGNET SYNCHRONOUS MOTORS	13
2.1	FIELD WEAKENING OPERATION OF PERMANENT MAGNET SYNCHRONOUS MOTORS	15
2.1.1	<i>Constant Voltage Constant Power Vector Control [8],[29].....</i>	<i>27</i>
2.1.2	<i>Constant Current Constant Power Vector Control [19] [30]</i>	<i>30</i>
2.1.3	<i>Optimum Current Vector Control [9].....</i>	<i>32</i>
3	CONVENTIONAL PHASE ADVANCEMENT METHOD	37
3.1	ANALYSIS OF A PERMANENT MAGNET SYNCHRONOUS MOTOR DRIVEN BY CONVENTIONAL PHASE TIMING ADVANCEMENT METHOD [37].	40
3.1.1	<i>Fundamental Frequency Model.....</i>	<i>44</i>
3.1.2	<i>Below Base Speed Operation (Constant Torque Zone, $n \leq 1$)</i>	<i>48</i>
3.1.3	<i>Operation above Base Speed (Constant Power Region, $n \geq 1$).....</i>	<i>50</i>
3.1.4	<i>“Optimal” Inductance for the Field-Weakening.....</i>	<i>53</i>
3.2	STEADY STATE PMSM CONTROL CONSIDERING WINDING RESISTANCE	56
3.2.1	<i>Constant Power Speed Ratio</i>	<i>61</i>
4	SIMULATIONS AND EXPERIMENTAL VERIFICATION OF CONVENTIONAL PHASE ADVANCEMENT METHOD FOR SURFACE PM MACHINES.....	63
4.1	SIMULINK BASED SIMULATION MODEL	63
4.2	SIMULATION RESULTS	70
4.3	MEASURED MACHINE DATA	72

4.4	EXPERIMENTAL SETUP	75
4.5	EXPERIMENTAL RESULTS AND CONCLUSION	102
5	INTRODUCTION – SWITCHED RELUCTANCE MOTORS.....	132
5.1	MODELING OF SWITCHED RELUCTANCE MOTORS [4][51].	137
6	LITERATURE REVIEW – SWITCHED RELUCTANCE MOTOR CONTROL.....	148
6.1.1	<i>Low Speed Voltage Control (Voltage PWM)[15],[59]</i>	<i>151</i>
6.1.2	<i>Low Speed Current Control [15],[59].....</i>	<i>153</i>
6.1.3	<i>High Speed Single Pulse Control of Switched Reluctance Motors</i>	<i>154</i>
6.2	LITERATURE REVIEW – HIGH SPEED SINGLE PULSE CONTROL	158
7	CONTINUOUS CONDUCTION ANALYSIS AND SIMULATION RESULTS	177
7.1	EXAMPLE MOTOR MODEL	178
7.1.1	<i>Nomenclature and Parameters of the Example Motor</i>	<i>181</i>
7.2	EXAMPLE MOTOR ANALYSIS	183
7.2.1	<i>Linear Model.....</i>	<i>184</i>
7.2.2	<i>Nonlinear Model</i>	<i>185</i>
7.2.3	<i>Nonlinear Model with Partial Derivatives.....</i>	<i>191</i>
7.2.4	<i>Nonlinear Model with Current Estimation from Flux-Linkage Data</i>	<i>191</i>
7.3	SIMULATION RESULTS	194
7.4	CONTINUOUS CONDUCTION ANALYSIS - FLAT UNALIGNED INDUCTANCE TYPE SRM.....	205
7.4.1	<i>Region I Analysis ($0 \leq \theta \leq (\alpha_r - \beta - \theta_a)$).....</i>	<i>211</i>
7.4.2	<i>Region II Analysis ($(\alpha_r - \beta - \theta_a) \leq \theta \leq \beta$).....</i>	<i>213</i>
7.4.3	<i>Region III Analysis ($\beta \leq \theta \leq [\alpha_r - \beta - (2 * \theta_{dwell} - \alpha_r)]$, $\beta \leq \theta \leq (2 * \alpha_r - 2 * \theta_{dwell} - \beta)$).....</i>	<i>214</i>
7.4.4	<i>Region IV Analysis ($(2 * \alpha_r - 2 * \theta_{dwell} - \beta) \leq \theta \leq (\alpha_r - \beta)$).....</i>	<i>215</i>

7.4.5	Region V Analysis ($(\alpha_r - \beta) \leq \theta \leq (\alpha_r - \beta + \theta_{commutation})$)	215
7.4.6	Region VI Analysis ($(\alpha_r - \beta + \theta_{commutation}) \leq \theta \leq \alpha_r$)	216
7.4.7	Analytical Results	219
7.4.8	Validation of Analytical Results	233
7.4.9	Controller Analysis	240
7.4.10	Constant Power Speed Ratio	253
7.5	CONTINUOUS CONDUCTION ANALYSIS - NON-FLAT UNALIGNED INDUCTANCE	256
7.5.1	Region I Analysis ($0 \leq \theta \leq (\alpha_r - \beta - \theta_{adv})$)	264
7.5.2	Region II Analysis ($(\alpha_r - \beta - \theta_{adv}) \leq \theta \leq \beta$)	266
7.5.3	Region III Analysis ($\beta \leq \theta \leq (\alpha_r - \theta_{dwell})$)	267
7.5.4	Region IV-a Analysis ($(\alpha_r - \theta_{dwell}) \leq \theta \leq \frac{\alpha_r}{2}$)	268
7.5.5	Region IV-b Analysis ($\frac{\alpha_r}{2} \leq \theta \leq \theta_{dwell}$)	269
7.5.6	Region V Analysis ($\theta_{dwell} \leq \theta \leq (\alpha_r - \beta)$)	270
7.5.7	Region VI Analysis ($(\alpha_r - \beta) \leq \theta \leq (\alpha_r - \beta + \theta_{commutation})$ $(\alpha_r - \beta) \leq \theta \leq (\alpha_r - \beta + \theta_{dwell} - \theta_{adv})$)	271
7.5.8	Region VII Analysis ($(\alpha_r - \beta + \theta_{commutation}) \leq \theta \leq \alpha_r$)	272
7.5.9	Analytical Results	274
7.5.10	Validation of Analytical Results (Simulation Results)	285
7.5.11	Controller Analysis	300
7.5.12	Constant Power Speed Ratio	304
8	CONCLUSION AND FUTURE WORK	309
8.1	SURFACE PERMANENT MAGNET SYNCHRONOUS MOTOR	309

8.2 SWITCHED RELUCTANCE MOTOR	312
Bibliography	316
Appendix	330
Vita	362

LIST OF TABLES

Table 2-1: Torque Equations [24].....	20
Table 4-1: Parameters of a Surface Permanent Magnet Synchronous Motor with Fractional-Slot Concentrated Windings.....	64
Table 4-2 : Machine per-phase Resistance and per-phase Inductance Measurement.	74
Table 4-3 : Measured No Load Losses and Machine Data.	80
Table 4-4 : 250V, 25% Load.....	104
Table 4-5 : 250V, 50% Load.....	105
Table 4-6 : 250V, 75% Load.....	106
Table 4-7: 250V, 100% Load.....	107
Table 4-8 : 300V, 25% Load.....	108
Table 4-9 : 300V, 50% Load.....	109
Table 4-10 : 300V, 75% Load.....	110
Table 4-11 : 300V, 100% Load.....	111
Table 4-12 : Current Comparison at 250V and 300V DC.	119
Table 4-13 : Minimum Current and Unity Power Factor Speed.	128
Table 4-14 : Calculated Torque Component of the Stator Current (with 300V DC).....	130
Table 7-1 : Flat Unaligned Inductance type SRM, Dwell = 31.	236
Table 7-2 : Flat Unaligned Inductance type SRM, Dwell = 31.	237
Table 7-3 : Flat Unaligned Inductance type SRM, Dwell = 31.	238
Table 7-4: Flat Unaligned Inductance type SRM, Dwell = 32.	239
Table 7-5 : Peak Current Required to get Rated Power.	248

Table 7-6 : Rated Power Development at High Speed.....	248
Figure 7-28 : CPSR Analysis – Flat Unaligned Inductance type SRM.	254
Table 7-7: CPSR of the Flat Unaligned Inductance type SRM with Discontinuous Conduction.	257
Table 7-8 : Non-flat Unaligned Inductance type SRM, Dwell = 31° (Linear Model and Non Linear Model).....	288
Table 7-9 : Non-flat Unaligned Inductance type SRM Dwell = 31° (Linear Model).	289
Table 7-10: Non-flat Unaligned Inductance type SRM Dwell = 31° (Non Linear Model).	290
Table 7-11 : Non-flat Unaligned Inductance type SRM Dwell = 31° (Linear Model). ...	291
Table 7-12: Non-flat Unaligned Inductance type SRM Dwell = 31° (Non Linear Model).	292
Table 7-13 : Current Regulator Set Point to get Rated Power.....	297
Table 7-14 : Rated Power at High Speed using Continuous Conduction.	298
Table 7-15 : CPSR of the Non Flat Unaligned Inductance type SRM with Discontinuous Conduction.	308

LIST OF FIGURES

Figure 1-1: Typical AC Drive Characteristics.....	2
Figure 1-2 : Electrical Equivalent Circuit of a Separately Excited DC Motor.....	4
Figure 1-3: AC Motor Classification Based on the Shape of Back EMF Waveform.....	7
Figure 2-1: Surface Permanent Magnet Motor - Cross Sectional View.	14
Figure 2-2: Interior Permanent Magnet Motor - Cross Sectional View.	16
Figure 2-3: Synchronous Reluctance Motor - Cross Sectional View.	17
Figure 2-4: Electrical Equivalent d-q Circuit of a Synchronous Motor in the Synchronously Rotating Reference Frame [23].....	20
Figure 2-5: Current and Voltage Limited Operation of Permanent Magnet Motors [8]. .	23
Figure 2-6: Below Base Speed Operation of Surface PM Machines [28].	26
Figure 2-7: Above Base Speed Operation of Surface PM Machines [8][9].....	28
Figure 2-8: Constant Current Constant Power Vector Control.	31
Figure 2-9: Optimum Current Vector Control.....	33
Figure 2-10: Scheme of Flux-Weakening Control System for Permanent Magnet Synchronous Motors [9].	34
Figure 2-11: Optimal Condition for Flux Weakening Operation of Surface PM Motors [31].	35
Figure 3-1: Comparison of Back-EMF and Applied Stator Voltage above Base Speed without Field-Weakening.	38
Figure 3-2: Comparison of Back EMF and Applied Voltage above Base Speed With Phase Advancement.	39

Figure 3-3: Motor / Inverter Schematic for a PMSM Driven by CPA [37].	41
Figure 3-4: Three Phase Waveforms.	42
Figure 3-5: Fundamental Frequency Model.	45
Figure 3-6: Vector Diagram of Conventional Phase Advancement Method.	57
Figure 4-1: Simulink Model for CPA driven PMSM Simulation.	65
Figure 4-2 : PMSM Motor Model	68
Figure 4-3 : Vehicle Dynamics.	69
Figure 4-4 : Simulation Results for CPA driven PMSM motor at Full Load (6kW) and 151 V_{dc} Supply Voltage.	71
Figure 4-5: No Load Losses Measurement Setup.	73
Figure 4-6 : Per Phase Stator Winding Inductance Measurement using LCR meter.	74
Figure 4-7 : Measured Back-EMF of a 6-kW Fractional-Slot Concentrated-Winding PMSM Motor at Base Speed (900 rpm).	76
Figure 4-8 : Measured Back-EMF of a 6-kW Fractional-Slot Concentrated-Winding PMSM Motor at 4000 rpm.	77
Figure 4-9 : Measured Back-EMF with FFT at Base Speed (900 rpm).	78
Figure 4-10 : Measured Back-EMF with FFT at 1800 rpm.	79
Figure 4-11: Measured No Load Losses of a 6-kW Fractional-Slot Concentrated- Winding Motor.	81
Figure 4-12 : Measured Back-EMF of a 6-kW Fractional-Slot Concentrated-Winding PMSM Motor.	82
Figure 4-13: Close up of the Experimental 6-kW Surface PM Motor.	83

Figure 4-14 : Index Pulse from Incremental Encoder on back-EMF at 900 rpm.....	85
Figure 4-15: Rotor Position Estimation.....	87
Figure 4-16 : Overall Electrical Schematics.....	88
Figure 4-17 : a. Motor & Dyne Coupling, b. Voltage & Current Sensors.....	90
Figure 4-18 : Overall Experimental Setup.	91
Figure 4-19 : Overall Test Schematics.	92
Figure 4-20 : Simulink Based OPAL RT Model.	96
Figure 4-21: Data Acquisition and Motor Control (OPAL RT Model).	97
Figure 4-22: Part of the CPA Based Controller for Surface PM Motor with Fractional-Slot Concentrated Windings.	98
Figure 4-23 : Modulation Index and Inverter Lead Angle Logic.	100
Figure 4-24: Details of the Sine Triangle type PWM Switching Scheme.	101
Figure 4-25 : Data Monitor (OPAL RT).....	103
Figure 4-26 : Speed Tracking.....	112
Figure 4-27: Measured Power Vs Speed, Torque Vs Speed and Current Vs Speed for 300V, & 100% Load.	114
Figure 4-28: Measured Losses.....	115
Figure 4-29 : Measure Inverter Efficiency.....	117
Figure 4-30 : Measured Motor Efficiency.....	118
Figure 4-31 : Measured Drive Efficiency.	121
Figure 4-32 : Comparison of Inverter Efficiency.	122
Figure 4-33 : Comparison of Motor Efficiency.	123

Figure 4-34 : Comparison of Total Drive Efficiency.	124
Figure 4-35: No Load Losses and Drive Efficiencies.	126
Figure 5-1 : Cross-Sectional View of a Four Phase 8/6 Switched Reluctance Motor. .	133
Figure 5-2: Asymmetrical Half-Bridge Voltage Source Inverter Topology for an 8/6 SRM Motor [11],[15].	135
Figure 5-3: Per Phase Equivalent Circuit of Switched Reluctance Motor.	139
Figure 5-4: Per Phase Inductance Profile of an 8/6 SRM Motor (Neglecting Saturation).	141
Figure 5-5: Flux-Linkage Vs Current Plot.	145
Figure 6-1: Firing Scheme of an 8/6 SRM Motor.	149
Figure 6-2: Voltage Control (Voltage PWM) [59].	152
Figure 6-3: Current Type SRM Control.....	155
Figure 6-4: Single Pulse High Speed Operation of SRM Motors.	157
Figure 6-5: Speed Control System for Switched Reluctance Motor Based on [65].	162
Figure 6-6: Inner Torque Control Loop for Switched Reluctance Motor based on [65].	163
Figure 6-7: Closed Loop High Speed Control Scheme for Switched Reluctance Motor Based on [12],[11].	165
Figure 6-8: Current Regulator Set Point as a Function of Output Torque [11].....	166
Figure 6-9: Advance Angle Estimation [11].	168
Figure 6-10: High Speed SRM Control Based on [11].	169

Figure 6-11: Closed Loop Torque Control Loop for Continuous Conduction Based on [75].	175
Figure 7-1: Flux-Linkage Vs Rotor Position Plot for the Example SRM Motor.....	179
Figure 7-2: Flux-Linkage Vs Current plot for the Example Motor.	180
Figure 7-3: Example Motor Data.	182
Figure 7-4: Maximum Co-Energy of the Example Motor with Peak Current of 600A...	183
Figure 7-5: Linear Magnetic Model of the Example Motor.....	186
Figure 7-6: Linear Inductance Profile of the Example Motor.	187
Figure 7-7: Simulink Model for the Example Motor [$L(\theta)$].	188
Figure 7-8: Inductance Profile of the Example SRM.	189
Figure 7-9: Simulink Model for the Example Motor Simulation [$L(\theta, i)$]......	190
Figure 7-10: Partial Derivatives for Nonlinear Model.	192
Figure 7-11: Simulink Model Based on Partial Derivatives.	193
Figure 7-12: Simulink Model of the Example Motor based on Current Estimation from Flux-Linkage Data.	195
Figure 7-13: Instantaneous Phase Current and Co-energy for the Example Motor when Producing Rated Power at Base Speed [78].	196
Figure 7-14: : Instantaneous Phase Current and Co-energy for the Example Motor when Producing Rated Power at 6 Times Base Speed (using model in Section 7.2.2).	197
Figure 7-15: Simulation Result of Discontinuous Conduction: Advance Angle = 22.5° , Dwell = 30, $I_{set} = 600A$ @ 6500 RPM (using model in 7.2.2).	200

Figure 7-16: Simulation Result of Continuous Conduction: Advance Angle = 22.5 , Dwell = 31, Iset = 600A @ 6500 RPM (using model in Section 7.2.2).	201
Figure 7-17 : Continuous conduction (n = 6, dwell = 31°, advance angle = 22.5°, and Ipeak = 600A).....	202
Figure 7-18: Inductance Profile Comparison for Linear Model and Non-Linear Model.	204
Figure 7-19: Location of Zero Volt-Sec Notches for Flat Unaligned Inductance type SRM Motor when Operated in Continuous Conduction (Matlab Simulation).	206
Figure 7-20: Flat Unaligned Inductance type SRM Analysis when Operated in Continuous Conduction.	207
Figure 7-21: Validation of Flat Unaligned Inductance Type SRM Motor Analysis, Speed = 6500 rpm (n=26), Dwell = 31°, Advance Angle = 23° and Current Regulator Set Point, Ipeak = 600A.	234
Figure 7-22 : Comparison Between Analytical and Simulation Results.	241
Figure 7-23 : Comparison Between Analytical and Simulation Results.	242
Figure 7-24 : Comparison Between Analytical and Simulation Results.	243
Figure 7-25 : Comparison Between Analytical and Simulation Results.	244
Figure 7-26 : Dwell Angle Vs Advance Angle (Speed = 3750 RPM, Ipeak = 500A). ...	245
Figure 7-27: Power Control in Continuous Conduction Mode.	247
Figure 7-28 : CPSR Analysis – Flat Unaligned Inductance type SRM.	254
Figure 7-29 : Non-Flat Unaligned Inductance Profile.....	258
Figure 7-30 : Notch Location for Non Flat Unaligned Inductance type SRM when Operated in Continuous Conduction Mode.	260

Figure 7-31 : Continuous Conduction Analysis – Non Flat Unaligned Inductance type SRM.	261
Figure 7-32: Validation of Non-flat Unaligned Inductance Type SRM Motor Analysis, Speed = 3750 rpm (n=15), Dwell = 31° , Advance Angle = 23° and Current Regulator Set Point, $I_{peak} = 600A$	286
Figure 7-33 : Average Power.	287
Figure 7-34: Comparison of Analytical Results with Simulation Results for a Non Flat Unaligned Inductance Profile type SRM Motor.....	294
Figure 7-35 : Comparison of Analytical and Simulation Results.....	295
Figure 7-36 : Comparison of Analytical and Simulation Results.....	296
Figure 7-38 : Comparison between Non Linear and Linear Analysis for Rated Output Power.	299
Figure 7-39: Dwell Angle Vs Advance Angle (Speed = 3750 RPM, $I_{peak} = 500A$).	301
Figure 7-40 : Power Control in Continuous Conduction Mode.	302
Figure 7-41 : Response to a Step Change in Current Regulator Set when Operating at 6500 RPM with Dwell Angles of 30.25° and 31°	303
Figure 7-42: CPSR Estimation with Single Pulse High Speed Operation of the Non flat Unaligned Inductance type SRM.	305

Abbreviations

RMS = Root Mean Square

EMF = Electro-Motive Force

PM = Permanent Magnet

IPM = Interior Permanent Magnet Motor

SPM = Surface Permanent Magnet Motor

IM = Induction Motor

PMSM = Permanent Magnet Synchronous Motor

CPSR = Constant Power Speed Ratio

SPWM = Sinusoidal Pulse Width Modulation

CPA = Conventional Phase Advancement Method

SRM = Switched Reluctance Motor

PI = Proportional + Integral type Controller

DC = Direct Current

1 INTRODUCTION

1.1 Electrical or Hybrid Electrical Transportation Vehicles

Air pollution concerns, oil dependence on politically unstable regions and high oil prices are some of the reasons that have caused a flurry of activity in the areas of efficient electrical or hybrid electrical vehicles. If only an internal combustion engine is used, application of brakes results into generation of heat energy (kinetic energy gets converted into heat energy). If an electric motor or a combination (motor and an internal combustion engine) is used, kinetic energy can be converted into regenerative power which can be used to recharge batteries. This improves overall vehicle efficiency. The selection of a particular motor technology depends on several factors like cost, efficiency, size, weight, noise level etc. Locomotives are a good example of a high starting torque requirement. When a train is started, it is typically accelerated with a rated torque to a constant coasting speed. Once it reaches this cruising speed, low but sufficient torque to overcome road losses is required. Occasionally, the train may be required to run at a much higher speed than the designed cruising speed. These desired characteristics of a traction vehicle fit well with a motor having a wide speed range. Many other applications such as fork-lifts, golf carts, excavators, dump trucks, construction vehicles, and mining shovels also require high torque at low speeds and higher speed range. Other examples of traction vehicles are various types of construction trucks. They require not only high torque capability but also high speed

operation, particularly when driving on state or interstate highways. With current technology, at low speed, most of the electrical drives can be controlled to produce high torque. Special control technique has to be applied in order to operate electrical traction vehicles at high speed. There are several reasons for this limited speed range. One of the reasons is the upper limits that are placed on the motor input voltage and motor current due to the limitation on available DC supply voltage (battery). Power electronics used in the voltage source inverter which converts this DC voltage in an AC voltage, also puts some limitations on voltage and current capacity. These limits not only restrict the maximum torque but also the maximum speed at which rated power can be produced. Figure 1-1 shows ideal as well as practical drive characteristics. In traction vehicle terminology, base speed (n_b) or the rated speed is the speed at which available motor input voltage (or inverter output voltage) will be at the maximum value.

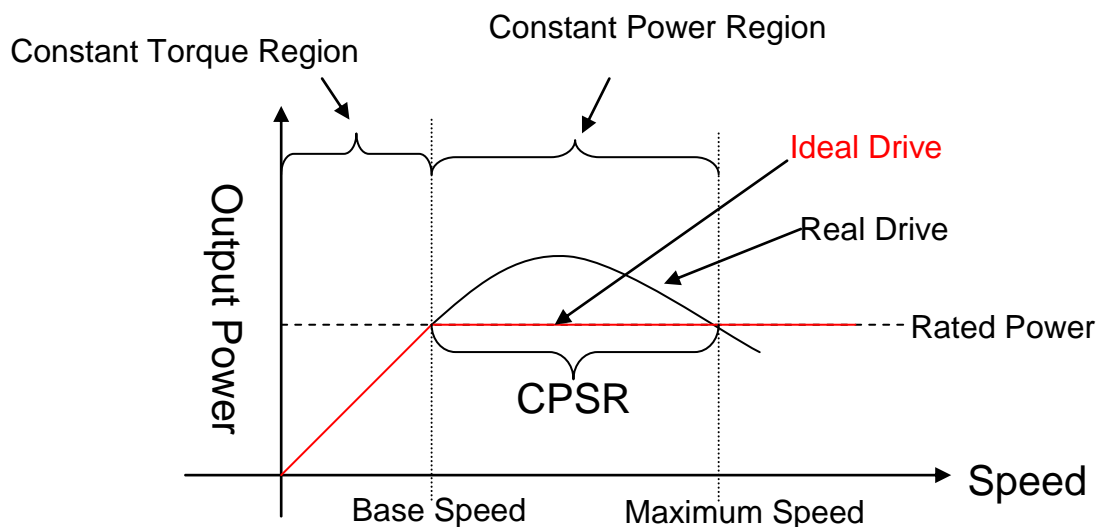


Figure 1-1: Typical AC Drive Characteristics.

Below this speed is the constant torque region. Above base speed, starts a constant power region.

AC drives do not have a natural flat output power characteristic at high speed. As the speed increases, output power increases. Once the applied voltage is at the maximum value, output power starts to decrease. At some speed, developed power drops below the rated power of the motor. The ratio of this highest speed at which the rated power can be developed to the base speed is called Constant Power Speed Ratio (CPSR) [1]. Widely used vector controlled induction motor drives can offer a CPSR of 4:1[1]. The next section describes a typical control scheme used to extend the high speed range of a separately excited DC motor.

1.2 Introduction to Field Weakening

Separately excited DC motors, if controlled properly, can provide ideal Torque / Power characteristics. To illustrate this, consider the steady state electrical model of a separately excited DC motor, as shown in Figure 1-2. . In this model, the armature circuit is represented by an ideal terminal supply voltage source V_t , winding resistor R_a , and generated back-EMF E_b . The back-EMF is generated due to the interaction between the armature circuit magnetic flux and the field circuit magnetic flux. In this type of an electrical motor, the air gap flux density is provided by the electromagnets which are energized by the controllable field current I_f .

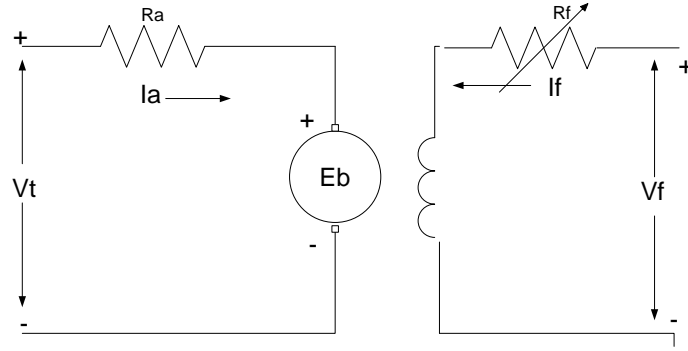


Figure 1-2 : Electrical Equivalent Circuit of a Separately Excited DC Motor.

Here V_f is the constant field supply voltage while R_f , which also includes field winding resistance, is a variable field resistance. Field resistance is normally used to control the amount of current in the field circuit, which in turn controls the air-gap flux density.

This representation is a Thevenin equivalent of the entire DC motor rotor structure.

Using the Krichhoff's voltage law for the armature circuit, we have,

$$V_t = E_b + I_a R_a \quad (1.1)$$

This can be rewritten as,

$$I_a = \frac{V_t - E_b}{R_a} \quad (1.2)$$

Back-EMF is given by,

$$E_b = K I_f \omega \quad (1.3)$$

The torque is given by,

$$T_e = K_t * I_f * I_a \quad (1.4)$$

Here ω = motor speed in rad/sec, and K_t , K_g are the motor design constants (torque and back EMF respectively). From Equation (1.4), it is clear that, in constant torque region, to keep the torque constant, field current I_f and the armature current I_a have to be kept constant or their product has to be maintained constant. I_f can be held constant by keeping field supply voltage V_f and field winding resistance R_f constant. From Equation (1.2), armature current I_a depends on the difference between the motor terminal voltage V_t and back-EMF E_b . As shown in Equation (1.3), E_b increases with speed due to its dependence on motor speed ω . Thus the converter output voltage must be increased to keep the armature current constant to keep the torque constant till base speed. At low speed, the rated armature current and the rated excitation flux can be used to obtain the rated motor torque. Because there is a limit on the available DC supply voltage, at some speed N_b , also called the base speed or the rated speed, the converter will reach its limiting output voltage $V_{t \max}$. Above this base speed, only way force the current into the motor is by reducing the back-EMF. From Equation(1.3), this can be done by reducing the field current I_f . In this region, output torque through its dependence on the field current and the armature current will also decrease with increase in the speed, i.e.,

$$T \propto \frac{1}{\omega} \quad (1.5)$$

Since Output Power, $P_e = T_e \omega$ (1.6)

Above base speed, the process of producing the rated power by lowering the air gap flux density (field flux $\psi_f = K\psi I_f$) to increase the speed range of an electrical motor is termed as the “flux weakening” or the “field weakening”.

1.3 Viable Candidates for Field Weakening Operation

Basic principles of electromagnetic induction were discovered in the early 1800's by Oersted, Gauss, and Faraday. By 1820, Hans Christian Oersted and Andre Marie Ampere had discovered that an electric current can produce a magnetic field. The next 15 years saw a flurry of cross-Atlantic experimentation and innovation, leading finally to a simple DC rotary motor. While experimenting in 1834, Thomas Davenport developed what we today know as a DC motor, complete with a brush and commutator (receiving U.S. Patent No. 132). After the development of the Ward Leonard system of Control [2] (Patent No. 463,802), DC motors became the motor of choice for loads that require precise control of speed and torque. The Induction Motor (IM) was invented by Nikola Tesla in 1888 [3]. His landmark paper in AIEE (May 15th, 1888) was entitled “A New Alternating Current Motor”. Once the concept of a “cage” was introduced, it was an easy step to the development of synchronous motors. The earliest recorded Switched Reluctance Motor (SRM) was one built by Davidson in Scotland in 1838 [4]. It did not become viable until the recent developments in high power switching devices such as Bipolar Junction Power Transistor (BJT) in the early 1980's. The development of Alnico magnets by Bell Laboratories in the 1930's triggered the development of Permanent

Magnet (PM) machines. In 1950's ceramic magnets became available. In 1960's commercial rare earth PMs became available. At present, neodymium-iron-boron (NdFeB) magnets are used for traction drive application. To aid in the choice of the field weakening scheme, these motors are classified as shown in Figure 1-3. The shape of the generated back-EMF is the classification criteria. Based on the example of Pillay and Krishnan [5] - [6], motors with the sinusoidal back-EMF are referred to as permanent magnet synchronous motors (PMSM) and the ones with trapezoidal back-EMF are referred to as brushless DC motors (BDCM). For PMSM motors based on [1], another distinction can be made between surface mounted PM motors (SPM) and interior mounted PM motors (IPM). There is another reluctance type motor termed "Synchronous Reluctance" [1].

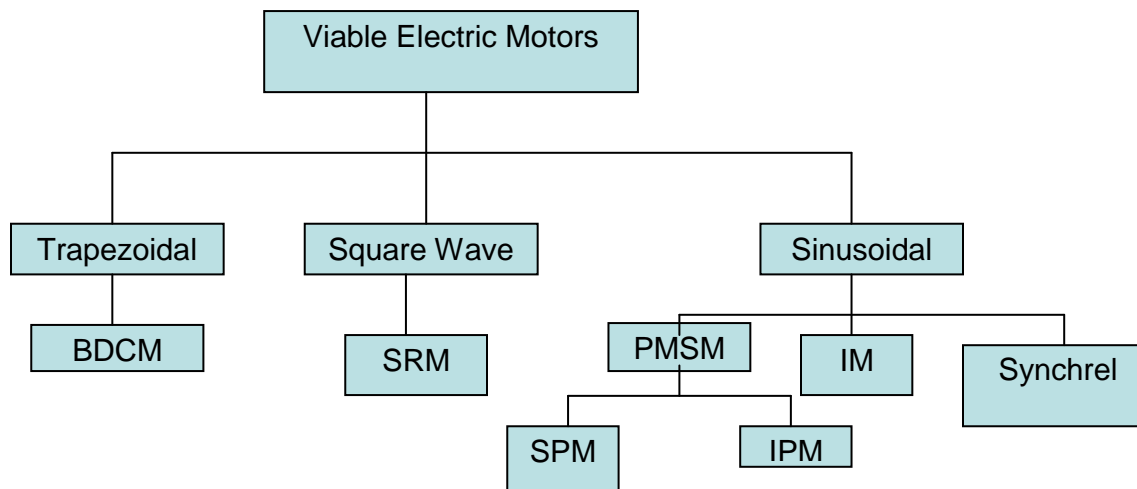


Figure 1-3: AC Motor Classification Based on the Shape of Back EMF Waveform.

Only induction motors have a controllable source of air gap flux density like that of a DC motor. The well-studied equivalent circuit of an induction motor can be used to derive the analytical expressions for its CPSR [7]. Analysis has shown that the induction motor does not have a natural “constant power” operating region [7]. During field weakening operation, when producing as much power as possible within the current rating of the motor, power output monotonically decreases with speed. The rate of decrease of developed power is related to drive parameters and indicate that several factors may reduce the rate of decrease of power with speed during field weakening [7]. The formulas indicate that while many model parameters influence the CPSR to some extent, it is the maximum permissible magnetizing current magnitude, DC supply voltage, base speed and torque requirement, and leakage inductances that have the greatest effect [7]. In situations where the motor design is fixed, the only parameters that can be varied by the drive designer are the DC supply voltage and power rating. This puts limits on the CPSR and prevents the use of a widely used induction motor for traction drive applications requiring a CPSR of 10:1 or more. In this research, the Surface Permanent Magnet Synchronous Motor and Switched Reluctance Motor have been considered for traction drive applications requiring a wide CPSR (10:1 or more).

1.4 Dissertation Objectives and Outline

The overall objective of this research was to increase the highest speed at which PMSM and SRM motors can produce their rated power without exceeding their current limits.

The rotor of the PMSM motor has surface permanent magnets resulting in smooth and constant torque with high power density. Due to the use of permanent magnets, permanent magnet synchronous motors have higher torque and higher efficiency [1], [8] than that of induction motors for the same size. In case of separately excited DC motors, there are two sets of windings resulting in “torque producing” and “field producing” currents. These currents are controlled independently, and in the constant power region, the field current is reduced to produce the rated power. In PMSM motors, there is only a stator winding and field flux is produced by the permanent magnets. As described in the Chapter 2, when the motor is in the constant power or field-weakening region, a part of this stator current has to be used to weaken the field produced by these permanent magnets and the remaining part of that current can produce the rated power. Chapter 2 reviews vector control based field-weakening methods that are typically used for the high speed operation of PMSM motors. These methods require an accurate measurement of the stator current. For a three phase motor, this means the use of six voltage and six current sensors. These measured currents and voltages are then converted to the “field component” and the “torque component”. Above motor base speed, the “field component” of the current is applied such that it opposes the magnetic field produced by the permanent magnets.

If not used properly, this traditional “field weakening” method can cause irreversible demagnetization of the rotor permanent magnets [9]. The need for three phase voltage and current measurement results in more drive hardware size, weight and cost. The three-phase to two-phase transformation means more mathematical complexity, slower

system response and more required computational power. Use of sensors also reduces the reliability of the control system.

The primary goal for this part of the research was to develop a simple high speed controller. For this research, a conventional phase advancement method was considered as a field-weakening control scheme. Cambier et al have a patent on this conventional phase advancement method for brushless DC motors [10]. Chapter 3 describes the adaptation of this CPA method for the surface permanent magnet synchronous motors. This chapter also describes the development of a real time controller based on this CPA method. A fundamental frequency model of PMSM motor was considered for realizing this high speed controller.

It has been shown that three simple equations form the basis of this high speed controller. Chapter 4 is focused on the implementation and experimental verification of the CPA based control method to widen the CPSR ratio of a surface PM motors. It is shown that with the CPA based controller, there is a well defined speed at which a PMSM motor operates at a unity power factor. At this speed, the resultant current is at the minimum value. Also, at this speed, the inverter efficiency is at its highest level. It is possible to adjust the machine design parameters such that this minimum speed will be the same as the nominal speed of the motor. Also, it has been shown that this CPA based method does not require any phase voltage or current measurements. This method does not require any three-phase to two-phase transformations, which reduces complexity, hardware size and implementation cost.

When compared with induction motors or permanent magnet motors, switched reluctance motors are simpler in design. The rotor of the SRM motor is nothing but a stack of steel laminations, making SRM simple in construction and low in cost. As there is no source of rotor excitation (permanent magnets or windings), SRMs are inherently fault-tolerant [11], and they can be used in very high speed or high temperature applications [12]. Use of a proper converter topology can avoid shoot-through faults and isolate the faulted phase, eliminating a possibility of drag torque and fire hazard during phase failure. In Chapter 6 and 7, it has been shown that this SRM structure results in a higher natural CPSR than PMSM motors [13], but it also results in more torque pulsation and acoustic noise. Therefore, the SRM is an ideal candidate for heavy off-road vehicles where vibrations and noise are generally not an issue.

Traditional SRM control is of a discontinuous type. For example, at the beginning of each cycle, the stator current starts from zero and returns back to zero. Chapter 6 reviews the existing constant torque and constant power region control strategies. In Chapter 7, it has been shown that this discontinuous type high speed control strategy itself is the limiter of the CSCR. Because of the non-linearity due to saturation and complex interdependence of the winding inductance, current and flux-linkages, with traditional discontinuous conduction, associated machine data is required to derive a look up table relating required peak current and output torque [14] , [15]. This data is typically obtained by FEA analysis or by carrying out a number of experiments. Even though, an SRM motor is low cost and fault tolerant, designing an SRM controller is tedious.

For this research, a continuous conduction based high speed control scheme has been considered. Switched Reluctance Drives Limited has patents (US 5469039, US 5545964, US 5563488) on continuous type control schemes. The primary goal for the second part of the research was to mathematically analyze the high speed operation of SRM motors when continuous conduction is used. Chapter 7 describes this mathematical analysis. It has been shown that if the speed-sensitive losses are ignored, the CPSR of an SRM motor can be infinite when a continuous conduction based high-speed control scheme is used [13] and the resultant average and RMS current are well below the rated value. At high speed, saturation is not an issue [16]. Using a linear magnetic model, analytical expressions have been derived relating resultant average motor power and average motor current to the machine design and control parameters. Analytical expressions relating required peak current to the desired output power have also been derived. In Section 7.4 and Section 7.5, required residual flux-linkage and resultant minimum current have been derived. For verification purposes, these analytical results have been compared with simulation results based on linear as well as non-linear models. In Chapter 7, it has been shown that the control variables required for continuous conduction based control scheme are same as the low-speed, discontinuous conduction based control scheme.

2 LITERATURE REVIEW: PERMANENT MAGNET SYNCHRONOUS MOTORS

Inverter driven permanent magnet synchronous motors (PMSM) are widely used in high performance variable frequency drive systems. The stator of a typical synchronous motor is the same as that of a standard induction motor (IM). It is made of a number of stampings slotted to receive stator windings. Permanent magnet synchronous motors also have sinusoidal flux distribution. This results in a sinusoidal back EMF and requires sinusoidal currents to produce constant torque. Unlike induction motors, the rotor of a synchronous motor has permanent magnets (PM) instead of electro-magnets. When compared to an induction motor, these rare earth permanent magnets create high density magnetic field. This results in higher efficiency and lighter weight [10]. Constant magnetic field also generates relatively constant torque for a constant stator current input [10]. This inherent characteristic of PMSM motors to produce a constant torque for a constant current is considered to be a drawback for applications in electric vehicles. Particularly in the constant power region, torque has to decrease with increase in speed in order to produce the constant rated power without exceeding current rating. PMSM motors also have higher power factor compared to that of an Induction Motor [5]. Figure 2-1 shows a cross-sectional view of a Surface PM Motor (SPM). In this type of a machine, the magnetic pole is constructed flush with the surface of the rotor. The rotor magnets have high permeability (close to that of the air, 1.06 for Nd-Fe-B). These permanent magnets appears as an air gap to the stator magneto-motive force [17].

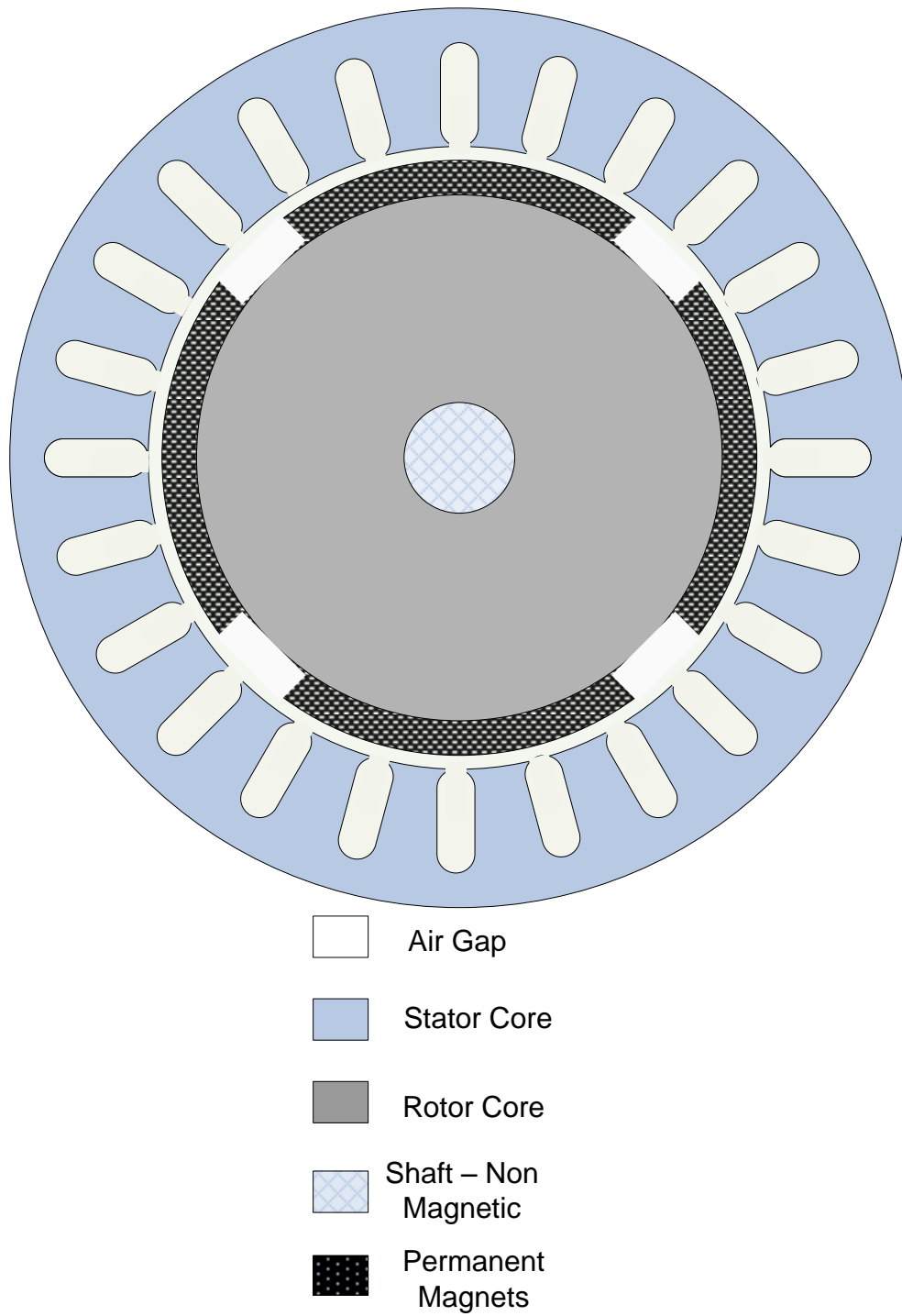


Figure 2-1: Surface Permanent Magnet Motor - Cross Sectional View.

Therefore, the air gap flux density between the stator and the rotor is uniform hence SPM is a non-salient type of machine. As a result only magnetic torque is produced.

The term salient means “protruding” or “sticking out” and a salient pole is a magnetic pole that sticks out from the surface of the rotor. Figure 2-2 shows a cross sectional view of an Interior Permanent Magnet motor (IPM). Here rotor magnets are inset into the rotor. Here, the air gap flux density between stator and rotor is not uniform. As a result both magnetic and reluctance torques are produced.

Figure 2-3 shows a cross sectional view of the synchronous reluctance motor. Here rotor has air gaps. As a result only reluctance torque is produced.

2.1 Field Weakening Operation of Permanent Magnet Synchronous Motors

Motors with sinusoidal operation can be characterized by parameters resolved into a quadrature-axis and a direct-axis component. The problem arises due to the speed dependency of machine inductances, whereupon the coefficients of differential equations (voltage equations), which describe the motor behavior, are time varying except when the motor is at standstill. After several configuration dependent transformations were developed, it was recognized that there is one “general” transformation which eliminates all time-varying inductances.

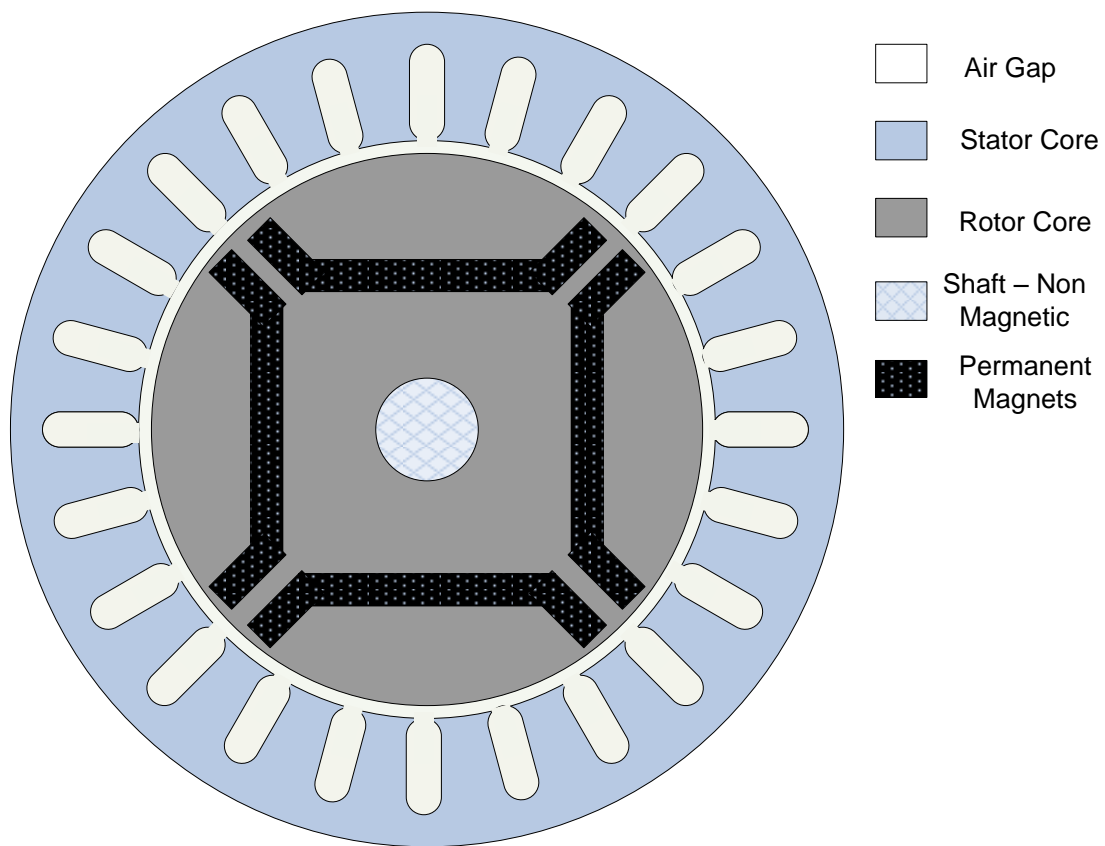


Figure 2-2: Interior Permanent Magnet Motor - Cross Sectional View.

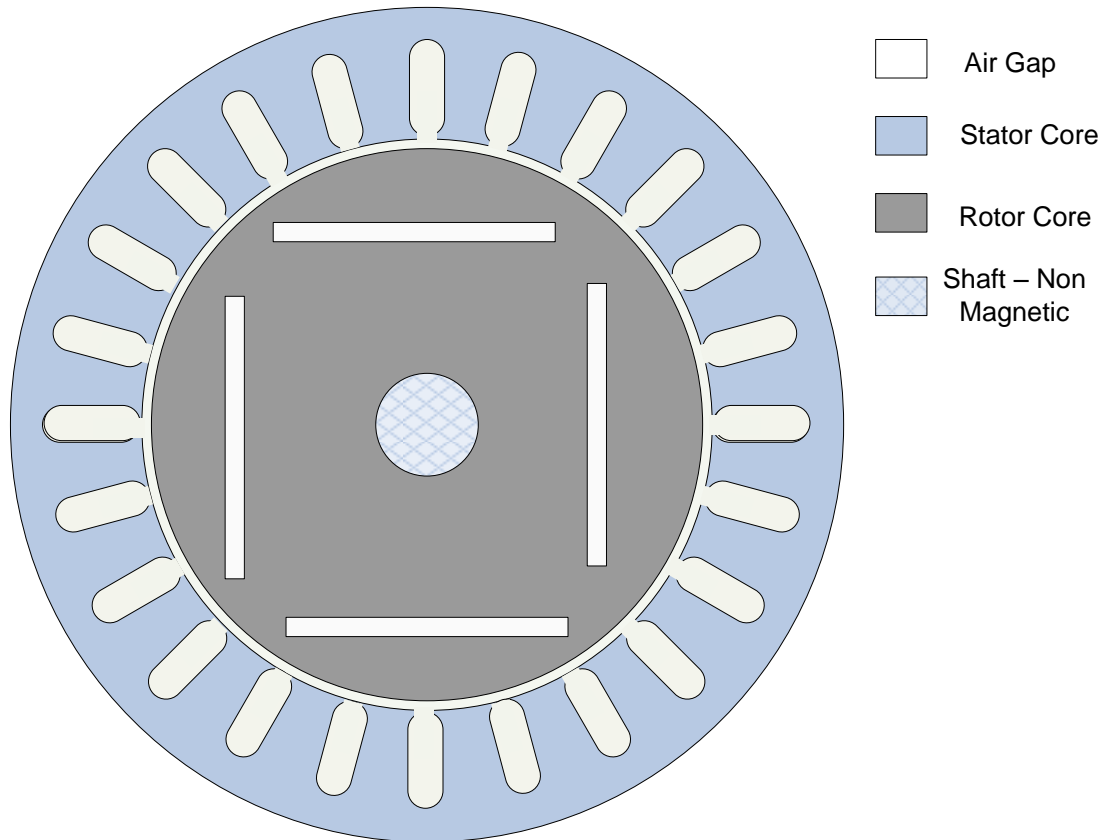


Figure 2-3: Synchronous Reluctance Motor - Cross Sectional View.

This can be done by referring the stator and rotor variables to a reference frame which may rotate at any angular velocity or remain stationary and termed “arbitrary-reference frame.”

This transformation may be expressed in vector notation as,

$$\underline{V}_{qdo} = K_s \underline{V}_{abc}, \quad (2.1)$$

Here, \underline{V}_{qdo} and \underline{V}_{abc} are the column vectors,

$$\underline{V}_{qdo}^T = [V_q, V_d, V_o], \quad \text{and} \quad \underline{V}_{abc}^T = [V_a, V_b, V_c],$$

V_a , V_b , and V_c are phase voltages. V_q , and V_d are quadrature-axis and direct-axis phase voltage components. V_o is a zero sequence voltage. In balanced three-phase operation, zero sequence currents or voltages are zero. Interested readers can refer to [18] for more information on a need to transfer three-phase currents and voltages to a two-phase d-q system. More information on d-q transformation theory can also be found in [19], [20] and [21]. The dynamic equations for a synchronous motor with saliency and permanent magnets can be defined as [5], [6], [20], and [22],

$$\begin{aligned} \frac{di_{qs}}{dt} &= \frac{1}{L_{qs}} (V_{qs} - R_s i_{qs} - \omega_e L_{ds} i_{ds} - E_f) \\ \frac{di_{ds}}{dt} &= \frac{1}{L_{ds}} (V_{ds} - R_s i_{ds} + \omega_e L_{qs} i_{qs}) \end{aligned} \quad (2.2)$$

Here R_s = stator per phase winding resistance, L_{qs} =q-axis inductance, L_{ds} = d-axis inductance, E_f = back-EMF due to magnetic flux, ω_e = electrical rotor speed, V_{qs} = q-axis voltage component, V_{ds} = d-axis voltage component, I_{qs} = q-axis current component, i_{ds} = d-axis current component. Equation (2.2) is consistent with the circuit of Figure 2-4.

Electromagnetic torque of a PM synchronous motor can be expressed as [22],

$$T_e = \frac{3}{2} \left(\frac{p}{2} \right) \left[(L_{ds} - L_{qs}) i_{ds} i_{qs} + \frac{E_f}{\omega_e} i_{qs} \right] \quad (2.3)$$

Here p = number of poles.

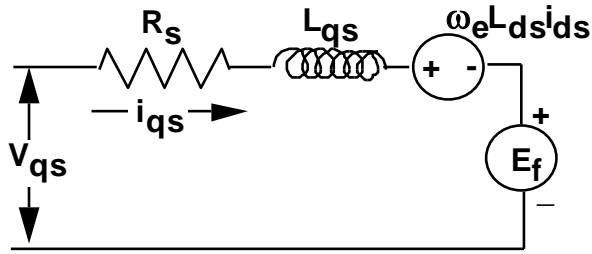
The torque equations take on different forms depending on the q-axis and d-axis inductance. Relationships are shown in the following Table 2-1.

Note that for surface PM motors, torque only depends on the q-axis (vertical component) current i.e.,

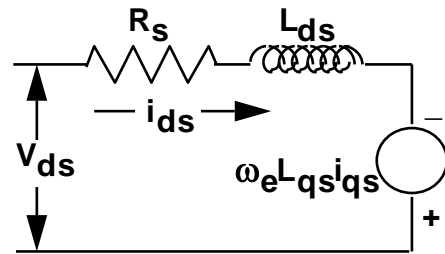
$$T_e = \frac{3}{2} \left(\frac{p}{2} \right) \left[\frac{E_f}{\omega_e} i_{qs} \right] \quad (2.4)$$

Making the assumptions¹ that the system is in the steady state where all derivatives are zero, and neglecting resistances,

¹ The subscript “s” has been dropped for currents, voltages and inductances.



a) Equivalent q-axis circuit.



b) Equivalent d-axis circuit.

Figure 2-4: Electrical Equivalent d-q Circuit of a Synchronous Motor in the Synchronously Rotating Reference Frame [23].

Table 2-1: Torque Equations [24]

MOTOR	PARAMETERS	TORQUE
SPM	$L_{ds} = L_{qs}$	$T_e = \frac{3}{2} \left(\frac{p}{2} \right) \frac{E_f i_{qs}}{\omega_e}$
IPM	$L_{ds} \neq L_{qs}$	$T_e = \left[(L_{ds} - L_{qs}) i_{ds} i_{qs} + \frac{E_f i_{qs}}{\omega_e} \right]$
Synchronous Reluctance	$E_f = 0$	$T_e = (L_{ds} - L_{qs}) i_{ds} i_{qs}$

Equation (2.2) now becomes

$$V_d = -\omega_e L_q i_q \quad (2.5)$$

And

$$V_q = \omega_e L_d i_d + E_f \quad (2.6)$$

These voltages are subject to the voltage limitations due to the limitation on available DC link voltage.

$$V_q^2 + V_d^2 \leq V_r^2 \quad (2.7)$$

Similarly, the current limitations due to limitations of the power devices used in the inverter system and winding insulations,

$$i_q^2 + i_d^2 \leq I_r^2 \quad (2.8)$$

Here, I_r = rated stator current value in amperes and, V_r = rated stator voltage value in volts.

Combining Equations (2.5) and (2.6), in Equation (2.7) , we have,

$$\left(\omega_e L_q i_q \right)^2 + \left(\omega_e L_d i_d + E_f \right)^2 \leq V_r^2 \quad (2.9)$$

Defining, $\frac{E_f}{\omega_e} = \psi_{mag} = \psi_f =$ flux linkages due to rotor permanent magnets,

Equation (2.9) becomes,

$$\left(\frac{i_d + \frac{\psi_{mag}}{L_d}}{\frac{V_r}{L_d \omega_e}} \right)^2 + \left(\frac{i_q}{\frac{V_r}{L_q \omega_e}} \right)^2 = 1 \quad (2.10)$$

In the i_d, i_q plane, Equation (2.10) is an ellipse centered at $-\frac{\psi_{mag}}{L_d}$. With rated voltage V_r fixed, this ellipse shrinks inversely with the speed of the motor, ω_e . Thus, one has a voltage-limit ellipse and a current-limit circle. We note that for the surface type permanent magnet motors, L_q and L_d are equal (due to non-saliency). Thus, the voltage-limit ellipse degenerates into a circle. The current limiting circle and the voltage circle are shown in Figure 2-5 [9]. At $\omega = \omega_o$ any control action must occur within the cross-hatched area. Below base speed, all the action occurs inside the current limiting circle.

Above base speed, the applied voltage is the maximum and the back-EMF exceeds the applied voltage. Consequently the back-EMF has to be reduced to produce torque in the constant power region. Unlike separately excited DC motors or induction motors, PM synchronous motors do not have a separate and controllable source of air-gap flux density. Therefore, a component of the stator current (the d-axis current) must be used to counter the air-gap flux density.

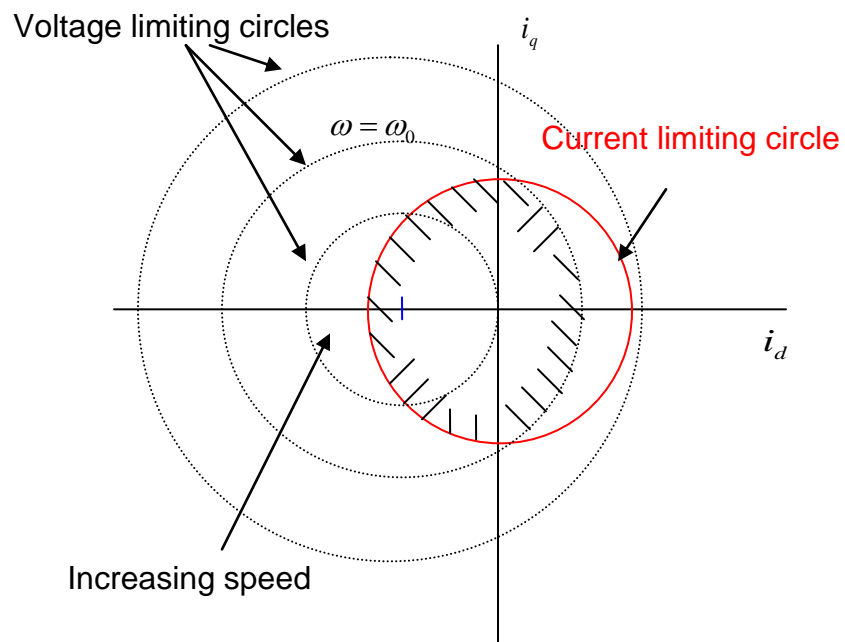


Figure 2-5: Current and Voltage Limited Operation of Permanent Magnet Motors [8].

The q-axis component of the stator current is then used to develop the required torque. This has led to the terminology “flux-weakening” [8]. Controllers that control both the magnitude and the phase angle of the stator excitation are termed as “vector controllers” [25]. Since this “vector control” also results in the control of spatial orientation of the electromagnetic field, the term “field orientation” [25] is also used. The flux weakening control [8] is very useful for high speed, constant power operation considering the voltage constraint. This is a desired characteristic in traction applications. Since part of the current is “wasted” in field weakening, surface PM machines have generally been considered to be poor candidates for achieving this wide constant power speed [1].

The center of the voltage limiting circle in Equation (2.10) is also called as the characteristic current of SPM machines, and is defined as,

$$I_{CH} = \frac{\psi_{mag}}{L_d} \quad (2.11)$$

Here ψ_{mag} is the RMS magnetic flux linkage and L_d is the d – axis inductance. This center should lie inside the current limiting circle (red circle in Figure 2-5). Theoretically SPM machines have infinite CPSR if $I_{CH} \leq I_{rated}$ [26]. For surface PM machines, this characteristic current is usually several times higher than the rated current of the machine [8]. With conventional distributed stator winding, due to the large effective air gap, inductance value of the SPM machines is typically low. Due to use of permanent magnets, the magnet flux linkage is quite high. This results in much higher value of the

characteristic current than the rated current, putting limits on achievable CPSR. It is also well known that when the rated current of the motor is equal to the characteristic current of the motor, flux weakening is optimal [1]. For this reason a wider CPSR can simply be achieved by adding a series of external inductors [17]. This technique increases weight, volume and losses [1]. Surface PM Machines with a fractional slot concentrated windings (FSCW) have considerably higher inductance, mainly due to higher slot leakage inductance [26], [27]. Surface PM Machines equipped with concentrated windings provide the highest power and torque density [26] compared to that of distributed windings. Due to the lower winding losses, FSCW machines also have superior thermal performance in the constant power region [26]. Although, distributed winding machines have the best inverter utilization. Without flux weakening, a machine must be designed to produce the rated torque over the entire speed range. This also requires over sizing of an inverter. Additionally, low inductance increases the switching requirements of power devices and causes high short circuit currents.

The electric torque produced by the surface PM machine is given by[22],

$$T_e = \frac{3}{2} \left(\frac{p}{2} \right) [\psi_{mag} i_q]$$

Here ψ_{mag} is the flux produced by the permanent magnets and p is the number of stator poles. For a given machine design, output torque only depends on the q-axis current. In the constant torque region (below base speed operation), maximum torque-per-amp is

produced by keeping the d-axis current is to zero [1], [8]. This is accomplished by maintaining the applied stator voltage in phase with the back-EMF. Figure 2-6 illustrates operation below base speed of a surface permanent magnet motor (generating maximum torque-per-amp.). Here ψ_a is the magnetic flux produced by the stator currents.

With rated voltage and rated current, at base speed the machine produces rated power. At and above base speed, the applied voltage will be at its rated value. As the speed increases above base speed, back-EMF will exceed the applied stator voltage, making it difficult to produce any torque. In this region, stator current vector has to be rotated counter clockwise. In doing so, part of this stator current vector (i.e. horizontal d-axis component) is used to reduce the air-gap flux.

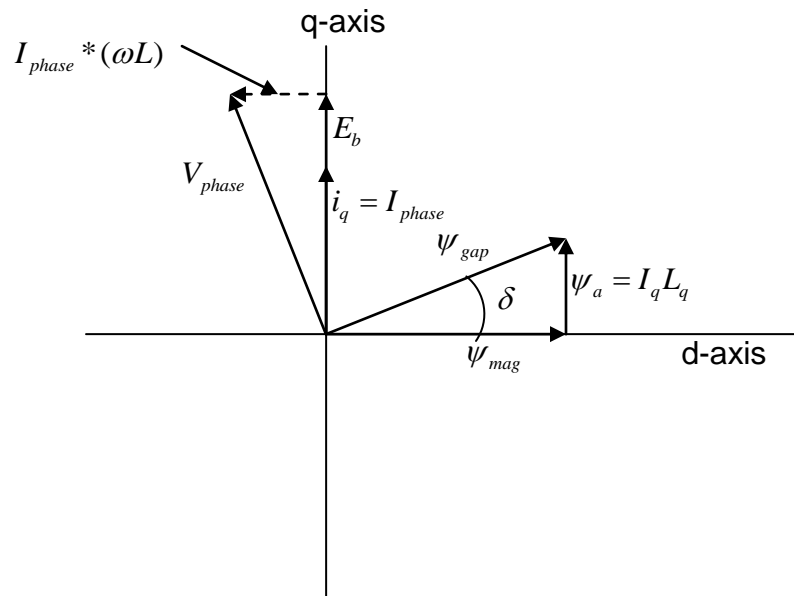


Figure 2-6: Below Base Speed Operation of Surface PM Machines [28].

This in turn reduces the generated back-EMF. The remaining vertical or q-axis component of the stator current is then used to produce the required torque. Figure 2-7 illustrates above base speed, field weakening operation of the Surface PM Machines.

As speed increases, current vector rotates more towards the direct-axis. At some speed, developed torque becomes zero as all of the current is used to reduce the back-EMF. In constant power zone, as the part of the current is used to oppose the magnetic field produced by the permanent magnets, magnet demagnetization due to the direct axis armature reaction must be prevented.

The demagnetization process is irreversible and it decreases the electro-magnetic torque [9]. Use of magnets with large coercive force helps with the above problem in field-weakening zone operation of permanent magnet synchronous motors [28]. The following sections describe some of the available field weakening techniques for surface PM machines.

2.1.1 Constant Voltage Constant Power Vector Control [8],[29]

From Table 2-1, developed mechanical power is given by²,

$$P_m = T_e \omega_e = \frac{3}{2} \left(\frac{p}{2} \right) E_b i_q \quad (2.12)$$

² $E_f = E_b = \text{Back_EMF}$

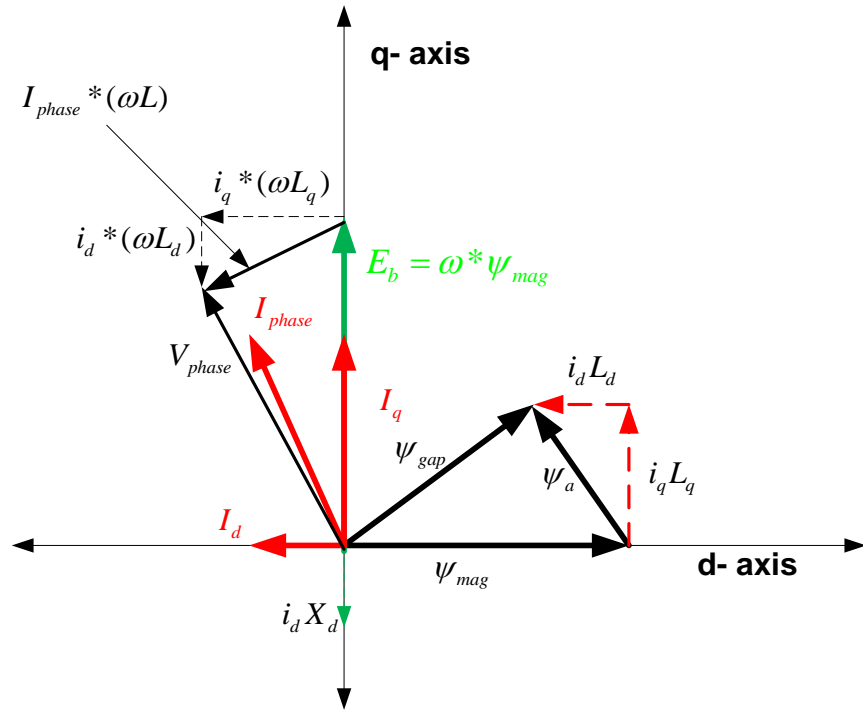


Figure 2-7: Above Base Speed Operation of Surface PM Machines [8][9].

Therefore, in the field-weakening zone, to keep power constant, the q-axis component of the stator current has to be changed with increase in speed.

At and above base speed ω_b , rated power can be developed using rated value of stator current, i.e,

From Equation(2.12),

$$P_{rated} = \frac{3}{2} \left(\frac{p}{2} \right) \psi_{mag} I_{rated} \omega_b = K I_{rated} \omega_b \quad (2.13)$$

Therefore, from Equation (2.12) and Equation (2.13), the q-axis component of the stator current can be derived as,

$$i_q = I_{rated} \frac{\omega_b}{\omega_e} \quad (2.14)$$

From Equation (2.5), the d-axis component of the applied stator voltage is,

$$V_d = -\omega_e L_q i_q = -\omega_e L_q * I_{rated} \frac{\omega_b}{\omega_e} = \omega_b L_q I_{rated} \quad (2.15)$$

Note that, in constant power region, this value is constant. In this zone, as the applied voltage is at its rated value, to keep the voltage constant, we have,

$$\begin{aligned} V_{s\max} &= \sqrt{V_d^2 + V_q^2}, \\ \therefore V_q &= \sqrt{V_{s\max}^2 - V_d^2} \end{aligned} \quad (2.16)$$

Note that the q-axis component of the applied stator voltage is also constant. From Equation(2.6),

$$\begin{aligned} V_q &= \omega_e L_d i_d + E_f = \sqrt{V_{s \max}^2 - V_d^2}, \\ \therefore i_d &= \frac{\sqrt{V_{s \max}^2 - V_d^2} - E_f}{\omega_e L_d} \end{aligned} \quad (2.17)$$

Note that, as speed increases, both the d-axis and q-axis components of the stator current decrease. In this control strategy, the current vector is controlled according to the Equation (2.14) and (2.17) to produce maximum available torque considering both current and voltage constraints.

2.1.2 Constant Current Constant Power Vector Control [19] [30]

In this control strategy, instead of applied voltage, in the field weakening zone, applied current is held constant. As explained in the previous section, Equation (2.14) implies constant power operation in the field-weakening zone. To keep stator current constant,

$$i_d = -\sqrt{I_s^2 - i_q^2} = -\sqrt{I_s^2 - \left(I_{rated} \frac{\omega_b}{\omega_e} \right)^2} \quad (2.18)$$

From Equation (2.15) , constant q-axis current means, the d-axis component of applied stator voltage will also be constant. So in this control strategy, the voltage vector moves along the line $V_d = \omega_b L_q I_s$. In contrast to the previous method, here q-axis component of the applied stator voltage decreases. Figure 2-8 illustrates constant current constant power control strategy.

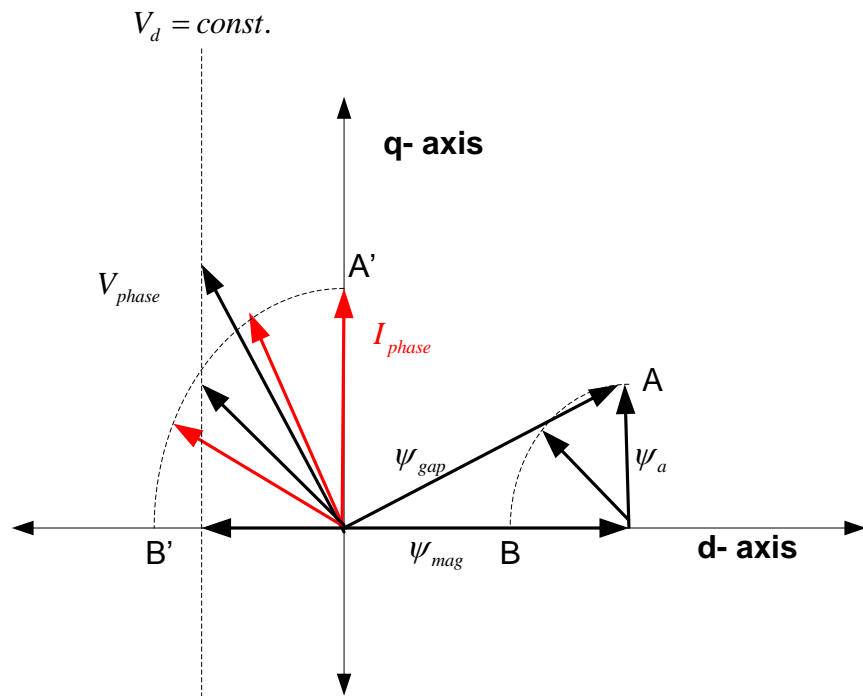


Figure 2-8: Constant Current Constant Power Vector Control.

2.1.3 Optimum Current Vector Control [9]

Figure 2-9 illustrates optimum current vector control strategy. Below base speed, voltage vector is adjusted such that current will be in phase with the back-EMF producing maximum torque-per-amp.

This can be done till point A. Point A is where current-limit circle intersects the voltage-limit circle corresponding to the base speed. Morimoto [9] has shown that the voltage-limited maximum power trajectory passes through the characteristics current point. So from base speed till point B (point where current-limit circle intersects the maximum power line), stator current can follow the current-limit circle. Note that this is not a constant power strategy. By this control strategy maximum allowable apparent power is produced. Figure 2-10 illustrates this field-weakening control scheme.

If the characteristic current of the motor is same as the rated current of the motor, i.e. $I_{CH} = I_{Rated}$, then the back-EMF (E_b), terminal voltage (V_{phase}), and the voltage drop across the phase inductance ($I_{phase} * (\omega L)$) form an isosceles triangle. This triangle grows at the same rate as the speed increases [31]. With this scenario, there is no theoretical limit on the maximum speed at which the motor can be operated [31]. The difference between the inductance voltage drop and back-EMF is what controls the maximum attainable speed; and the closer this ratio is to unity, the higher is the attainable speed [31]. Figure 2-11 illustrates the same. Here V_{phase} is the applied phase voltage, I_{phase} is the resultant per phase stator current, L is the per phase winding inductance, and E_b is the generated back EMF.

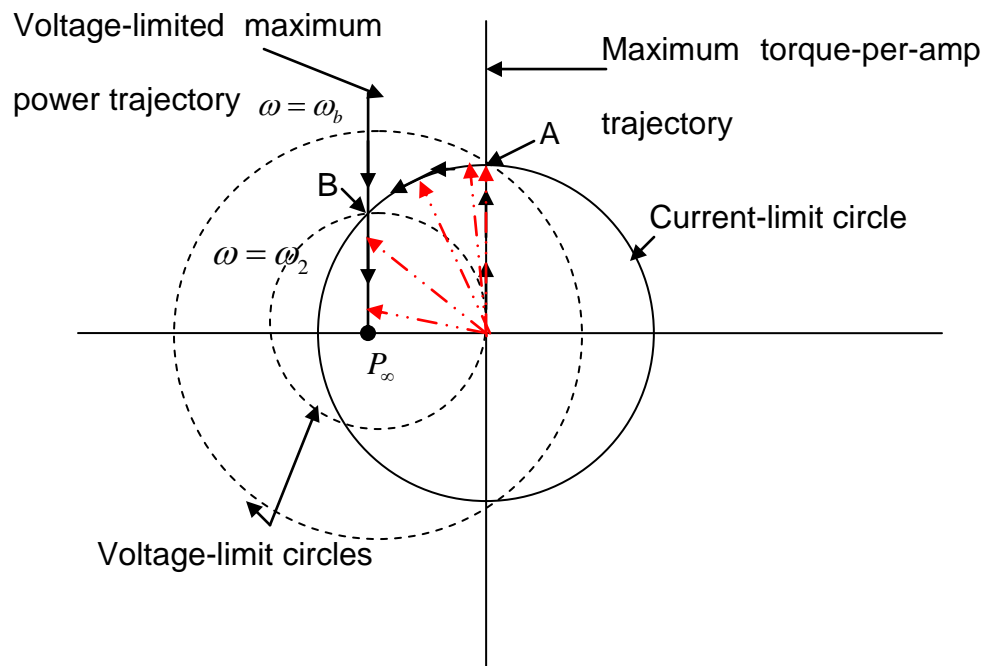


Figure 2-9: Optimum Current Vector Control.

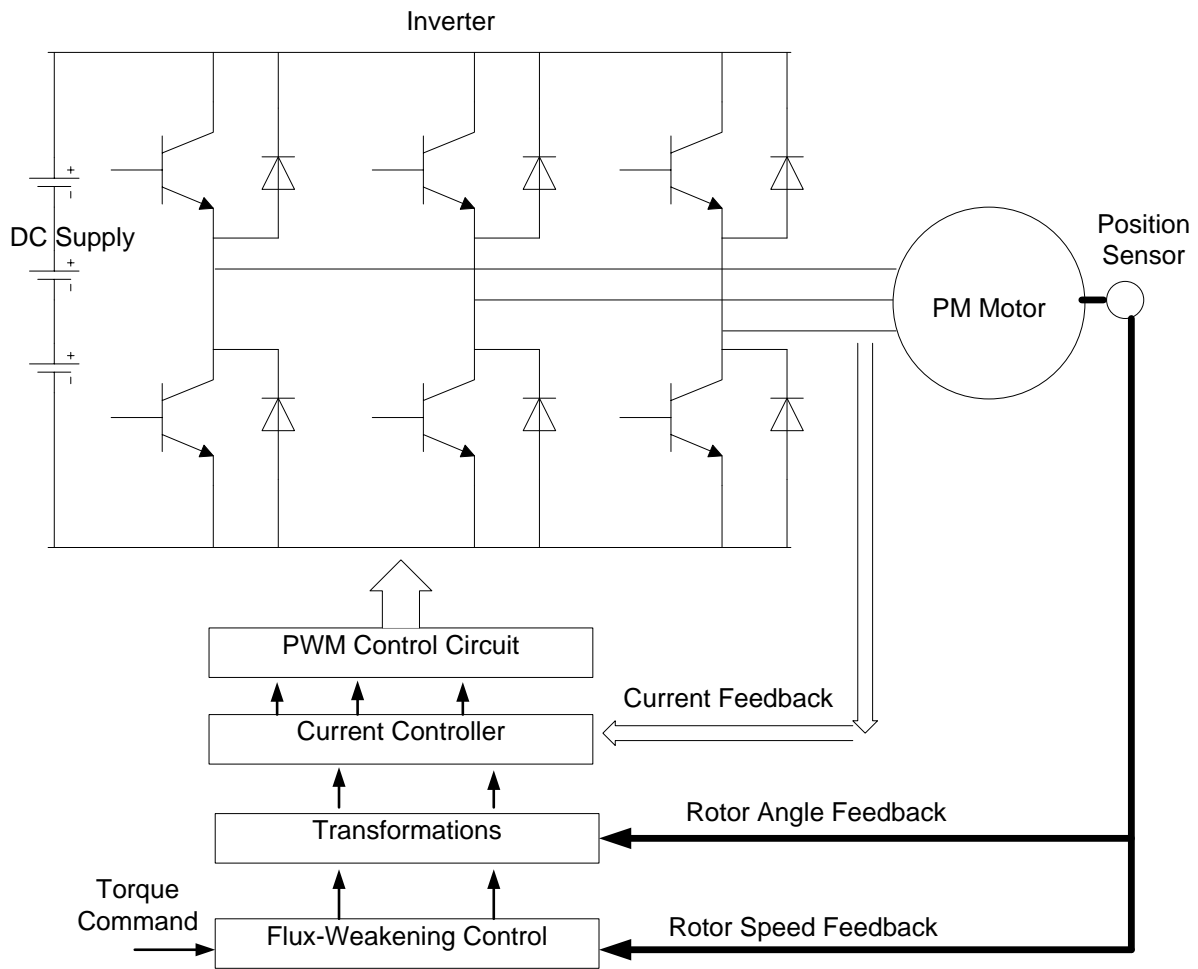


Figure 2-10: Scheme of Flux-Weakening Control System for Permanent Magnet Synchronous Motors [9].

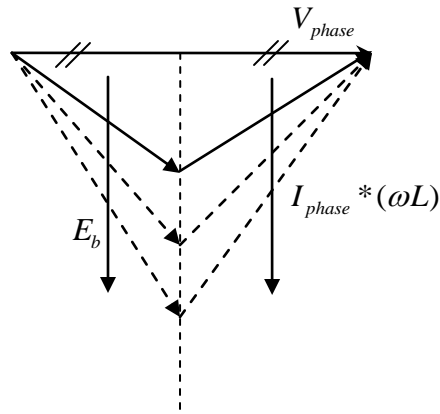


Figure 2-11: Optimal Condition for Flux Weakening Operation of Surface PM Motors [31].

Interested readers can refer to [32] for more information on field-weakening type vector control schemes used for PM machines.

Slemon [33] questioned whether the flux weakening is the optimal approach to achieve constant power range for some traction drives. He suggested re-rating motors such that full voltage is available till the maximum attainable speed rather than just till the base speed. Maximum torque-per-amp can be produced over most of the speed range by making the field due to the stator current lead that of the rotor magnets by $\pi/2$ radians. In other words, the current should be in phase with the back-EMF. As maximum speed is approached, the angle between stator and rotor magnetic fields can be decreased to achieve nearly unity power factor to make the best use of available power [34]. By avoiding constant power operation and using re-rating approach, Chapman et al [35] claimed to produce higher power levels from smaller low cost PM machines. He also

outlined design choices (gear ratio, rearranging motor windings, and extending constant volts per hertz by providing a frequency range above rated value) intended to avoid flux weakening and improve power per unit mass ratio. Nipp [36] suggested that the extension of speed range of PMSM is possible by connecting different coil groups of the stator winding in different configurations. This approach requires larger motors to be used for smaller applications increasing size, weight and cost. Otherwise it requires extra voltage, increasing power electronics rating and hence size, cost and weight.

3 CONVENTIONAL PHASE ADVANCEMENT METHOD

Above base speed, the internal back-EMF exceeds maximum available supply voltage. Thus as the speed of the motor approaches the base speed, the ability of an inverter to force current into motor winding diminishes. This causes torque reduction and ultimately puts limitation on the achievable maximum speed.

In Figure 3-1, the red curve represents applied voltage and the black curve represents generated back-EMF. Note that back-EMF exceeds the applied voltage making it difficult to force any current into the motor.

In vector control, as discussed in the previous chapter, above base speed, d-axis current is applied such that it reduces the resultant air-gap magnetic field. This causes reduction in generated back-EMF. This helps the inverter to force current into the motor winding and develop the required torque at higher speeds. This traditional “flux weakening” method, if not used properly, can cause irreversible demagnetization of the rotor permanent magnets [9].

Vector control requires information about the phase currents and voltages. These three-phase quantities have to be transformed into equivalent d-q values. Based on control, error values (d-q) have to be transformed back to the three phase values. Based on this information along with Pulse Width Modulation technique used, inverter switches are turned ON or OFF.

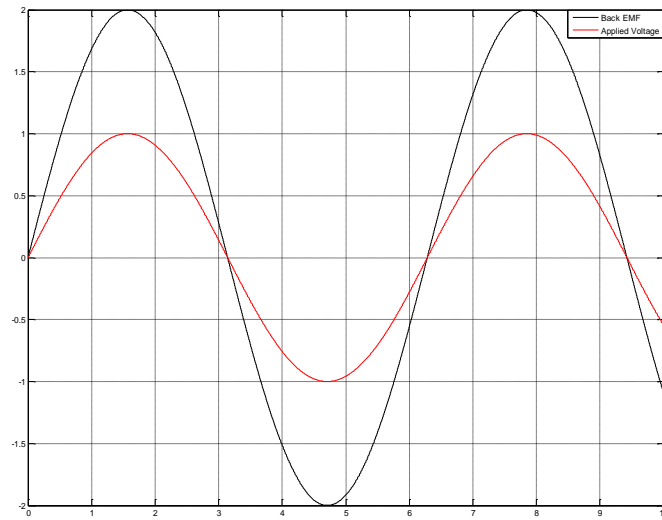


Figure 3-1: Comparison of Back-EMF and Applied Stator Voltage above Base Speed without Field-Weakening.

This means vector control requires precise information about the phase currents and phase voltages. This implies more drive hardware, size and weight. An Abc-dq transformation means more mathematical complexity, slower system response and more required computational power. The primary goal of this research was to reduce this mathematical complexity. This can be done by avoiding vector control type field weakening scheme which also reduces the need for voltage and current sensors.

The phase timing advancement technique (described in [10] for brushless DC motors) is one of the possible solutions. Above base speed, this technique prematurely turns ON inverter switches. This premature switching results in an application of voltage to the motor winding when the instantaneous value of the back EMF of the corresponding motor winding is less than the applied voltage. Figure 3-2 illustrates this phase advancement technique.

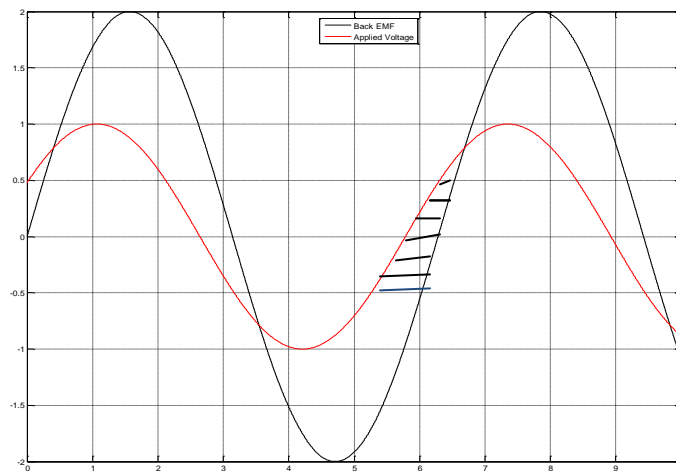


Figure 3-2: Back EMF and Applied Voltage above Base Speed With Phase Advancement.

Phase timing advancement results in “pre-charging” of the winding with current. By the time the rotor rotates to a position where generated back-EMF exceeds applied voltage, current in the winding has already been raised to a level that can produce significant torque even though the same current starts decreasing due to the negative relative voltage applied across the motor inductance. This results in significant increase in maximum motor speed at which constant power can be developed.

3.1 Analysis of a Permanent Magnet Synchronous Motor Driven by Conventional Phase Timing Advancement Method [37].

Figure 3-3 shows a schematic of a three-phase PMSM driven by a voltage-source inverter (VSI). Figure 3-3 also defines some of the parameters and notations used in this discussion. Here p = number of poles, N =actual mechanical rotor speed in revolutions per minute (rpm), N_b = mechanical base speed in rpm, n = relative speed = $\frac{N}{N_b}$, Ω_b = base speed in electrical radians/sec, $= \frac{p}{2} * 2\pi * \frac{N_b}{60}$, Ω = actual rotor speed in electrical radians/sec, $= n\Omega_b$, E_b = rms magnitude of the phase-to-neutral emf at base speed, I_R = rated rms motor current, P_R = rated output power = $3E_b I_R$, L_s = self inductance per phase, L_o = leakage inductance per phase, M = mutual inductance, L = equivalent inductance per phase = $L_o + L_s + M$, R = winding resistance per phase, v_{an} =applied phase A to neutral voltage, e_{an} = phase A to neutral back-EMF and, e_{ab} = phase A to phase B (line-to-line) back-EMF.

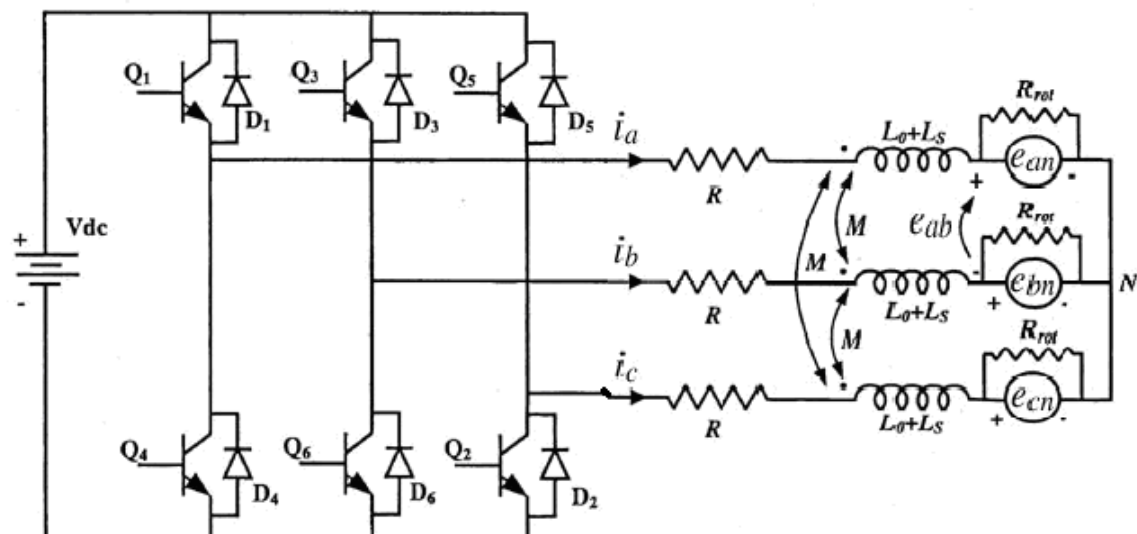


Figure 3-3: Motor / Inverter Schematic for a PMSM Driven by CPA [37].

First part of the Figure 3-3, is a typical voltage source inverter configuration. Here DC supply voltage is denoted by V_{dc} . Typically a battery is used as a DC supply source. Q_1 , Q_2 , Q_3 , Q_4 , Q_5 , and Q_6 are solid state power electronics switches. Typically IGBTs are used as inverter switches. Similarly D_1 , D_2 , D_3 , D_4 , D_5 , and D_6 are bypass diodes. Switches in an inverter of Figure 3-3, can be controlled by a well known method called as sinusoidal pulse width modulation (SPWM) technique. This inverter switching scheme uses a triangular carrier wave (green color waveform shown in Figure 3-4, V_{tri}) and three sinusoidal reference waveforms (shown in blue for phase A , yellow for phase B and, red for phase C, i.e. $V_{control}$) to decide the switching pattern. For phase A, if $V_{control} > V_{tri}$, upper switch Q_1 is turned ON , similarly when $V_{control} < V_{tri}$, lower switch Q_4 is turned ON.



Figure 3-4: Three Phase Waveforms.

Simultaneous switching of both of these switches in one inverter leg will result in short circuit of a DC supply. As it takes a small but finite time for switches to change the state, to avoid short circuit usually a dead time is inserted between changes of state. The amplitude and frequency of an inverter output waveform (applied stator voltage) is determined by the amplitude and frequency of the $V_{control}$ waveform. This frequency is called the fundamental frequency. Usually the amplitude of the triangular waveform is kept at unity and the amplitude of a sinusoidal control waveform is changed. The ratio of $V_{control} / V_{tri}$ is called the modulation index m_a . When the modulation index m_a is more than 1, the inverter is said to be operating in an over-modulation region and the switching waveform looks like a square wave. Maximum value of the m_a is $4/\pi$. The frequency of V_{tri} waveform is called the switching frequency. The switching frequency is usually in KHz to obtain a sinusoidal shape in the resultant stator current.

The remaining part of Figure 3-3 is a typical PMSM motor model. Resistors R and R_{rot} , represent the copper losses and the speed sensitive rotational losses of a typical PMSM motor respectively. The value of R_{rot} can be calculated for any given speed using the least-squares fit of a back-EMF data and the least squares-fit of rotational no-load losses data. At relative speed n , the value of $R_{rot}(n)$ is calculated as,

$$R_{rot}(n) = \frac{3(nE_b)^2}{P_{rot}(n)} \quad (3.1)$$

3.1.1 Fundamental Frequency Model

The main focus of this section is on the application of conventional phase advancement for field weakening operation of surface PM motors. The objective is to focus on constant power speed ratio, efficiency, and steady state control. This discussion is greatly simplified by neglecting the motor losses. Unless otherwise specified, the discussion in the remainder of this section and the next one assumes that the winding resistance R_s is zero and the rotational loss resistance R_{rot} , is infinite. Equations developed in this section give a good insight into the performance of a surface PM motor when used for traction drive application using CPA method.

Figure 3-5 shows a per phase, fundamental frequency model of a surface PM motor driven by a voltage source inverter. This is equivalent to one of the three phases in Figure 3-3. The first part (DC supply + an inverter section) of the Figure 3-3, is replaced by the resultant, inverter output AC voltage ($V \angle \delta$). Vector \tilde{V} represents line-to-neutral supply voltage at fundamental frequency. The frequency of this supply voltage is the same as the frequency of the $V_{control}$ waveform while the RMS magnitude of the supply voltage depends on the modulation index.

$$V = \frac{1}{\sqrt{2}} * m_a * \frac{V_{dc}}{2}, \quad (3.2)$$

In Figure 3-5, R is stator winding resistance (which will be neglected for initial analysis). This value can be obtained from measured machine data.

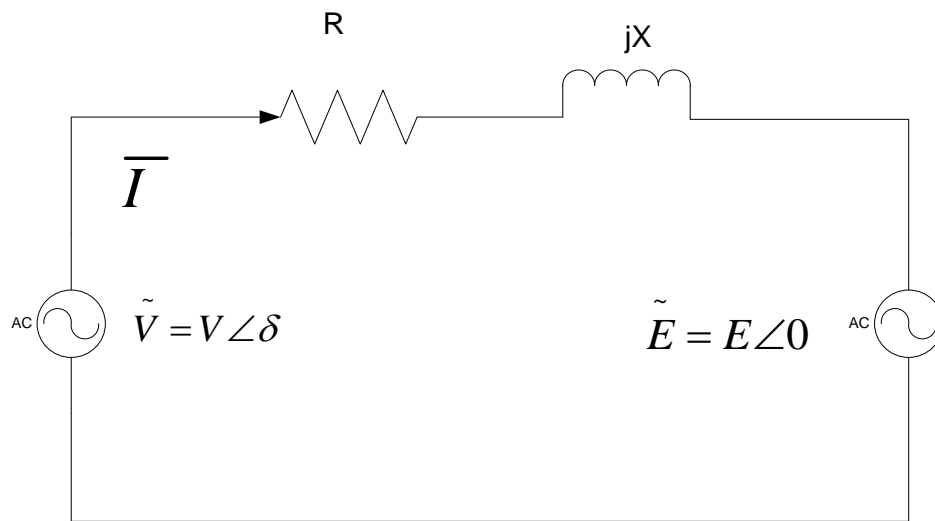


Figure 3-5: Fundamental Frequency Model.

Similarly, the motor per phase winding reactance can be expressed as,

$$\begin{aligned}
 X &= \Omega L \\
 X &= \frac{\Omega}{\Omega_b} \Omega_b L \\
 X &= nX_b
 \end{aligned} \tag{3.3}$$

Value of per-phase stator winding inductance (L) can also be obtained from the measured machine data. Here X_b is the per-phase winding reactance at base speed and n is the relative speed of the motor compared to the base speed. Vector \tilde{E} represents the phase-to-neutral generated motor back-EMF. This vector is chosen as a reference vector. Its phase angle will always be zero. Magnitude of this back-EMF is linear in motor speed. The voltage constant K_v , has units of RMS volts per electrical radian per second. Thus, the RMS value of the back-EMF at any motor speed is given by,

$$\begin{aligned}
 E &= K_v \Omega \\
 E &= \frac{\Omega}{\Omega_b} \Omega_b K_v \\
 E &= nE_b
 \end{aligned} \tag{3.4}$$

Here E_b is the RMS magnitude of line-to-neutral back-EMF at base speed and n is the relative motor speed compared to the base speed. A detailed PSICE simulator was developed to analyze the performance of a PM synchronous motor, controlled by PWM when operating at a constant speed, based on the fundamental frequency model. This

model of the motor drive is applicable at a selectable but constant speed. As the motor speed increases, generated back-EMF increases. Supply voltage has to be increased proportionally. Based on the available DC supply voltage, base speed n_b , can be defined as the highest speed at which applied voltage will be at its rated value. At this point, modulation index $m_a = 4/\pi$ and $V = \sqrt{2} * V_{dc}$. The base speed is also the highest speed at which rated torque is required, and can be produced. Power developed at this point is the rated power. True base speed n_{bt} , is exactly same as the actual base speed when the dc supply voltage is the minimum value that permits rated torque to be developed at the base speed. For sinusoidal PWM, we have,

$$V_{out} = \frac{1}{\sqrt{2}} * m_a * \frac{V_{dc}}{2}, \quad (3.5)$$

From Figure 3-5, we have,

$$\tilde{V} = \bar{I} * (R + jnX_b) + (n\bar{E}_b) \quad (3.6)$$

Assume that the rated current is in phase with back-EMF to produce maximum torque-per-amp.

Neglecting resistance, at base speed ($n = 1$), with modulation index at $4/\pi$, we have,

$$V_{dc_min} = \frac{\pi}{\sqrt{2}} \sqrt{E_b^2 + (X_b I_r)^2} \quad (3.7)$$

Here I_r is the rated RMS stator winding current. Note that Equation (3.7) insures that sufficient dc supply voltage is provided so that at base speed, the driving voltage is sufficient not only to overcome the back-EMF voltage but also internal impedance of the motor. If the DC supply voltage is less than V_{dc_min} , it will not be possible to develop the rated torque at the specified base speed and the true base speed will be less than the specified value. If the DC supply voltage is larger than V_{dc_min} , then the true base speed will be greater than the specified value. Letting the true base speed be denoted as n_{bt} we have,

$$n_{bt} = \frac{V_{dc}}{V_{dc_min}} n_b \quad (3.8)$$

When the DC supply is larger than the minimum, the rated torque can be developed at a speed higher than the base speed resulting in greater power conversion capability. However, the drive control can be configured to preclude this extra capability restricting the maximum power above base speed to the rated power. Even though control may be used to constrain the torque speed envelope, the addition of surplus dc supply voltage may allow reduced current magnitude at higher speeds, thereby reducing inverter and motor copper losses and improving efficiency. This possibility is discussed further.

3.1.2 Below Base Speed Operation (Constant Torque Zone, $n \leq 1$)

In the constant torque zone, both the magnitude of the applied stator voltage V , and the angle δ can be adjusted. This allows motor current to be in phase with the back-EMF.

From Figure 3-5, voltage magnitude V , and inverter lead angle δ can be calculated as follows;

$$\begin{aligned}
 \tilde{V} &= nE_b + jnIX_b \\
 &= \sqrt{(nE_b)^2 + (nIX_b)^2} \angle \tan^{-1} \left(\frac{nIX_b}{nE_b} \right) \\
 &= n\sqrt{E_b^2 + (X_b I)^2} \angle \tan^{-1} \left(\frac{IX_b}{E_b} \right) \\
 &= V \angle \delta
 \end{aligned} \tag{3.9}$$

Note that inverter lead angle does not depend on the speed. It only depends on the current required to produce desired torque. It also depends on motor design parameters at base speed such as phase reactance and back-EMF.

Equation (3.9) applied to Figure 3-5, neglecting resistance, we have RMS current,

$$\tilde{I} = \frac{V \angle \delta - nE_b \angle 0}{jnX_b} = \frac{V \sin \delta}{nX_b} + j \frac{(nE_b - V \cos \delta)}{nX_b} \tag{3.10}$$

As speed increases, the modulation index has to be increased from 0 to $4/\pi$ so that the applied voltage overcomes back-EMF and the winding reactance voltage drop. From Equation (3.9), it can be seen that, for the constant current, the applied voltage vector extends from the origin at constant δ until it reaches its maximum value. Assuming that the DC supply voltage is minimum given by Equation (3.7), modulation index is $4/\pi$, and stator current is the rated current, maximum phase voltage magnitude can be calculated as,

$$V_{\max} = \sqrt{(E_b^2) + (X_b I_r)^2} \quad (3.11)$$

Similarly, inverter lead angle is given by,

$$\delta = \tan^{-1} \left(\frac{I_r X_b}{E_b} \right) \quad (3.12)$$

With the rated current, the power developed at the base speed will be the rated power.

Since the current is in phase with the back-EMF, for 3-phase rated power P_r , we have,

$$P_r = 3E_b I_r \quad (3.13)$$

At base speed, the constant torque region ends. If applied DC voltage is more than (3.7), the true base speed will be more than the designed base speed. Although control can be used such that applied voltage is limited to the designed base speed value. Above base speed starts constant power region.

3.1.3 Operation above Base Speed (Constant Power Region, $n \geq 1$)

Above base speed voltage magnitude $V = V_{\max}$ i.e. sinusoidal PMW is operating in the over-modulation region. Neglecting the armature resistance, from Figure 3-5, current vector is given by,

$$\begin{aligned} \tilde{I} &= \frac{V_{\max}}{nX_b} \sin \delta + j \left[\frac{E_b}{X_b} - \frac{V_{\max}}{nX_b} \cos \delta \right], \\ \tilde{I} &= I_r + jI_x \end{aligned} \quad (3.14)$$

It can be seen from Equation (3.14) that this stator current has two parts a) Real part – which is responsible for mechanical torque production, and b) Imaginary part.

Here I_r is the component of motor current which is in phase with the back-EMF. This component is like a q-axis current component in the d-q model and it can be referred to as a torque producing current component. I_x is the component of a phase current that is orthogonal to the back-EMF and results in no net torque production. This component is like a d-axis component of the current in the d-q model and can be referred to as a field weakening current. Total motor current has RMS magnitude,

$$I = \sqrt{I_r^2 + I_x^2},$$

$$I = \frac{\sqrt{V_{\max}^2 - n2V_{\max}E_b \cos \delta + n^2E_b^2}}{nX_b} \quad (3.15)$$

From Figure 3-5, the apparent inverter output power (or motor input power) can be derived as follows,

$$S_{in} = \tilde{V} * \tilde{I}^*,$$

$$S_{in} = (V_{\max} \angle \delta) * \left(\frac{V_{\max} \angle \delta - nE_b \angle 0}{jnX_b} \right)^* \quad (3.16)$$

Therefore motor input power is given by,

$$P_{in} = 3 \operatorname{Re}(\tilde{V} \tilde{I}^*),$$

$$P_{in} = 3 \frac{V_{\max} E_b}{X_b} \sin \delta \quad (3.17)$$

Similarly, total motor output power is given by,

$$\begin{aligned} P_m &= 3 \operatorname{Re}(\tilde{E} \tilde{I}^*), \\ P_m &= 3 \frac{V_{\max} E_b}{X_b} \sin \delta \end{aligned} \quad (3.18)$$

and

$$P_{\max} = 3 \frac{V_{\max} E_b}{X_b} \quad (3.19)$$

Here P_{\max} , is the maximum power that can possibly be converted to mechanical form. This power corresponds to the lead angle δ being 90° . From Equation (3.17) and Equation (3.18), it can be seen that, motor output power is equal to the motor input power. As we have neglected the winding resistance, efficiency is 100%. Since the losses are zero, all the power from first part of the Figure 3-5 is transferred to the second part of the figure. Common value of this power is,

$$P_m = P_{in} = 3 \frac{V_{\max} E_b}{X_b} \sin \delta \quad (3.20)$$

This expression shows that, it is easy to control surface PM motor to deliver rated power in constant power zone. Inverter lead angle δ , has to be held fixed at a value that causes motor output power in Equation (3.20) to be equal to the rated power of the motor given by Equation (3.13). We have,

$$\delta = \sin^{-1} \left(\frac{X_b P_r}{3 V_{\max} E_b} \right) \quad (3.21)$$

While constant lead angle control allows the PMSM to operate at a constant power above base speed, it is not a certainty that doing so results in operation within the rated motor current limit. The critical factor is the motor inductance as shown in the next section.

3.1.4 “Optimal” Inductance for the Field-Weakening

Observe from Equations (3.14) that as the speed approaches infinity, motor current magnitude approaches a limiting value given by,

$$\begin{aligned}\lim_{n \rightarrow \infty} \tilde{I} &= \lim_{n \rightarrow \infty} \left\{ \frac{V_{\max}}{nX_b} \sin \delta + j \left[\frac{E_b}{X_b} - \frac{V_{\max}}{nX_b} \cos \delta \right] \right\}, \\ \lim_{n \rightarrow \infty} I_r &= \lim_{n \rightarrow \infty} \frac{V_{\max}}{nX_b} \sin \delta = 0 \\ \lim_{n \rightarrow \infty} I_x &= \lim_{n \rightarrow \infty} \left(\frac{E_b}{X_b} - \frac{V_{\max}}{nX_b} \cos \delta \right) = \frac{E_b}{X_b} = \frac{E_b}{\Omega_b L}\end{aligned}\tag{3.22}$$

Equation (3.15) gives the value of RMS motor current, when operating at any speed above base speed. Equation (3.21) gives the value of the lead angle δ such that the rated power is produced in the constant torque zone. In order to keep the current required to produce this rated power below the rated current value I_R , we have ,

$$\begin{aligned}I &= \frac{\sqrt{V_{\max}^2 - 2nV_{\max}E_b \cos \delta + n^2E_b^2}}{nX_b} \\ I &= \frac{\sqrt{V_{\max}^2 + n(n-2)E_b^2}}{n\Omega_b L}, \\ I &\leq I_r\end{aligned}\tag{3.23}$$

As speed goes to infinity, we have,

$$\lim_{n \rightarrow \infty} I = \lim_{n \rightarrow \infty} \frac{\sqrt{V_{\max}^2 + n(n-2)E_b^2}}{nX_b} = \frac{E_b}{X_b} = \frac{E_b}{\Omega_b L} = I_{CH} \quad (3.24)$$

The limiting RMS current magnitude in Equation (3.24) is called as the “characteristic current” of the motor and is denoted as I_{CH} . This is the same as Equation (2.11). Note that the characteristic current depends only on the motor parameters at base speed such as back-EMF and winding reactance. This current is independent of required motor load and DC supply voltage. Also note that, from Equation (3.22), as speed increases, torque producing current I_r approaches zero. The limiting current at high speed is solely due to field weakening current component I_x . This result has a positive implication for being able to operate over a wide CPSR while remaining within the motor current rating. Unfortunately, there is also an adverse implication towards efficiency when operating at high speed and partial load conditions. The impact on efficiency is considered later. At the moment, we consider the positive impact on CPSR when the machine inductance is sufficiently large.

If the limiting RMS current in Equation(3.24), which is the characteristic current, is less than or equal to the rated current I_R , then we have an inductance requirement that yields an infinite CPSR,

$$L_{\infty} = \frac{E_b}{\Omega_b I_R} \quad (3.25)$$

This inductance value is sometimes cited as the “optimal” value for field weakening [27], [31], [8]. Theoretically, any surface permanent magnet synchronous machine having an inductance value equal to Equation (3.25) or higher, will have an infinite CPSR.

In the constant power region, there is a well defined speed at which current magnitude is minimal. Setting the derivative of Equation (3.15) with respect to relative speed n , equal to zero and solving for this speed yields,

$$n_{\min} = \frac{V_{\max}}{E_b \cos \delta} . \quad (3.26)$$

With this value of n substituted into Equation (3.15), the minimum current can found.

$$I_{\min} = \frac{P}{3V_{\max}} \quad (3.27)$$

Note that this minimum current magnitude is independent of motor parameters and depends linearly on the developed power and inversely on the maximum fundamental frequency component of the inverter output voltage. Since V_{\max} can be increased by raising the dc supply voltage, there may be a reduction in motor and inverter losses when V_{dc} is increased above the minimum level required to sustain rated power at base speed. It can be shown that for speeds less than n_{\min} , the inverter power factor is lagging; while for speeds above n_{\min} , the inverter power factor is leading. Thus, the inverter operates at the optimum unity power factor condition at only one speed, namely

n_{min} . Figure 3-6 illustrates this conventional phase advancement control strategy when used for the flux weakening of surface permanent magnet synchronous machines.

In this figure, red vector represents the stator current. Up to base speed, the current is maintained in phase with the back-EMF. This produces the maximum torque per amp. Simulation and the experimental results (as described later) suggest that, from base speed till n_{min} , stator current decreases with increase in speed to the minimum value. At this speed, current is phase with the applied voltage. So power factor is unity. Below this speed, the power factor is lagging. Above n_{min} , the current increases with speed and approaches the characteristic current. If this characteristic current is less than the rated current of the motor, theoretically surface PM machines have infinite CPSR. Above n_{min} , the power factor is leading as the back-EMF exceeds the rated supply voltage.

3.2 Steady State PMSM Control Considering Winding Resistance

The mathematical analysis given in previous section neglected winding resistance. Neglecting these factors makes the analysis simpler. It leads to compact expressions which provide considerable insight into the control of surface PM motors for traction drive application, using conventional phase advancement method. Stator current can be considered as a control variable. Depending on the load (torque/power) requirement, the required motor current can be estimated. This required motor current can be achieved by controlling the magnitude and the angle of applied stator voltage.

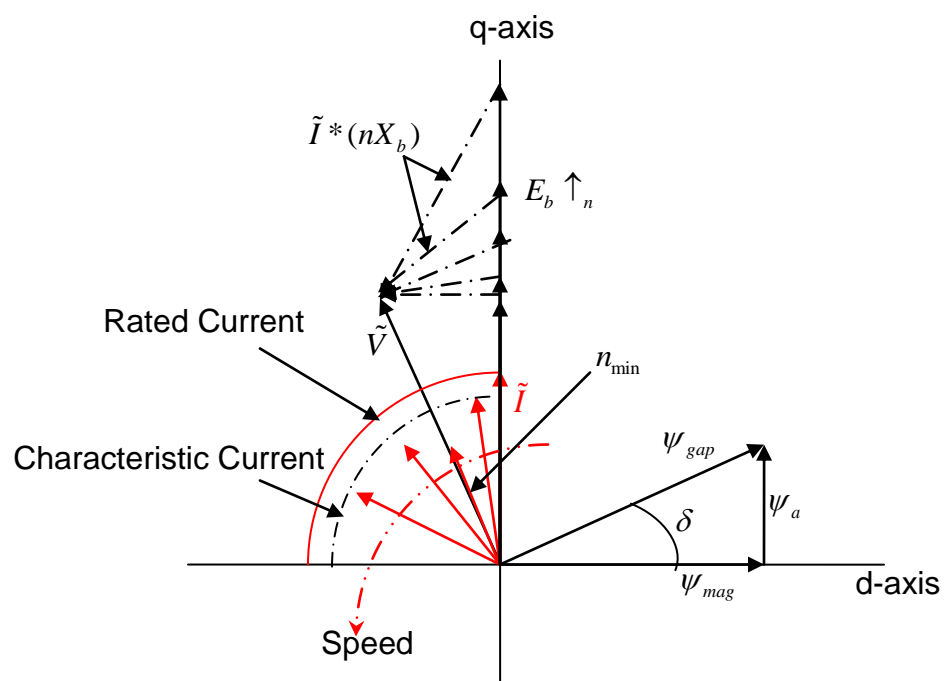


Figure 3-6: Vector Diagram of Conventional Phase Advancement Method.

When a DC supply is used, an inverter is needed to convert DC voltage into AC motor input voltage. If sinusoidal PWM is used to control the inverter, the magnitude and the frequency of the inverter output voltage (motor input voltage) can be controlled by controlling the modulation index and frequency of the control waveform. So ultimately the control variables are the modulation index, the frequency of the control waveform and the inverter lead angle. Based on the speed information, generated back-EMF and per phase winding reactance can be computed. Based on this information along with required output voltage information, the modulation index can be calculated.

In the constant torque mode (below base speed), both the amplitude modulation index and the inverter lead angle can be adjusted. This allows the motor current to be placed in phase with the motor back-EMF. Required motor current based on the torque demand is given by,

$$I_{req} = \frac{T}{3K_t} \quad (3.28)$$

Here K_t is the torque constant. From fundamental frequency model in Figure 3-5, with $X = n X_b$, the applied fundamental frequency voltage required to drive this current into the motor is,

$$V \angle \delta = (nE_b) + I_{req}^* (R + jnX_b)$$

$$V \angle \delta = \sqrt{(nE_b + RI_{req})^2 + (nX_b I_{req})^2} \angle \tan^{-1} \left(\frac{nX_b I_{req}}{nE_b + RI_{req}} \right) \quad (3.29)$$

Based on the required voltage magnitude in (3.29), the modulation index required to generate this inverter output (motor input) voltage is given by,

$$m_a = \frac{V}{\left(\frac{V_{dc}}{2\sqrt{2}}\right)} = \frac{2\sqrt{2} * \sqrt{(nE_b + RI_{req})^2 + (nX_b I_{req})^2}}{V_{dc}} \quad (3.30)$$

While the inverter lead angle is given by,

$$\delta = \tan^{-1} \left(\frac{nX_b I_{req}}{nE_b + RI_{req}} \right) \quad (3.31)$$

Note that both, the amplitude modulation index and the inverter lead angle depend on the motor speed. If the DC supply is more than the minimum required, then the constant torque control region ends at the “true base speed” n_{bt} . At this point amplitude modulation index will be equal to $\frac{4}{\pi}$. Equating m_a to $4/\pi$ in Equation (3.30), true base speed is the solution of,

$$\frac{4}{\pi} = \frac{2\sqrt{2} * \sqrt{(n_{bt}E_b + RI_r)^2 + (n_{bt}X_b I_r)^2}}{V_{dc}} \quad (3.32)$$

i.e.

$$n_{bt} = \frac{\sqrt{2 * \left(\frac{V_{dc}}{\pi}\right)^2 * (E_b^2 + X_b^2 I_r^2) - (RX_b I_r^2)^2 - (E_b RI_r)}}{(E_b^2 + X_b^2 I_r^2)} \quad (3.33)$$

Up to this true base speed, the modulation index will increase linearly from 0 to 1 and non-linearly from 1 to $4/\pi$ with increase in speed.

Above base speed starts the constant power region. Torque producing (and hence power producing) component of the stator current required for sustaining speed and load is given by,

$$I_r = \frac{P}{3nE_b} \quad (3.34)$$

Here P is the desired output power. Since the applied voltage is at the rated value,

$$m_a = \frac{4}{\pi} \quad (3.35)$$

From Figure 3-5, we have,

$$\tilde{I} = \frac{V \angle \delta - E \angle 0}{R + jnX_b} = \frac{V \angle \delta - E \angle 0}{Z \angle \theta_z} = \frac{V \angle (\delta - \theta_z) - nE_b \angle (-\theta_z)}{Z} \quad (3.36)$$

For desired motor output power P , we have,

$$\begin{aligned} \frac{P}{3} &= \text{Re}(\tilde{E} \tilde{I}^*) \\ \frac{P}{3} &= \text{Re} \left(\frac{nE_b V \angle (\theta_z - \delta)}{Z} - \frac{(nE_b)^2 \angle \theta_z}{Z} \right) \\ \frac{P}{3} &= \frac{nE_b V \cos(\theta_z - \delta)}{Z} - \frac{(nE_b)^2 \cos \theta_z}{Z} \end{aligned} \quad (3.37)$$

With $V = V_{max}$, the appropriate inverter lead angle is,

$$\delta = \theta_z - \cos^{-1} \left(\frac{\frac{ZP}{3} + (nE_b)^2 \cos \theta_z}{nE_b V_{\max}} \right) \quad (3.38)$$

Here,

$$\begin{aligned} V_{\max} &= \frac{\sqrt{2} * V_{dc}}{\pi} \\ Z &= \sqrt{R^2 + (nX_b)^2} \\ \theta_z &= \tan^{-1} \left(\frac{nX_b}{R} \right) \end{aligned} \quad (3.39)$$

The lead angle of Equation (3.38) assures that the required rated power is developed beyond base speed but it does not guarantee that the RMS motor current magnitude is within the motor current ratings unless the per-phase winding inductance is L_{∞} or greater.

3.2.1 Constant Power Speed Ratio

Theoretically the CPSR is infinite when the phase inductance of PMSM motor is greater than L_{∞} . For a finite CPSR requirement, Equation (3.23) can be modified to find the minimum per phase inductance required to achieve the desired CPSR.

$$L_{\min} = \frac{\sqrt{V_{\max}^2 + CPSR(CPSR-2)E_b^2}}{CPSR * \omega_b I_r} \quad (3.40)$$

Substituting the value for V_{\max} from Equation (3.11), we have,

$$L_{\min} = \sqrt{\frac{CPSR-1}{CPSR+1}} * \frac{E_b}{\omega_b I_r} \quad (3.41)$$

If $L < L_{\infty}$ i.e. if the per phase winding inductance is less than the inductance which guarantees that the characteristic current of the motor is less than the rated current of the motor, then the resulting finite CPSR is given by,

$$CPSR = \frac{E_b^2 + (X_b I_r)^2}{E_b^2 - (X_b I_r)^2} \quad (3.42)$$

4 SIMULATIONS and EXPERIMENTAL VERIFICATION of CONVENTIONAL PHASE ADVANCEMENT METHOD FOR SURFACE PM MACHINES.

A 30-pole, 6-kW, and 6000 rpm prototype of a permanent magnet synchronous motor (PMSM) with fractional-slot concentrated-windings was designed and developed by the University of Wisconsin, Madison [27]. Compared to the regular PMSMs with distributed winding, this machine has significantly more inductance [27], making it an ideal candidate for field weakening type control scheme. In April 2006, this prototype was delivered to the Oak Ridge National Laboratory (ORNL) for testing the CPA based controller. The control scheme based on conventional phase timing advancement is very simple compared to the vector control based field weakening scheme. It is low-cost because this control method does not require current or phase voltage sensors.

The following table shows parameters of the surface permanent magnet motor with fractional-slot concentrated windings used for simulation and experimental verification purpose.

4.1 Simulink Based Simulation Model

Figure 4-1 shows the algorithm for simulating a CPA based PSMS drive. This model assumes that the motor parameters, which includes per phase inductance, resistance, and back-EMF are known.

Table 4-1: Parameters of a Surface Permanent Magnet Synchronous Motor with Fractional-Slot Concentrated Windings.

Parameter	Measured value
Number of Poles, p	30
Base Speed, N_b	900 RPM
Back-EMF at Base Speed, E_b	49.45
Voltage Constant, K_v	0.03497
Rated Power, P_r	6 kW
Rated Torque, T_r	63.66 Nm
Rated RMS Current, I_r	40.44 A
Per Phase Winding Resistance, R	76 m Ω
Per Phase Inductance, L	1.3 mH

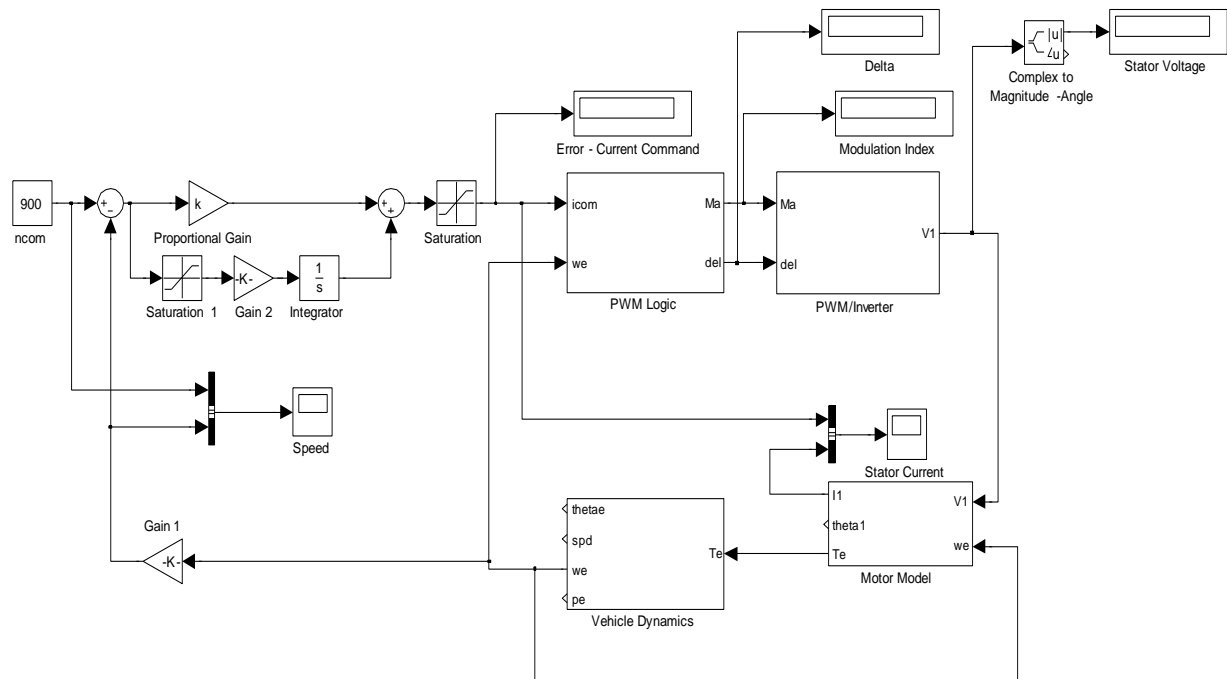


Figure 4-1: Simulink Model for CPA driven PMSM Simulation.

Here $ncom$ is the speed command. Speed error is generated by comparing $ncom$ with speed feedback from the *vehicle dynamics* block. This error, processed through a PI controller, is used as the stator current command. Based on this current requirement, required stator voltage magnitude and angle is calculated by using Equation (3.29). Based on the speed feedback, current command, and region of operation (constant torque or constant power), PWM Logic block calculates the modulation index and inverter lead angle by using Equations (3.28), (3.30), and (3.31) or Equations (3.34), (3.35). PWM / Inverter block represents the inverter model. Magnitude of the generated voltage is nothing but $Ma * \frac{V_{DC}}{2\sqrt{2}}$ and δ is the angle of this motor input voltage. Motor Model block, based on the information about applied voltage, along with the information about per-phase inductance, resistance and back-EMF, estimates the resultant stator current by using Equation (3.36). Based on this stator current, output torque is calculated using the Equation (3.13).

This output torque is then compared with the load torque information obtained from the road load equations. Following differential equation describes the Vehicle Dynamics block. We have,

$$J \dot{\omega}_m + D\omega_m = T_e - T_l \quad (4.1)$$

Here J is the motor inertia constant; D is the damping constant, T_e is the electrical torque generated by the motor, T_l is the load torque (also called as a road load) and ω_m

is the mechanical speed (in rad/sec). Following set of equations represent typical *road load* model [38]. We have,

$$F_{total} = F_{rr} + F_{ad} + F_{cr} \quad (4.2)$$

Here F_{rr} is the rolling resistance, F_{ad} is the aerodynamic drag, and F_{cr} is the climbing resistance. The rolling resistance is given by,

$$F_{rr} = f_r . m . g \quad (4.3)$$

Where m is the vehicle mass, g gravitational acceleration constant and f_r is tire rolling resistance coefficient. The aerodynamic drag is given by,

$$F_{ad} = \frac{1}{2} . \rho . C_D . A_f . (v + v_0)^2 \quad (4.4)$$

Where ρ is the air density, C_D is the aerodynamic drag coefficient, A_f is the vehicle frontal area, v is the vehicle velocity and v_0 is the head wind velocity. The climbing resistance is given by,

$$F_{cr} = m . g . \sin \theta \quad (4.5)$$

Here, θ is the grade angle. Figure 4-2 shows the motor model block in detail. Figure 4-3 illustrates the vehicle dynamics block in detail.



4.2 Simulation Results

Figure 4-4 shows simulation results of a PMSM motor driven by a CPA method. Note that there is a well defined speed ($n_{\min} = 1794$ RPM) at which current is minimum (30.5 A). Here rated current is 43 A, base speed is 900 RPM, rated power is 6 kW, and rated torque is 63 Nm and the DC supply voltage is 151 V. During simulations, back-EMF was assumed to 46.5 V and per phase inductance was assumed to be $764 \mu H$. Up to the base speed, rated current is required to produce the rated torque. Developed power increases linearly with speed as $P_m = T\omega_m$. Inverter lead angle δ (between back-EMF and the supply voltage), given by the Equation(3.31), increases rapidly with the speed.

In this region applied stator voltage also increases as the speed increases. The magnitude of this applied voltage is given by the Equation (3.29). Above base speed is the constant power or the field-weakening region. In this region, torque decreases as the speed increases. Current also decreases with speed increase until it hits the minimum value I_{\min} given by the Equation (3.27). The speed at which this minimum current is reached is given by the Equation (3.26). At this point the inverter power factor is unity. Below this point, power factor is lagging, and above this point, power factor will be leading. After n_{\min} , current increases slowly and approaches the characteristic current of the motor ($I_{CH} = 43.0$ A) given by the Equation (3.24). In the constant power region, the magnitude of the applied stator voltage is constant ($V_{\max} = 67.97$ V), given by the Equation (3.39). The inverter lead angle δ is given by the Equation (3.38).

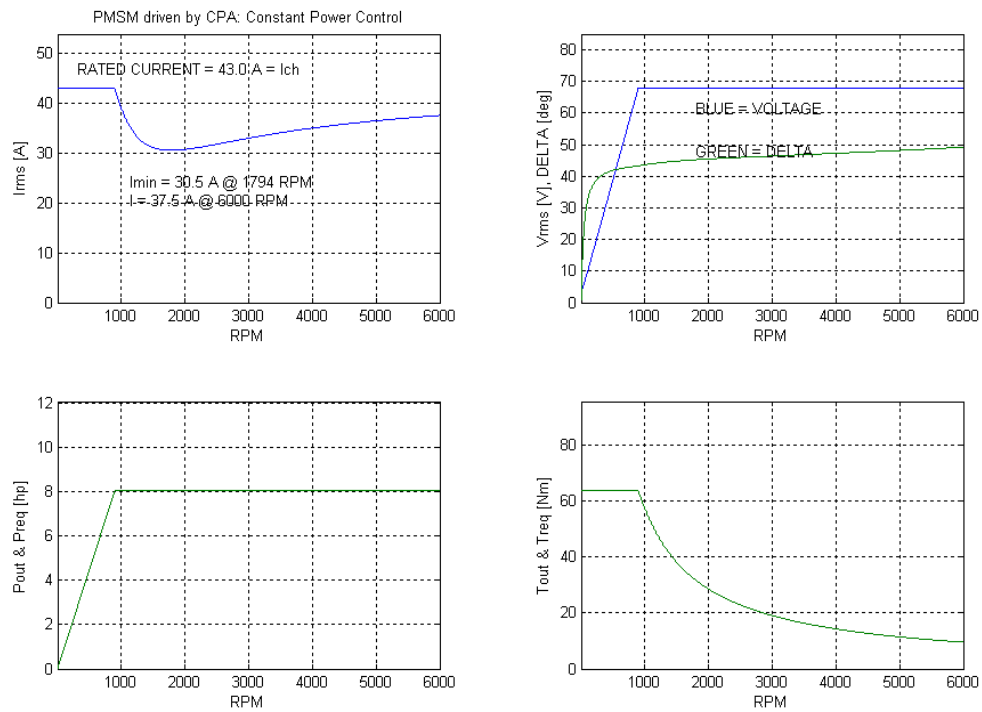


Figure 4-4 : Simulation Results for CPA driven PMSM motor at Full Load (6kW) and 151 V_{dc} Supply Voltage.

Simulation results (both Matlab based and PSpice based) confirmed that if conventional phase advancement method is used, the experimental surface permanent magnet motor with fractional-slot concentrated-windings can produce the rated power at 6000 RPM. It can be seen in Figure 4-4 that the current required to produce this rated power is same as the rated current of the motor. Per phase inductance value of the actual experimental motor was 1.3 mH and back-EMF was 49.5 V which results in characteristic current = 26.9 A. The rated current of the experimental motor was 40.44 A.

4.3 Measured Machine Data

Figure 4-5 shows measurement setup for no-load losses. First part of this figure shows a cross-sectional view of experimental 6 kW motor. The second part of this figure shows the dynamometer that was used to run this motor at different speeds to measure back-EMF at different speeds. The second part also shows Agilent 4284A precision LCR meter. Figure 4-6 shows the LCR meter that was used for the per-phase stator winding inductance measurement. Per phase stator winding resistance measurement was carried out using Agilent 3458A digital multi meter. Table 4-2 lists all the measured data along with the data obtained from FEA analysis and analytical prediction [27]. For no-load losses measurement, Surface PM Motor was connected to a dynamometer (DynLOC IV). Stator windings were connected to a Tektronix TDS5104B oscilloscope. Using the DynLoc IV control panel, the machine was rotated at different speeds.

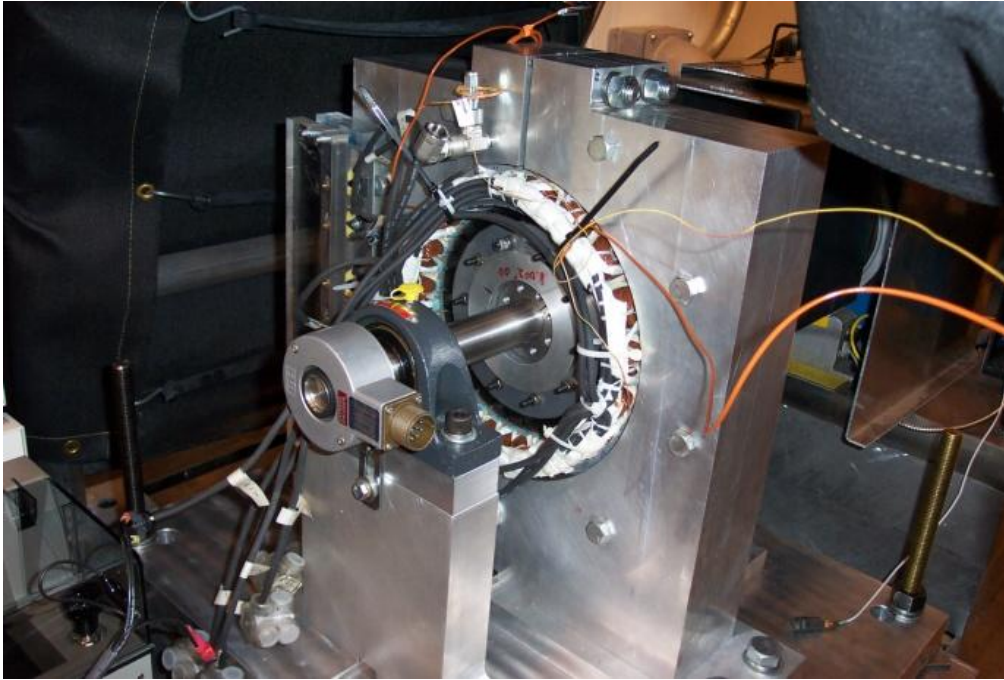


Figure 4-5: No Load Losses Measurement Setup.

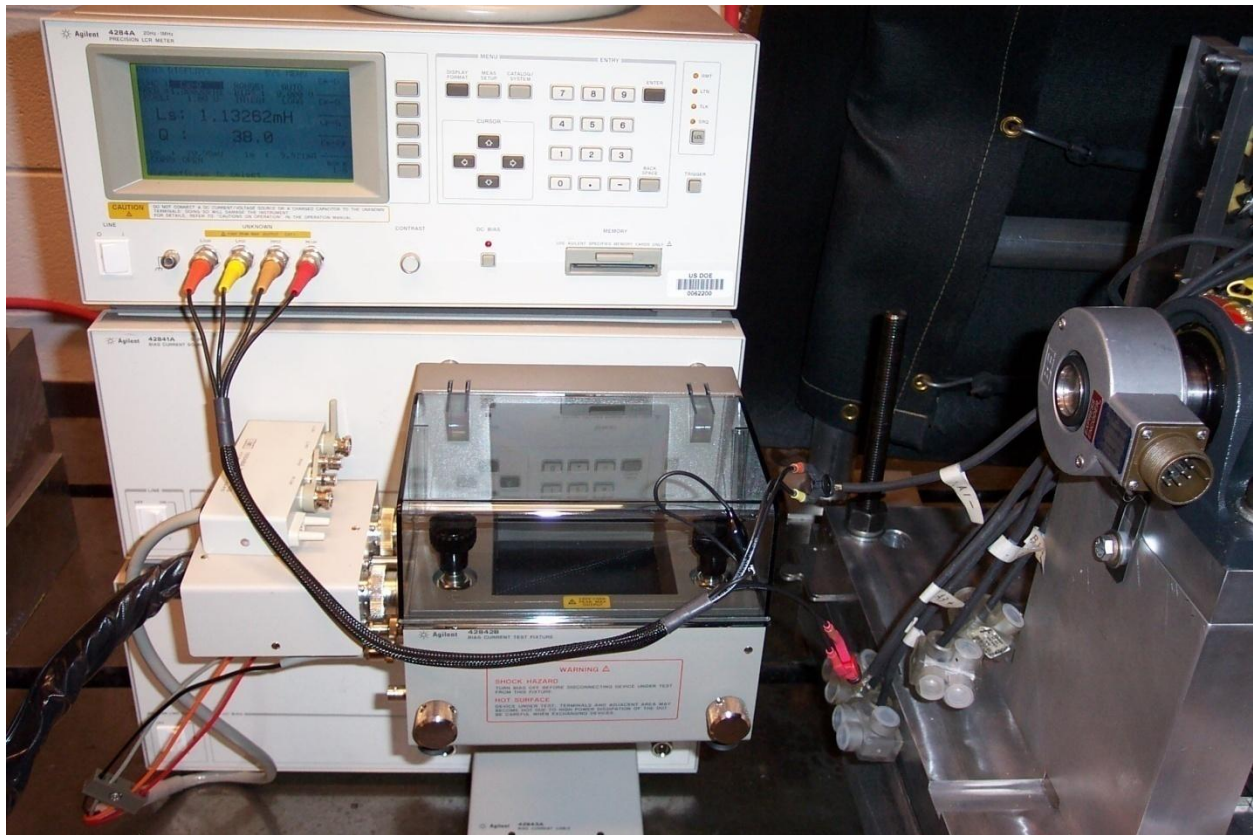


Figure 4-6 : Per Phase Stator Winding Inductance Measurement using LCR meter.

Table 4-2 : Machine per-phase Resistance and per-phase Inductance Measurement.

	Resistance		Inductance, Frequency \approx 1kHz		
				Voltage = 1V	Voltage = 10 V
Phase A	0.07535 Ω	75 m Ω		1.13 mH	1.185 mH
Phase B	0.07683 Ω	76 m Ω		1.18 mH	1.1899 mH
Phase C	0.07560 Ω	75 m Ω		1.14 mH	1.1968 mH
Analytical Prediction		63 m Ω		1.03 mH	
FEA prediction				1.16 mH	
Wisconsin Measured		71 m Ω		1.3 mH	

Figure 4-7 shows captured back-EMF waveform at base speed (900 rpm) and 4000 rpm. Figure 4-8, Figure 4-9 and Figure 4-10 shows the measured back-EMF with its Fast Fourier Transform. The purple line is the back-EMF, and the yellow graph is its FFT. A 3rd harmonic can be noticed on these figures. Stator windings of a three phase PMSM motor usually have a common neutral point as they are usually connected in Y format. This type of connection results in the cancelation of 3rd and all the triplen harmonics. From these figures, it can also be seen that the surface PM motor with fractional-slot concentrated-windings type motor has sinusoidal shaped back-EMF. Using the dynamometer, the experimental motor was rotated at 0 – 4000 rpm in the steps of 100 rpm. At each speed, peak to peak, and RMS value of the fundamental frequency component of the back-EMF was recorded. Table 4-3 lists all this measured data.

Figure 4-11 shows measured no-load losses. Figure 4-12 shows RMS values of the back-EMF along with its least square fit. This is used to calculate the voltage constant K_v in Equation (3.4). Since there is no load attached to the motor, torque required by the dyne to keep the motor speed constant is only the no-load power loss ($P = T * \omega$) at that speed.

4.4 Experimental Setup

Figure 4-13 shows a close up of the experimental, 6-kW surface permanent magnet motor with fractional-slot concentrated-windings.

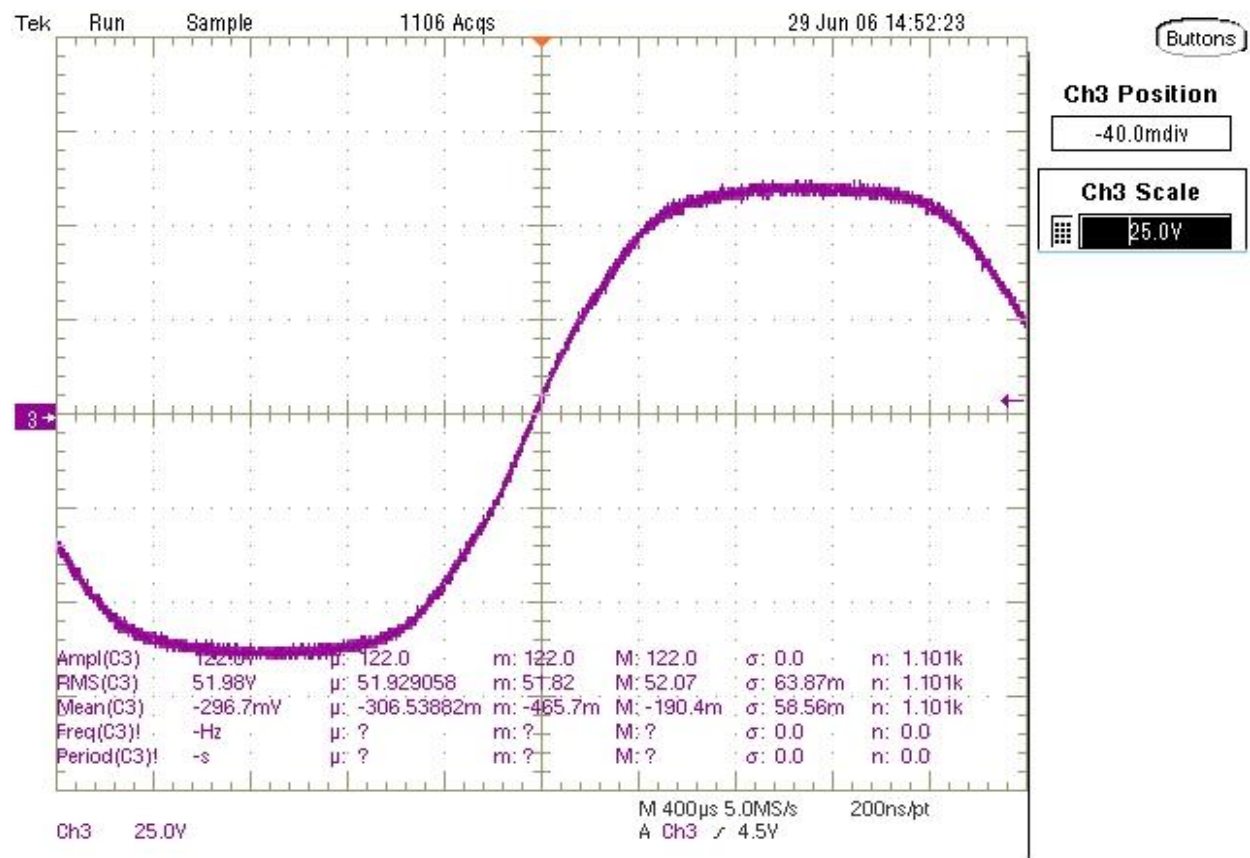


Figure 4-7 : Measured Back-EMF of a 6-kW Fractional-Slot Concentrated-Winding PMSM Motor at Base Speed (900 rpm).

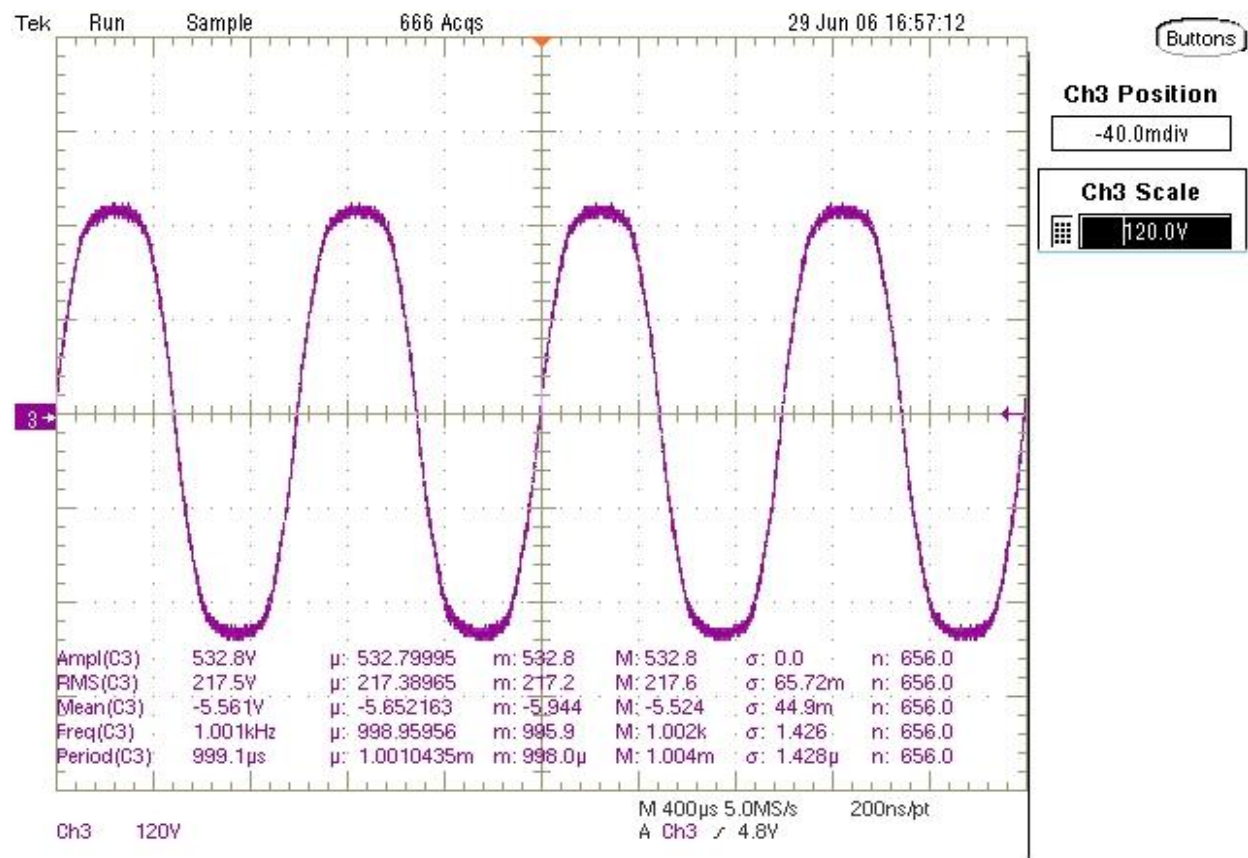


Figure 4-8 : Measured Back-EMF of a 6-kW Fractional-Slot Concentrated-Winding PMSM Motor at 4000 rpm.

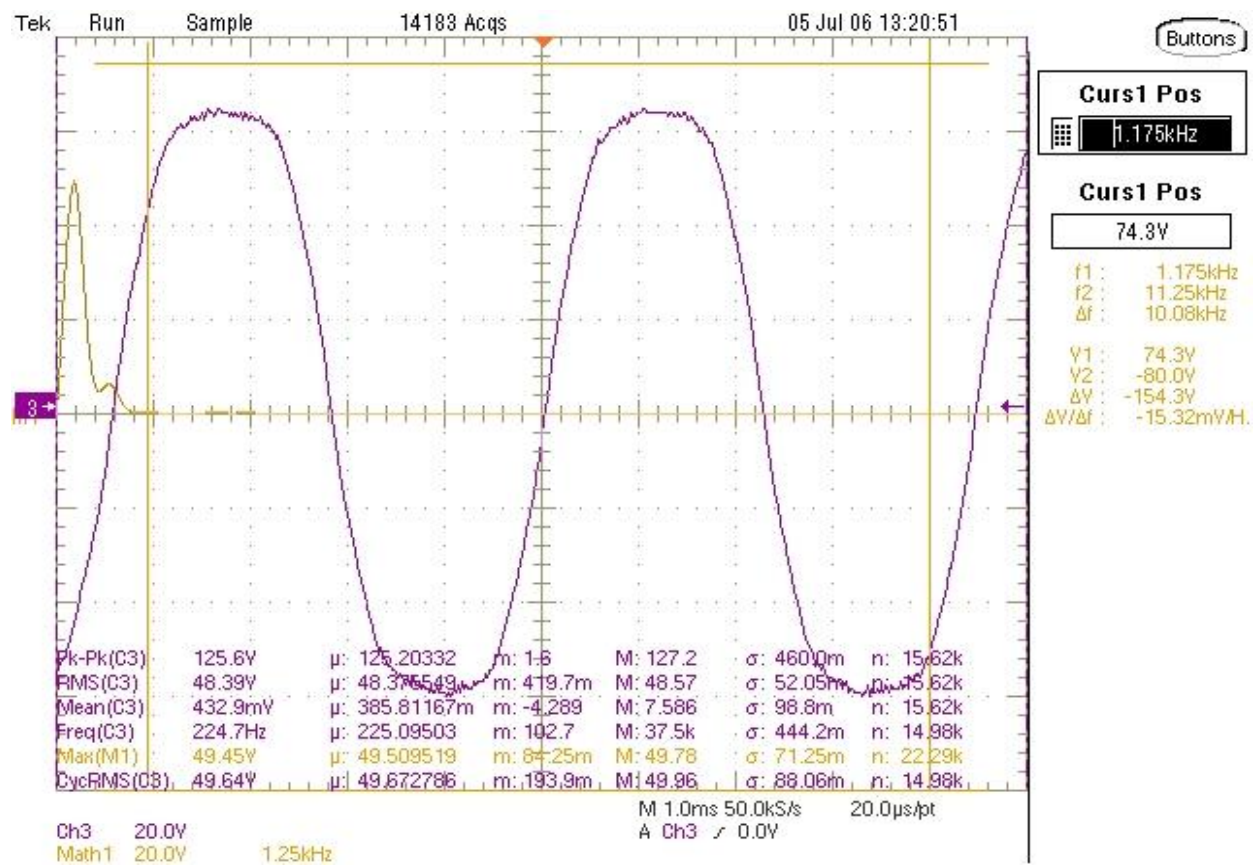


Figure 4-9 : Measured Back-EMF with FFT at Base Speed (900 rpm).

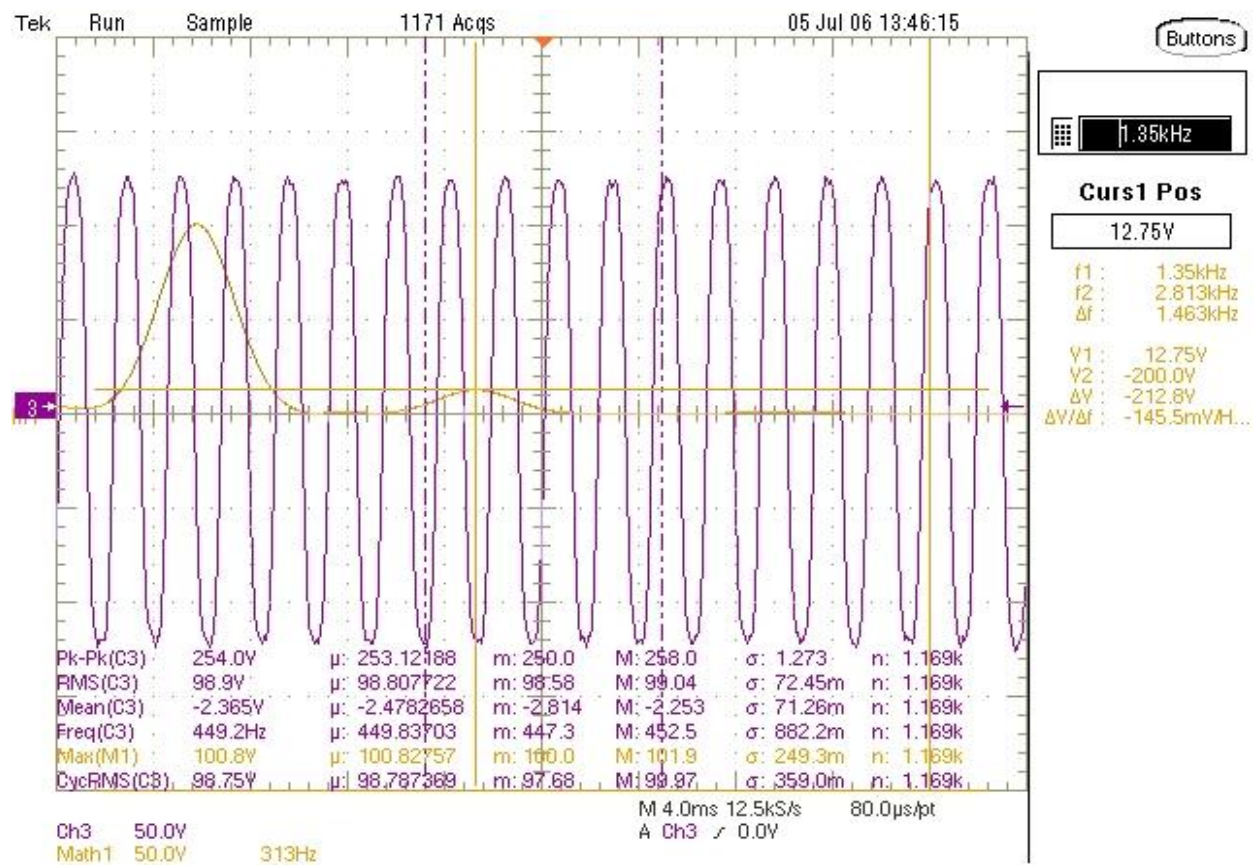


Figure 4-10 : Measured Back-EMF with FFT at 1800 rpm.

Table 4-3 : Measured No Load Losses and Machine Data.

Speed	Measured Power	Calculated Power	Torque	Peak - Peak Amplitude	Cycle RMS	FFC	Frequency
(RPM)	(Watts)	(Watts)	(Nm)	(Volts)	(Volts)	Volts (RMS)	(Hz)
100	0	0	0.0	13.00	5.53		25
200	0	0	0.0	27.00	11.00		50
300	0	6.2832	0.2	40.00	16.54		75
450	0	23.5619	0.5	64.00	24.91	24.47	112.9
600	0	0	0.0	81.00	33.05		150
700	100	102.6254	1.4	95.20	38.60		175
800	0	0	0.0	108.00	44.02		200
900	100	84.823	0.9	125.60	49.64	49.45	224.7
1000	100	125.6637	1.2	135.00	55.00		250
1400	200	175.9292	1.2	190.40	77.10		350
1800	200	245.0442	1.3	254.00	100.80	98.75	449.2
2000	100	146.6077	0.7	268.80	110.10		500
2200	400	414.6904	1.8	296.40	121.00		550
2600	500	517.3156	1.9	348.80	142.60		650
2700	500	508.938	1.8	375.00	148.20	149.1	674.8
3000	600	628.3185	2.0	399.60	164.20		750
3400	700	747.6991	2.1	456.00	185.90		850
3600	800	791.6813	2.1	498.00	197.90	197.4	899.5
3800	800	835.6636	2.1	508.80	206.90		950
4000	900	879.6459	2.1	532.80	217.30		1000

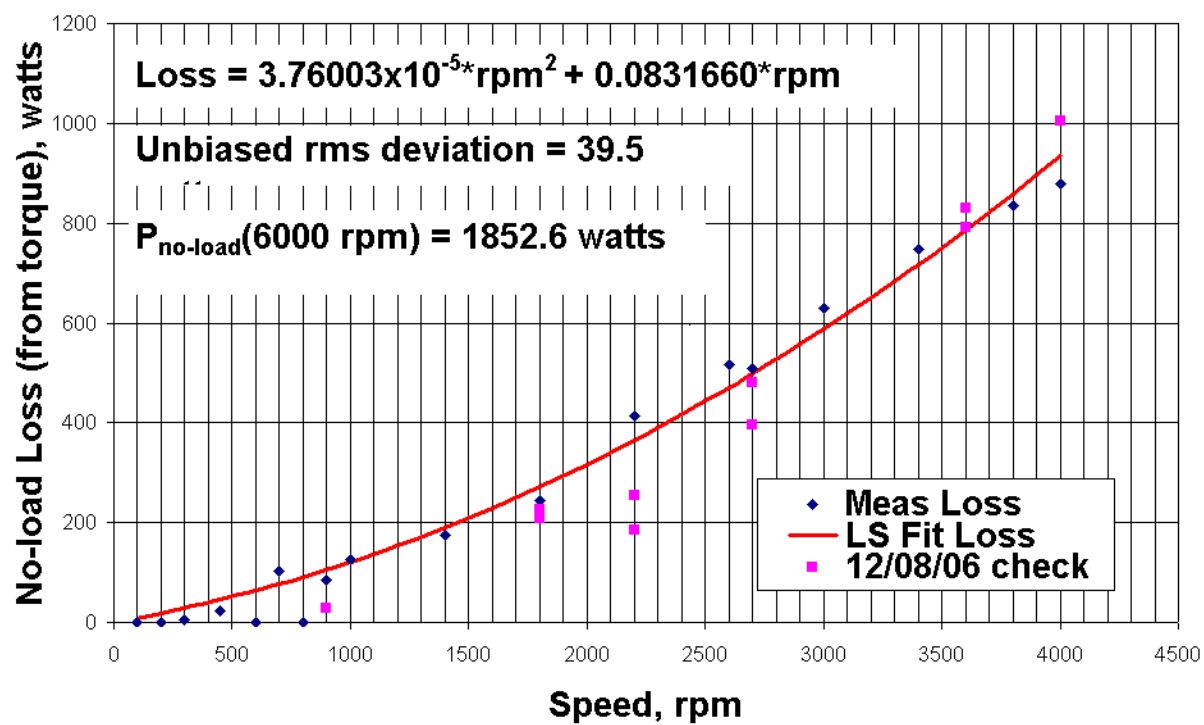


Figure 4-11: Measured No Load Losses of a 6-kW Fractional-Slot Concentrated-Winding Motor.

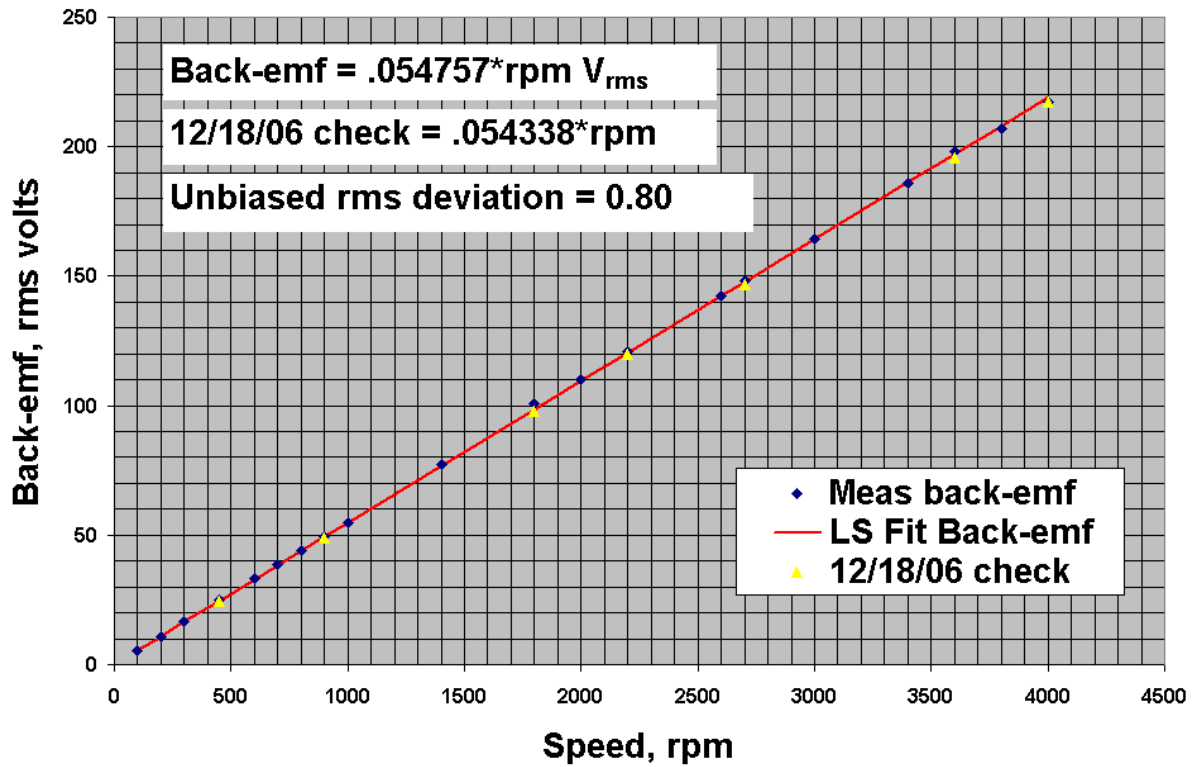


Figure 4-12 : Measured Back-EMF of a 6-kW Fractional-Slot Concentrated-Winding PMSM Motor.

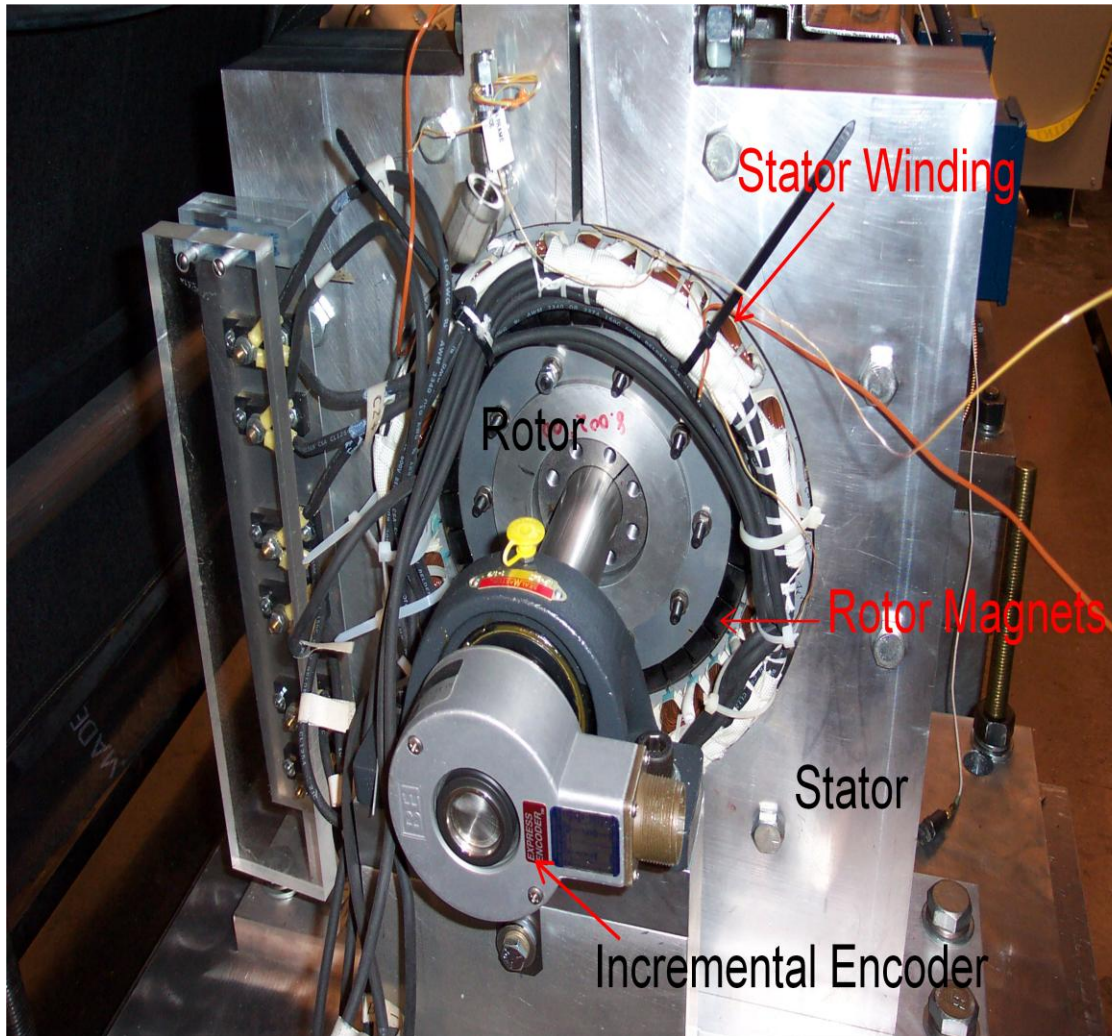


Figure 4-13: Close up of the Experimental 6-kW Surface PM Motor.

Stator, stator windings, rotor, rotor permanent magnets, and incremental encoder can be seen in this figure.

It is very important to know the exact rotor position of the synchronous motors because if the applied stator voltage is 180° out of phase with the back-EMF, the resulting large current can damage the motor windings. An incremental encoder was used to measure the speed and the rotor position of the experimental motor. HS35 type incremental optical encoder from BEI industry was used. Incremental encoders typically have three output pulses, namely A, B and Z. This particular encoder has 1024 pulses (A and B) per mechanical revolution. Because of the offset between pulse A and pulse B, a 4X resolution can be obtained (by using rising and falling edge of Pulse A and B) to measure the speed and to estimate the rotor position. There is also one pulse per mechanical revolution, also called as a reference pulse or a Z pulse. This Z pulse is usually used to reset the rotor angle measurement counter after 360°.

Figure 4-14 shows these Z pulse (pink) along with the generated back-EMF at 900 rpm. The angle difference between the index pulse and the nearest zero-crossing (with rising voltage) of the back-EMF is recorded. Since the encoder is fixed on the rotor shaft, this offset remains constant over the entire speed range. So when the motor is running, Z pulse is detected by connecting it to the digital input terminal of the OPAL RT system. An event detection block (hardware + software) was used. When this pulse is detected, a recorded offset degree from this point gives the zero-crossing of the back-EMF waveform. This was considered as a zero degrees i.e. $\theta = 0$.

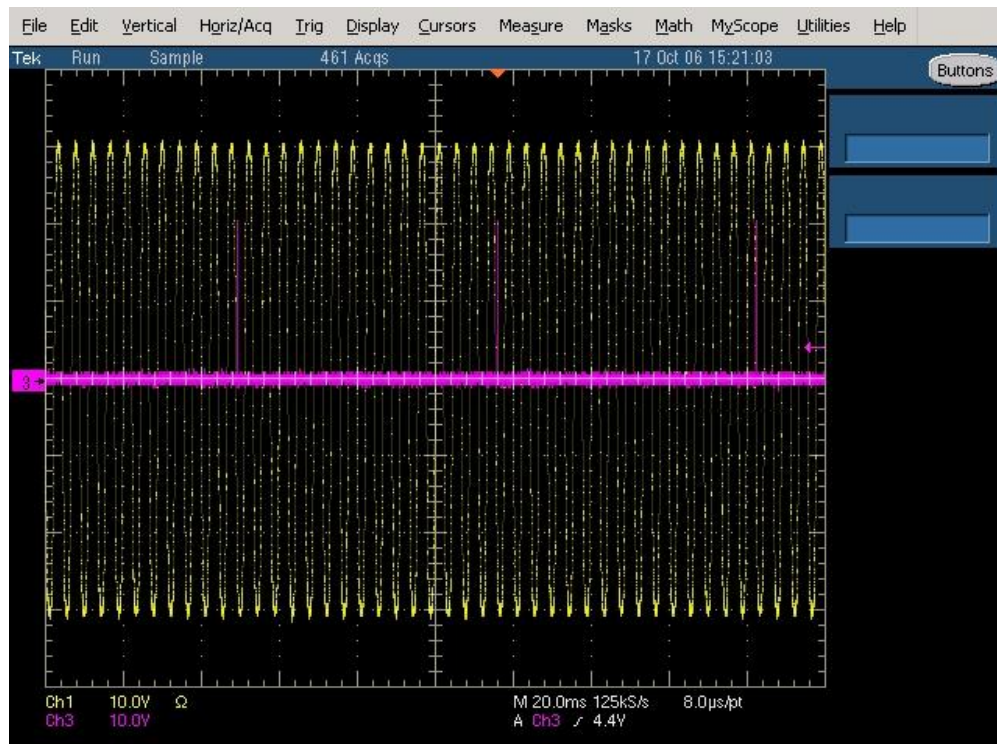


Figure 4-14 : Index Pulse from Incremental Encoder on back-EMF at 900 rpm.

Now, if the inverter lead angle is δ , then the equivalent rotor position is Index pulse + offset - δ . Measurements were carried out to find out the offset angle between the reference Z pulse of the incremental encoder and the zero crossing of the back-EMF waveform. The motor was driven by the dynamometer so that the back-EMF and the Z pulse could be displayed on the oscilloscope. The calculated offset was 207.50. Figure 4-15 illustrates the same.

Figure 4-16 shows the electrical connection diagram of the experimental setup. A three phase 480V, 200A power supply was connected to the Danfoss VLT 5252 inverter. A 12 AWG cable was used to provide power to the inverter control logic through a 20A circuit breaker. A 600V, 600A, Robicon DC power supply was connected to the inverter with two 4/0 AWG cables. The positive cable was routed through the current and voltage sensor to measure available DC voltage, DC current and resultant DC power. Three phase inverter output was connected to the motor using 4/0 AWG cables through a 200A fuse disconnect with a 100A fuse. These cables were also routed through the voltage and current sensors to measure motor input current, motor input voltage and resultant motor input power. For safety purpose, the DC power supply, inverter and motor were connected to a common ground (to the test bedplate on which the motor was mounted). This test bedplate was in turn connected to the main building ground. Four LEM CV3-500 voltage sensors were used to measure inverter input and motor input voltages. For these voltage sensors, nominal voltage is 350V while peak voltage is 500V. Conversion ratio is 500V/10V which means when the voltage on the cables through the sensor is 500V, output of the sensor will be 10V.

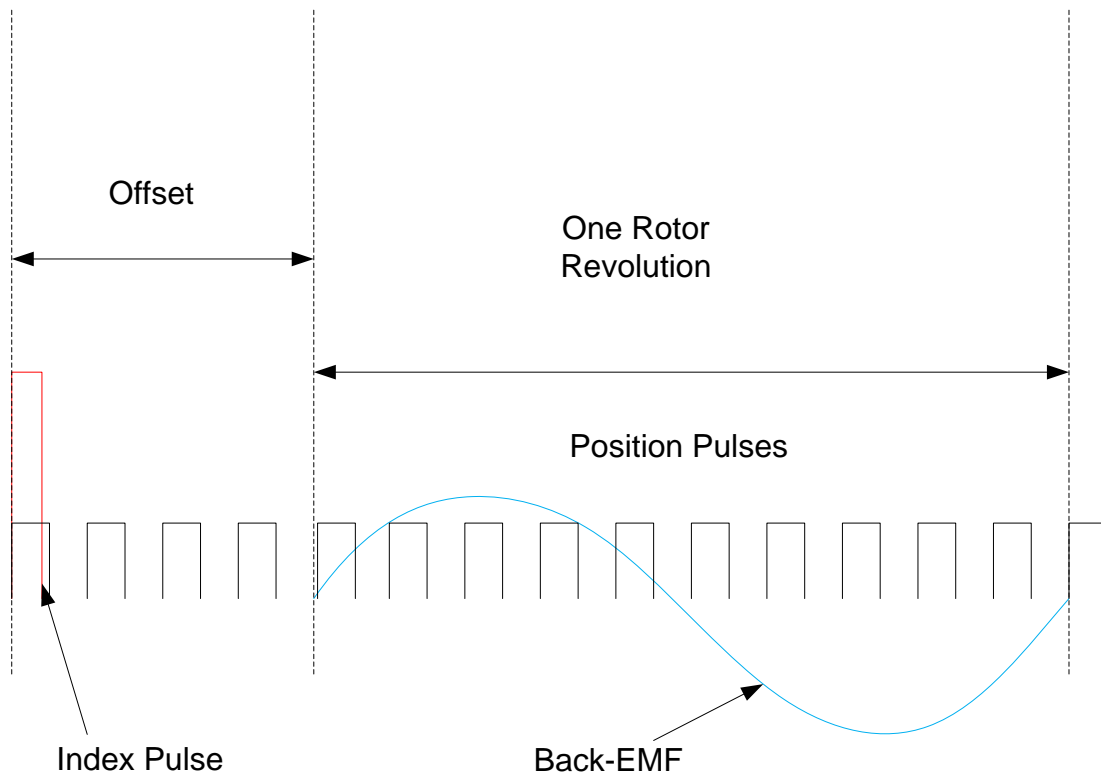
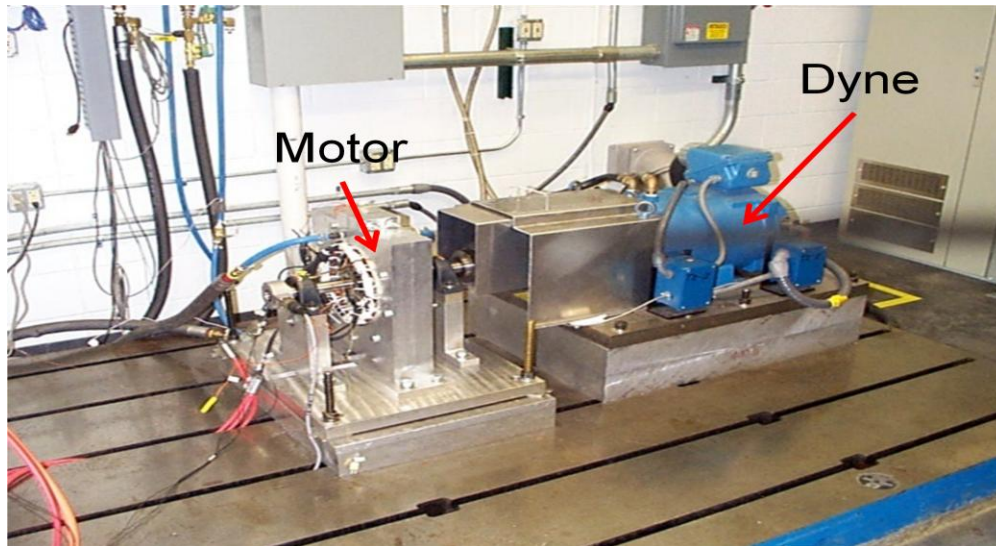


Figure 4-15: Rotor Position Estimation.

Four LEM LC300S current sensors were used to measure inverter input currents. For these sensors, nominal current is 300A while peak current is 500A. Conversion ratio is 1:2000. Additionally, three LEM LT100-P/SP 33 current sensors were used to measure motor input current (inverter output current).

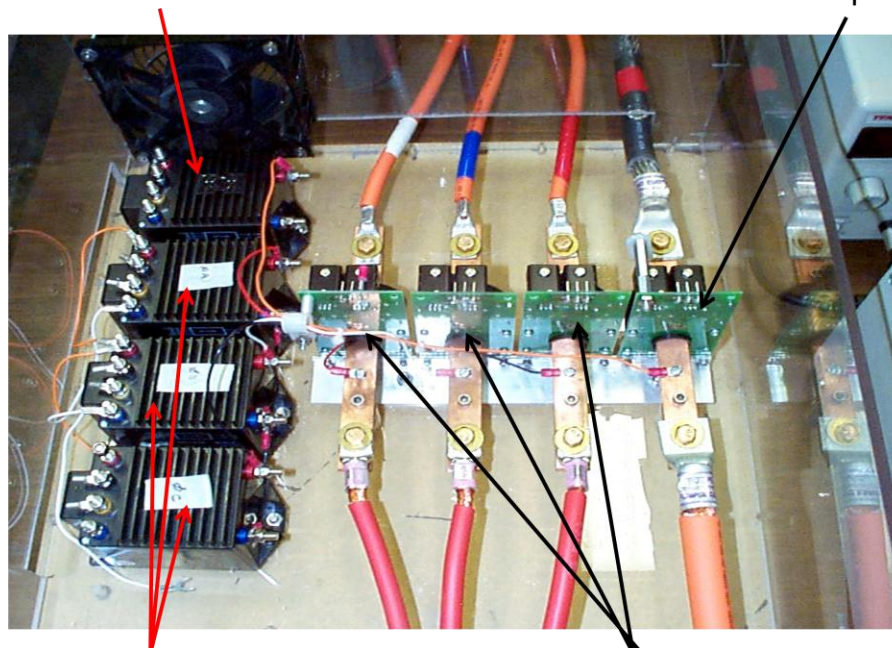
Figure 4-17 shows the setup of these sensors. The output of these voltage and current sensors was connected to a power analyzer (Yokogawa PZ4000). Based on the measured voltage and current information provided by the sensors, this analyzer computed inverter input power (DC Power) and motor input power (or inverter output power). The dyne control panel displayed the information about motor output torque and shaft power. Figure 4-18 shows a view of the overall setup. Figure 4-19 shows an overall schematic of the same.

The Danfoss VLT 5252 inverter is designed to be used with an induction motor. In order to use it with the experimental surface PM motor, the inverter's control logic was bypassed. Only the switching part along with over-current, over-voltage, over temperature protection and dynamic braking capability was used. Two sets of interface cards compatible with the Danfoss inverter were ordered from Aalborg University in Denmark. One of these cards converted IGBT gate signals (switching information) from the controller to the fiber optic signal to reduce noise interference. The second card converted this fiber optic signal back to the digital signals. The second card was mounted on the inverter. This second card also monitored for over-voltage, over-current, over-temperature conditions, and if required, could shut down the inverter.



DC Voltage Sensor for
Inverter Input Voltage

DC Current Sensor for
Inverter Input Current



Motor Input Voltage
Sensors

Motor Input Current
Sensors

Figure 4-17 : a. Motor & Dyne Coupling, b. Voltage & Current Sensors.

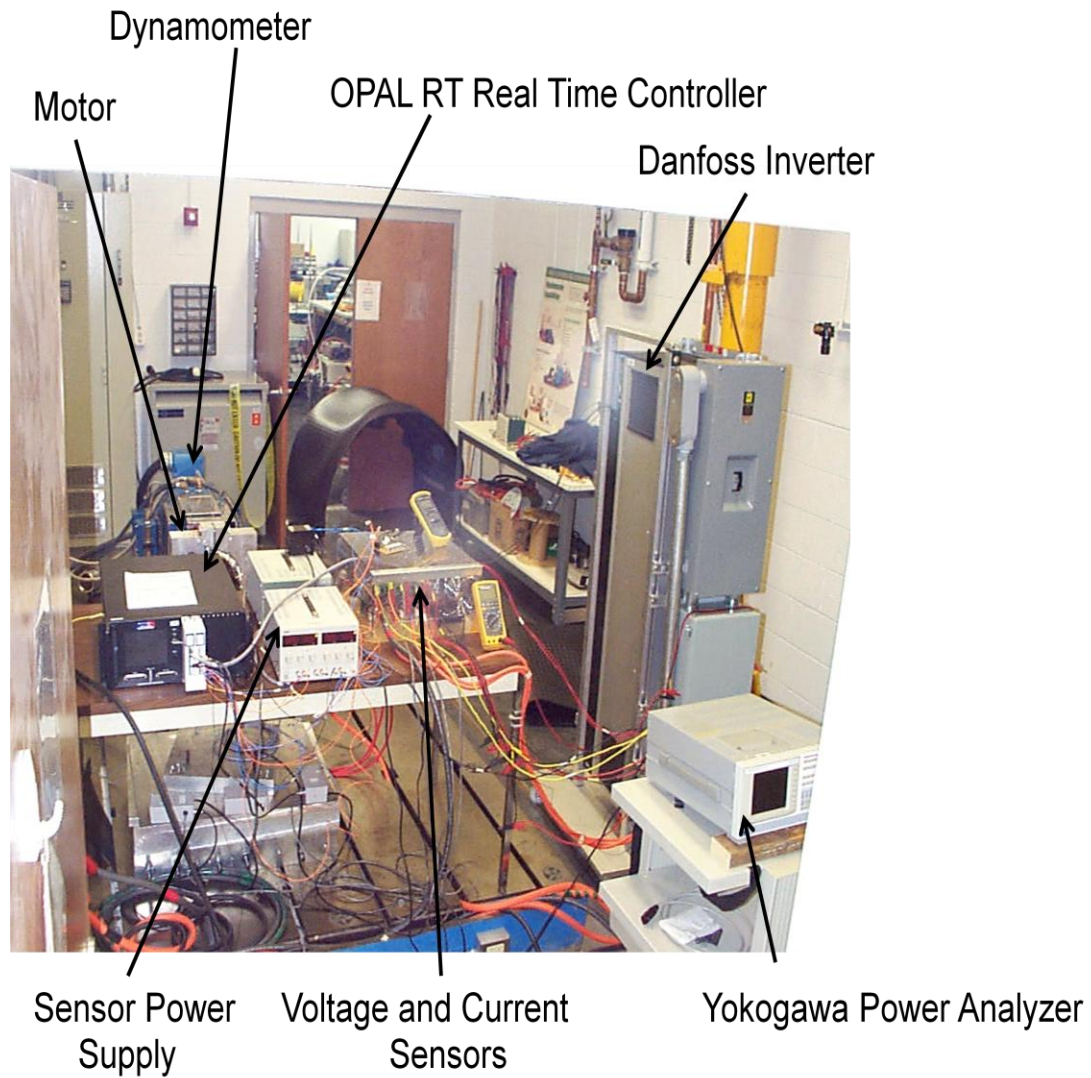


Figure 4-18 : Overall Experimental Setup.

Another modification to the Danfoss VLT 5252 was a set of DC connectors, to allow power from a 600 V, 600 A Robicon DC power supply to be connected directly to the inverter's DC link. In doing so, the converter part of the Danfoss drive was bypassed. Although not used during this testing, the inverter DC link can be supplied by 3-phase, 480 V power from AC source which is then rectified and used to charge the DC link.

OPAL RT based real time controller with 3.2 GHz speed (800 MHz bus speed) with a QNX 6.2 operating system was used. OPAL RT OP5340 card with 16 analog inputs was used to monitor the stator and rotor, currents and voltages; along with rotor position, motor speed, DC supply voltage and DC supply current.

OPAL RT OP5311 with 16 digital inputs card was used to monitor Z, A and B incremental encoder pulses. OPAL RT OP5312 card with 16 digital outputs was used to send the PWM switching signals to the inverter IGBT's. These signals were sent to the Danfoss inverter via the Alborg University interface cards. All these signal conditioning cards were mounted on the "target" PC which has the QNX based operating system. A Toshiba laptop was used as a "host" PC to compile and download the control model generated in the Simulink. This compiled model was then downloaded to the "target" PC via Ethernet cable from the host PC to the target PC. The host computer was also used to monitor all the feedback (motor speed, motor voltages, motor currents and DC supply voltage and current). A GP-IB cable transmitted data from the Yokogawa PZ400 power analyzer, to a data readout program installed on separate Dell desktop in the control room.

A typical motor (or experiment) startup procedure was:

1. Connect the 3-phase, 480V auxiliary power source to provide the power to the inverter's internal circuitry followed by a restart using a push button on the Alborg card, (to clear faults).
2. Turn ON the motor and dyne cooling system.
3. Turn ON the dyne power supply.
4. Compile Simulink based control model in the host PC, and download control model to the target OPAL RT PC; 5. RUN the controller without enabling inverter gate switching.
6. Connect the DC power supply and increase the applied DC voltage from zero to the desired DC link value in order to avoid high inrush current.
7. Start the dyne in a speed mode and increase the motor speed to 400 RPM.
8. Set the desired speed command through the host PC, release the dyne by turning the speed mode OFF and ENABLE the inverter gate signal switching. Once the dyne speed mode is turned off, OPAL RT controller starts controlling the motor speed. An absolute type encoder can provide the accurate rotor position. If this type of encoder is used, PMSM motor can be started from the standstill by the controller alone. With an incremental type encoder, unless the motor is rotating, the initial rotor position cannot be detected. Without accurate information about the rotor position, voltage cannot be applied to a synchronous motor to avoid high inrush current.

9. Turn the dyne back ON but in torque mode; 10. Start loading the motor to the desired load condition.

At this point, the controller should be able to maintain the commanded speed while developing the required torque.

Figure 4-20 shows the overall OPAL RT control model. SM_Encoder has all the control logic, data acquisition, and signal conditioning program. SC_Encoder_interface has all the monitoring blocks. Figure 4-21 shows the inside of SM_Encoder.

Upper portion of the Figure 4-21 is speed and rotor position estimation algorithm. Here encoder pulses A,B and Z are connected to the digital input card of the OPAL RT system. An even detection block measures the number of A and B pulses. Note that this particular encoder produces 1024 pulses per revolution. Based on the encoder feedback, the rotor position and number of revolutions per minute (RPM) is estimated. Z pulse or the index pulse is also detected and used to reset the rotor position counter. This is the speed and rotor position feedback. Middle portion of the Figure 4-21 is a currents and voltages measurement algorithm. Output of the voltage and current sensor is connected to the analog input card on the OPAL RT system. Phase voltages and currents were measured for monitoring purpose only. During simulations, it was detected that DC voltage value had the greatest effect on the controller. Therefore, only the DC voltage feedback was used for control purpose. The lower portion of the Figure 4-21, is the actual CPA based controller. Figure 4-22 shows this conventional phase advancement based controller.

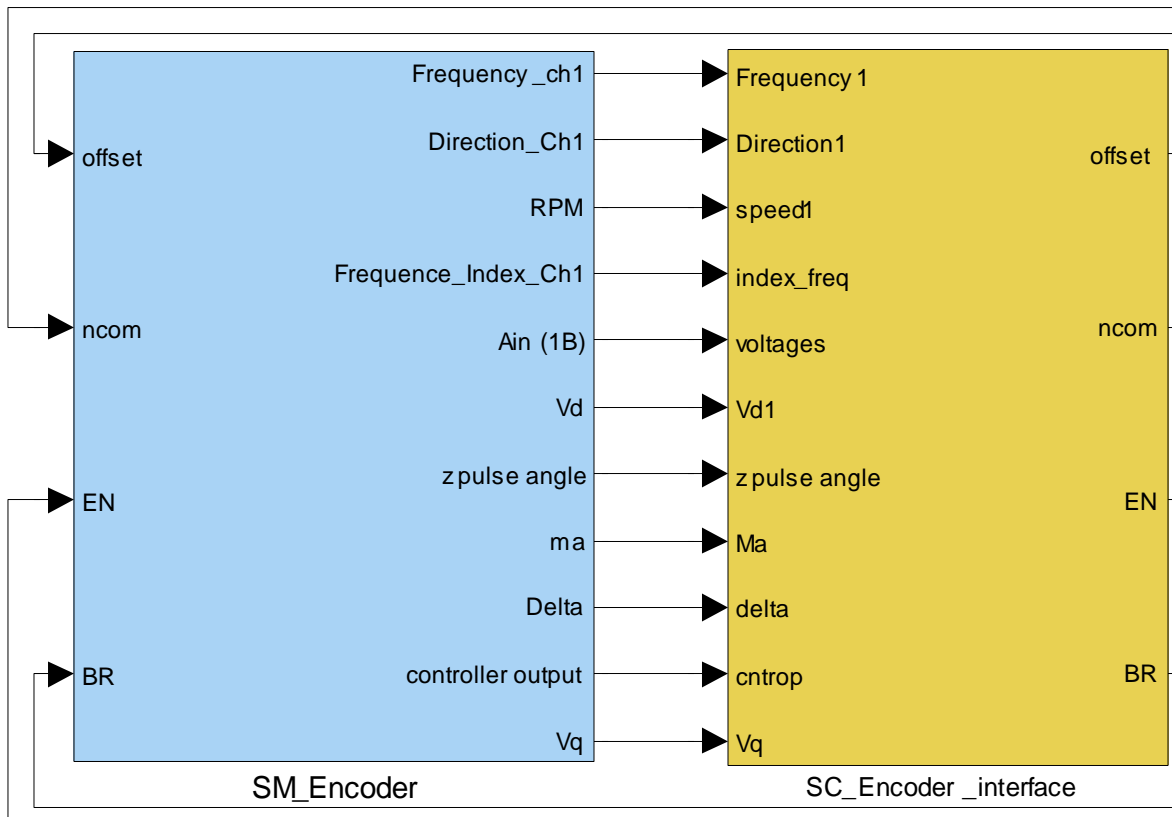


Figure 4-20 : Simulink Based OPAL RT Model.

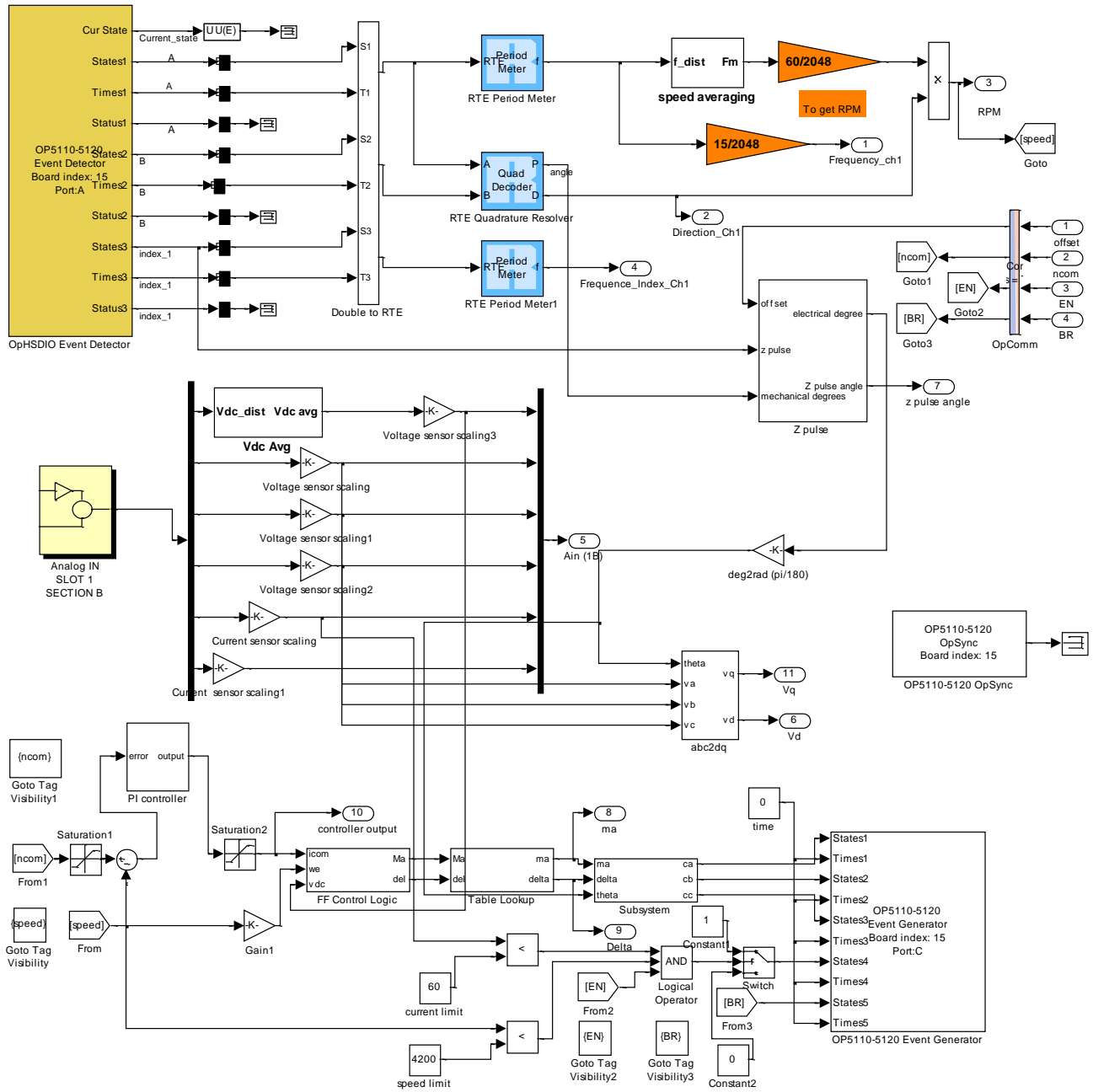


Figure 4-21: Data Acquisition and Motor Control (OPAL RT Model).



Here n_{com} is the speed command set by the operator using the user interface. Speed feedback is then compared with the desired speed command. Through a PI controller, this error is converted to a current command. In the constant torque zone (below base speed), based on the DC voltage feedback, the required current is then converted into the required modulation index by using Equation (3.30) and required inverter lead angle by using Equation (3.31). In the constant power region (above base speed), modulation index is fixed at $4/\pi$ and the inverter lead angle is calculated by using Equation (3.38).

Figure 4-23 shows the details of the actual Controller. Based the rotor position feedback, this calculated modulation index and the inverter lead angle is then converted to the appropriate PWM switching signals. Figure 4-24 shows the details of the sine-triangle type PWM switching scheme.

As described in Chapter 3, in sinusoidal PMW, a sine wave is compared with the triangular waveform. The amplitude of the triangular waveform is kept constant. PWM switching frequency is nothing but the frequency of this triangular waveform. During experimentation 9 kHz switching frequency was used. Amplitude of the sine waveform is nothing but the scaled modulation index. Frequency of the sine waveform is same as the frequency of the motor. Figure 4-24 shows the details for PWM logic.

Angle of the sine waveform is obtained by adding the calculated inverter lead angle to the measured rotor position. Generated switching signals are then applied to the Danfoss inverter IGBT's through an OPAL RT digital output card and Alborg University interface card.

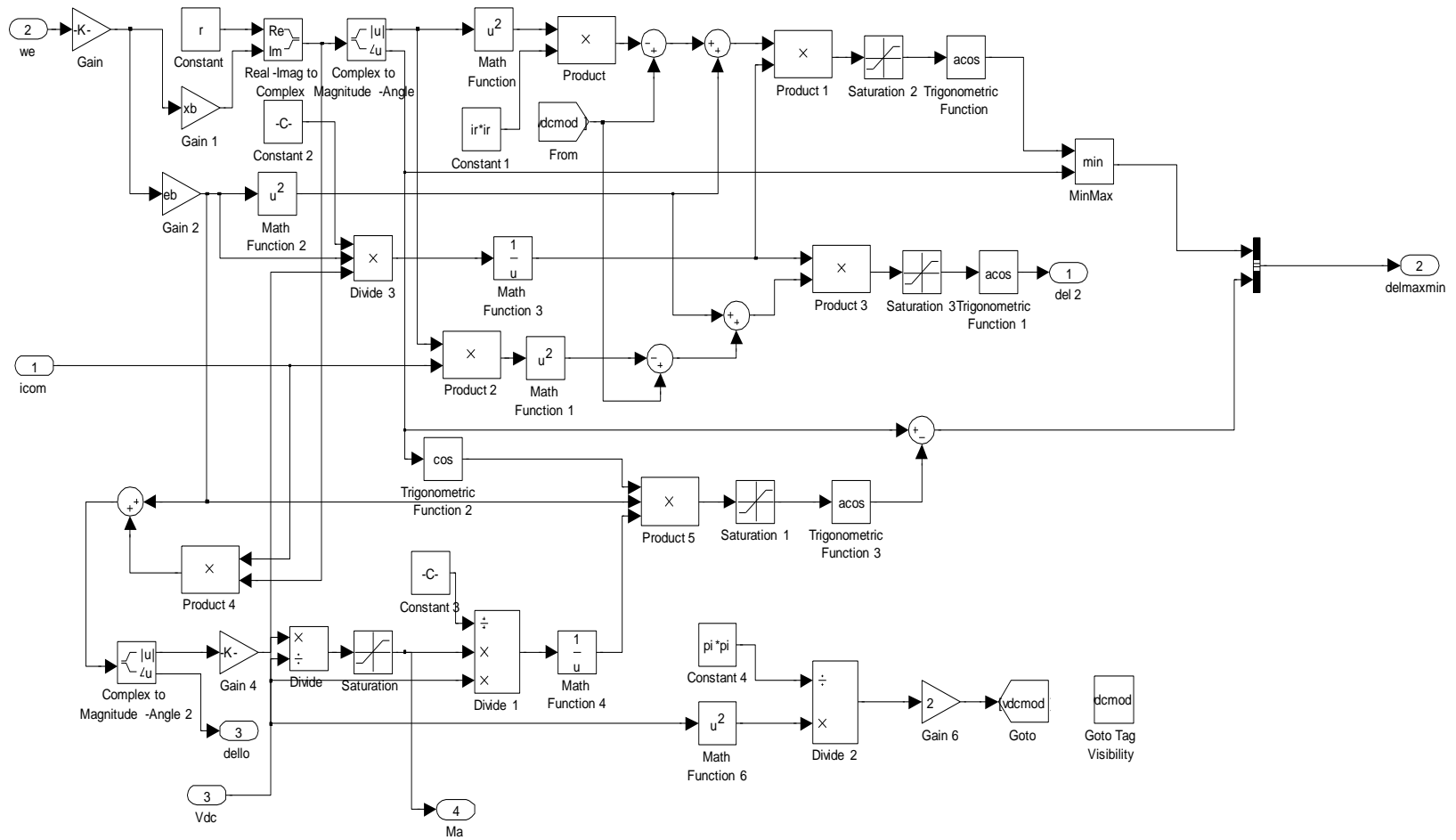


Figure 4-23 : Modulation Index and Inverter Lead Angle Logic.

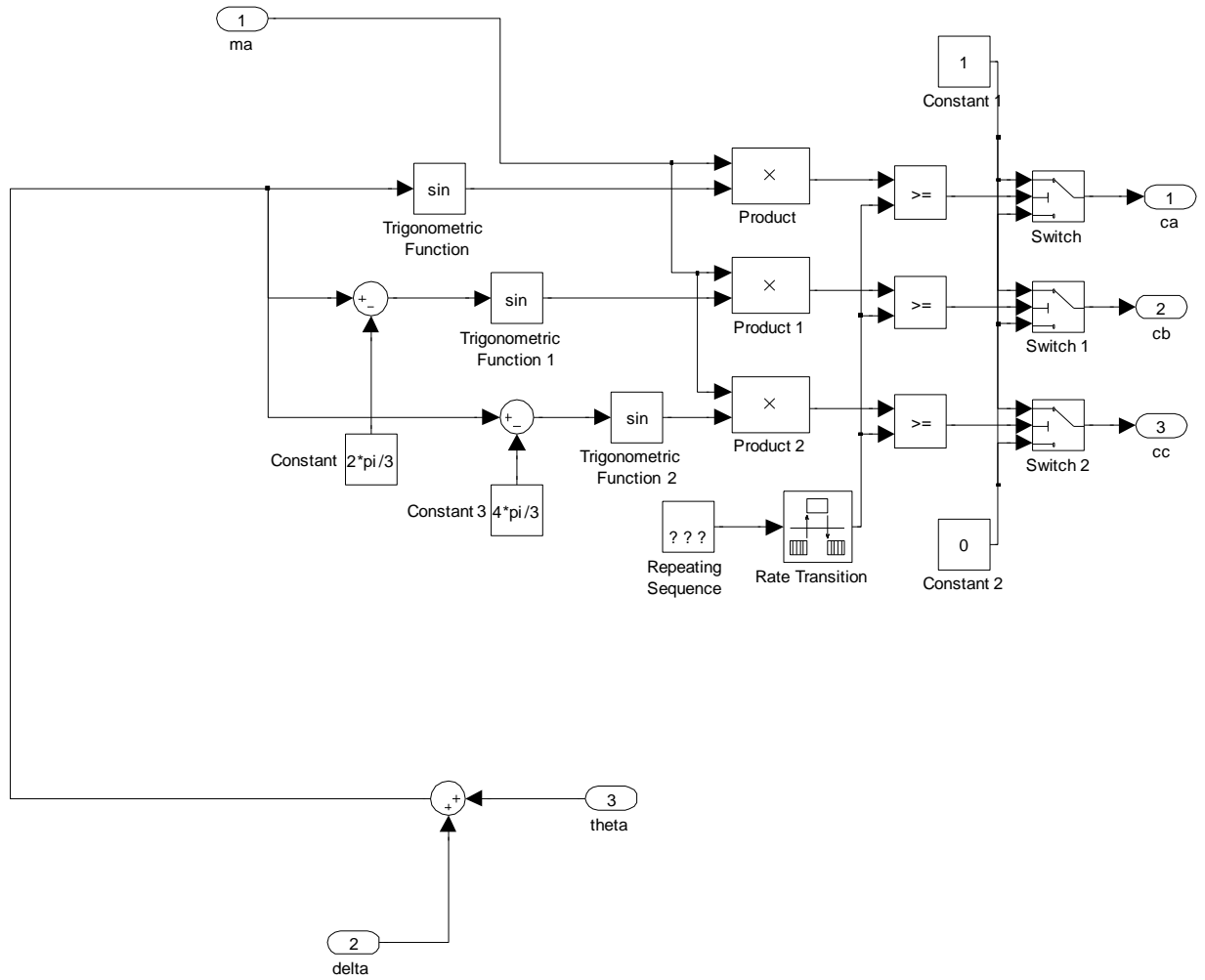


Figure 4-24: Details of the Sine Triangle type PWM Switching Scheme.

The inverter, then converts available DC voltage from the Robicon DC power supply into motor input voltage ($V\angle\delta$). These phase voltages are then applied to the motor stator winding leads through voltage and current sensors. Figure 4-25 shows the inside of SC_Encoder_interface. When the Simulink model is running on the host PC, this is the only part of the model that is displayed and changed. Through this interface, a speed command is entered. Desired motor torque can be controlled through Dyne's control panel.

4.5 Experimental Results and Conclusion

Tests were carried out at 450, 900, 2000, 3000 and 4000 RPM. For each of these speeds, applied load was varied from 0% to 100% in the steps of 25%. These sets of measurements were carried out at 300V DC and at 250V DC. Table 4-4, Table 4-5, Table 4-6, Table 4-7, Table 4-8, Table 4-9, Table 4-10, Table 4-11 show the measured torque, stator voltages, stator currents, DC voltage and DC current at each of these test points.

Figure 4-26 shows the response of CPA based control system to a step change in the speed. Here the yellow line indicates step change in speed command and the pink graph indicates the response of the motor. Speed command has been changed from 900 RPM to 1800 RPM.

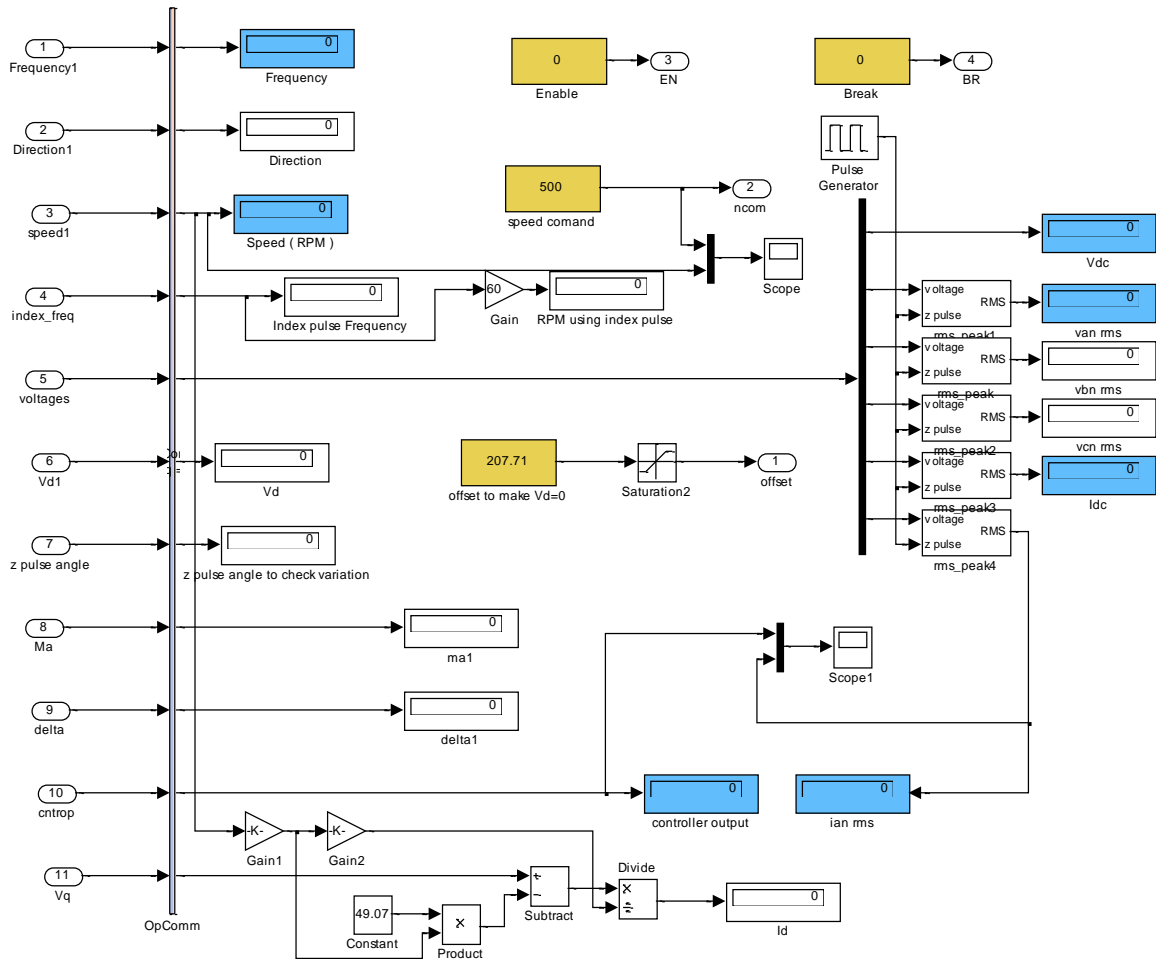


Figure 4-25 : Data Monitor (OPAL RT).

Table 4-4 : 250V, 25% Load

						25%							
	MOTOR				INVERTER							SOURCE	
6-kW 36/30 FSCW SAM loss VLT 5252 controlled by Aalborg card interfaced to OPAL-RT											Robicon dc supply		
RPM	Torque, N-m	Power, kW	$v_{an},$ V_{rms}	i_a, A_{rms}	$v_{bn},$ V_{rms}	i_b, A_{rms}	$v_{cn},$ V_{rms}	i_c, A_{rms}	Power to Motor, kW	Measured Loss, kW	$v_{supply},$ V_{dc}	$i_{supply},$ A_{dc}	Power to inverter, kW
450													
900	15.9	1498.5	86.93	12.35	86.72	11.99	86.75	12.3	1574	75.5	253.31	6.5	1648
2000	7.2	1507.2	118.4	11.84	118.8	11.13	118.8	12.4	1762	254.8	250.82	7.2	1766
3000	4.8	1508	121.5	11.16	120.9	10.87	121.1	10.2	1899	391	253.11	7.57	1905
4000	3.6	1508	120.7	14.07	125.3	13.48	123.2	14	2226	718	253.23	8.8	2228

Table 4-5 : 250V, 50% Load

						50%							
	MOTOR				INVERTER							SOURCE	
6-kW 36/30 FSCW SPM Danfoss VLT 5252 controlled by Aalborg card interfaced to OPAL-RT											Robicon dc supply		
RPM	Torque, N-m	Power, kW	v_{an}, V_{rms}	i_a, A_{rms}	v_{bn}, V_{rms}	i_b, A_{rms}	v_{cn}, V_{rms}	i_c, A_{rms}	Power to Motor, kW	Measured Loss, kW	v_{supply}, V_{dc}	i_{supply}, A_{dc}	Power to inverter, kW
450													
900	31.9	3006.5	94.6	21.81	94.79	21.81	94.6	21.78	3073	66.5	253.35	12.73	3197
2000	14.3	2995	118.26	14.03	118.1	14.21	119.04	15.04	3192	197	250.77	12.89	3203
3000	9.6	3016.9	121.06	12.85	121.1	12.92	120.89	12.98	3318	301.1	253.27	12.97	3401
4000	7.2	3015.9	122.34	15.73	121.3	15.9	124.93	15.48	3634	618.1	253.32	14.47	3651

Table 4-6 : 250V, 75% Load

						75%							
	MOTOR				INVERTER							SOURCE	
6-kW 36/30 FSCW SPM Danfoss VLT 5252 controlled by Aalborg card interfaced to OPAL-RT											Robicon dc supply		
RPM	Torque, N-m	Power, kW	v_{an}, V_{rms}	$i_a,$ A_{rms}	$v_{bn},$ V_{rms}	$i_b,$ A_{rms}	$v_{cn},$ V_{rms}	i_c, A_{rms}	Power to Motor, kW	Measured Loss, kW	$v_{supply},$ V_{dc}	$i_{supply},$ A_{dc}	Power to inverter, kW
450													
900	47.7	4500.6	102.72	31.96	102.52	31.8	102.6	32.03	4688	187.4	253.34	19.24	4865
2000	21.5	4500.7	118.56	19.53	117.84	19.92	117.5	19.9	4690	189.3	250.72	18.76	4739
3000	14.4	4522.4	120.68	16.32	120.86	16.14	120.8	16.01	4868	345.6	253.15	19.09	4903
4000	10.8	4523.9	124.15	17.34	122.6	18.21	121.1	18.58	5122	598.1	253.19	20.4	5138

Table 4-7: 250V, 100% Load

						100%							
	MOTOR				INVERTER							SOURCE	
6-kW 36/30 FSCW SPM Infoss VLT 5252 controlled by Aalborg card interfaced to OPAL-RT											Robicon dc supply		
RPM	Torque, N-m	Power, kW	v_{an}, V_{rms}	i_a, A_{rms}	v_{bn}, V_{rms}	i_b, A_{rms}	v_{cn}, V_{rms}	i_c, A_{rms}	Power to Motor, kW	Measured Loss, kW	v_{supply}, V_{dc}	i_{supply}, A_{dc}	Power to inverter, kW
450													
900	63.7	6010.3	111.96	45.44	112	45	111.86	45.1	6406	395.7	252.94	26.28	6623
2000	28.7	6010.9	119.77	22.78	119.6	23.5	119.88	24.16	6138	127.1	253.4	24.43	6179
3000	19.1	6000.4	120.65	20.16	120.5	20	120.5	21.04	6277	276.6	253.02	25.2	6324
4000	14.4	6031.9	120.76	22.26	124	21.2	122.35	22.4	6520	488.1	253.13	26.09	6549

Table 4-8 : 300V, 25% Load

						25%							
	MOTOR				INVERTER							SOURCE	
6-kW 36/30 FSCW SPM Danfoss VLT 5252 controlled by Aalborg card interfaced to OPAL-RT											Robicon dc supply		
RPM	Torque, N-m	Power, kW	v_{an}, V_{rms}	i_a, A_{rms}	v_{bn}, V_{rms}	i_b, A_{rms}	v_{cn}, V_{rms}	i_c, A_{rms}	Power to Motor, kW	Measured Loss, kW	v_{supply}, V_{dc}	i_{supply}, A_{dc}	Power to inverter, kW
450	15.9	749.27	81.3	11.61	81.11	11.35	81.04	11.38	784	34.73	300.58	3.03	873
900	16	1508	98.89	12.94	98.89	12.63	98.7	12.74	1609	101	307.73	5.42	1678
2000	7.2	1508	136.79	17.58	134.3	15.58	138.69	16.55	1742	234	302.44	6.13	1842
3000	4.8	1507.5	146.52	7.46	146.3	7.67	146.28	7.7	1942	434.5	307.7	6.43	1938
4000	3.6	1508	150.1	11.52	144.1	12.61	149.33	12.06	2236	728	307.48	7.28	2262

Table 4-9 : 300V, 50% Load

						50%							
	MOTOR				INVERTER							SOURCE	
6-kW 36/30 FSCW SPMDanfoss VLT 5252 controlled by Aalborg card interfaced to OPAL-RT											Robicon dc supply		
RPM	Torque, N-m	Power, kW	v_{an}, V_{rms}	i_a, A_{rms}	v_{bn}, V_{rms}	i_b, A_{rms}	v_{cn}, V_{rms}	i_c, A_{rms}	Power to Motor, kW	Measured Loss, kW	v_{supply}, V_{dc}	i_{supply}, A_{dc}	Power to inverter, kW
450	31.8	1498.5	81.56	21.39	81.46	21.45	81.58	21.33	1532	33.5	300.71	5.55	1680
900	31.8	2997.1	103.58	21.8	103.48	21.81	103.38	21.87	3073	75.9	300.57	10.84	3264
2000	14.3	2995	135.77	15.58	134.3	16.78	133.34	15.79	3244	249	302.83	10.85	3285
3000	9.5	2985.5	146.32	10.32	146	10.67	146.08	10.31	3390	404.5	307.7	10.96	3384
4000	7.2	3016.7	148.13	13.3	146.82	13.27	148.34	13.18	3687	670.3	307.4	11.99	3709

Table 4-10 : 300V, 75% Load

						75%							
	MOTOR				INVERTER							SOURCE	
6-kW 36/30 FSCW SPM Danfoss VLT 5252 controlled by Aalborg card interfaced to OPAL-RT											Robicon dc supply		
RPM	Torque, N-m	Power, kW	V _{an} , V _{rms}	i _a , A _{rms}	V _{bn} , V _{rms}	i _b , A _{rms}	V _{cn} , V _{rms}	i _c , A _{rms}	Power to Motor, kW	Measured Loss, kW	V _{supply} , V _{dc}	i _{supply} , A _{dc}	Power to inverter, kW
450	47.7	2247.8	85.9	36.2	85.86	35.83	85.79	36.09	2537	289.2	300.78	9.42	2841
900	47.7	4495.6	112.9	32	112.79	31.8	112.91	32.04	4645	149.4	300.5	16.33	4926
2000	21.5	4502.9	138.82	19.8	132.09	18.94	135.83	20.81	4702.9	200	302.74	15.65	4747
3000	14.3	4494	146.07	13.42	146.09	13.44	145.84	13.73	4874	380	307.62	15.97	4877
4000	10.7	4483.1	147.24	15.53	148.5	15.91	146.82	15.76	5096	612	307.4	17	5111

Table 4-11 : 300V, 100% Load.

						100%							
	MOTOR				INVERTER							SOURCE	
6-kW 36/30 FSCW SPM Danfoss VLT 5252 controlled by Aalborg card interfaced to OPAL-RT											Robicon dc supply		
RPM	Torque, N-m	Power, kW	v_{an}, V_{rms}	i_a, A_{rms}	v_{bn}, V_{rms}	i_b, A_{rms}	v_{cn}, V_{rms}	i_c, A_{rms}	Power to Motor, kW	Measured Loss, kW	v_{supply}, V_{dc}	i_{supply}, A_{dc}	Power to inverter, kW
450	63.7	3001.8	90.86	45.4	90.65	45.17	90.83	45.41	3501	499.2	300.75	12.4	3725
900	63.7	6003.6	120.63	44.7	120.63	44.1	120.74	44.54	6511	507.4	300.26	22.35	6703
2000	28.6	5990	139.62	29	137.83	26.8	135.73	29.21	6195	205	302.52	20.82	6315
3000	19.1	6000.4	145.75	18.7	145.9	18.79	146.03	18.68	6327	326.6	307.62	20.59	6362
4000	14.4	6030.4	146.43	19.4	146.25	20.43	149.36	18.63	6571	540.6	307.35	21.42	6612

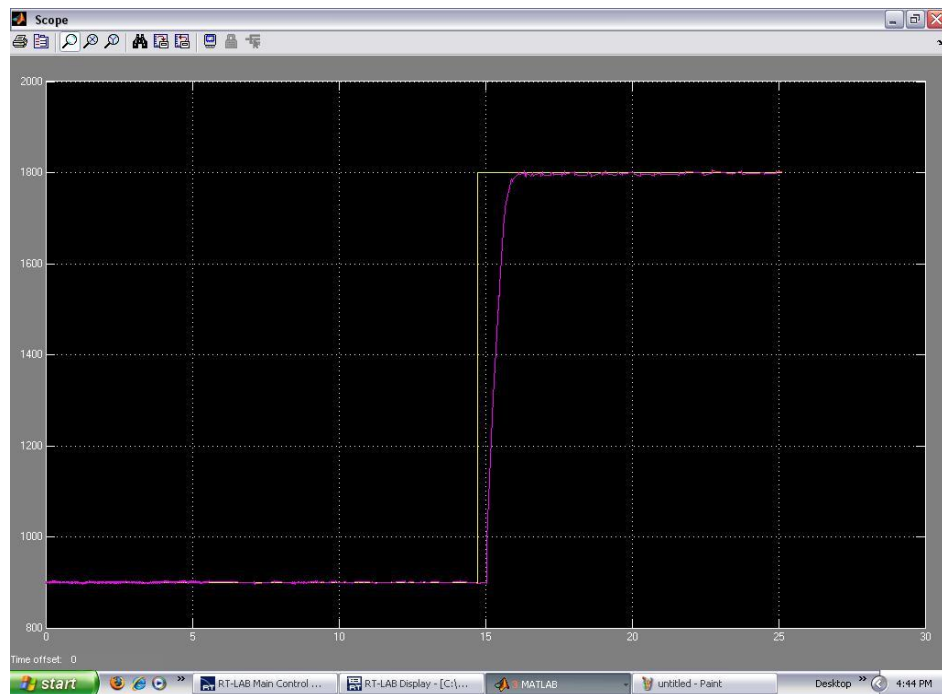
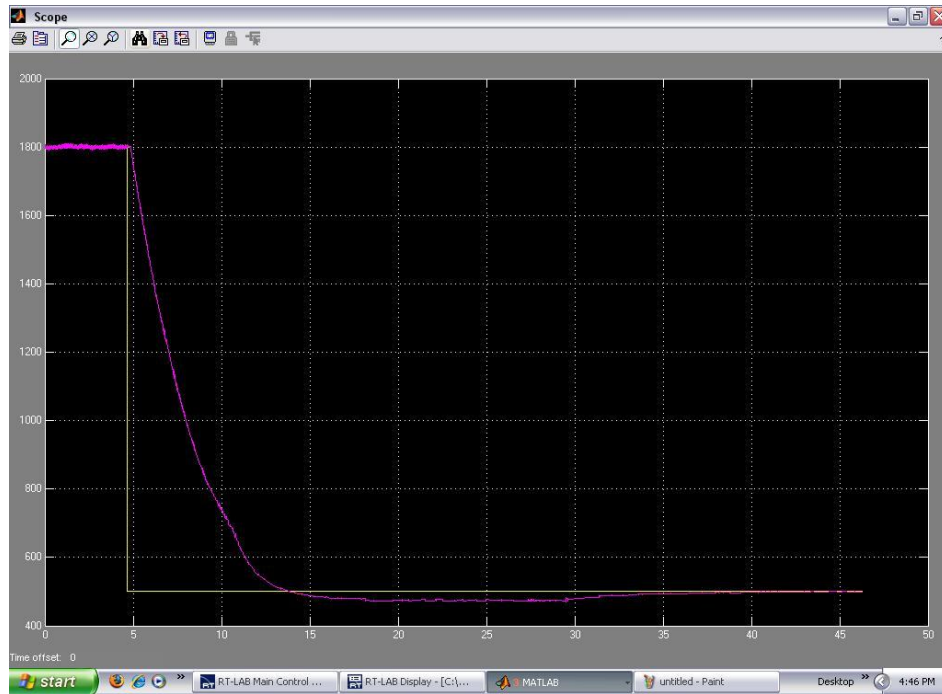


Figure 4-26 : Speed Tracking.

Since the main focus of this experiment was to test the CPA method to extend the constant power speed ratio, proportional and integral gain values were kept moderate ($K_p = 0.25$, $K_i = 0.05$). By proper tune up, the motor speed response can be improved to have one overshoot but no undershoots to avoid stress on mechanical couplings. When speed command was reduced from 1800 rpm to 900 rpm, no control action was taken. Losses and inertia of the motor was used to reduce the speed. Once the speed was reduced to the new set point value, controller would engage to keep the speed constant.

From Figure 4-27, up to base speed (i.e. 900 RPM), in constant torque region, rated torque can be produced and required stator current is the rated current of the motor. In this zone, developed motor output power increases linearly with the speed. After base speed, in the constant power or field weakening zone, rated power can be produced. As the power was kept constant, with increase in speed, generated torque will be reduced. With this torque, stator current also decreased. Initially this stator current hits the minimum value (given by Equation (3.27)) and then, slowly, it approaches the characteristics current (given by Equation (3.24)). Figure 4-28 lists measured losses. Below base speed, losses are proportional to the developed power (or load). The rotor of surface PM machine has permanent magnets. When the machine is rotated, magnetic flux due to rotor permanent magnets causes eddy currents (core losses). High losses can be noticed especially at the higher speeds. Results in the Figure 4-28 confirms successful suppression of these eddy current losses in the magnets and rotor core that are generated by the significant air gap sub-harmonic field components.

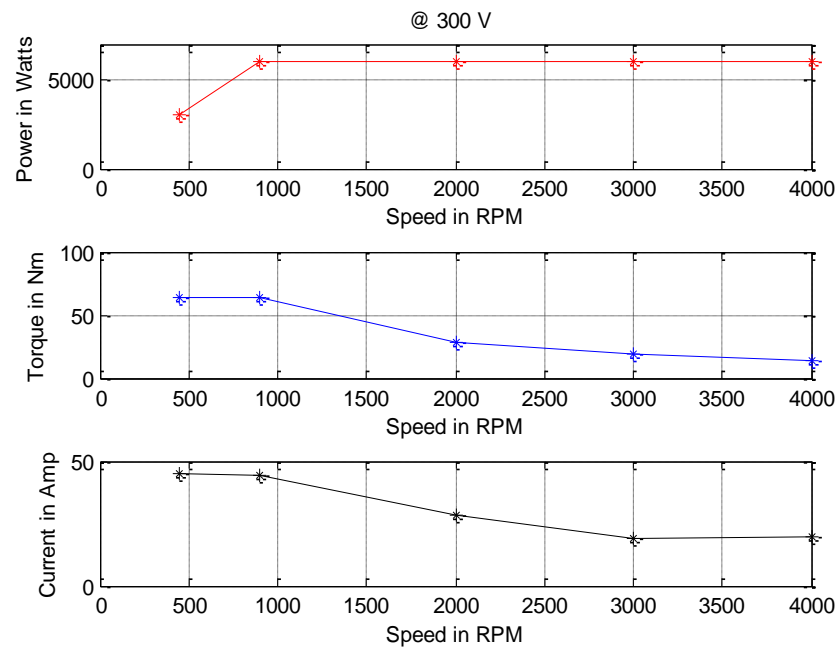


Figure 4-27: Measured Power Vs Speed, Torque Vs Speed and Current Vs Speed for 300V, & 100% Load.

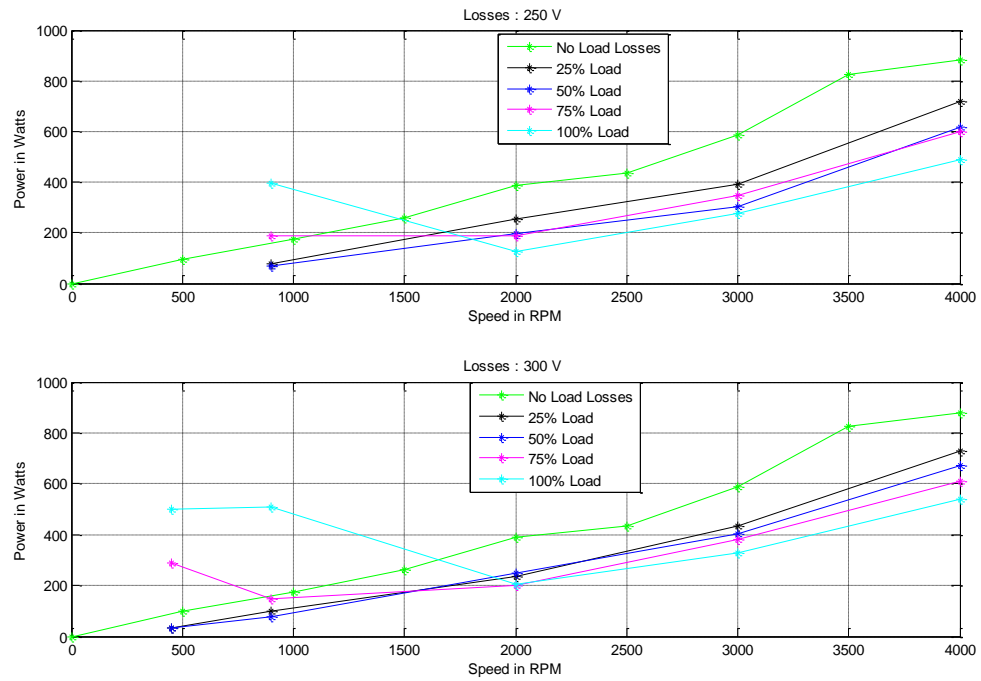


Figure 4-28: Measured Losses.

This is a significant result since these losses have been considered to be one of the key potential obstacles to using fractional-slot concentrated windings for high-speed operation [27]. Above base speed, as the current approaches the characteristic value, which is independent of the load condition (or required power output), losses, defined as the difference between the motor input power and the motor output power, are more for partial loads. Below base speed losses are proportional to the power output.

Figure 4-29 shows measured inverter efficiency. Below base speed, the inverter is operating in the linear modulation region. In this region switching losses are high. Above base speed, inverter operates in the over-modulation region or six-step operation. Switching waveform is more like a square wave. In this region switching losses are less. From Figure 4-29 it can be noticed that inverter efficiency is very high in the constant power region. Between rated base speed and true base speed, inverter operates in the non-linear region. Here modulation index is between 1 and $4/\pi$. Figure 4-30 shows measured motor efficiency. In the constant torque region, motor efficiency is good (above 90%). In constant power region, motor current approaches a constant value. This value does not depend on the developed shaft power. Current required to produce 25% of the power is almost the same as the current required to produce 100% of the power. Hence current related losses are almost the same which means partial load efficiency is poor. This can be seen in the Figure 4-30 and Table 4-12. For the most operating conditions, motor efficiency is close to 90%. It can be seen that the partial load efficiency is poor especially at high speed.

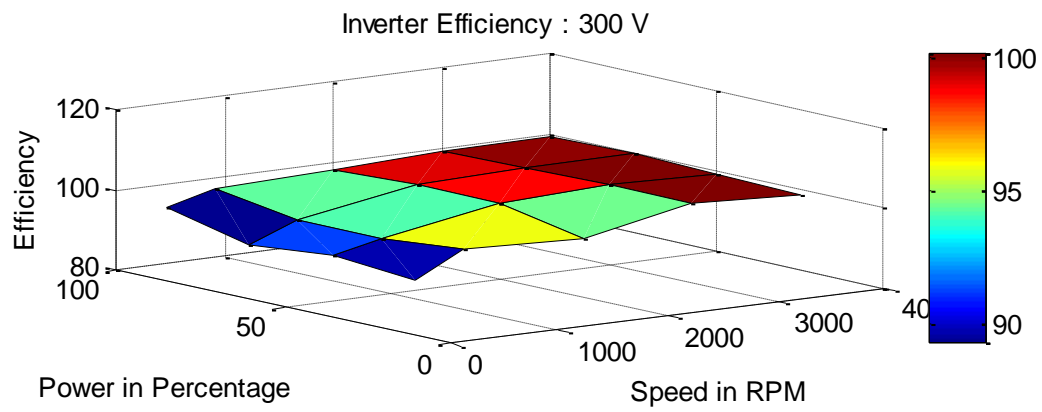
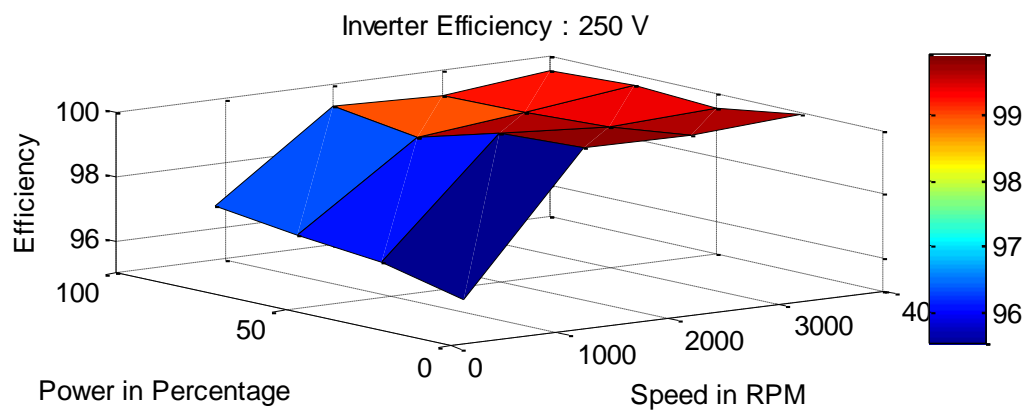


Figure 4-29 : Measure Inverter Efficiency.

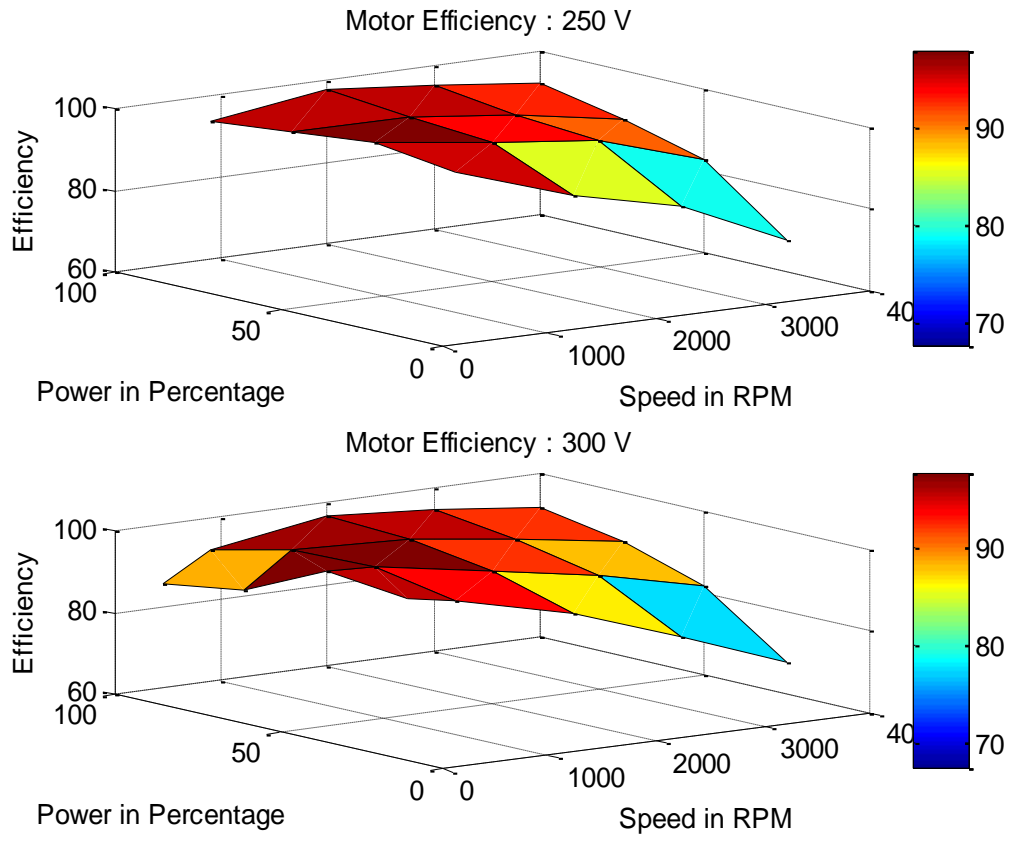


Figure 4-30 : Measured Motor Efficiency.

Table 4-12 : Current Comparison at 250V and 300V DC.

Speed (RPM)	Load	Average RMS Current with 250V DC (Amp)	Average RMS Current with 300V DC (Amp)
450	25%		11.4467
	50%		21.39
	75%		36.04
	100%		45.31
900	25%	12.2	12.77
	50%	21.8	21.8267
	75%	31.93	31.9467
	100%	45.1833	44.4567
2000	25%	11.78	16.57
	50%	14.4267	16.05
	75%	19.7833	19.85
	100%	23.47	28.3433
3000	25%	10.74	7.61
	50%	12.9167	10.4333
	75%	16.1567	13.53
	100%	20.4033	18.73
4000	25%	13.84	12.0633
	50%	15.7033	13.25
	75%	18.0433	15.7333
	100%	21.9367	19.4733

In general, even with the traditional vector control schemes, partial load efficiency of the Surface PM motors, especially at high speeds, is not good [39], [40]. Partial load efficiency is particularly important if the traction application requires high speed cruising operation at light loads. For fractional-slot concentrated-windings surface PM machines, maximizing the power/torque density leads to higher number of poles (experimental machine has 30 poles). This results in high electrical frequencies [41]. In addition to the stator core losses + rotor losses, high electrical frequencies generate additional AC losses in the stator windings of these machines [42], [43], [44].

Care must be taken in the control system itself to reduce these losses. Dual Mode Inverter control [45] is one method to increase the partial load efficiency of surface PM machines. This method makes the motor current proportional to the developed power which increases partial load efficiency. This is done by connecting a pair anti-parallel thyristors in series with each of the motor phase. Firing of these thyristors can be controlled to achieve better partial load efficiency. This increases overall reactance which minimizes the motor current. Traditional vector control can also be modified to increase the partial load efficiency of the fractional-slot concentrated windings PM synchronous motors [41]. In this control method, a suitable combination of d-axis component and a q-axis component of the stator current is estimated by carrying out a number of simulations or experiments. Figure 4-31 shows measured overall drive efficiency. Figure 4-32, Figure 4-33, and Figure 4-34 shows comparison of inverter, motor and drive efficiencies at 250V and 300V DC power supply.

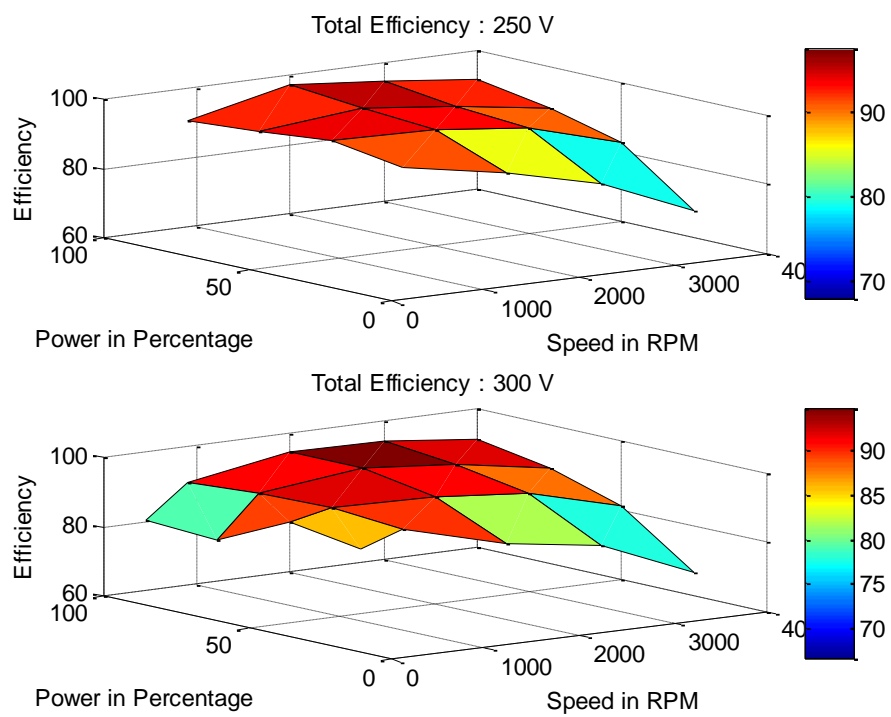


Figure 4-31 : Measured Drive Efficiency.

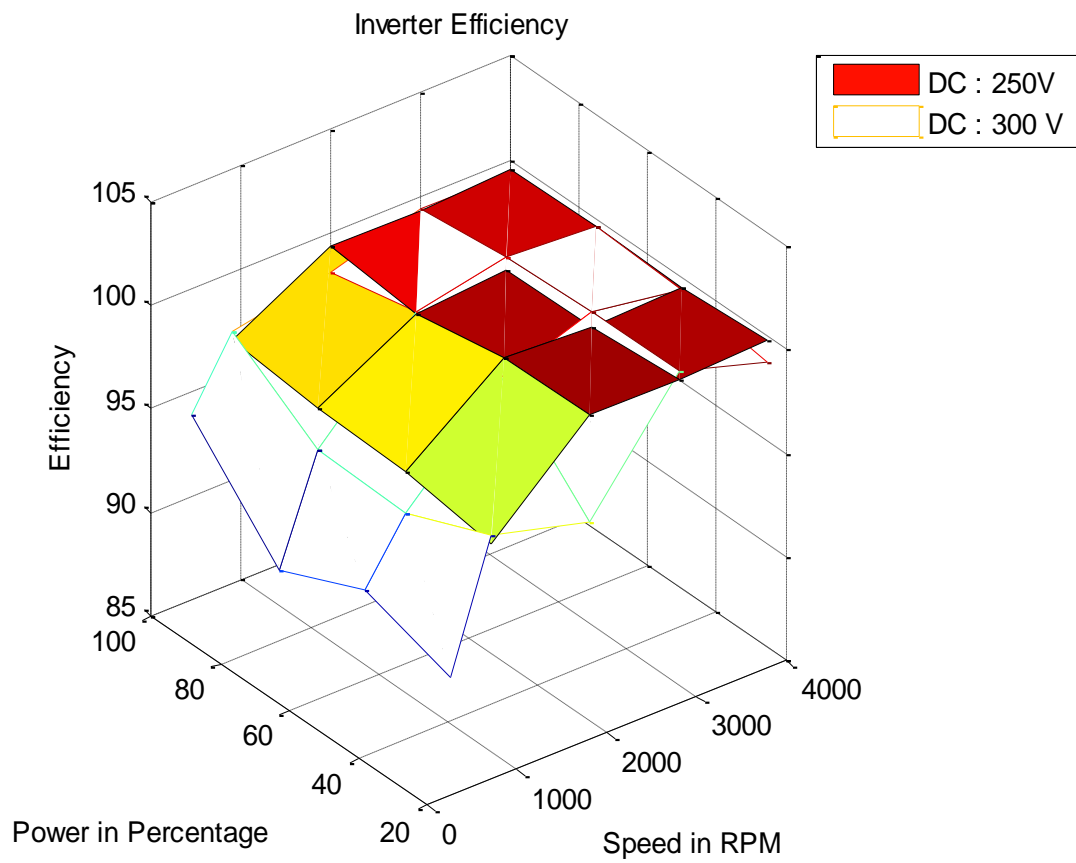


Figure 4-32 : Comparison of Inverter Efficiency.

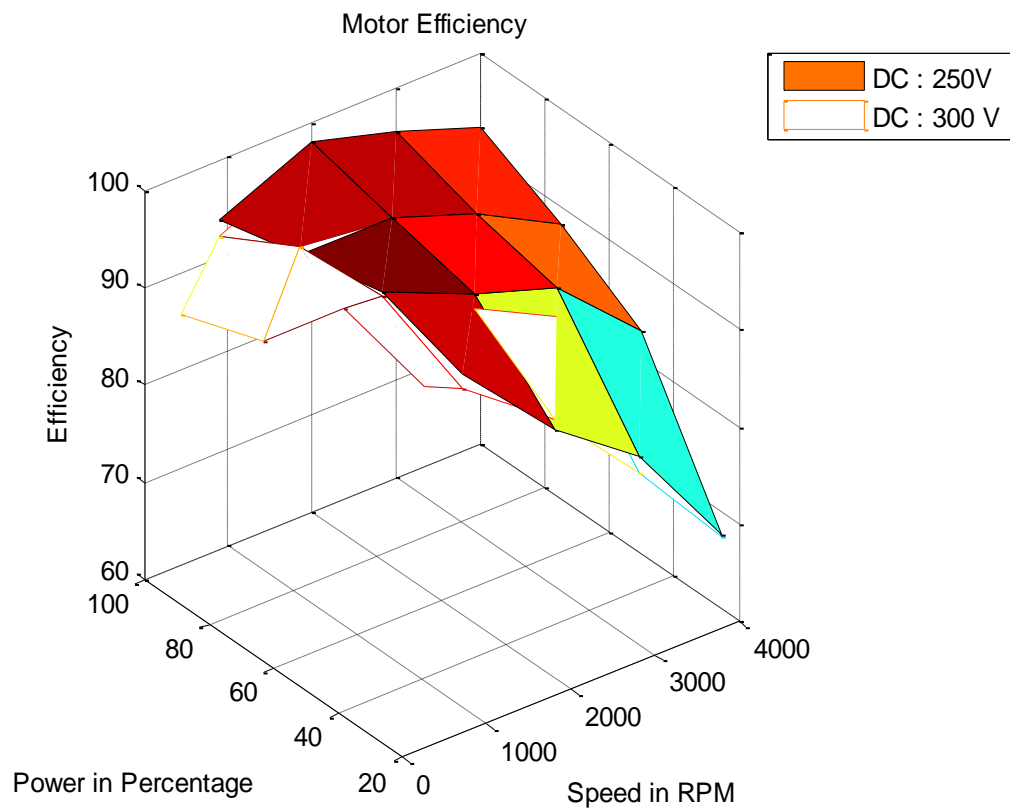


Figure 4-33 : Comparison of Motor Efficiency.

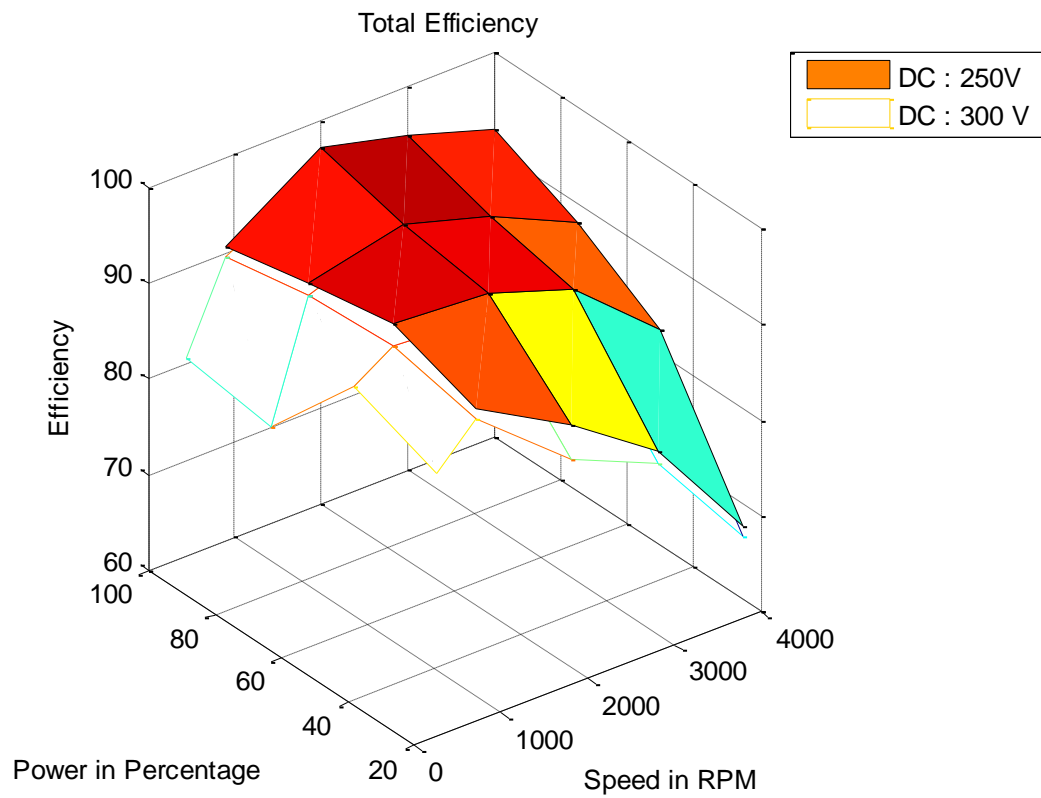


Figure 4-34 : Comparison of Total Drive Efficiency.

It can be seen from the Figure 4-33 that, for both voltages, motor efficiency is almost same. Inverter efficiency is also almost same, except for a speed range from base speed up to the true base speed. Table 4-12 compares stator currents for these two voltages. It can be seen from the Table 4-12 that, up to base speed, required stator current is almost equal for 250V and 300V. From rated base speed (900 RPM) till the n_{min} , current with 300V DC supply is more than the current with 250V DC supply. So the current related losses are more with 300V DC supply than 250V DC Supply. Also, note that for this speed range, sinusoidal PWM operates in the non-linear region.

For the non-linear region, a look up table was used to adjust the modulation index to avoid unstable operation. This lookup table was designed for a 250V operation. For 300V operation, because of time constrain, same lookup table was used. This can be a possible reason for more current during the non-linear region with 300V than 250V power supply. This non-linear region can be avoided by changing modulation index linearly from 0 to 1 up to the base speed and above base speed operation, the inverter can be operated in the six-step or square wave operation as reported in [27]. As expected, above n_{min} , stator current with 300V DC supply is less than with the 250V DC supply. So in this speed range, the motor and inverter efficiency should be better with more voltage. Although as speed increases, stator current approaches to the characteristic current which does not depend on the applied voltage or the load conditions.

Figure 4-35 shows the comparison between the no-load losses and motor and drive efficiency. No load losses were measured in two different ways.

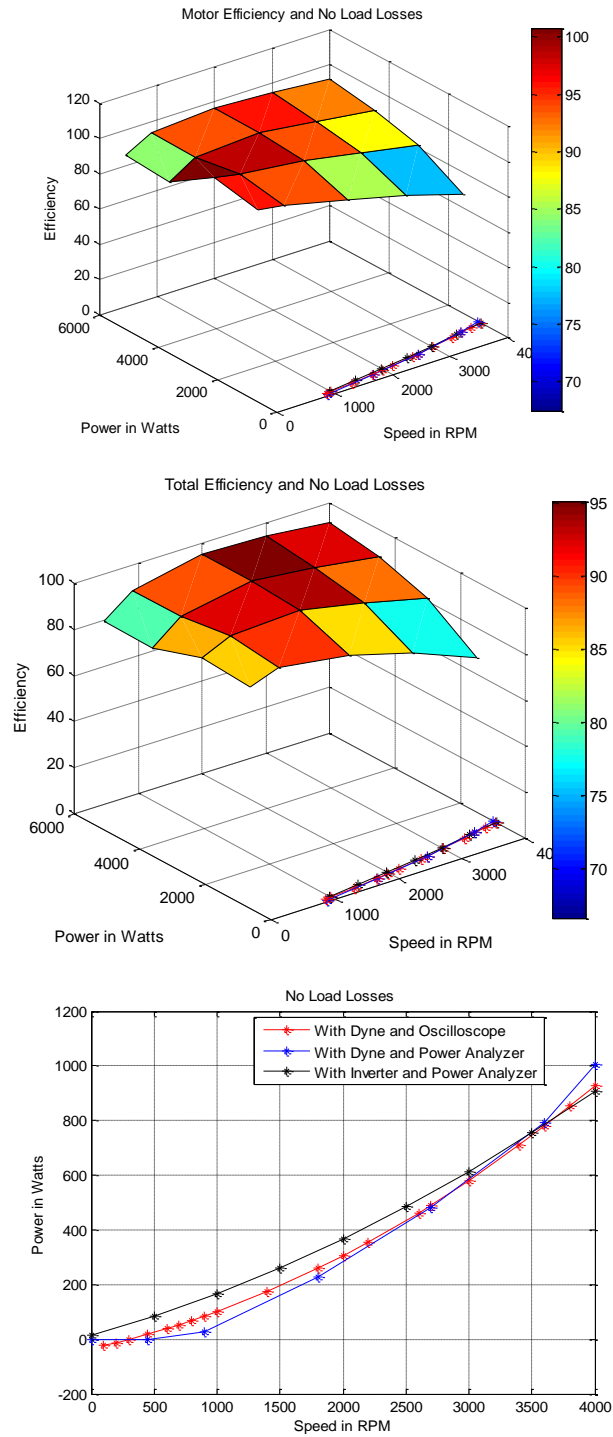


Figure 4-35: No Load Losses and Drive Efficiencies.

Dyne was used to rotate the motor at different speeds. Amount of power used by the dyne to rotate the motor at a constant speed is nothing but the no-load electrical losses plus mechanical losses. Similarly, an inverter can be used to run the motor at different speed with no load attached to it. Amount of power used by the inverter to keep the motor speed constant is again nothing but the no-load losses. When the supplied voltage is more than the minimum required DC voltage (given by Equation (3.7)), true base is more than the design base speed. From Equation (3.33) true base speed, or the speed at which modulation index will be $4/\pi$, is given by,

$$n_{bt} = \frac{\sqrt{2 * \left(\frac{V_{dc}}{\pi}\right)^2 * (E_b^2 + X_b^2 I_r^2) - (R^2 X_b^2 I_r^4) - (E_b R I_r)}}{(E_b^2 + X_b^2 I_r^2)}$$

Using parameters from Table 4-1, with 250V DC supply, true base speed will be 1117 rpm. With 300V DC supply, true base speed will be 1344 rpm.

From Equation (3.26), we have, $n_{min} = \frac{V_{max}}{E_b \cos \delta}$. From Equation (3.27), we have,

$$I_{min} = \frac{P}{3V_{max}}. \text{ Using } V_{max} = \frac{\sqrt{2} * V_{dc}}{\pi}, \text{ and } \delta = \sin^{-1} \left(\frac{X_b P_r}{3V_{max} E_b} \right), \text{ We can calculate Table 4-13.}$$

As discussed earlier, more voltage means, lower minimum current. So if the drive spends a good amount of time at certain speed, proper voltage can be selected so that this speed coincides with minimum speed. Also note that at this speed, power factor is unity. Inverter control scheme can also be designed such that at this speed, it will operate in square wave operation reducing both switching and conduction losses.

Table 4-13 : Minimum Current and Unity Power Factor Speed.

	$V_{dc} = 300 V_{dc}$			$V_{dc} = 250 V_{dc}$		
	$V_{max} = 135 V_{rms}$			$V_{max} = 112.5 V_{rms}$		
Power, watts	N_{min} Rpm	I_{min} A_{rms}		N_{min} rpm	I_{min} A_{rms}	
1500	2481	3.70		2076	4.44	
3000	2556	7.40		2169	8.88	
4500	2698	11.10		2357	13.33	
6000	2943	14.81		2728	17.77	

We have, motor output power $P_{shaft} = 3I_r n E_b$, which leads to $I_r = \frac{P_{shaft}}{3nE_b}$. Here I_r is the real or torque producing component of the stator current. Table 4-14 shows the calculated value of real part of the stator current from the measurements. Since the inverter lead angle was not recorded, it is not possible to accurately estimate the equivalent q-axis and d-axis component of the stator current. From Table 4-14, up to base speed, for the same load, the q-axis current is constant. Above base speed, the q-axis current decreases continuously. As described in section 2.1.1, in constant voltage constant power control strategy, above base speed, both the d-axis and the q-axis components of the stator current decreases. As described in section 2.1.2, in constant current constant power strategy, above base speed, the stator current is constant. As described in section 2.1.3, in optimum current vector control scheme, up to base speed the current is in phase with the back-EMF. That means the d-axis current is zero. From the base speed to the speed at which current-limiting circle intersects the voltage-limited maximum power trajectory, the d-axis current increases. Above this speed, d-axis current remains constant while the q-axis current decreases continuously. In CPA method, below base speed, the current is in phase with the back-EMF. Above base speed, the current initially decreases to the minimum value and then increases to the constant value (characteristic current).

Experimental results prove that, conventional phase advancement based traction drive control system does not require any type of current feedback.

Table 4-14 : Calculated Torque Component of the Stator Current (with 300V DC).

RPM	Relative speed, n	Shaft Power, kW	I_{rms}	Torque Current	Load
450	0.5	749	11.45	10.1	25%
450	0.5	1499	21.39	20.2	50%
450	0.5	2248	36.04	30.3	75%
450	0.5	3002	45.31	40.47	100%
900	1	1508	12.77	10.17	25%
900	1	2997	21.83	20.2	50%
900	1	4496	31.95	30.3	75%
900	1	6004	44.46	40.47	100%
2000	2.222	1508	16.57	4.57	25%
2000	2.222	2995	16.05	9.08	50%
2000	2.222	4503	19.85	13.66	75%
2000	2.222	5990	28.34	18.17	100%
3000	3.333	1508	7.61	3.05	25%
3000	3.333	2986	10.43	6.04	50%
3000	3.333	4494	13.53	9.09	75%
3000	3.333	6000	18.73	12.13	100%
4000	4.444	1508	12.063	2.29	25%
4000	4.444	3017	13.25	4.58	50%
4000	4.444	4483	15.73	6.8	75%
4000	4.444	6030	19.47	9.15	100%

This method can extend the constant power region of a surface PM motor with phase inductance greater than L_∞ . With the help of speed and rotor position information along with load requirement, the desired current is calculated by solving a simple fundamental power transfer equation between two voltages sources (applied voltage and back-EMF).

It can be seen from the experimental results that the rated power can be produced at any speed above base speed with the required current being less than the rated current of the motor. Below base speed, both modulation index and voltage angle are changed while above base speed, only voltage angle is changed. Compared to the traditional vector control scheme, this method is easy to implement and the required computational power is less. It was possible to implement a time step of 50 μs and a switching frequency of 9 kHz.

In the constant power region, since the part of the stator current is used to oppose the magnetic flux produced by the permanent magnets, improper control technique can lead to irreversible demagnetization of the rotor permanent magnets.

Use of the permanent magnets on the rotor prevents the use PMSM motors for high speed application. Since there is always a field excitation, faulted stator phase cannot be safely isolated to continue the use of motor. For these operating conditions, Switched Reluctance Motors, described in the next chapter, have advantages over the PMSM motors.

5 INTRODUCTION – SWITCHED RELUCTANCE MOTORS

Light electric or hybrid electric vehicles, such as passenger vehicles, have a modest constant power speed range (CPSR) requirement of 4 to perhaps 6:1. Such performance can be achieved with traction drives incorporating a variety of popular motor types including induction, permanent magnet and switched reluctance machines. For passenger vehicle applications, the switched reluctance motor (SRM) is often ruled out based on torque pulsations, mechanical vibration, and acoustical noise despite recent and on-going research addressing these issues [46]. Traction drives for heavy vehicles may require a CPSR of 10:1 or more. In addition, heavy vehicles, especially off-road vehicles, are more tolerant to torque ripple, noise, and vibration. The potentially low motor/inverter cost of the SRM can make it an attractive candidate for such applications provided the CPSR can be shown to easily exceed a CPSR of 10:1. High CPSR means drive can operate at high cruising speed. SRM motors are robust because of their ability to run under failure conditions [15]. In SRM motors, torque/speed characteristics is not defined solely by the machine manufacturer hence an extreme wide range of these characteristics can be obtained by simply alternating control scheme for phase timings [47]. The switched reluctance motor (SRM) has double saliency meaning it has a saliency in the stator as well as saliency in the rotor. Figure 5-1 shows a cross sectional view of the four phase 8/6 SRM motor.

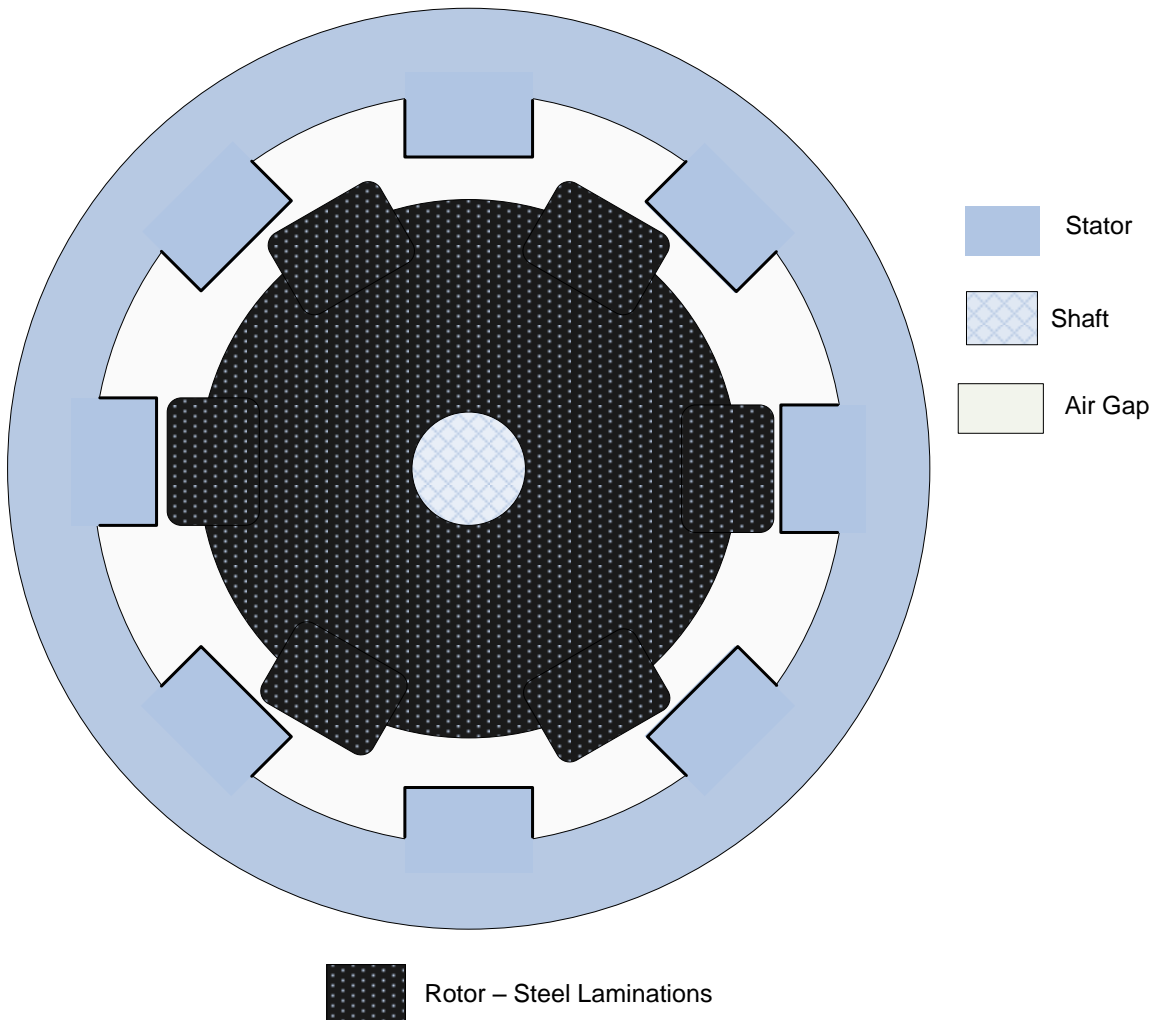


Figure 5-1 : Cross-Sectional View of a Four Phase 8/6 Switched Reluctance Motor.

The machine rotor does not have any windings or permanent magnets; it is a low cost stack of laminations. This makes the motor structure very rugged and low cost. As there are no permanent magnets or winding on the rotor, SRM motors can be used for very high speed applications [48], [11]. Lack of permanent magnets on the rotor structure also allows the use of the SRM in very high temperature environment [48]. Instead of the usual sinusoidally distributed windings, SRM motors typically have concentrated windings on the stator poles. These windings can be externally wound form and then slipped over the silent stator poles [48]. This makes stator assembly process very simple, inexpensive and also reduces the maintenance time during failures. The possibility of a phase-to-phase fault is low, as the motor windings are both physically and magnetically isolated from one another [48]. If a proper converter topology is used, a faulted phase can be isolated. As there is no excitation in the rotor, rotor poles cannot generate power into the faulted phase. This eliminates a possibility of drag torque or fire hazard during phase failure [48]. Use of proper converter topology also avoids shoot through faults (short-circuit of the source). This makes SRM motors robust, fault tolerant and a good candidate for heavy traction drives especially the ones which are used in harsh environmental conditions. For smooth torque production, four phase SRM motors are generally preferred [15]. Each phase of the motor is made up of two coils wound around diametrically opposite stator poles. These two coils are connected electrically in series such that their magnetic fluxes are added.

Each stator-pole pair can be energized by an asymmetrical half bridge converter whose topology is shown in Figure 5-2.

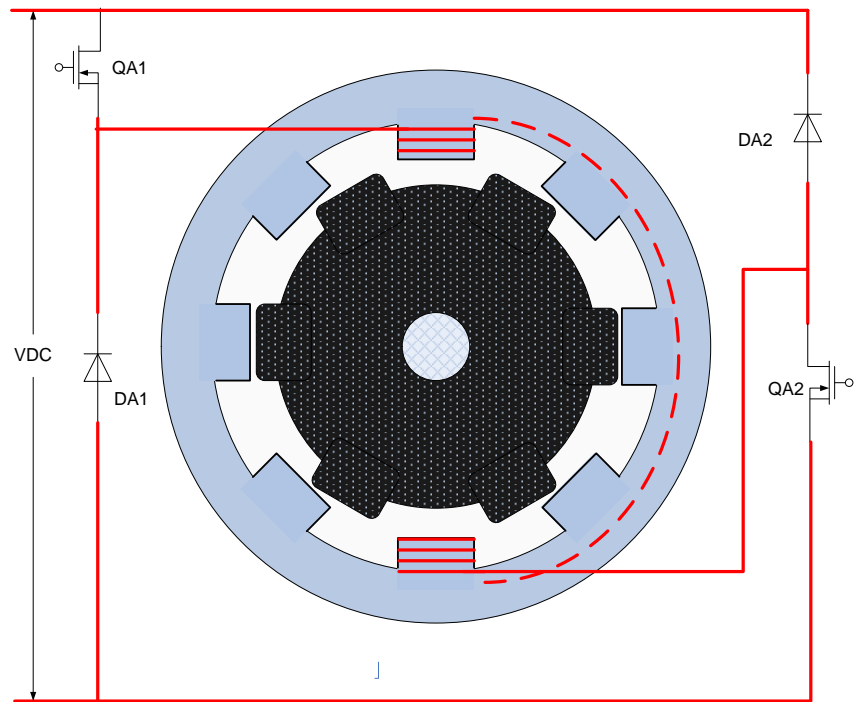
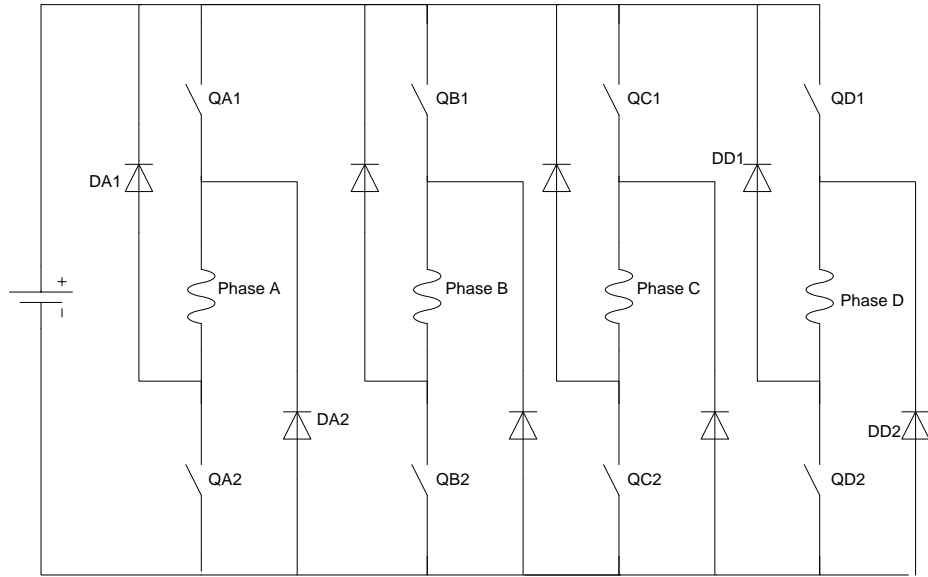


Figure 5-2: Asymmetrical Half-Bridge Voltage Source Inverter Topology for an 8/6 SRM Motor
[11],[15].

Here a power electronics switch (IGBT, MOSFET etc.) is connected in between positive terminal of the DC supply voltage and one end of the stator pole pair winding. A second switch is connected between the negative terminal of the DC supply voltage and the other end of the stator pole pair winding. Bypass diodes are also connected across the stator winding as shown in Figure 5-2. The input DC power supply can be either a battery or a rectified and filtered AC supply. The DC supply can be fixed or variable in magnitude. In some known drives, the power supply includes a resonant circuit which produces a DC voltage which rapidly varies between zero and a predetermined value to allow zero voltage switching of the power switches [49].

As pointed out by Becerra et. al. in [50], the torque in SRM motor is produced due to the tendency of a magnetic circuit to align itself to a position of least reluctance. As shown in Figure 5-2, full DC voltage is applied across the phase winding (phase A) by turning ON switches QA1 and QA2. This causes current buildup in that phase. This current sets up a magnetic field which causes a magnetic pull on the nearest rotor pole pair. This magnetic flux enters the rotor structure through one rotor pole and leaves the rotor structure through the other pole of that rotor pole pair. That rotor pole pair then aligns itself to the energized stator pole pair.

This is the position of minimum reluctance (as seen by the stator current). This is also a position of least stored energy. Once the rotor is at the completely aligned position, both the switches are turned OFF. This converter also provides a path for continuity of inductor currents through the bypass diodes when excitation is removed from a coil.

All machine phases are excited sequentially and synchronously with the help of a rotor position encoder to produce unidirectional torque. Torque in the SRM is developed as a solenoidal force as opposed to the Lorentz force that drives most motors, where both the stator and rotor produces magnetic field [51].

5.1 Modeling of Switched Reluctance Motors [4][51].

Coupling between phases of the SRM is weak [15], allowing model of each phase to be developed and solved independently. For one phase, we have coil terminal voltage,

$$V_s = iR + \frac{d\lambda(\theta, i)}{dt}, \quad (5.1)$$

Here, V_s = voltage applied to the winding by the converter, i = winding current, λ = magnetic flux linkage of the winding, R = winding resistance, and θ = rotor position.

Equation (5.1) is nonlinear due to the nonlinear dependence of the flux linkages λ , on the rotor position θ , and the winding current i . The differential equation can be expanded as,

$$V_s = iR + \left(\frac{\partial \lambda(\theta, i)}{\partial i} \frac{di}{dt} \right) + \left(\frac{\partial \lambda(\theta, i)}{\partial \theta} \frac{d\theta}{dt} \right) \quad (5.2)$$

Where $\frac{d\theta}{dt} = \omega$ i.e. the motor speed in rad/sec, and we have,

$$V_s = iR + \left(\frac{\partial \lambda(\theta, i)}{\partial i} \frac{di}{dt} \right) + \left(\frac{\partial \lambda(\theta, i)}{\partial \theta} \omega \right) \quad (5.3)$$

Defining incremental inductance,

$$l(\theta, i) = \frac{\partial \lambda(\theta, i)}{\partial i} \quad (5.4)$$

and pseudo back-EMF,

$$e(\theta, i, \omega) = \omega \cdot \frac{\partial \lambda(\theta, i)}{\partial \theta} \quad (5.5)$$

we have,

$$V_s = iR + l(\theta, i) \cdot \frac{di}{dt} + e(\theta, i, \omega) \quad (5.6)$$

The term $e(\theta, i, \omega)$ is called as a pseudo back-EMF because, unlike surface PM Motors, not all of the instantaneous power associated with $e(\theta, i, \omega)$ is converted to the mechanical form.

Some part of this power is a stored energy, associated with the charge and discharge of the coil inductance, and rest is converted to mechanical form. The stored energy component has a zero average value. From the Equation(5.6), we can write the per phase equivalent circuit of SRM as shown in the Figure 5-3.

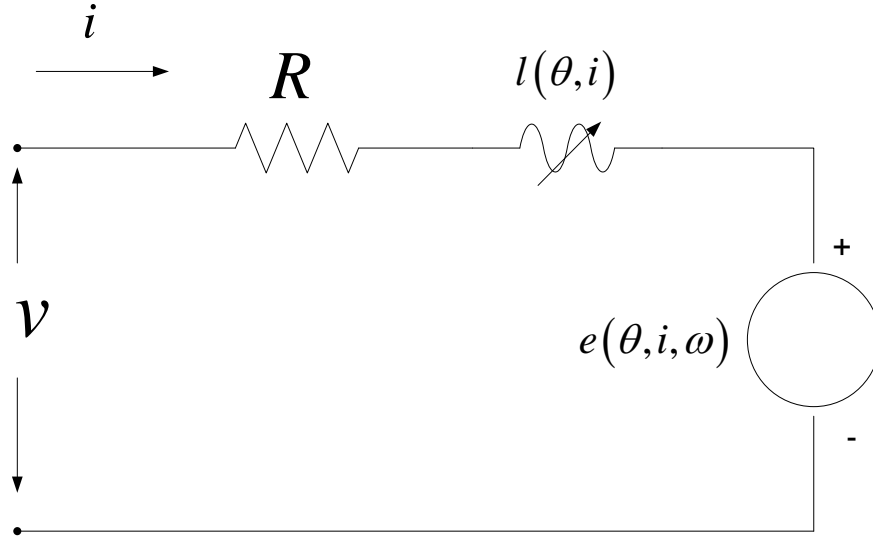


Figure 5-3: Per Phase Equivalent Circuit of Switched Reluctance Motor.

For the simplicity of initial analysis, saturation of magnetic flux-linkage is ignored. Incremental inductance, which depends on both the rotor position and current, can be considered as a linear inductance which depends only on the rotor position. Equation (5.3) and (5.6) can be modified to the following form.

$$V_s = iR + L \frac{di}{dt} + \omega i \frac{dL}{d\theta} \quad (5.7)$$

Multiplying by current i , we get,

$$V_s i = i^2 R + Li \frac{di}{dt} + \omega i^2 \frac{dL}{d\theta} \quad (5.8)$$

From the Figure 5-3, power converted to mechanical form is,

P_m = Power Supplied – Resistive Loss – Power Stored in an Inductor. Therefore,

$$P_m = V_s i - i^2 R - \left(\frac{d}{dt} \frac{1}{2} Li^2 \right) \quad (5.9)$$

Here ,

$$\begin{aligned} \frac{d}{dt} \left(\frac{1}{2} Li^2 \right) &= Li \frac{di}{dt} + \frac{1}{2} i^2 \frac{dL}{dt} \\ \frac{d}{dt} \left(\frac{1}{2} Li^2 \right) &= Li \frac{di}{dt} + \frac{1}{2} i^2 \omega \frac{dL}{d\theta} \end{aligned} \quad (5.10)$$

After substituting the Equations (5.8) and (5.10) into the Equation (5.9), we get,

$$\begin{aligned} P_m &= \frac{1}{2} \omega i^2 \frac{dL}{d\theta} \\ T_m &= \frac{P_m}{\omega} = \frac{1}{2} i^2 \frac{dL}{d\theta} \end{aligned} \quad (5.11)$$

From above equation, it is clear that torque (T_m) does not depend on the direction of the stator current (because of square term) and can only be developed when the inductance changes. Motoring torque can only be produced in the direction of rising inductance. The shape and magnitude of the produced torque depends mainly on the shape and magnitude of the phase current. Therefore the torque control in switched reluctance drives is attained through the current control [52]. Figure 5-4 shows per phase inductance profile with respect to the rotor angular position and required stator current profile to produce the motoring torque.

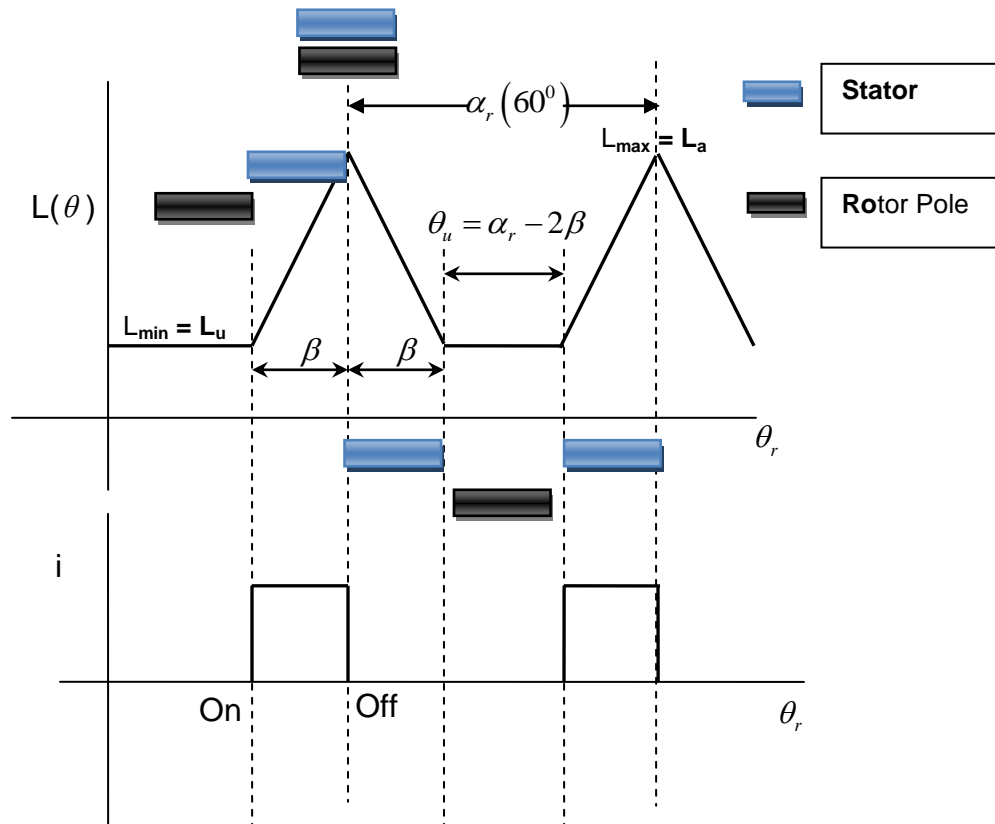


Figure 5-4: Per Phase Inductance Profile of an 8/6 SRM Motor (Neglecting Saturation).

Here saturation is neglected. When a rotor pole pair is aligned with the stator pole pair, it is a minimum reluctance (or maximum inductance) position for that phase. This position is also called as a “completely aligned” position. When the center of the rotor pole pair is aligned with the center line between two adjacent stator pole pairs, this is the maximum reluctance (or minimum inductance) position. This position is also called the “completely unaligned” position. If N_r is the number of rotor poles, then the rotor pole pitch,

$$\alpha_r = \frac{2\pi}{N_r} \quad (5.12)$$

This evaluates to be 60° for an 8/6 SRM motor which means the per phase inductance profile repeats itself every 60° . We have, β_s = stator pole arc length and β_r = rotor pole arc length. These lengths are assumed to be equal (i.e. $\beta_s = \beta_r = \beta$). Inductance profile for other phases can be obtained by delaying this profile by,

$$\begin{aligned} \theta &= 2\pi \left(\frac{1}{N_r} - \frac{1}{N_s} \right), \\ \theta &= 2\pi \left(\frac{1}{6} - \frac{1}{8} \right) = \frac{\pi}{12} \end{aligned} \quad (5.13)$$

i.e. by $15^\circ, 30^\circ$ and 45° . Here N_s is the number of stator poles. As it can be seen in Figure 5-4, $dL/d\theta$ changes sign at full alignment, therefore the pseudo back-EMF $e(\theta, i, \omega)$ also changes its sign at the full alignment.

The torque equation can be rewritten as follows,

$$T_e = \frac{1}{2} i^2 \frac{dL}{d\theta} = \frac{1}{2} i^2 \left(\frac{L_{\max} - L_{\min}}{\beta} \right) \quad (5.14)$$

Since the current switching to produce torque is based on the reluctance profile, this machine is called as a switched reluctance motor [4]. Figure 5-4 also shows the ideal current profile required to produce motoring torque. A current pulse is applied when the rotor pole pair starts aligning with the stator pole pair (i.e. when magnetic overlap begins). The current pulse is removed at the completely aligned position. This is done to avoid generation of braking torque (negative torque). As shown later, a significant amount of magnetic saturation can be observed especially around completely aligned position. Because of magnetic saturation, per phase inductance depends not only on the rotor position but also on the amount of current in the stator winding. Equation (5.14) is only valid for unsaturated conditions. Considering saturation, the most accurate way to calculate average power is to rewrite (5.1) as,

$$d\lambda(\theta, i) = (v - iR) dt \quad (5.15)$$

Then multiplying by phase current and integrating over an interval of T , the total average power developed by all *four phases* is given by ,

$$\begin{aligned} P_m &= \text{average power converted to mechanical form} \\ &= \frac{4}{T} \int_0^T i(v - iR) dt \\ &= \frac{4}{T} \int_{\lambda(0)}^{\lambda(T)} i d\lambda \end{aligned} \quad (5.16)$$

The minimum-averaging interval corresponds to one rotor pole pitch, i.e. 60° or $\pi/3$ radians for an 8/6 motor. With the substitution,

$$\omega T = \frac{\pi}{3} \quad (5.17)$$

Equation (5.16) becomes,

$$\begin{aligned} P_m &= \omega \frac{12}{\pi} \int_{\lambda(0)}^{\lambda(\pi/3)} i \, d\lambda \\ T_m &= \frac{P_m}{\omega} = \frac{12}{\pi} \int_{\lambda(0)}^{\lambda(\pi/3)} i \, d\lambda \\ &= \frac{12}{\pi} W \end{aligned} \quad (5.18)$$

Where

$$W = \int_{\lambda(0)}^{\lambda(\pi/3)} i \, d\lambda \quad (5.19)$$

is the work done in moving one pole pitch and is also called as the co-energy. The co-energy W is shown graphically in Figure 5-5.

It is the area enclosed by a plot of current $i(t)$ vs. flux-linkage $\lambda(t)$. No saturation can be observed if the rotor is held constant at completely unaligned position (i.e. in between two stator poles), and increased current will be a straight line (OAE) on $i(t)$ vs. $\lambda(t)$ plot. Saturation is not observed, as the winding reluctance (mainly due to the air) is at maximum possible value. With rotor held at completely aligned position, $i(t)$ vs. $\lambda(t)$ will follow the path OCF. Since the winding reluctance is at minimum possible value, saturation can be observed.

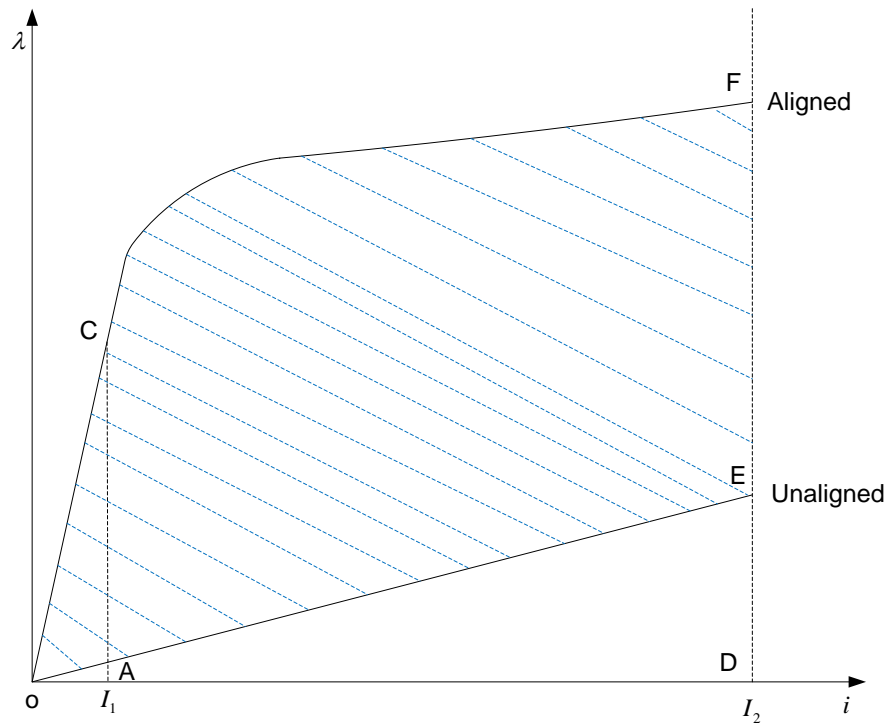


Figure 5-5: Flux-Linkage Vs Current Plot.

Now suppose the rotor pole is at completely unaligned position and current (I_2) is applied to the adjacent stator coil. Since the reluctance is at maximum, current will increase slowly and it will set up magnetic flux. This will cause the rotor pole to move in to minimum reluctance position (i.e. aligned position).

During this rotor movement, graph will follow the path OAE. Full DC voltage is applied across that particular phase such that, by the time rotor moves to the on-set of alignment position, stator current will rise to the required (or rated) value. At point E (at on-set of alignment), magnetic overlap will start i.e. the rotor pole will start aligning with the stator pole. Now from point E to point F, the current can be held constant to the desired value to produce desired torque during the increasing inductance region. Point F is the fully aligned position. At this point, both the switches are turned OFF. As there is still current in the phase winding, negative DC voltage needs to be applied through the bypass diodes. Current will start decreasing and it will follow FCO path. If there is still current at complete alignment position, reversed back-EMF will reduce current more rapidly. During alignment, due to the low reluctance saturation can be observed (path FCO). For a given peak current, maximum torque that can be produced is determined by the area between the aligned and unaligned flux linkage curves (OAEFCO).

In general, the average torque produced over one revolution is,

$$T_{avg} = q \frac{W}{\alpha_r} \quad (5.20)$$

Here, q is the number of phases and W is the co-energy. In general, control of the switched reluctance motor requires; when to turn on the switches (i.e. an advance

angle), when to turn off the switches (i.e. dwell angle), and amount of current (current regulator set point I_{set}).

Next chapter describes this SRM control especially high speed control. Switched Reluctance Drives Limited holds a number of patents (including high speed control) on different SRM control strategies. Interested readers can refer to [53], [54], [55], [56], [57], [58].

6 LITERATURE REVIEW – SWITCHED RELUCTANCE MOTOR CONTROL

Control requirements for four-quadrant operation can only be met by high-speed real-time controllers which operate with phase currents directly. Desired average torque can be obtained by controlling when the current pulse is applied, when the current pulse is removed and how much current is applied. This can be done by setting an advance angle θ_{adv} , a dwell angle θ_{dwell} and a current regulator set point i_{set} [15], [12], [11]. For an advance angle and a dwell angle selection, the point at which magnetic overlap starts is taken as a reference point. This is the point at which stator pole and rotor pole are at the on-set of alignment. Since it takes finite amount of time for current to rise (due to the winding impedance and back-EMF), the current pulse is applied in advance to this point, such that the current reaches the desired peak value (I_{set}) just before this magnetic overlap position. For example, in Figure 6-1, Phase A can be energized by turning on power electronics switches QA1 and QA2 at an advance angle θ_{adv} . This applies full DC supply voltage across the phase A stator winding. During the constant inductance region, i.e. when the rotor pole is in between two adjacent stator poles, the generated back-EMF $e(\theta, i, \omega) = \omega * \frac{\partial \lambda(\theta, i)}{\partial \theta} = \omega * i * \frac{\partial L(\theta, i)}{\partial \theta}$ is low or zero. So the current rise is rapid, causing increasing magnetic flux to be established in the machine. This region is called the “fluxing” region.

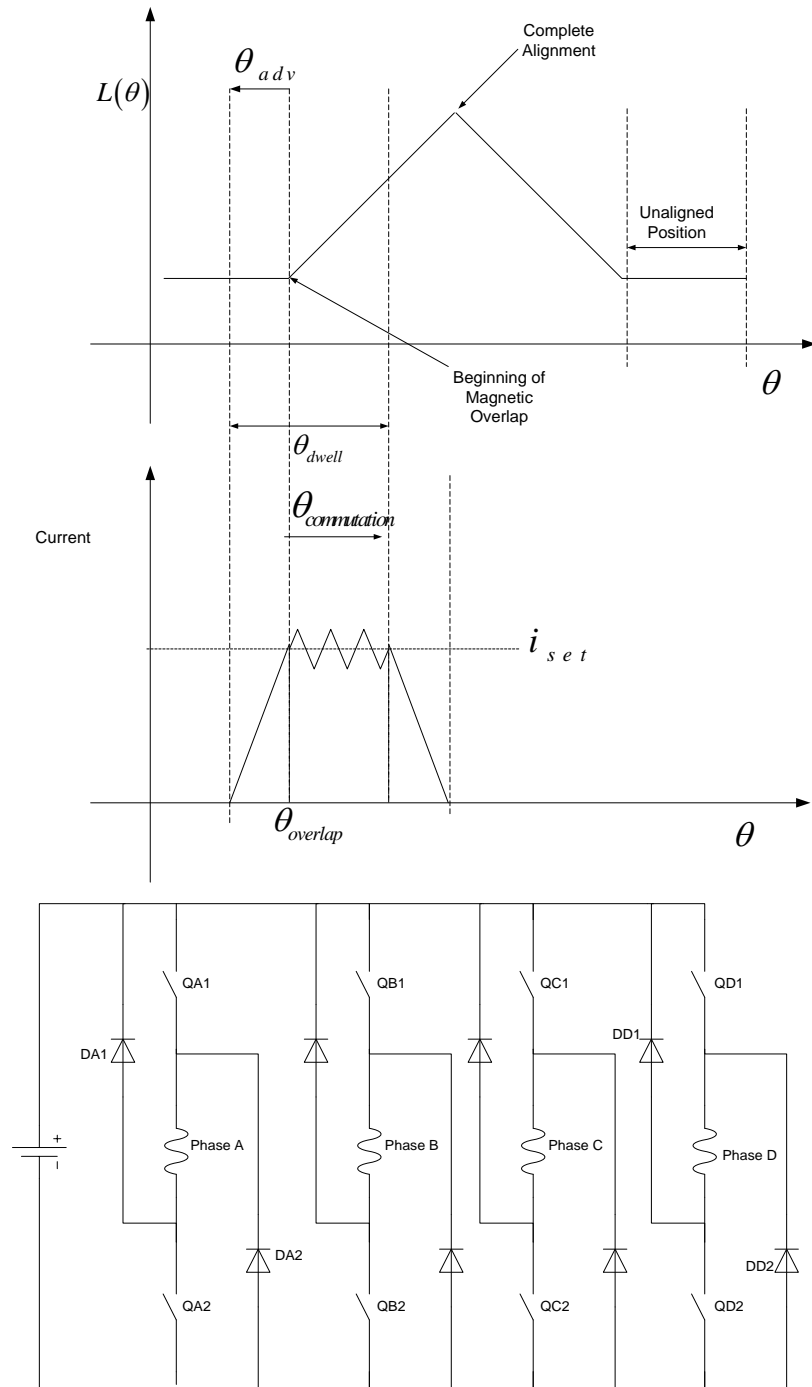


Figure 6-1: Firing Scheme of an 8/6 SRM Motor.

The magnetic flux produced in the air gap acts on the rotor poles to produce a motoring torque. This is due to the tendency of the magnetic circuit to align itself to the minimum reluctance (maximum inductance) position.

As long as the inductance remains nearly constant, there is no or little back-EMF and full supply voltage is available to force the increasing current. When rotor pole starts aligning with the stator pole, rising inductance generates a back-EMF which consumes an increasing portion of the supply voltage. Assuming that the peak current is reached at the on-set of alignment, during magnetic overlap, the phase current has to be controlled to the desired value (or the rated value). Literature [15], suggests that a hysteresis type current regulator can be used.

In a closed loop control system, measured phase current is compared with the current regulator set point. If the measured phase current is more than the current regulator set-point plus the hysteresis band, one of the switches in the pair is turned OFF while other switch is still ON. Turning one switch OFF while remaining switch of that pair is still ON, imposes a zero voltage on the stator winding through one of the bypass diodes. The back-EMF causes the current to decline. When phase current falls below the current regulator set-point minus the hysteresis band, both the switches are turned back ON. This again imposes a full DC voltage and the phase current rises.

Turning one switch ON or OFF while the other switch of that pair is still ON is called as a “soft-switching”. To avoid braking or negative torque, both the switches are usually turned OFF before the complete alignment. At the completely aligned position, the back-

EMF reverses, so if the supply voltage hasn't reversed, current will start increasing again. For this reason, the turn OFF angle or the "commutation angle" at which both switches are turned OFF is before full alignment and is reduced as the speed increases. If the phase current is still flowing at the commutation, the bypass diodes DA1 and DA2 will go on reversing the full supply voltage across the winding. Reversed back-EMF and negative supply voltage will reduce the phase current back to zero. That particular phase remains de-energized with zero voltage across it until the next stroke begins.

The region, in which negative DC voltage is applied through the bypass diodes, is called the "de-fluxing" region. Simultaneously turning both switches across a phase winding OFF is called as a "hard-switching". While the choice of the reference or "zero position" is an arbitrary choice, that choice does affect the numerical values of the advance and commutation angles calculated in the analysis part. The conduction interval, or the dwell angle, is independent of the reference point. Figure 6-1 summarizes this entire operation.

At low speed, chopping the voltage waveform is necessary to control the current as the phase winding usually does not have sufficient impedance or back-EMF to limit stator current.

6.1.1 Low Speed Voltage Control (Voltage PWM)[15],[59]

The simplest way to control the current at low speed is by soft chopping. The voltage control scheme is illustrated in Figure 6-2.

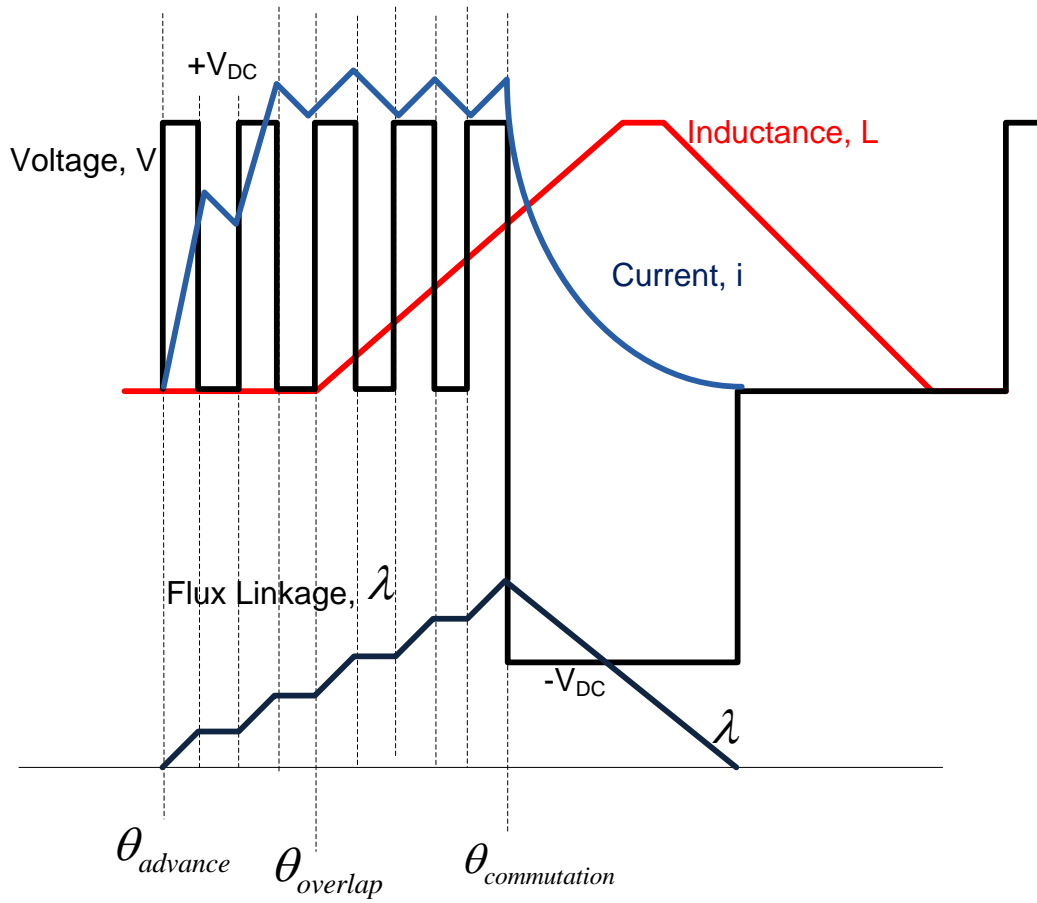


Figure 6-2: Voltage Control (Voltage PWM) [59].

In this scheme, one switch is left ON while the other switch is turned ON and OFF at a higher frequency with a fixed duty cycle $D = \frac{t_{ON}}{T}$. So instead of just controlling the current during magnetic overlap, the duty cycle is kept constant during the entire fluxing region (i.e. for entire dwell period). From the advance angle to the turn OFF angle, fixed duty cycle voltage pulses are applied to the phase winding. During unaligned region, the current increases rapidly. At the turn OFF angle, current is rapidly reduced by turning OFF both the switches, and applying negative DC voltage through the bypass diodes. Instead of soft chopping, hard chopping can also be used to control the current magnitude during the fluxing region but it increases current ripple by a large factor. Soft chopping produces lower acoustic noise, less EMI, and less DC ripple current in the supply and reduces the filter capacitance requirement. In the voltage type control strategy, turn on angle, turn off angle and duty cycle are the main control variables. As speed increases, the duty cycle has to be increased to maintain the current. When this duty cycle D becomes unity, the motor enters into a single pulse high speed operation mode. During soft chopping, the average voltage applied to the phase winding is DVs.

6.1.2 Low Speed Current Control [15],[59]

Most traction drives are current controlled drives [60]. In this type of control strategy, phase is magnetized using full supply voltage. Once the current approaches the set point value, current is controlled around that value by hysteresis type of a control scheme. After turn OFF angle, for de-fluxing, full negative voltage is applied by turning both switches OFF. If the switching frequency is high and sufficient DC voltage is

available, the resulting current waveform is almost like a square wave. Figure 6-3 shows a typical current control strategy.

In current type control, as the supply voltage is fixed, switched ON time decreases as the incremental inductance of the winding increases (i.e. towards the tail end of the magnetic overlap). In this type of control strategy, turn on angle, turn off angle, and current regulator set point are the main control parameters. Once the current reaches a desired value (i_{set}), current can also be controlled around this value by Current Regulated Pulse-Width-Modulation (CRPWM) type control.

More information on CRPWM can be found in [61]. In contrast to the hysteresis type current regulators, CRPWM controllers allow a precise definition of the switching frequency. However, implementation of CRPWM is more complex and it is machine parameter sensitive [62], [63], [64]. Hysteresis type current control is much simpler to implement. In comparison to CRPWM, average switching frequency in hysteresis type control is lower. High frequency chopping, especially towards the tail end of the fluxing region, results in a ripple current component on the DC link which must be supplied by the DC link filter capacitor.

6.1.3 High Speed Single Pulse Control of Switched Reluctance Motors

Since there is no field excitation in the rotor (like permanent magnets or electromagnets), Switched Reluctance Motors do not have a “d-q transformation” or “field oriented” or “field weakening” type control [15]. As the speed increases, at some speed, back-EMF exceeds the supplied DC voltage.

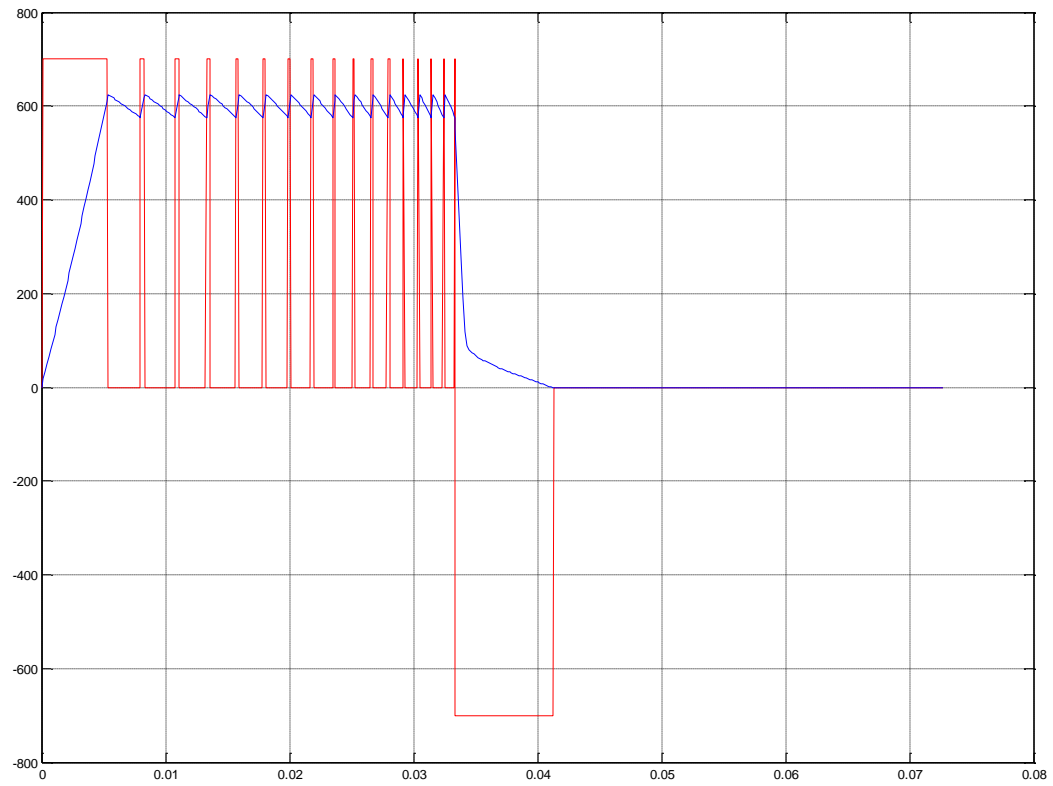


Figure 6-3: Current Type SRM Control.

This speed is also called as a rated speed or the base speed. This base speed is given by,

$$\omega_b = \frac{V_s \beta}{I_{rated} \Delta L} \quad (6.1)$$

When the rotor pole is in between two stator poles, the back-EMF is very low (almost zero). With suitable advance angle, desired current can be reached before magnetic overlap starts. At magnetic overlap (i.e. at the on-set of alignment), back-EMF rises instantaneously. Above base speed, even though the phase current is at the set point value, as the back-EMF exceeds the applied voltage, during magnetic overlap phase current starts decreasing. Therefore the drive operates in a "single-pulse" mode of operation. Figure 6-4 shows a typical "single pulse" high speed operation of a switched reluctance drive. In such a mode of operation, the applied voltage is a square wave as current barely reaches the rated current. After some speed, even with the increased advance angle, current does not reach the rated current value. With speed, peak current decreases. With peak current, developed power decreases, putting a limit on the CPSR. In high speed single pulse mode of operation, control variables are the advance angle and dwell angle.

It is well known that the values of $\theta_{advance}$ and θ_{dwell} can be predetermined using simulations or experiments and stored in the controller memory. Switching angles can be kept constant which results in simple and low-cost control, but drive operating speed range is limited and also it does not optimize the drive efficiency.

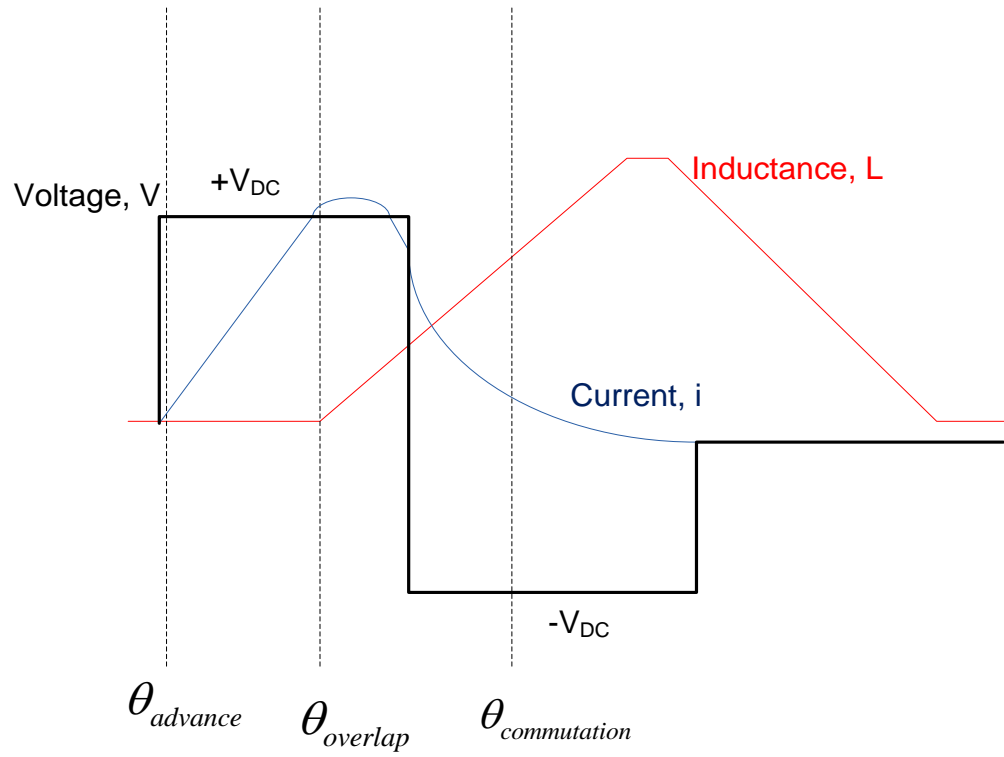


Figure 6-4: Single Pulse High Speed Operation of SRM Motors.

Turn-off angle can also be shifted synchronously with the turn-on angle (dwell angle can be kept constant) while advance angle is changed. Other extreme in realizing traction control is variation of all control variables i.e. advance angle, dwell angle and current set point. Implementation becomes complex. Advance angle can also be calculated in real time, which optimizes the output power and hence efficiency [65]. Large torque oscillations can be observed when the advance angle is changed in increments [61] . This can be avoided if the change is continuous (smaller).

Similar behavior can be observed during the change from one control strategy to another, if a combination of strategies is used to optimize the drive efficiency and drive operating area. Significant research has been done to estimate and optimize these control parameters especially for below base speed operation [59],[15]. The following section lists some of the control methods especially for high speed operation.

6.2 Literature Review – High Speed Single Pulse Control

Switched reluctance motors have three distinct regions of operation [47]. Below base speed, current has to be controlled to the rated value or desired value using voltage pulse width modulation or hysteresis band current control. Above base speed, applied voltage is at the rated value and the current can only be controlled by adjusting advance and dwell angle. In this region, the applied voltage is a square wave and resulting current is a single pulse. When operated with the fixed voltage and fixed switching angles, developed torque falls naturally as ω^2 . By increasing conduction angle in

proportion to speed, torque can be made to fall linearly in an inversely proportional way. As the advance angle is increased, there comes a point where the current pulse occupies half of the α_r . When the fluxing region exceeds $\alpha_r/2$ degrees, resultant current never returns back to zero as the de-fluxing region becomes shorter than the fluxing region. This case is similar to applying a DC voltage to a purely inductive circuit. With each additional stroke, this causes continuous current build up. To avoid this, dwell angle has to be limited to 50% of the stroke length. In the 3rd region of operation, voltage is at the rated value and irrespective of the advance and the dwell angle the current does not reach to the rated value. Current is still in single pulse mode and by keeping advance and dwell angles fixed, the motor can be operated with its intrinsic characteristics. Depending on the motor design, it is still possible to develop rated power even though peak current is below the rated value. However, developed power decreases rapidly and CPSR is limited.

When the rotor pole is in between two stator poles (unaligned region), $\frac{dL}{d\theta} = 0$.

Neglecting resistance R, we have,

$$v = L(\theta) \frac{di}{dt} \quad (6.2)$$

Here $L(\theta) = L_u$ unaligned inductance which is constant in this case, and $v = V_s$ (DC supply voltage, with both switches ON). Therefore,

$$V_s = L_u \frac{di}{dt} \quad (6.3)$$

And $i(0)=0$ i.e. current starts from zero at the beginning of the cycle and returns back to zero. Rewriting the Equation (6.3), we get,

$$\frac{di}{dt} = \frac{V_s}{L_u},$$

$$i(t) = \frac{V_s}{L_u} t \quad (6.4)$$

$$\therefore t = \frac{L_u I_{set}}{V_s}$$

Therefore,

$$\theta = \omega t = \omega \frac{L_u I_{set}}{V_s},$$

Hence the advance angle which guarantees that the required peak current I_{set} is reached at the on-set of alignment is given by,

$$\theta_{adv} = \omega \frac{L_u I_{set}}{V_s} \quad (6.5)$$

Bose [65] and MacMinn [11] have used this formula to calculate the advance angle as speed increases to produce the desired or rated power. This formula neglects the winding resistance and assumes that the back-EMF is zero during the constant inductance region (unaligned region). Since the advance angle has to be limited to the

unaligned region, we have $\theta_{adv} \leq \theta_{unaligned} = \alpha_r - 2\beta$. This puts the limit on the highest speed.

$$\omega \leq \frac{(\alpha_r - 2\beta)V_s}{L_u I_{set}} \quad (6.6)$$

Equation (6.6) gives the maximum attainable speed considering limits on the advancement angle to avoid continuous current. Ray et al. [66] used experiments to calculate the advance angle required to get desired power as a function of speed and load.

Bose et al. [65] used the speed control loop with the inner torque control loop for SRM motors. Figure 6-5 illustrates this control strategy. In this control strategy, speed feedback is compared with the speed command. Generated speed error is then converted to the torque command through the PI controller. This torque command is then converted to the peak current set point. The inner torque control loop is shown in Figure 6-6. Using this current set point, along with the speed feedback and the DC supply voltage feedback, advance angle or a turn ON angle is calculated based on the Equation (6.5). Based on this advance angle, commutation angle or the turn OFF angle is estimated from the predetermined values stored in the memory. Turn OFF angle is first reduced linearly from the maximum allowable angle (which avoids braking torque) to the half of that value. Above base speed turn off angle is kept constant. The relationship between the torque, the phase current, and the firing angles is highly non-linear and vary as functions of speed and load [67] , [15], [65].

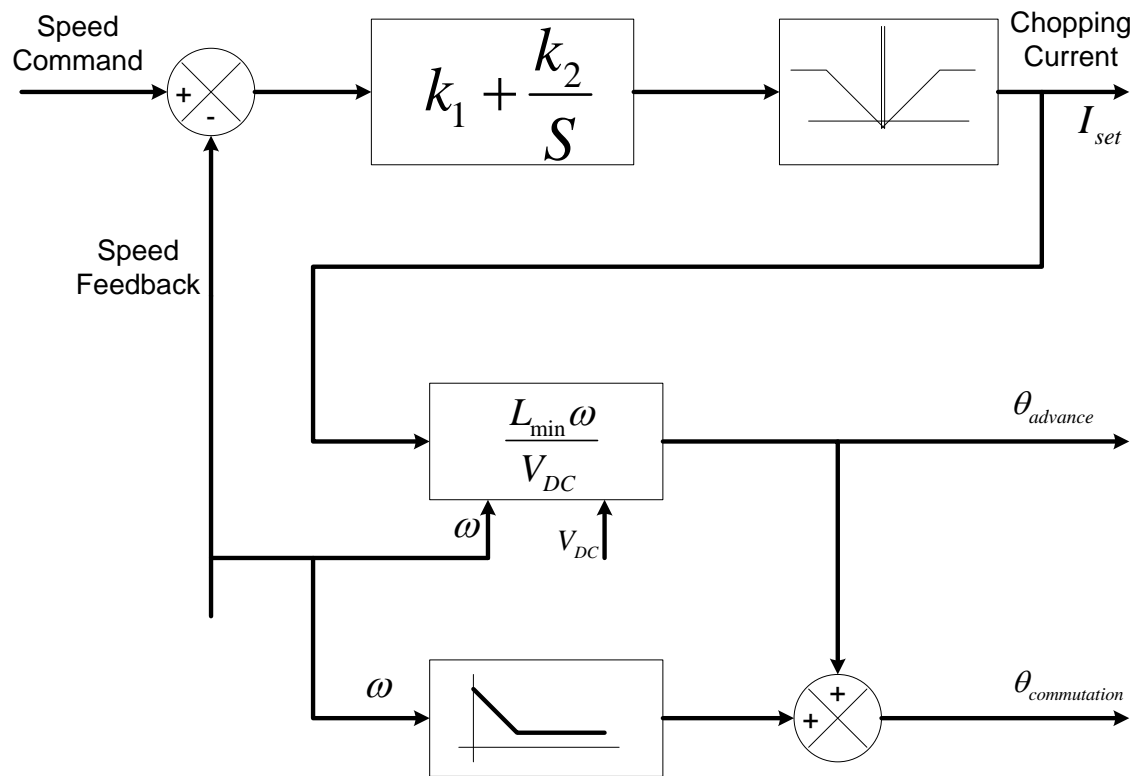


Figure 6-5: Speed Control System for Switched Reluctance Motor Based on [65].

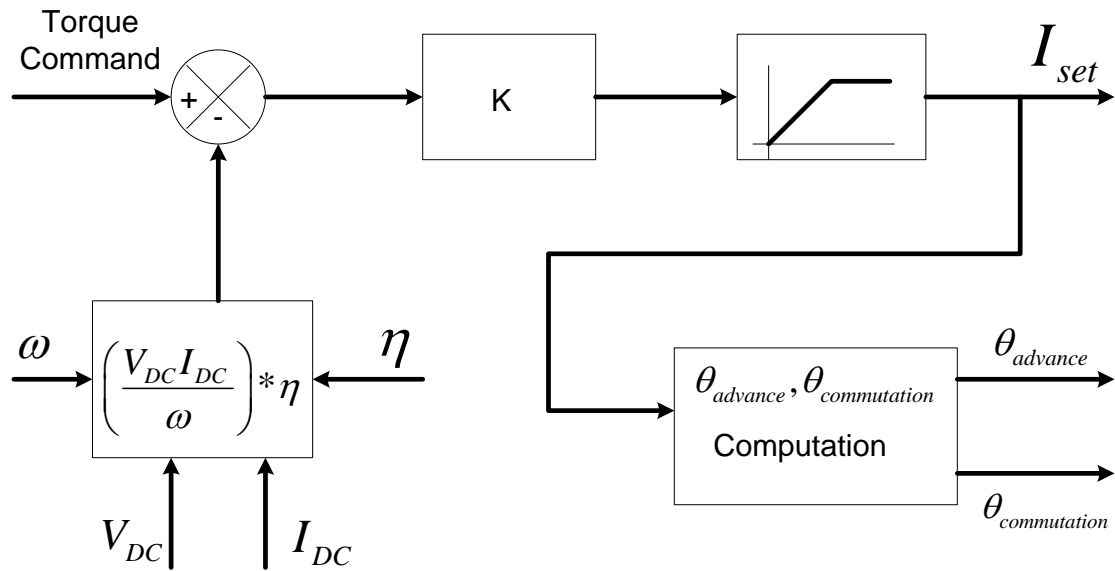


Figure 6-6: Inner Torque Control Loop for Switched Reluctance Motor based on [65].

If the converter efficiency is known, then based on the DC supply voltage, DC current, and the speed feedback, torque can be roughly calculated as follows,

$$T_e = \left(\frac{V_{DC} I_{DC}}{\omega} \right) * \eta \quad (6.7)$$

According to [65], a high gain torque loop inside a speed control loop, linearizes the overall control system. It enhances the speed response and also allows higher controller gains within the stability limits for the speed loop. This method provides better performance than the fixed angle type control strategies.

MacMinn et al.[12],[11] have proposed a closed loop control strategy for a very high speed, starter-generator switched-reluctance aircraft engine. This control method is shown in the Figure 6-7. This control method is very similar to Bose's [65] method except a phase current feedback is added and inner torque control loop is open. Since the torque feedback is not always feasible. Figure 6-8 (taken from [11]) shows the output torque as a function of current regulator set point (I_{set}). Using curve fitting, various values of the current regulator set point as a function of desired output torque can be calculated and stored in the controller memory. These values can be obtained through simulations or through the experiments. Based on the torque requirement, current regulator set point is estimated. Based on this current regulator set point, along with the DC voltage and speed feedback, advance angle is calculated by using Equation (6.5). Turn on angle (advance angle) is advanced such that the phase current

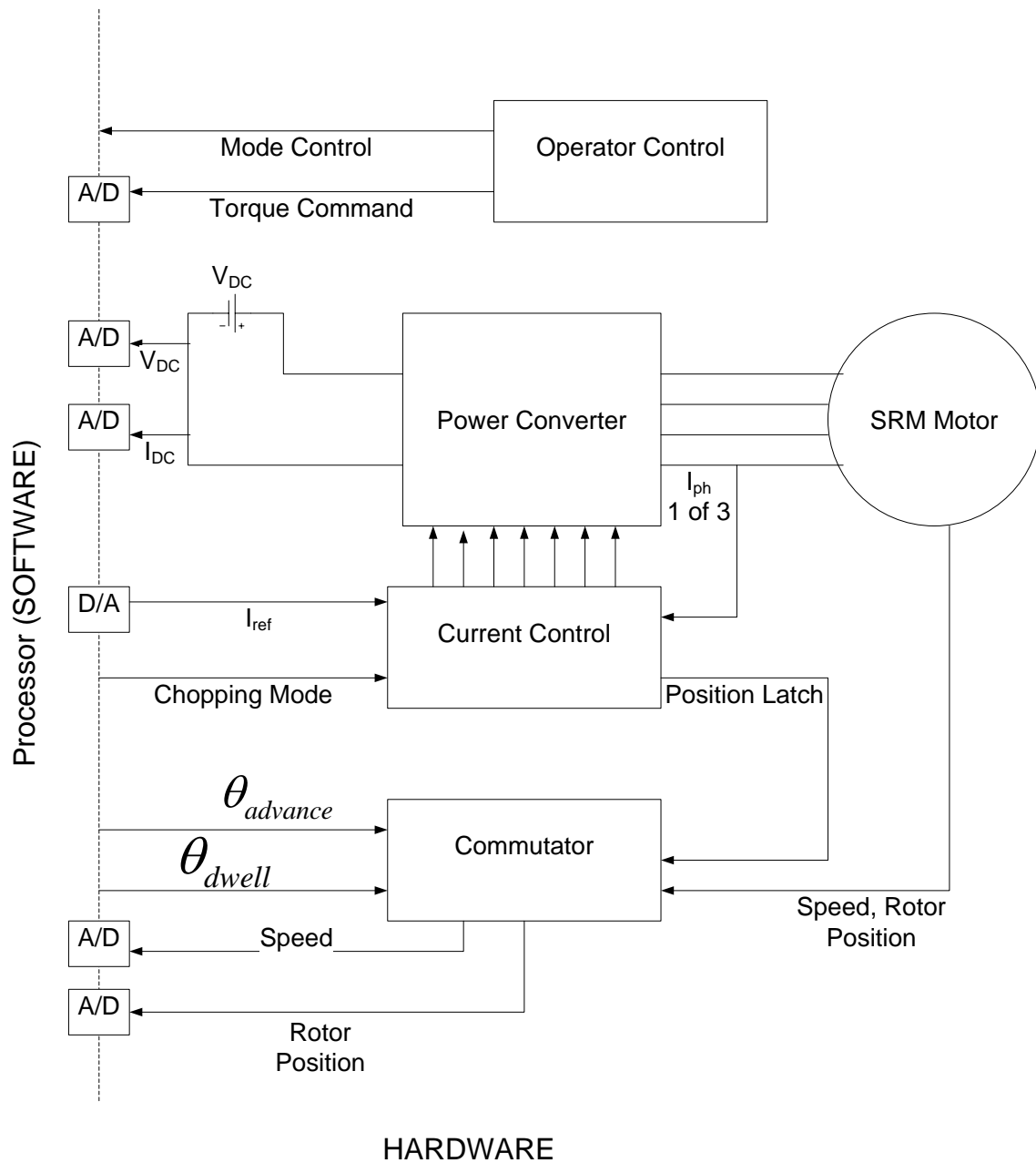


Figure 6-7: Closed Loop High Speed Control Scheme for Switched Reluctance Motor Based on [12],[11].

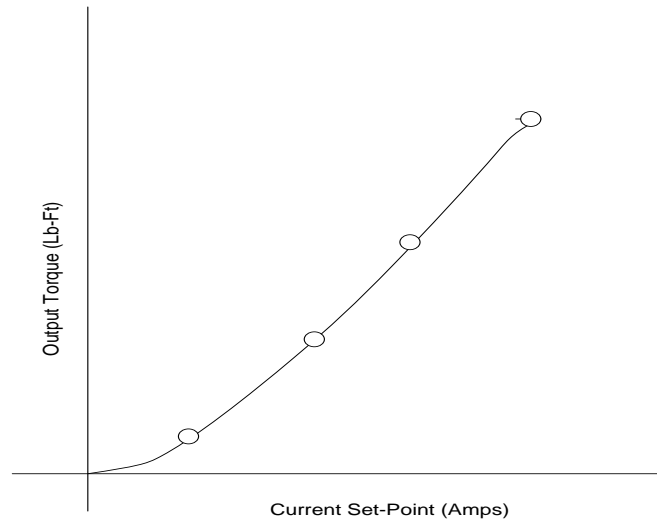


Figure 6-8: Current Regulator Set Point as a Function of Output Torque [11].

reaches the commanded value (which produce desired torque) at the on-set of magnetic overlap position.

The advance angle controller is shown in Figure 6-9. Advance angle control loop makes sure that the set point peak current is reached at the on-set magnetic overlap position. For this control strategy, entire motor speed range was divided into two categories: First is the low speed range where maximum current can be attained and the second is the high speed region where back-EMF is so high that the maximum current cannot be attained. In the second region, the current set-point is fixed to the rated value and motor torque is controlled by controlling the advance angle and turn OFF angle. Figure 6-10 shows this high speed SRM control strategy.

According to [11], in this high speed control strategy, dwell angle (θ_{dwell}) regulates the output torque and the turn on angle ($\theta_{advance}$) regulates the machine efficiency. For the second region operation (high speed, single pulse) MacMinn et al. used curve fitting methods to formulate the equations to estimate an advance and dwell angle from the torque command [11].

$$\begin{aligned}\theta_{dwell} &= G_1 T_{command} \omega^n - G_2 V_{DC} + G_3 \\ \theta_{advance} &= G_4 \theta_{dwell} - G_5 V_{DC} \theta_{dwell} - G_6 V_{DC} + G_7 \omega + G_8\end{aligned}\tag{6.8}$$

Here, constants G_4, G_5 and G_6 were chosen such that, with constant θ_{dwell} , $\theta_{advance}$ will decrease with increase in V_{DC} while, with constant V_{DC} , $\theta_{advance}$ will increase with increase in θ_{dwell} .

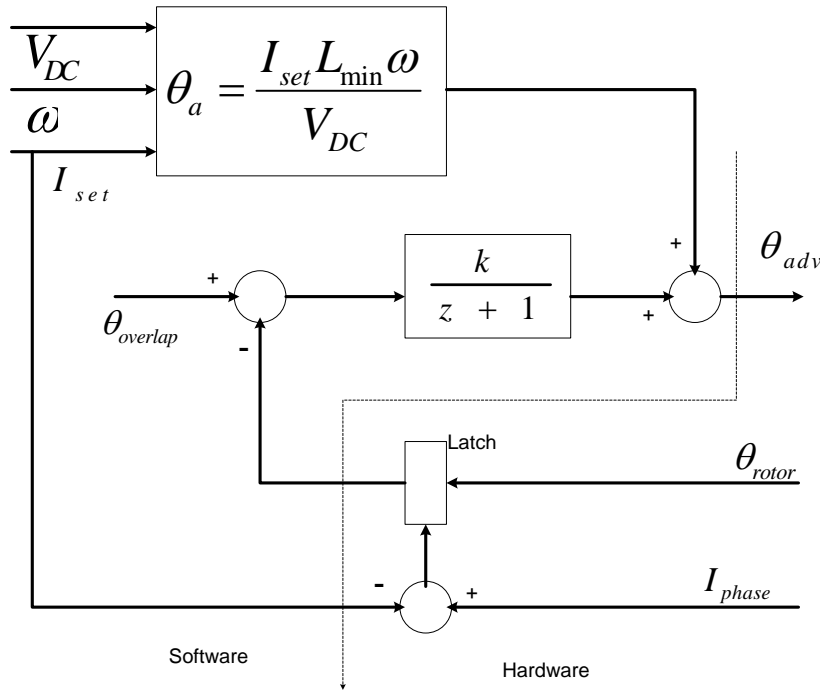


Figure 6-9: Advance Angle Estimation [11].

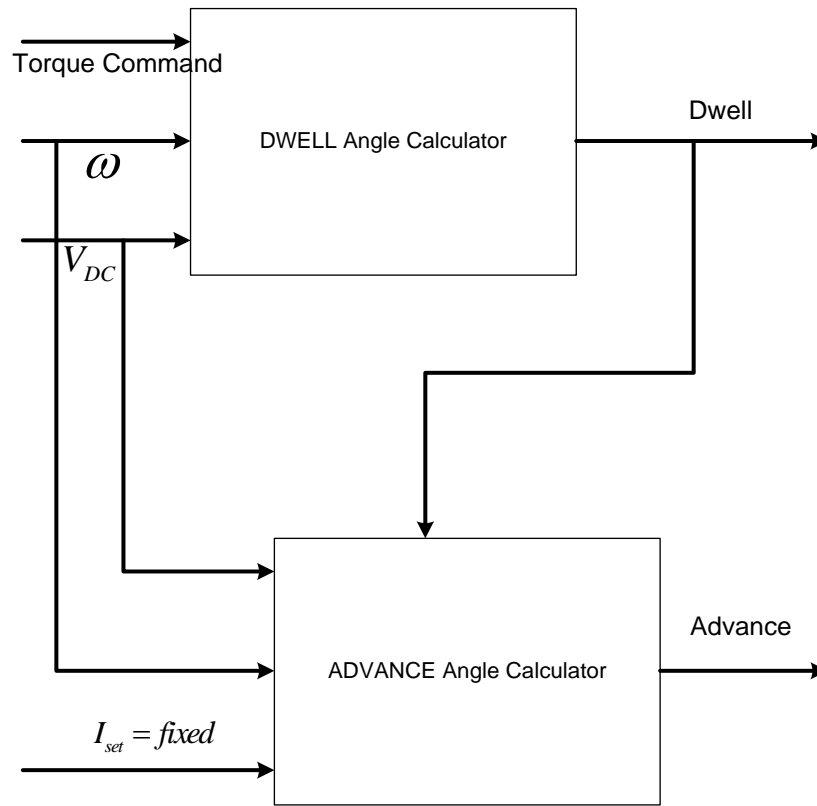


Figure 6-10: High Speed SRM Control Based on [11].

According to Fahimi et al. [67], [68]; the constant power region or high speed region starts when the back EMF exceeds the effective DC bus voltage and ends when the continuous conduction starts i.e. required dwell angle to produce desired torque is at 50% of the stroke length. To optimize the torque-per-amp, one should adjust the turn ON instance ($\theta_{advance}$) such that the peak current matches the position at which maximum torque occurs. Fahimi et al. suggested advancing the turn-on instance from an unaligned position using following equation [67], [68],

$$\Delta\theta = \frac{L_u I_{\max} \omega}{V_s} - \left(\frac{\pi}{N_r} - \left(\min(\beta_s, \beta_r) + \frac{|\beta_s - \beta_r|}{2} \right) \right) \quad (6.9)$$

[67] claims that the control strategy which uses above equation (described in the reference [68]), allows operation to speeds as high as 6 times the base speed. This paper also describes a sensorless control of SRM at super high speeds.

In single pulse motoring operation, build-up of the flux linkage is governed by the Faraday's Law [4], [69].

$$\lambda_{peak} = \frac{1}{\omega} \int_{\theta_{ON}}^{\theta_{OFF}} (V_{DC} - Ri) d\theta + \lambda_0 \quad (6.10)$$

Neglecting phase winding resistance and assuming that it is discontinuous conduction i.e. at the end of de-fluxing region, current and flux-linkage is reduced to zero value (i.e. $\lambda_0 = 0$), we have,

$$\lambda_{peak} = \frac{V_{DC}}{\omega} \theta_{dwell} \quad (6.11)$$

As the peak value of the flux-linkage decides the iron loss in the motor, dwell has to be kept to the minimum [69]. Equation (6.5) guarantees that the peak current is reached at the on-set of alignment. In unaligned inductance region, as the back-EMF is almost zero, current rise is linear ($di/dt = V_{DC}/L_u$). Current in the flat inductance region does not contribute to the torque production whereas it increases the copper loss in the motor. Moving the current closer the magnetic overlap position will reduce the copper loss but to produce the same torque, the dwell has to be increased. Increased dwell increases the peak value of the flux-linkage. Kioskeridis et al. [69], claim to have optimized the turn ON and turn OFF angles for high speed single-pulse operation by finding the best balance between copper loss and iron loss, i.e. between the minimum dwell and the minimum advance angle. These values were determined using simulations and by carrying out experiments. The SRM motor was rotated at a constant speed and at a constant torque and the advance angle and the dwell angle was changed to find out the best combination by measuring losses at each of those points. Kim et al. in [70], describe a scheme for advance angle estimation for a single-pulse high speed operation. To find out the turn ON angle which results in the maximum efficiency, 3D characteristics of the estimated motor efficiency and torque as a function of the advance and the commutation angle was investigated using extensive simulations. First for a given speed, a set of combinations of the advance angle and the commutation angle which produces same torque was calculated. From that set a combination which results

in maximum efficiency was then identified and recorded. According to [70] efficiency is more sensitive to the advance angle than to the turn OFF angle.

All of the above mentioned SRM control strategies are of discontinuous type. Meaning, at the beginning of the fluxing region (i.e. when the DC voltage is applied), phase current starts from the zero and at the end of de-fluxing region (i.e. when the negative DC supply voltage is applied), it returns back to the zero. Above base speed, back – EMF, whose magnitude increases as the speed increases, exceeds the applied DC voltage. Therefore the peak current decreases. With the peak current, co-energy area decreases and hence the developed power reduces below the rated power. With discontinuous type conduction, speeds as high as 6 times the base speed can be achieved which means CPSR is limited to 6:1 [68].

According to Yahia [71], CPSR increases with the increase in the magnetic saliency ratio i.e. the ratio of the aligned inductance to the unaligned inductance. CPSR and output power also increases with the increase in the duration of inductance rise [71]. Morel [72] and Vujcic [73] lists the machine parameters that can be changed to achieve wider constant power range.

Another way to increase the CPSR is by allowing continuous conduction. When the conduction angle (dwell) is more than the half of the total cycle, current and flux-linkage fail to return back to the zero as the de-fluxing region is less than the fluxing region. So with each cycle, progressive growth of the current and the flux-linkage occurs resulting in an unstable condition. Once the current has grown to the desired or rated value, it

can be controlled by keeping the fluxing region exactly equal to half of the cycle (i.e. one stroke, in an 8/6 motor: 60°). If the de-fluxing region is maintained to the remaining half of the stroke length, this growth can be sustained. This allows the motor to produce the rated torque at much higher speeds.

Switched Reluctance Drives Limited has patents (US 5469039, US 5545964, US 5563488) on continuous conduction mainly for switched reluctance generators. According to these patents, turn OFF angle is kept almost constant (it is decreased a little bit as speed increases). Turn ON is initially changed such that it results in the current growth from stroke to stroke. Once the desired peak current is reached, a feedback control loop keeps the turn ON angle constant. If the load current is increased, resultant error, through the PI controller causes the advance angle to increase. Since turn OFF (or commutation) angle is constant, this increases fluxing region (dwell angle). Resultant flux build-up causes increase in the peak current. Once the current rises above new required set point, advance angle decreases back and stabilizes to a new equilibrium point. As described in the next chapter, peak current set point can be used to regulate the output power but for a given speed and the dwell angle, advance angle can be changed to maximize the output power rather than to regulate the output power.

According to Korkosz et al. [74], by careful selection of control angles, with continuous conduction, the rated power can be produced for a wide speed range. Although this paper fails to elaborate the requirements on the dwell angle to initiate and maintain the continuous conduction and the control method used/needed to stabilize the current growth once continuous conduction is initiated. The paper provides the data from

simulations as well as experiment based results with mild continuous conduction. According to the author, the advance angle does not depend on the speed and once a certain speed is exceeded, phase current can stabilize itself during continuous conduction [69]. Authors of that paper used polar calculations and ANSYS to obtain the coefficients of the differential equations to implement the SRM motor model.

Rekik [75] used following torque control loop to stabilize the continuous conduction. Figure 6-11 illustrates the same. Here, torque command is converted to a current command. This current is then compared to the actual motor current and the error is converted to a dwell angle deviation command through the PI controller.

This difference is then added to the dwell angle necessary to initiate and maintain continuous conduction. From the steady state, if the torque command is stepped up, dwell angle will be increased, which increases fluxing region. This leads to the progressive growth of the phase current. Increased current in turn increases the output torque. According to [75], by this method, twice the rated torque can be developed without exceeding the rated current. Rekik et al. claim that the resultant RMS current can be kept constant to the rated value, independent of the speed. Since with the continuous conduction twice the rated torque can be produced, transient over-torque can be provided in the field-weakening operation for a fixed DC voltage. Interested readers can find more information about this control strategy in [16]. This paper also lists the advantages of a switched reluctance motor when operated in the field-weakening zone, with and without continuous conduction mode, over the induction and the surface permanent magnet motors.

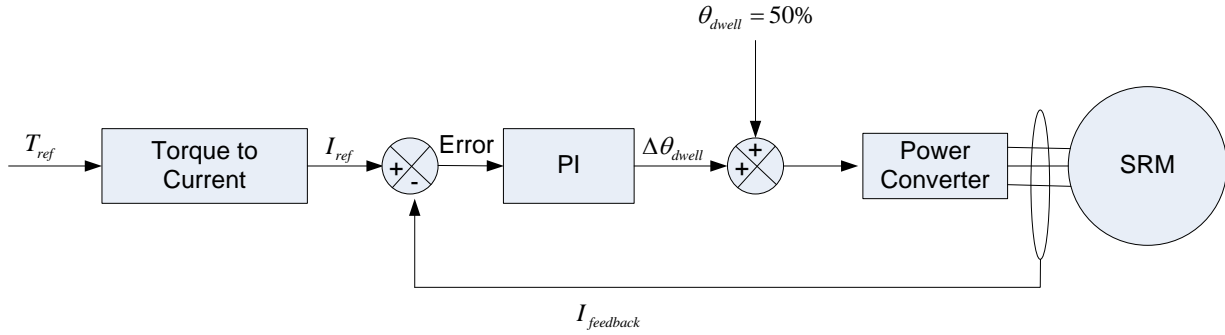


Figure 6-11: Closed Loop Torque Control Loop for Continuous Conduction Based on [75].

Long et. al. [76] and Rekik et al. [75], suggested that for a machine operating with conventional discontinuous current, extended speed operation can be achieved by reducing the number of turns per pole, but this reduces torque-per-amp at or below the base speed. At extended speeds, reducing the number of turns per pole reduces the effective the back EMF. It allows an improvement in the power capability within the DC link voltage constraint. According to Long et al., continuous phase current excitation enhances the extended power capability at extended speeds without significantly compromising the system or machine efficiencies [76]. Machines with continuous current can be designed with more number of turns per pole to increase the torque-per-amp at or below base speed. This reduces the inverter current rating and hence silicon requirement [76].

In continuous conduction, phase current starts from a non-zero value and grows with every stroke. As described earlier, this phenomenon can be controlled. In SRDL patents, as described earlier, growing phase current is controlled to the desired value,

by changing the advance angle with turn OFF angle almost fixed. In the references [75] and [16], phase current is controlled by changing the dwell angle while the advance angle is just used to maximize the efficiency. In both of these continuous conduction type control methods, dwell angle is changed (50% +) to regulate the output power. Literature available on these two continuous conduction type control schemes does not give any details on what is the continuous conduction, how it is initiated, how the current growth is stabilized, what is the relationship between developed output power and control / machine parameters, what happens to the average current and what are the key parameters. The primary goal of this research was to answer these questions. Next chapter describes the analysis of continuous conduction using linear magnetic model.

7 CONTINUOUS CONDUCTION ANALYSIS AND SIMULATION RESULTS

The continuous conduction type control scheme discussed here is very similar to that typically used to control low speed operation (i.e. discontinuous conduction mode type control). The relevant control quantities are the advance angle, the dwell angle and the current regulator set point. It is shown that the dwell angle is the key factor and must be sufficiently large to sustain the continuous conduction, but excessive values are shown to reduce the motor efficiency. Advance angle is then set at an “optimum” value that maximizes energy conversion and control of the developed power is achieved by raising/lowering the peak current regulator set point. This control results in the developed power that is directly proportional to the motor current magnitude, achieving good efficiency at partial as well as full load conditions. Dynamic response can be sluggish when the dwell is set at the minimum value necessary to support the continuous conduction for steady state operation. A sophisticated controller that will widen the dwell during transient intervals in order to improve speed of response and then collapse the dwell to minimum requirement during steady speed operation can resolve this potential problem. The remainder of this chapter is organized in six sections. Section 7.1 contains a description of the parameters of an example SRM motor intended for a 26:1 CPSR application that is used as an illustration throughout the chapter. This section also reviews the linear model theory predicting an infinite CPSR for the SRM operating in continuous conduction. If the speed sensitive losses are

ignored, linear magnetic model predicts that the CPSR of the SRM motor can be infinite when the continuous conduction type high speed control scheme is used [13]. A linear magnetic model does not provide accurate results for analyzing low speed performance, but it has been shown to be accurate in predicting high-speed performance of switched reluctance motor in continuous as well as discontinuous conduction mode [13]. Section 7.2 describes different simulation models of the example motor. Section 7.3 provides the simulation results for the continuous conduction type control scheme. Section 7.4 and 7.5 describe the mathematical analysis of the example motor when continuous conduction type control scheme is used for the operation of the SRM motor in the constant power region. This mathematical analysis tries to answer some of the questions like how SRM goes into the continuous conduction, how the current growth is contained, which control and machine design parameters affect the output power and resultant average current, what happens to the average current and some insight into the continuous conduction based SRM controller. For verification purpose, the simulation results have been compared with the analytical results.

7.1 Example Motor Model

Data for the example motor was obtained by using a program [77] designed by the Oak Ridge National Laboratory. The motor is a four phase 8/6 SRM design. Flux linkage data obtained from the design program for one phase is displayed in the Figure 7-1, and Figure 7-2. The data has been displayed for one pole pitch which is 60° for an 8/6 machine. The flux linkage data for this phase would repeat itself in each 60° interval.

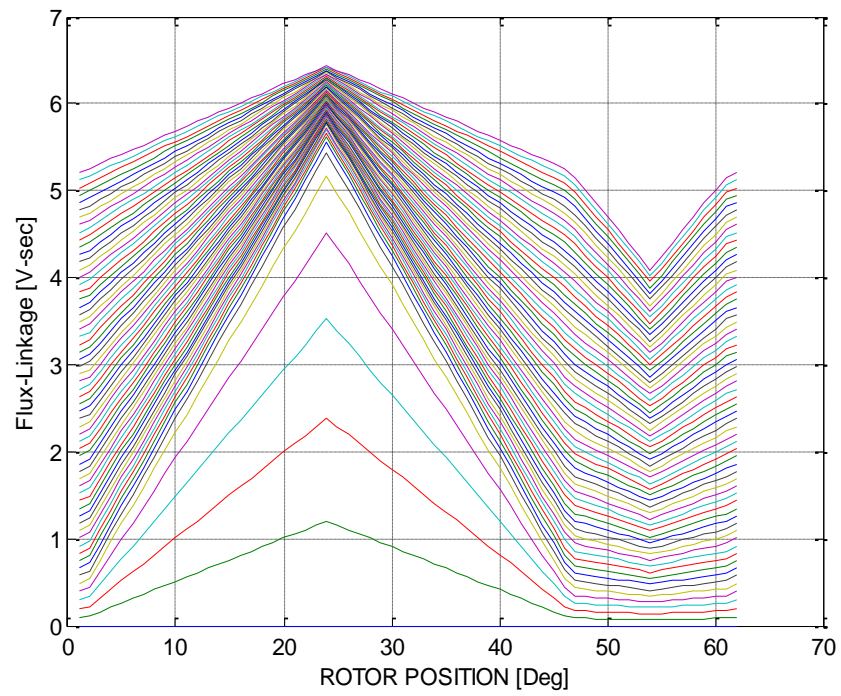


Figure 7-1: Flux-Linkage Vs Rotor Position Plot for the Example SRM Motor.

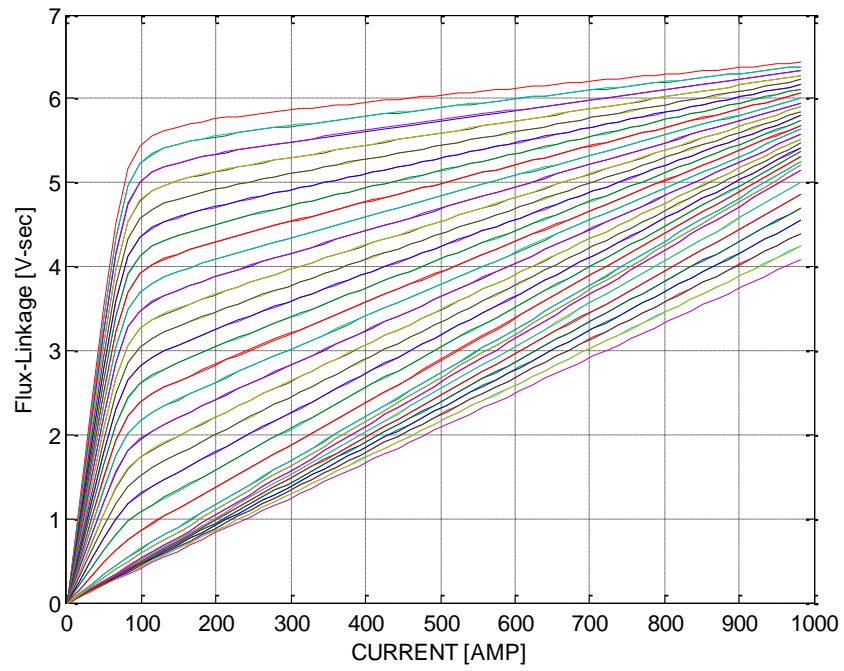


Figure 7-2: Flux-Linkage Vs Current plot for the Example Motor.

Flux linkage data for the other three phases can be generated by delaying the data in Figure 7-3 by 15° , 30° and 45° . Flux linkages values dependent on both the rotor position and the winding current. In Figure 7-1, the flux linkages are plotted versus rotor position, in one degree increments, with winding current as a parameter. The winding current varies from 0 to 983.607 amps in the steps of 16.394 amperes. The peak of the flux linkage curves occurs at 22.5° which is the “completely aligned” position while the minimum flux linkage occurs at 52.5° which is the “completely unaligned” position. In this position the rotor pole is exactly in between two adjacent stator poles. The “zero degree” position has been chosen corresponding to the condition where the rotor and stator poles are “point-to-point” i.e. at the onset of alignment or the on-set of magnetic/physical overlap. In Figure 7-2 data is displayed with the rotor position as parameter. Rotor position is varied from 0° to 60° in the steps of 1° . In Figure 7-3, saturation can be observed for the currents greater than 300A during magnetic overlap.

7.1.1 Nomenclature and Parameters of the Example Motor

N_b = Base Speed (250 RPM), R = Winding Resistance Per Phase (0.014Ω), I_p = Peak Current (650 A), I_{rms} = Rated RMS Current (450 A), P_r = Rated Power (320 HP), CPSR = 26 (Top Speed 6500 RPM), L_a = inductance in aligned position (73.38mH), L_u = inductance in the unaligned position (4.15mH), $\Delta L = L_a - L_u = (69.23\text{mH})$, β = pole arc (22.5°), α_r = pole pitch (60), θ_{adv} = advance angle, V_s = DC supply voltage (700 V).

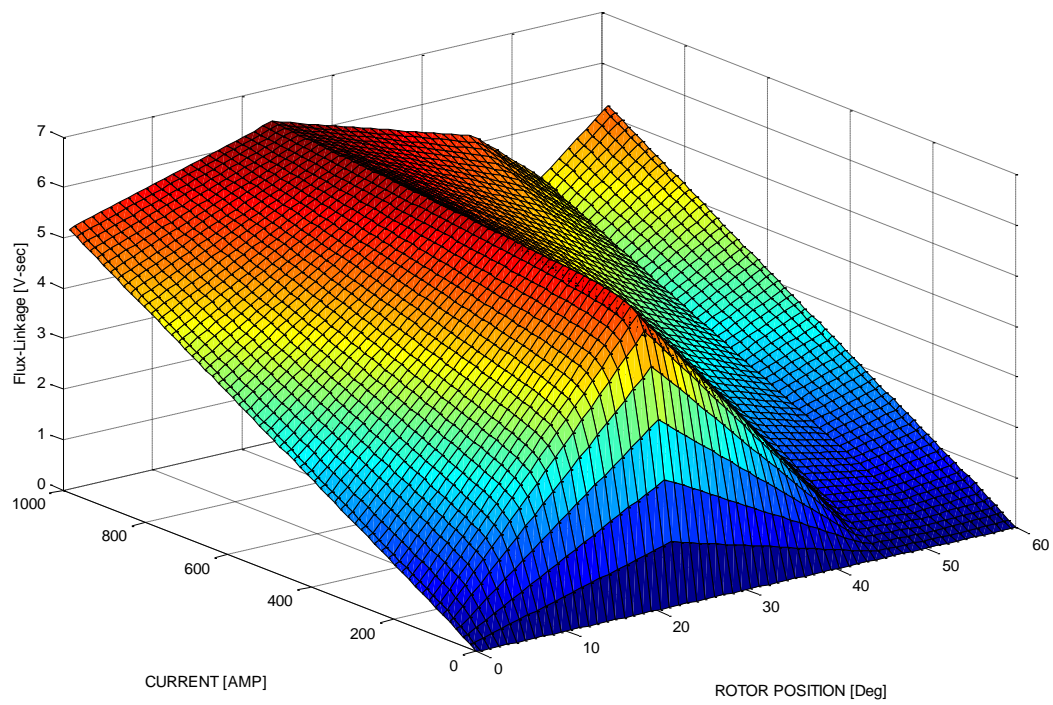


Figure 7-3: Example Motor Data.

7.2 Example Motor Analysis

It is assumed that the SRM is driven by a voltage source inverter (VSI) whose topology is shown in the Figure 5-2. To use a reference other than the on-set of alignment position (as shown in Figure 6-1) would simply involve adding a fixed constant to the values of advance and commutation angles derived in this chapter. For the example motor with a peak current of 600 amps, the maximum co-energy area is shown in the Figure 7-4. The enclosed area is 2472 joules. Applying Equation (5.18), the maximum torque that could possibly be developed with a peak current of 600 amps is 9442 Nm. If this torque can be developed at the specified base speed of 250 rpm then the developed power would be 247.2 kW or 331.4 hp. The ability to operate at this torque and the power level at the specified base speed will depend on having an adequate DC supply voltage.

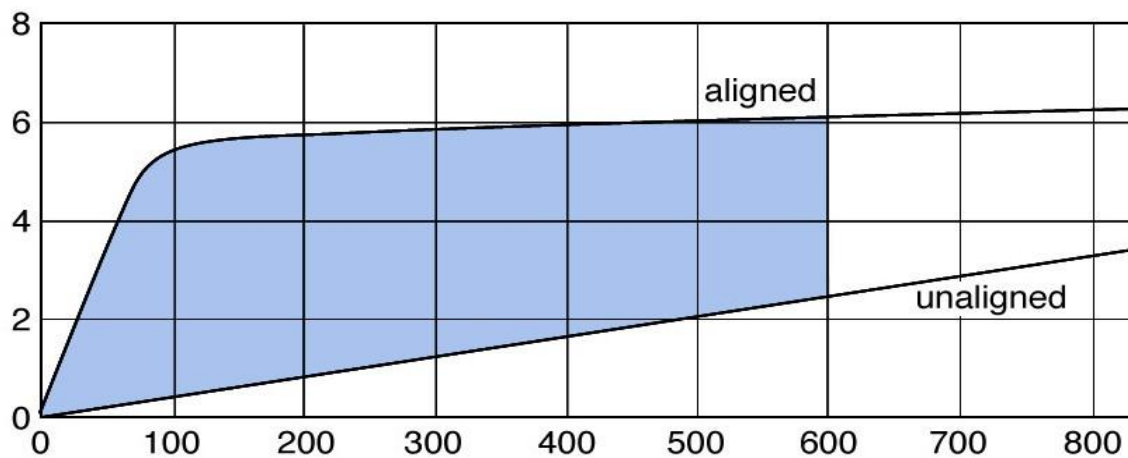


Figure 7-4: Maximum Co-Energy of the Example Motor with Peak Current of 600A.

7.2.1 Linear Model

For flux-linkages, we have,

$$\lambda(\theta, i) = l(\theta, i) * i \quad (7.1)$$

Ignoring saturation we have,

$$\lambda(\theta) = L(\theta) * i \quad (7.2)$$

For linear mode it is assumed that the flux-linkages only depend on the rotor position and not the current level. Another way to determine the flux-linkages is,

$$\lambda = \int (V_s - iR) dt \quad (7.3)$$

Using above equations for flux-linkages, the motor current can be calculated by the following equation.

$$i = \frac{\int (V_s - iR) dt}{L(\theta)} \quad (7.4)$$

So based on the DC supply voltage information, along with per phase winding resistance and per phase winding inductance information, it is possible to estimate the phase current. For a linear model which ignores saturation, per phase inductance information can be obtained by dividing the flux linkage data in Figure 7-3 by the

corresponding current. The linear inductance profile for the example model over one pole pitch is shown in the Figure 7-5. This graph was obtained by the division of the flux-linkage data by the corresponding current (16.393 A). Note that the inductance during the unaligned region is not perfectly flat. An idealized linear inductance profile having a constant inductance in the unaligned zone was developed using Matlab and Simulink to carry out the continuous conduction analysis and simulations for high-speed operation. First part of the Figure 7-6 shows this flat unaligned inductance profile while second part shows non-flat (similar to the actual example motor profile) unaligned inductance profile. Figure 7-7 shows the Simulink based linear model which uses this linear per phase inductance profile.

7.2.2 Nonlinear Model

Considering current dependent saturation, phase current can be estimated as follows,

$$i = \frac{\int (V_s - iR) dt}{L(\theta, i)} \quad (7.5)$$

Here per phase inductance profile not only depends on the rotor position, it also depends on the phase current. Inductance profile needed for the above equation can be obtained by dividing the flux-linkage data of Figure 7-3 by the current for a fixed rotor angle. Figure 7-8 shows this resultant per phase inductance profile which incorporates the current dependence. Figure 7-9 shows the Simulink based non-linear model developed to carry out simulations for comparison with the linear model at high speed.

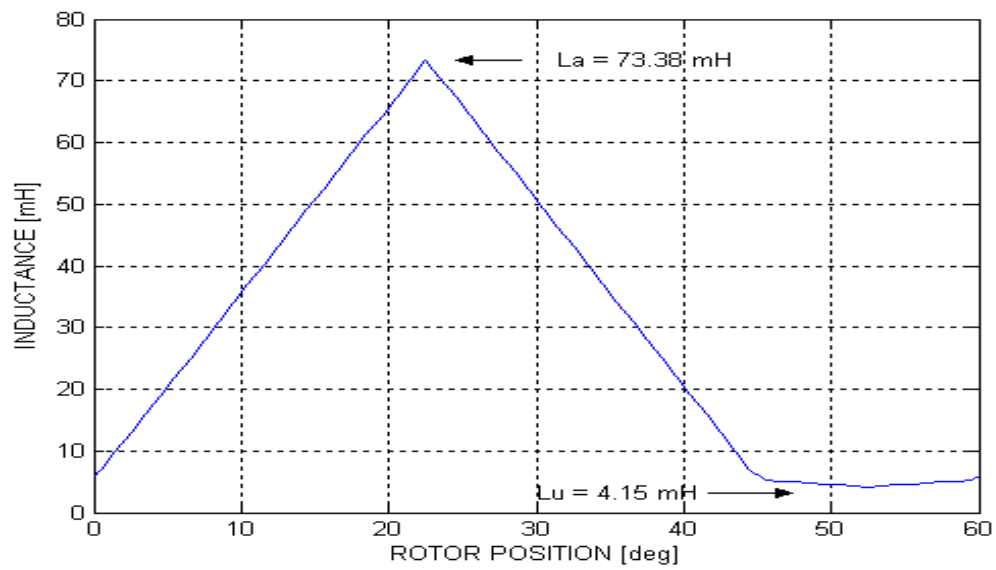


Figure 7-5: Linear Magnetic Model of the Example Motor.

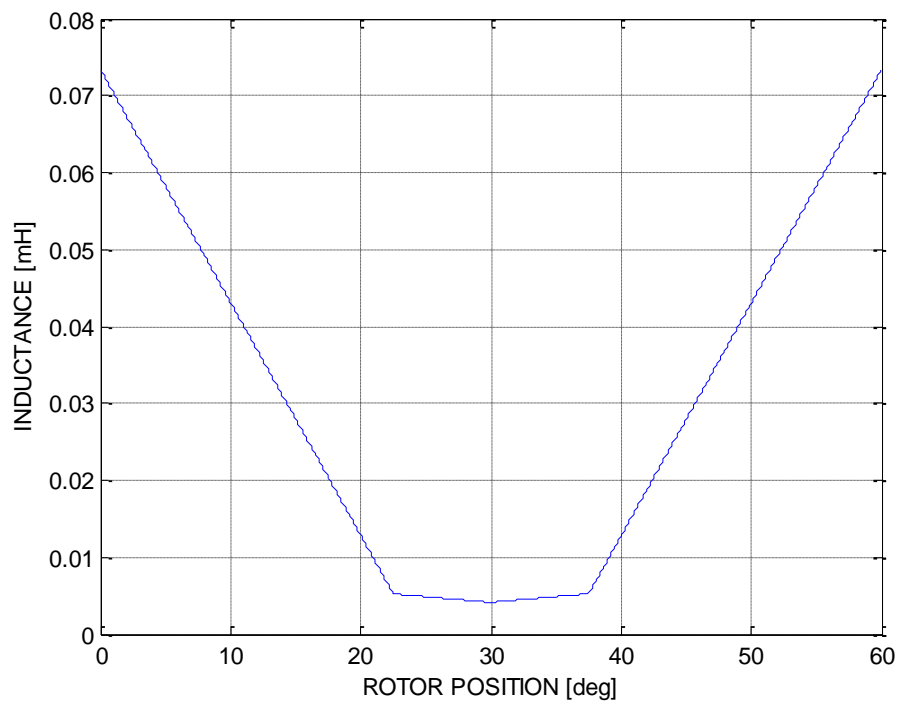
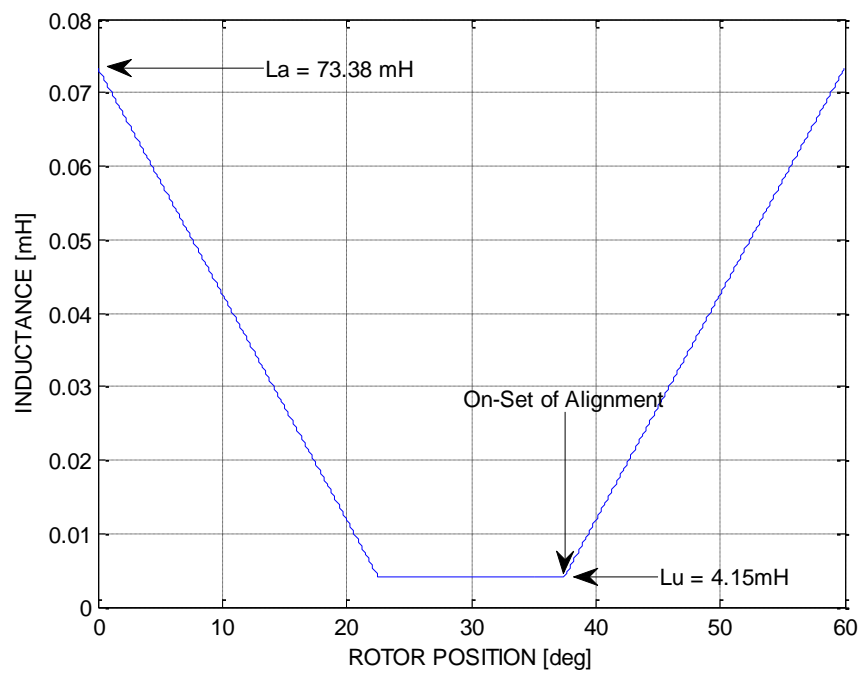


Figure 7-6: Linear Inductance Profile of the Example Motor.

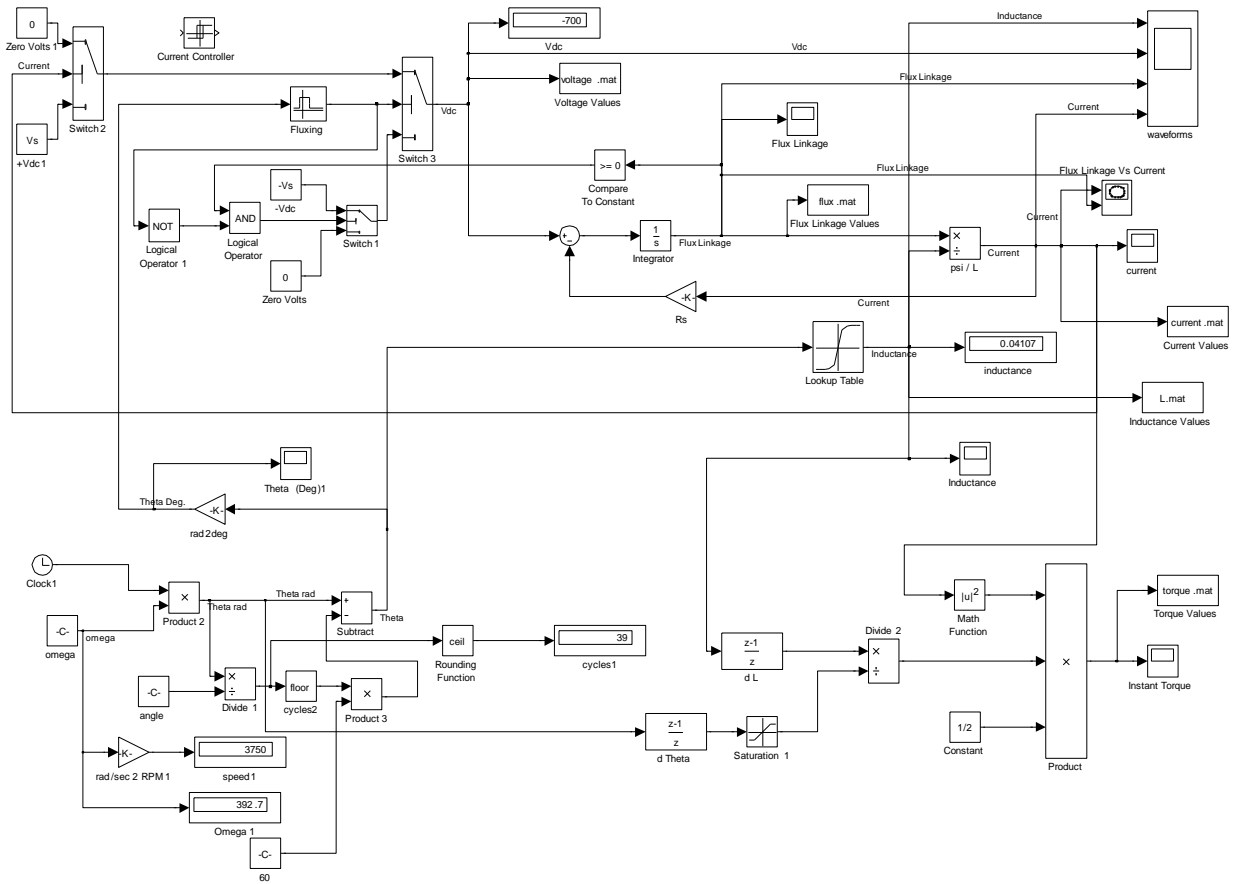


Figure 7-7: Simulink Model for the Example Motor [L(θ)].

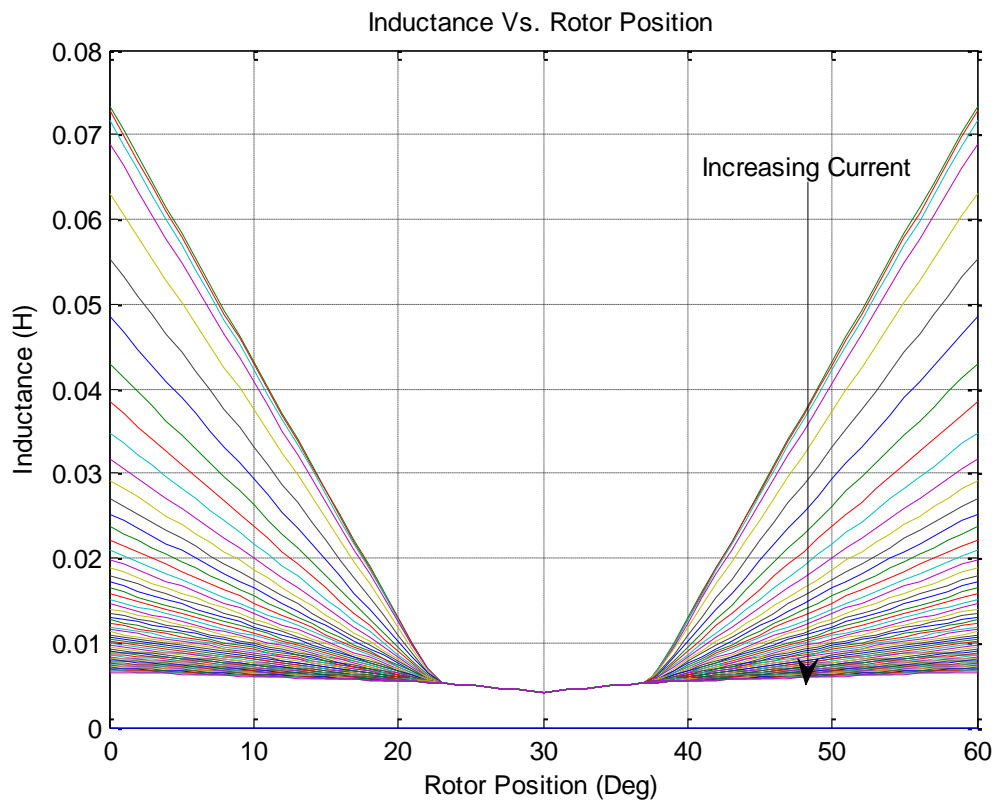


Figure 7-8: Inductance Profile of the Example SRM.

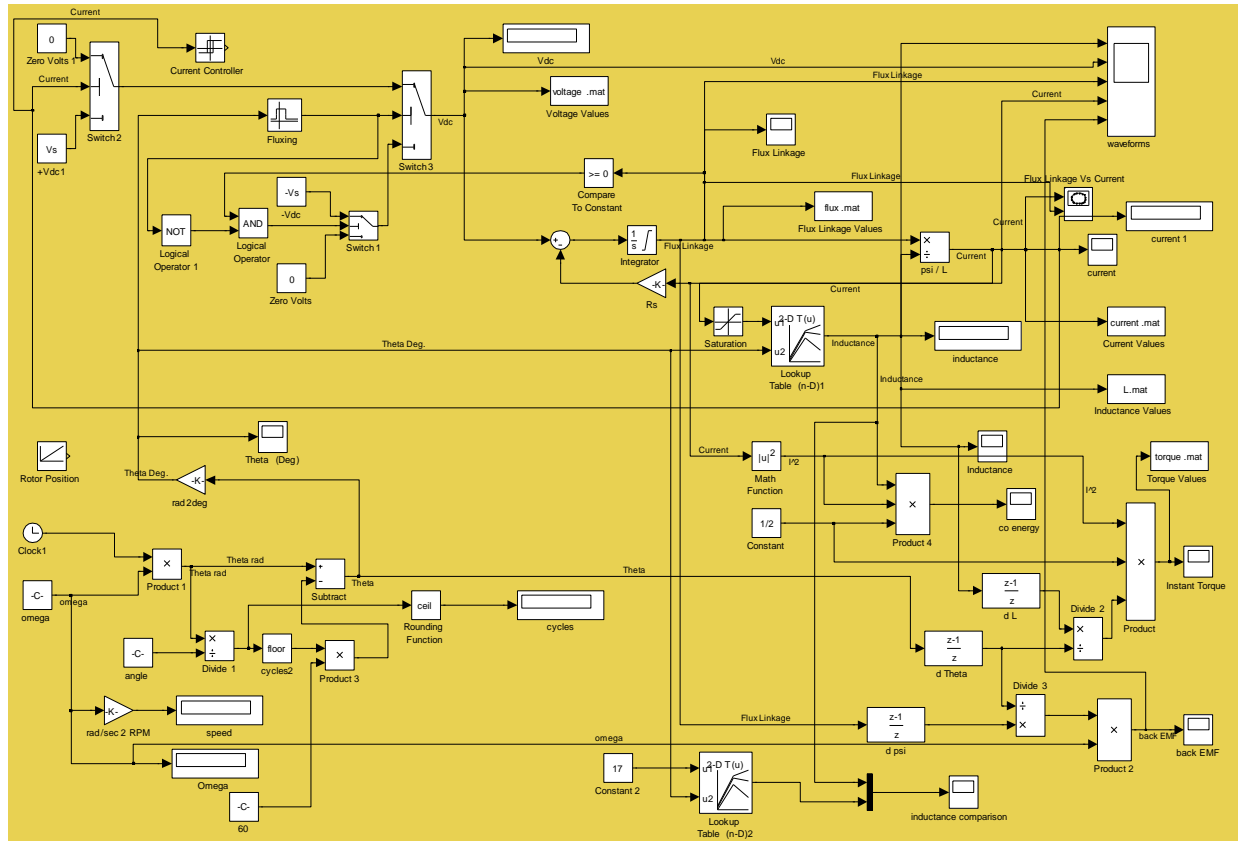


Figure 7-9: Simulink Model for the Example Motor Simulation [$L(\theta, i)$].

7.2.3 Nonlinear Model with Partial Derivatives

From Equation (5.3) applied voltage can be given by the following equation,

$$V_s = iR + \left(\frac{\partial \lambda(\theta, i)}{\partial i} \cdot \frac{di}{dt} \right) + \left(\frac{\partial \lambda(\theta, i)}{\partial \theta} \cdot \omega \right) \quad (7.6)$$

This equation can be modified to the following form to estimate the phase current,

$$\frac{di}{dt} = \frac{1}{\frac{\partial \lambda(\theta, i)}{\partial i}} \left[(V_s - iR) - \left(\frac{\partial \lambda(\theta, i)}{\partial \theta} \cdot \omega \right) \right] \quad (7.7)$$

The partial derivatives required in above equation to calculate phase current can be derived from the example motor data shown in the Figure 7-3. Interested readers can refer to [51] , [15], and [4] for more information on various mathematical methods those can be used to manipulate the flux-linkage data $\lambda(\theta, i)$ to obtain the partial derivatives

$$\left. \frac{\partial \lambda(\theta, i)}{\partial \theta} \right|_{i=\text{constant}} \quad \text{and} \quad \left. \frac{\partial \lambda(\theta, i)}{\partial i} \right|_{\theta=\text{constant}} .$$

Figure 7-10 shows these partial derivatives obtained using Matlab. Figure 7-11 shows the Simulink based motor model which uses these partial derivatives and Equation (7.7) to estimate the phase current. During the analysis, this model was not used.

7.2.4 Nonlinear Model with Current Estimation from Flux-Linkage Data

By using piecewise cubic spline interpolation (Matlab command interp1), it is possible to manipulate the flux-linkage data $\lambda(\theta, i)$, in the Figure 7-3, to estimate the phase current as a function of the flux-linkage and the rotor position i.e. $i(\lambda, \theta)$.

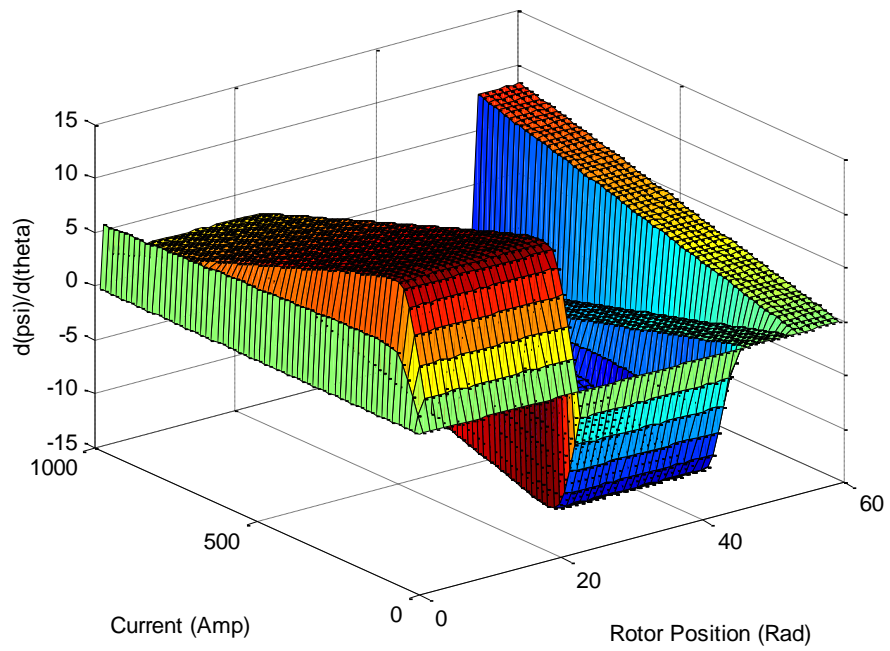
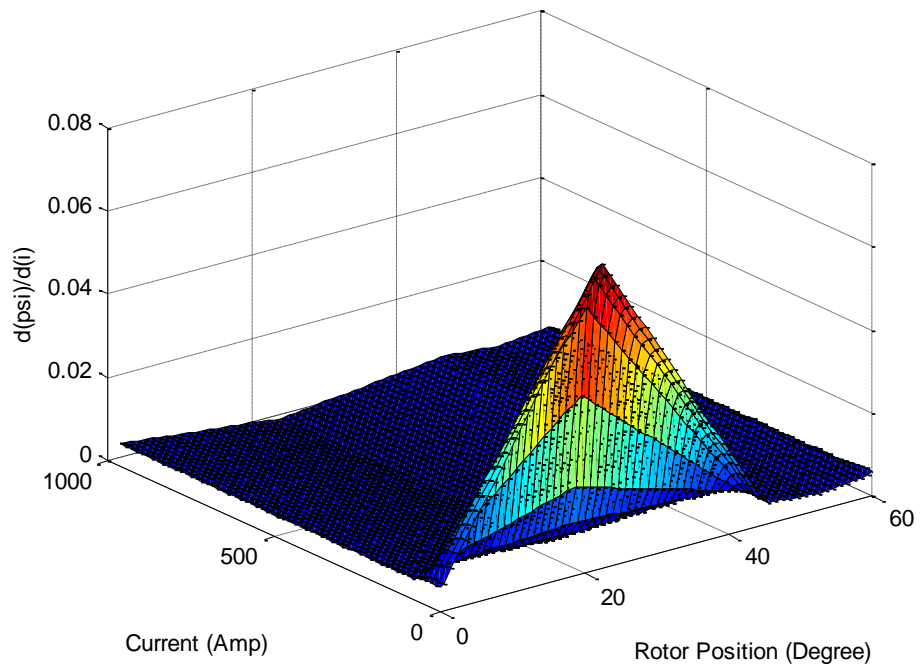


Figure 7-10: Partial Derivatives for Nonlinear Model.

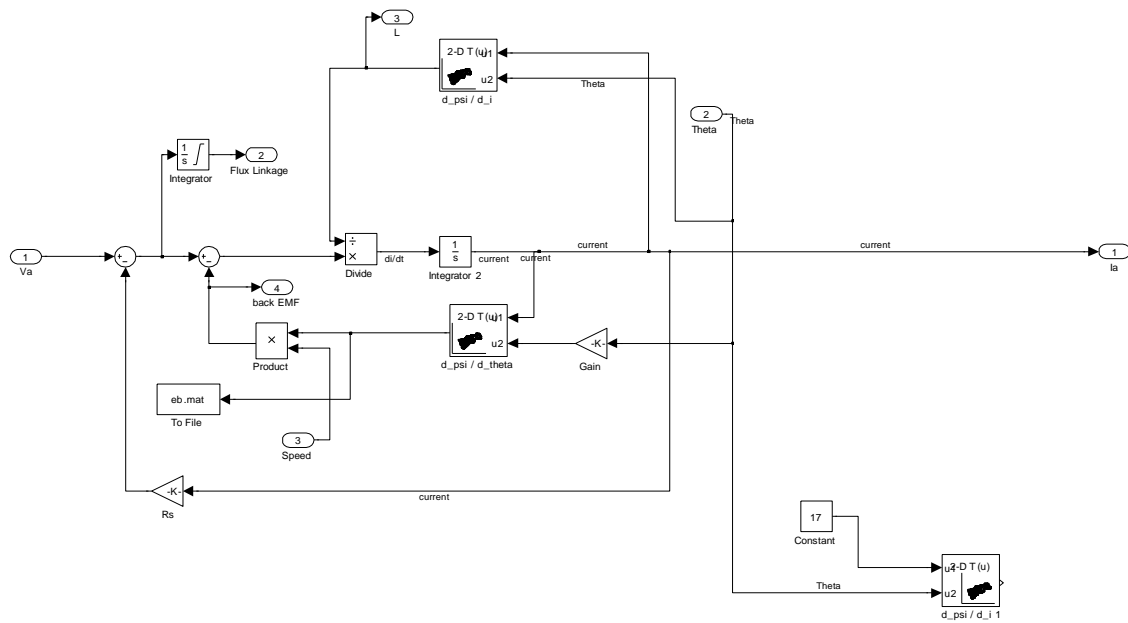
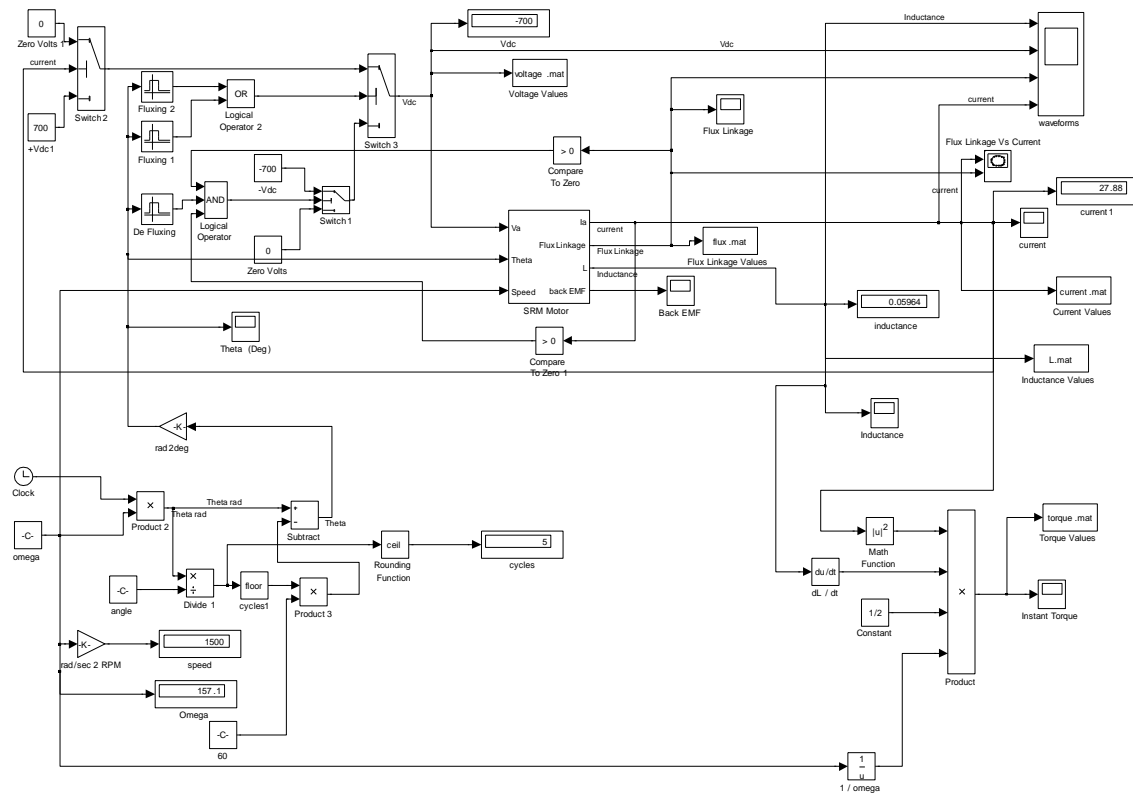


Figure 7-11: Simulink Model Based on Partial Derivatives.

Figure 7-12 shows the Simulink based non-linear SRM model which uses this $i(\lambda, \theta)$ data to estimate the phase current based on the flux-linkage $(\int (V_s - iR) dt)$ information and the rotor position $(\int \omega dt)$ information. Next section shows the simulation results based on these SRM models.

7.3 Simulation Results

Conventional SRM control involves discontinuous winding current. The winding current starts at zero and at the end of each stroke it returns back to zero. This type of control is effective at low speed while the motor impedance and the back-EMF are low and supply voltage is adequate to rapidly drive substantial current into the winding. As speed increases, the back-EMF and winding impedance increases. The peak motor current decreases with speed.

Figure 7-13 shows simulations of the instantaneous current in one phase of the example motor over one rotor revolution and a co-energy plot at the base speed of 250 RPM ($n = 1$).

Figure 7-14 shows simulations of the instantaneous current in one phase of the example motor over one rotor revolution and a co-energy plot at 6 times base speed (1500 RPM), when producing rated power. Here the advance angle was set to 24.75° and dwell angle was set to 30° . Note that for both speeds the minimum winding current is zero i.e. it is a discontinuous mode of operation.

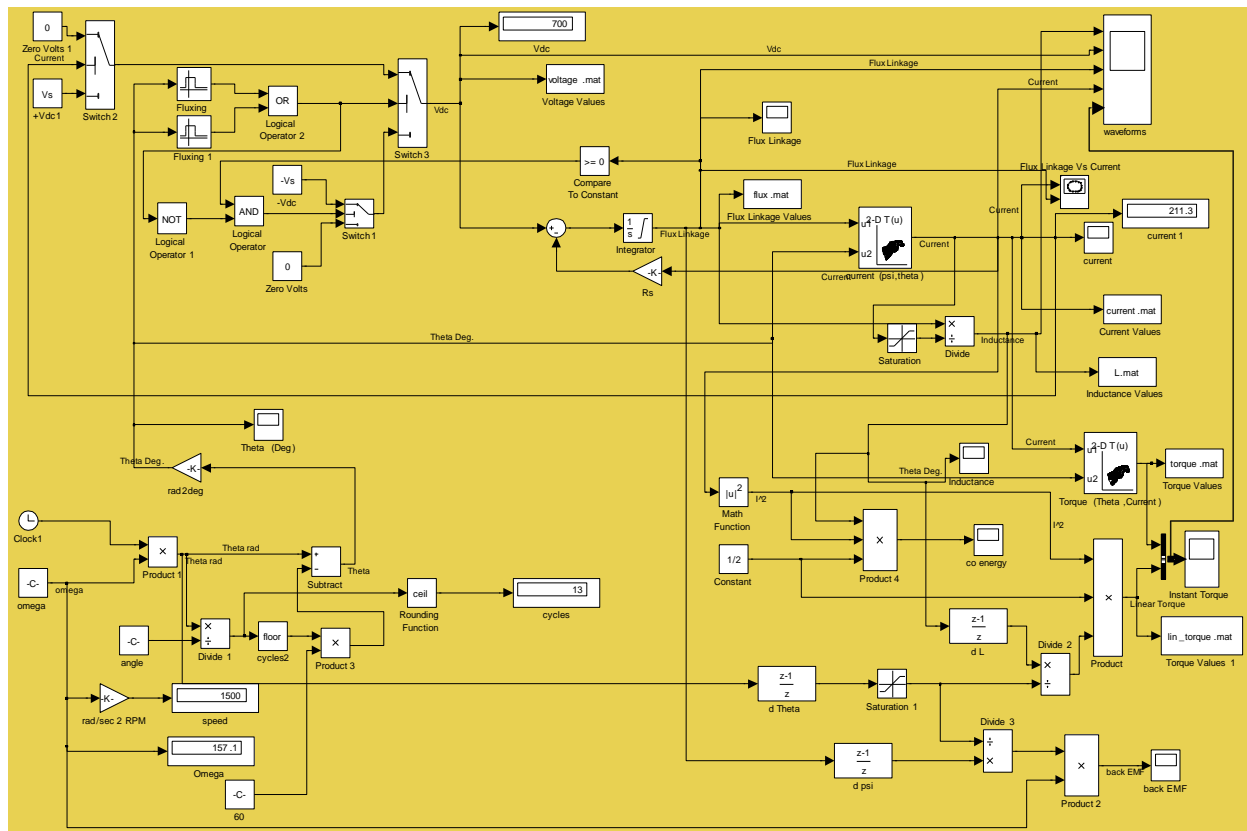


Figure 7-12: Simulink Model of the Example Motor based on Current Estimation from Flux-Linkage Data.

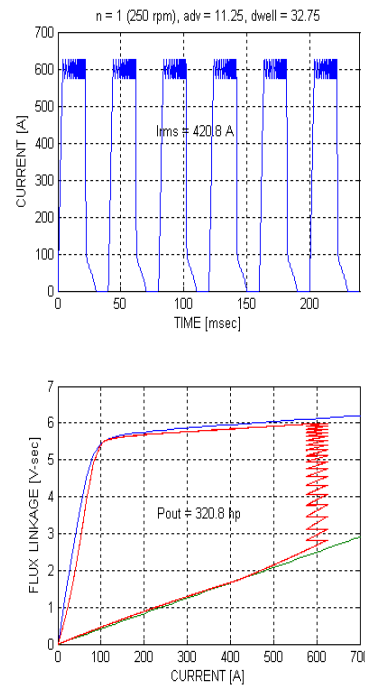


Figure 7-13: Instantaneous Phase Current and Co-energy for the Example Motor when Producing Rated Power at Base Speed [78].

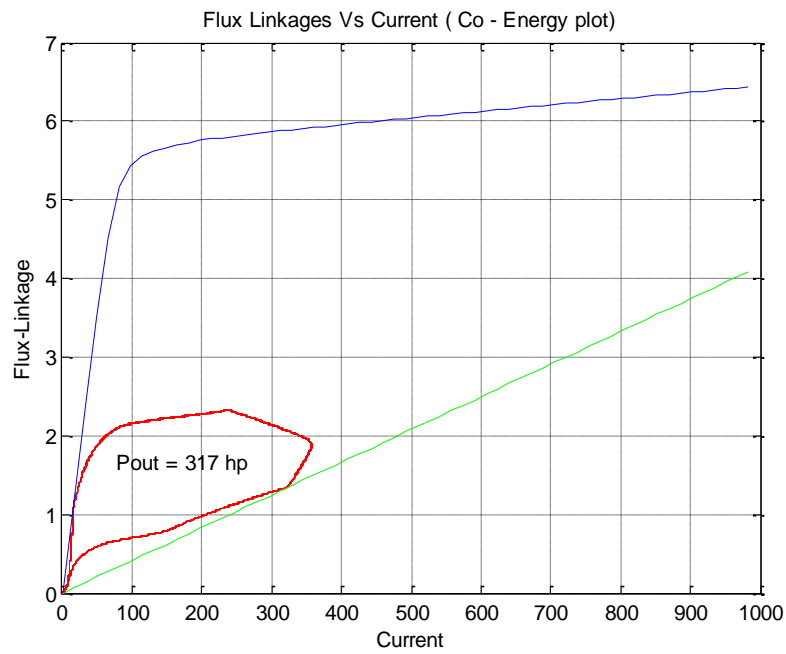
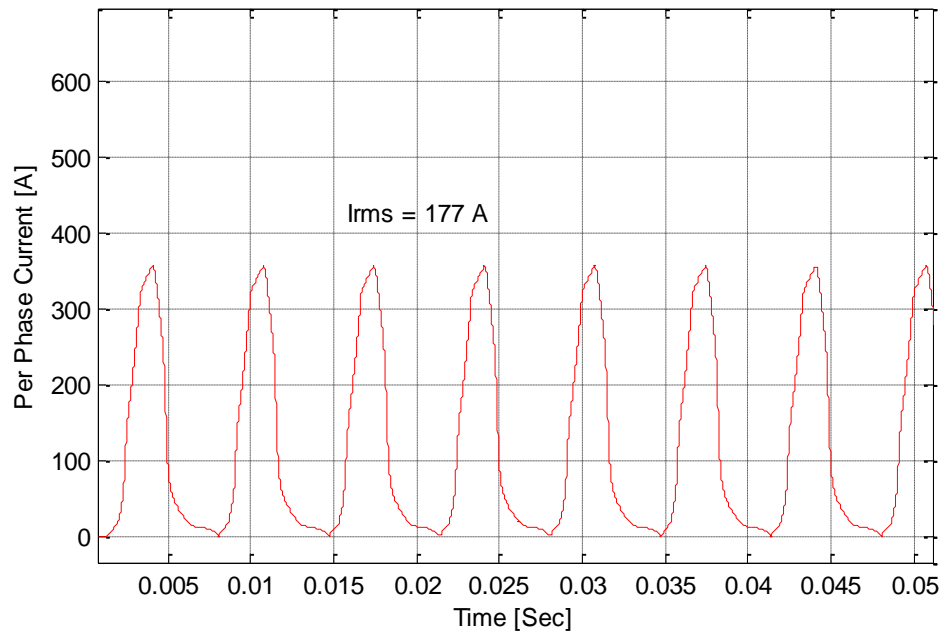


Figure 7-14: : Instantaneous Phase Current and Co-energy for the Example Motor when Producing Rated Power at 6 Times Base Speed (using model in Section 7.2.2).

Unfortunately the co-energy decreases faster than the reciprocal of speed and therefore the CPSR is finite when the SRM is controlled using discontinuous type control scheme. In case of the example motor, as Figure 7-13 indicates, the CPSR is 6:1. That is the relative speed of 6 is the highest speed at which rated power (320 hp) can be developed. At speeds above 1500 rpm, developed power will be less than 320 hp.

In continuous conduction, the minimum winding current is greater than zero. By selecting a dwell angle more than 50% of the stroke length or the rotor pole pitch α_r (30° for the 8/6 example motor), the fluxing region (or the magnetizing region) is kept more than the de-fluxing (or the de-magnetizing) region. That is, if the dwell is 31° , de-fluxing region will be $\alpha_r - \theta_{dwell} = 60^\circ - 31^\circ = 29^\circ$. At the end of each stroke, flux returns to a higher value than the start value. At the end of each stroke, residual value of the flux linkage and hence the minimum current increases. Peak current also increases with each stroke. Once the desired peak current (current regulator set point) is reached, current regulator will impose a short zero volt-sec interval (in this case $31^\circ - 29^\circ = 2^\circ$) in the fluxing region by turning OFF one of the switches. By doing so, it will make both the fluxing region and the de-fluxing region of equal width. During periodic steady state, with continuous conduction, it is necessary that there be a precise positive and negative volt-second applied to the winding during each stroke such that the winding current starts and returns to the same minimum value at the end of each stroke. So during steady state, both fluxing region and de-fluxing region will be of the same width (in this case 29°) guarantying desired peak current during each stroke.

Figure 7-15 and Figure 7-16 shows the example motor operating at the desired top speed of 6500 rpm for discontinuous and continuous conduction respectively. In both cases the set point of the peak current regulator is 600A, and the advance angle is 22.5° . The two cases differ slightly in dwell angle. In the discontinuous conduction case the dwell is 30° which is not adequate to trigger continuous conduction; while in the continuous conduction case the dwell angle is one degree wider at 31° .

Figure 7-15 shows that when operating with discontinuous conduction, at 6500 RPM small current is driven into the motor. The RMS current is about 33A, and the developed power is about 60hp which is far less than the 320hp rating. With continuous conduction, RMS current is about 333A which is within the 425A rating and the developed power is about 670hp, which is more than twice the rated power developed with the rated current at the specified base speed. Note that the current regulator operates one time during each stroke (during fluxing region) to limit the peak current to the 600A value (current regulator set-point). The current regulator kicks in because the dwell is slightly greater than 50% of the stroke length. Figure 7-17 illustrates how continuous conduction is started and how it is stabilized. The co-energy plot in the Figure 7-16 justifies the use of a linear inductance model to predict SRM performance during continuous conduction at high speed. When the winding current is large (600A in this case), the rotor is in the vicinity of the unaligned position where magnetic saturation is not a factor. When the rotor is in the vicinity of the aligned position where magnetic saturation is generally a factor, the winding current is at the minimum value, which is too low to involve the nonlinearity or saturation.

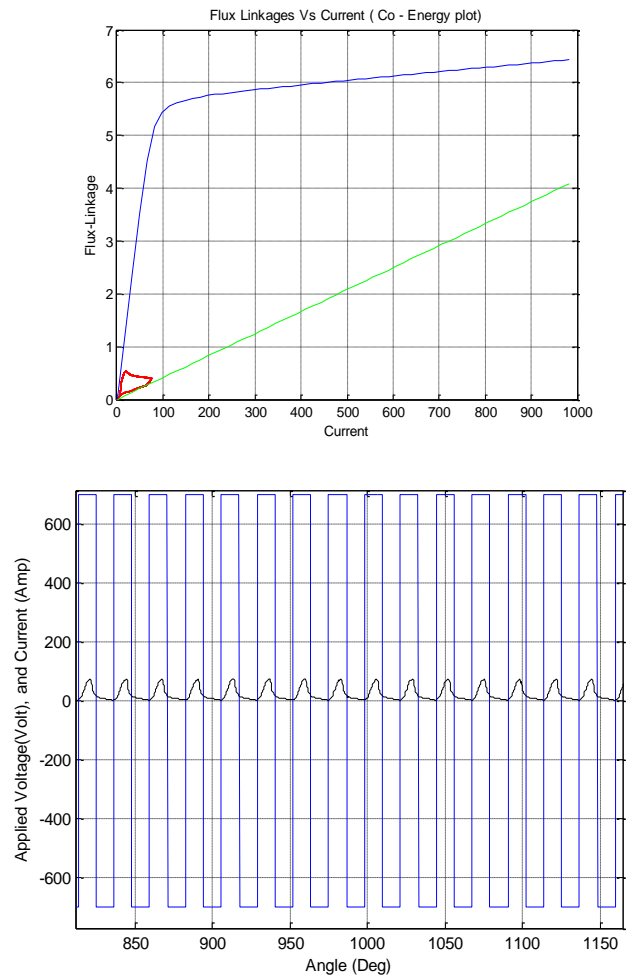


Figure 7-15: Simulation Result of Discontinuous Conduction: Advance Angle = 22.5 , Dwell = 30, Iset = 600A @ 6500 RPM (using model in 7.2.2).

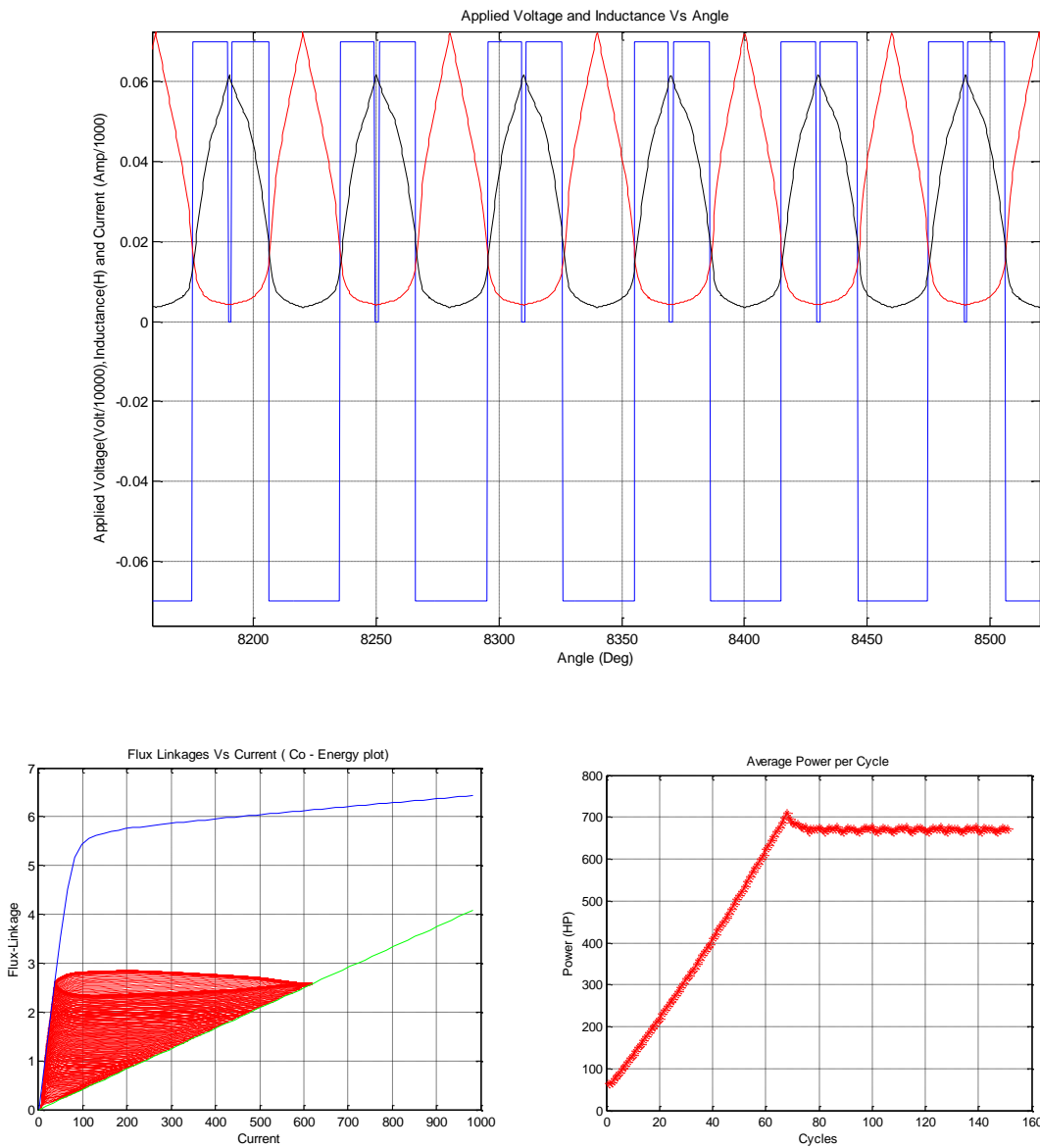


Figure 7-16: Simulation Result of Continuous Conduction: Advance Angle = 22.5 , Dwell = 31, Iset = 600A @ 6500 RPM (using model in Section 7.2.2).

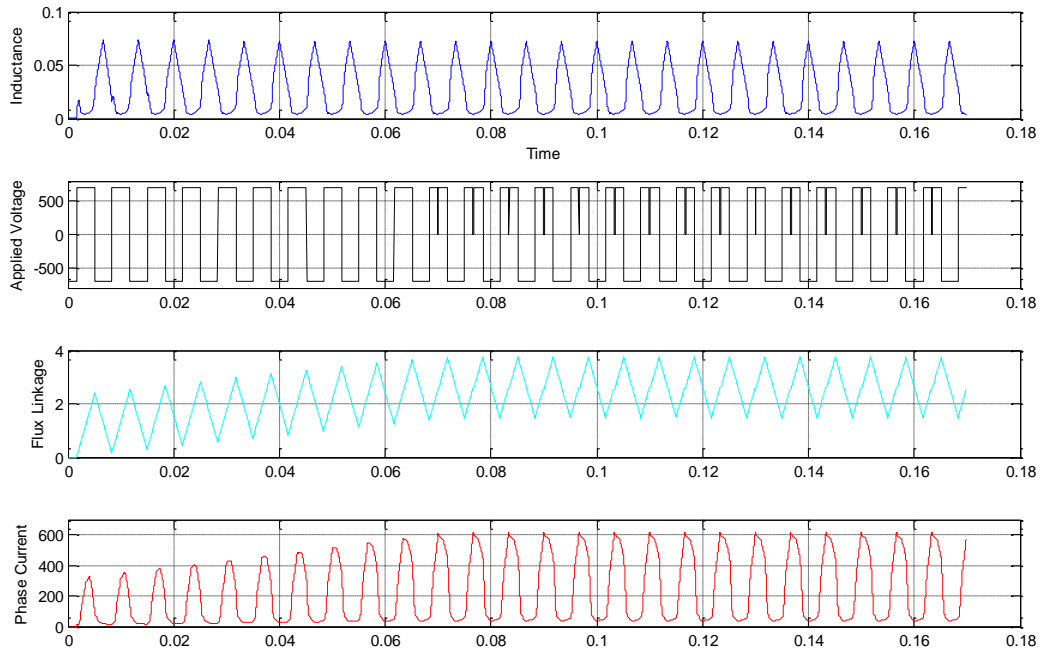


Figure 7-17 : Continuous conduction ($n = 6$, dwell = 31° , advance angle = 22.5° , and $I_{peak} = 600A$).

Values predicted by nonlinear simulations for RMS current is 332.75 A (using model described in section 7.2.4) and 333.37 A (using model described in section 7.2.2) while the average power is 670.27 hp (using model described in section 7.2.4) and 671.40 hp (using model described in section 7.2.2). The linear model predicted corresponding values to be 324.5A and 653.1hp. The difference is due to the small nonlinearities introduced by the saturation effect.

However, as described later, current regulator set point required to get the rated power (320hp) at 6500 RPM is about 364A. With this set point, values predicted by nonlinear simulations for RMS current is 189.27 A (using model described in section 7.2.4) and 189.36 A (using model described in section 7.2.2) while average power is 355.25 hp (using model described in section 7.2.4) and 355.49 hp (using model described in section 7.2.2).

The linear model predicted corresponding values to be 166A and 336.67hp. The use of linear model, simplifies the analysis of switched reluctance motors when operated in continuous conduction mode. Figure 7-18 shows the comparison between linear model inductance profile and nonlinear model inductance profile for the RMS current around 333 A.

Next section describes this mathematical analysis when SRM is operated in continuous conduction mode at high speed. Formulas are derived using the linear inductance profile (i.e. per phase inductance only depends on the rotor position). They give a considerable insight into continuous conduction.

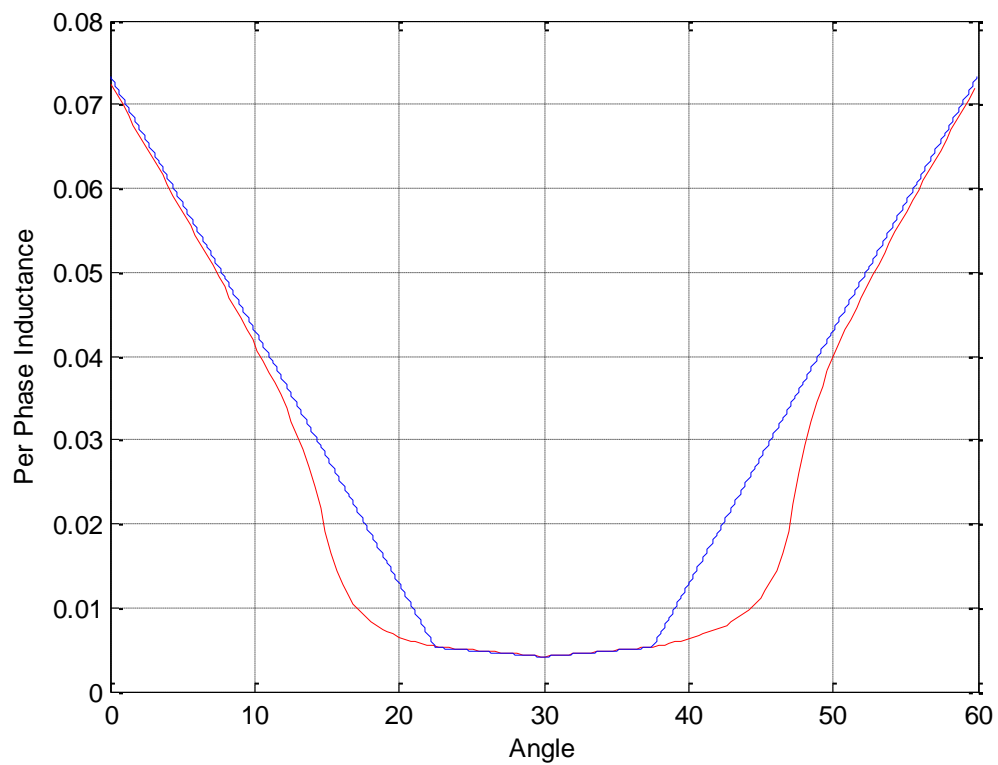


Figure 7-18: Inductance Profile Comparison for Linear Model and Non-Linear Model.

As of now, there is no literature available describing mathematical analysis of the switched reluctance motors when operated in the continuous conduction mode with current regulator to stabilize the growth. Mathematical analysis was carried out in two parts. In the first part, the inductance profile was assumed to be constant in unaligned region. In the second part, the inductance profile was assumed to be non-flat in unaligned region.

7.4 Continuous Conduction Analysis - Flat Unaligned Inductance type SRM

Simulation results suggest that, once the desired peak current is achieved by forcing more fluxing region than a de-fluxing region, a zero volt-sec notch required to sustain and stabilize the growing current, occurs just before the on-set of alignment. Figure 7-19 shows the location of the zero volt-sec notch during periodic steady state. For analysis purpose, entire stroke length (one rotor pole pitch) is divided into six parts. Figure 7-20 shows the waveforms used to carry out mathematical analysis. The first waveform is the inductance profile; the second waveform is the applied DC voltage, the third waveform is the flux-linkage and the fourth waveform is the current waveform.

For each region, the flux-linkage value is estimated by using following equation,

$$\lambda(\theta) = \int V_s(\theta) d\theta \quad (7.8)$$

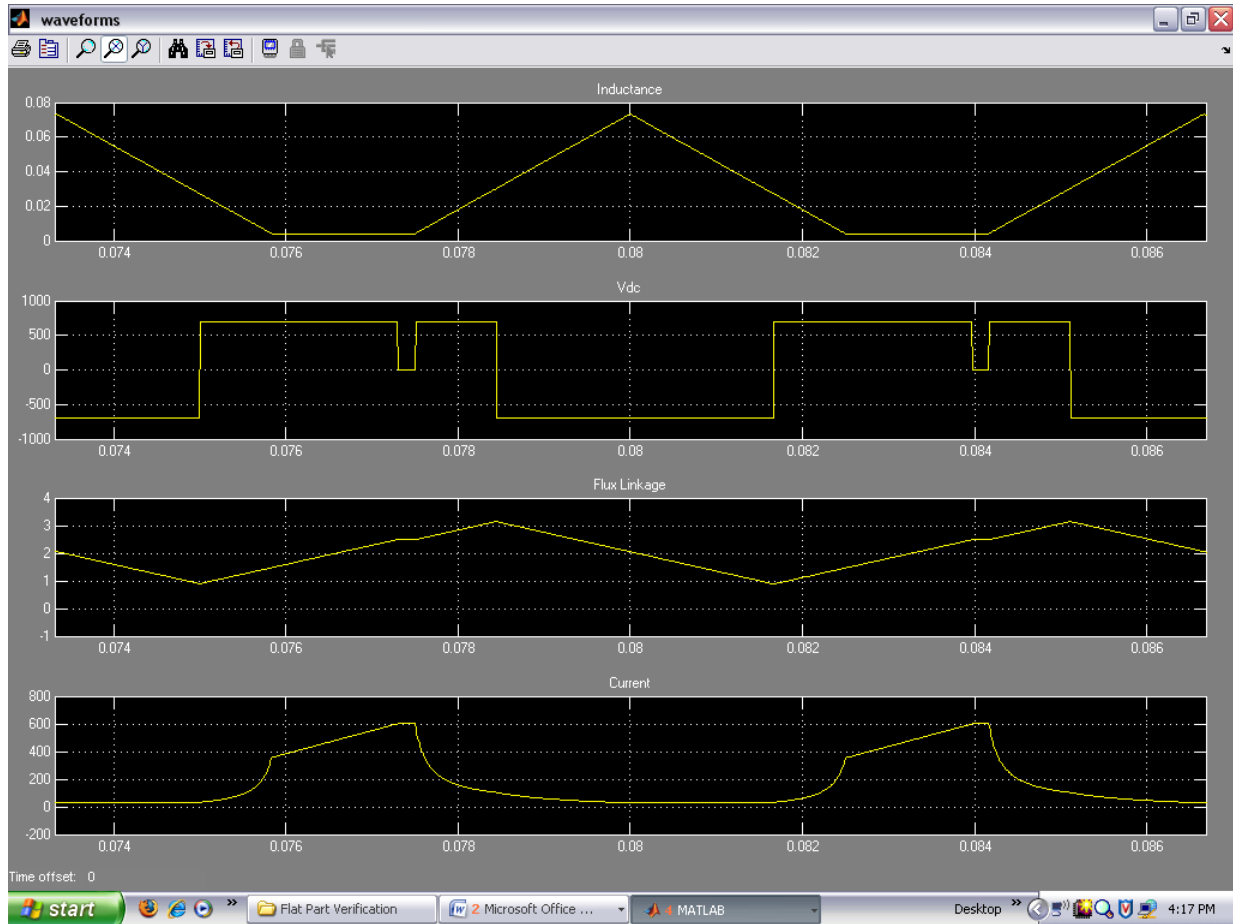


Figure 7-19: Location of Zero Volt-Sec Notches for Flat Unaligned Inductance type SRM Motor when Operated in Continuous Conduction (Matlab Simulation).

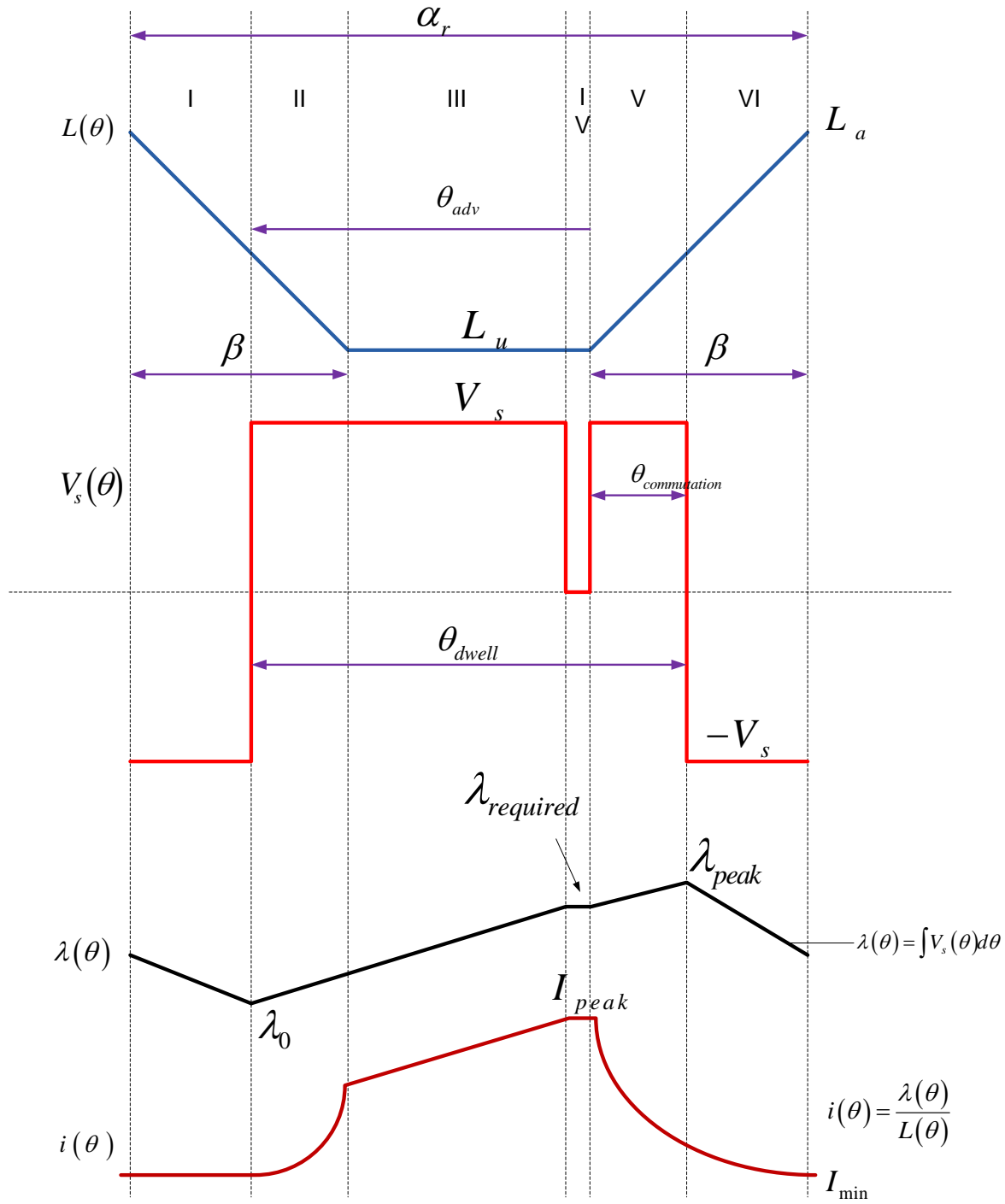


Figure 7-20: Flat Unaligned Inductance type SRM Analysis when Operated in Continuous Conduction.

Using this equation and the equation for the per phase inductance profile, current waveform equation can be derived using,³

$$i(\theta) = \frac{\lambda(\theta)}{L(\theta)} \quad (7.9)$$

Based on the flux-linkage and current waveform equation developed power can be estimated from the co-energy plot. i.e.

$$P_m = \omega \frac{12}{\pi} \int_{\theta} i d\lambda \quad (7.10)$$

Assume that flux-linkage starts from zero. Since with the continuous conduction, the fluxing-region is greater than the de-fluxing region. Hence the residual value of the flux-linkage increases with each stroke. So, at what λ_0 or λ_{peak} the required peak current is achieved? One way to find this is based on the peak current requirement. Let I_{peak} be the required current regulator set point (peak current). Then we have,

$$\lambda_{required} = I_{peak} * L(\theta) \quad (7.11)$$

³ $\theta_{commutation} = \theta_{dwell} - \theta_{adv}$

Similar to the traditional SRM control, with an advance angle greater than zero, peak of the current occurs just at the on-set of alignment. Therefore, $L = L_u$ (unaligned inductance). Therefore,

$$\lambda_{required} = I_{peak} * L_u \quad (7.12)$$

For $I_{peak} = 600A$ and $L_u = 4.15mH$, the required flux-linkage is $\lambda_{required} = 600 * 4.15 * 10^{-3} = 2.49Wb$. Now assume that the advance angle (θ_{adv}) is specified. As described earlier, in order to sustain the continuous conduction, it is required to maintain the precise balance of positive and negative volt-sec i.e. fluxing region has to be equal to de-fluxing region. Since, in continuous conduction, initially the fluxing region is greater than the de-fluxing region, current builds up with each cycle. Once the desired peak current is reached, equilibrium can be enforced by applying a zero volt-sec interval in the fluxing region. So if the dwell (fluxing region) is 32° , the de-fluxing region will be 28° (for 8/6 SRM), then the balancing zero volt-sec notch width will be 4° . That is during periodic steady state, zero volt-sec will have a width of,

$$2\left(\theta_{dwell} - \frac{\alpha_r}{2}\right) = (2\theta_{dwell} - \alpha_r)^0$$

Because of this notch, the fluxing region will be divided into two sub regions. Before this notch, the fluxing region will be: $\theta_{adv} - (2 * \theta_{dwell} - \alpha_r)^\circ$. So if the dwell is 31° and the advance angle is 22.5° , then first fluxing region will have a width of 20° . Since the

current reaches the peak value at the end of this first fluxing region, based on the current regulator set point, we can find the required residual flux linkage (λ_0) to get this current. Specifically we have,

$$\begin{aligned} y = mx + c &\Rightarrow \lambda_{required} = \frac{V_s}{\omega} * [\theta_a - (2 * \theta_{dwell} - \alpha_r)] + \lambda_0, \\ \lambda_{required} &= \frac{V_s}{\omega} * [\theta_a - (2 * \theta_{dwell} - \alpha_r)] + \lambda_0, \end{aligned} \quad (7.13)$$

Here $\lambda_{required}$ is given by Equation (7.12).

$$\begin{aligned} \therefore L_u * I_{peak} &= \frac{V_s}{\omega} * [\theta_a - (2 * \theta_{dwell} - \alpha_r)] + \lambda_0, \\ \therefore \lambda_0 &= L_u * I_{peak} - \frac{V_s}{\omega} * (\theta_a + \alpha_r - 2 * \theta_{dwell}) \end{aligned} \quad (7.14)$$

With an advance angle of 22.5°, a dwell angle of 31°, to reach a set point of 600A , we need,

$$\begin{aligned} \lambda_0 &= L_u * I_{peak} - \frac{V_s}{\omega} * (\theta_a + \alpha_r - 2 * \theta_{dwell}), \\ \lambda_0 &= (4.15 * 10^{-3} * 600) - \left(\frac{700}{2 * \pi * 6 * 250/60} \right) * \left[(22.5 + 60 - 62) * \left(\frac{\pi}{180} \right) \right], \end{aligned}$$

$$\lambda_0 = 0.89 \text{ Wb.}$$

Per phase winding inductance in the region I and II is given by⁴:

⁴ K = arbitrary constant.

$$L(\theta) = \frac{-\Delta L}{\beta} * \theta + k \quad (7.15)$$

When $\theta = 0$, $L(\theta) = L_a$, the value of phase inductance at complete alignment.

$$\therefore L(\theta) = L_a - \frac{\Delta L}{\beta} \theta, \quad (7.16)$$

7.4.1 Region I Analysis ($0 \leq \theta \leq (\alpha_r - \beta - \theta_a)$)

The flux Linkage waveform in region I is given by:

$$\lambda(\theta) = \frac{-V_s}{\omega} \theta + k$$

When $\theta = (\alpha_r - \beta - \theta_{adv})$, $\lambda(\theta) = \lambda_0$. Value of λ_0 is given by Equation (7.13). Therefore,

$$\therefore \lambda(\theta) = L_u I_{peak} - \left[\frac{V_s}{\omega} * (\theta + \beta - 2\theta_{commutation}) \right] \quad (7.17)$$

and

$$\therefore d\lambda(\theta) = \frac{-V_s}{\omega} * d\theta \quad (7.18)$$

Using Equations (7.17) and (7.16), phase current in region I is given by,

$$I(\theta) = \frac{\lambda(\theta)}{L(\theta)}$$

$$I(\theta) = \frac{L_u * I_{peak} - \left[\frac{V_s}{\omega} * (\theta + \beta - 2 * \theta_{commutation}) \right]}{L_a - \frac{\Delta L}{\beta} * \theta} \quad (7.19)$$

Using this current and Equation (7.18) in (5.18), power produced in the region I is given by,

$$\begin{aligned}
 P(\theta) &= \int_{\theta=0}^{\theta=(\alpha_r-\beta-\theta_a)} \lambda(\theta) * di(\theta) = \int_{\theta=0}^{\theta=(\alpha_r-\beta-\theta_a)} i(\theta) * d\lambda(\theta) \\
 \therefore P_1 &= \int_{\theta=0}^{\theta=(\alpha_r-\beta-\theta_a)} i(\theta) * d\lambda(\theta) \\
 \therefore P_1 &= \int_{\theta=0}^{\theta=(\alpha_r-\beta-\theta_a)} \frac{L_u * I_{peak} - \left[\frac{V_s}{\omega} * (\theta + \beta - 2 * \theta_{commutation}) \right]}{L_a - \frac{\Delta L}{\beta} * \theta} * \frac{-V_s}{\omega} * d\theta \\
 \therefore P_1 &= \frac{-V_s}{\omega} * \int_{\theta=0}^{\theta=(\alpha_r-\beta-\theta_a)} \frac{L_u * I_{peak} - \left[\frac{V_s}{\omega} * (\theta + \beta - 2 * \theta_{commutation}) \right]}{L_a - \frac{\Delta L}{\beta} * \theta} * d\theta \\
 \therefore P_1 &= \frac{V_s L_u I_{peak}}{\omega} \frac{\beta}{\Delta L} \ln \left(\frac{\frac{\beta}{\Delta L} L_a - (\alpha_r - \beta - \theta_a)}{\frac{\beta}{\Delta L} L_a} \right) - \left(\frac{V_s}{\omega} \right)^2 \frac{\beta}{\Delta L} (\alpha_r - \beta - \theta_a) \\
 &\quad - \left(\frac{V_s}{\omega} \right)^2 \frac{\beta}{\Delta L} \left((\beta - 2 * \theta_{commutation}) + \frac{\beta}{\Delta L} L_a \right) \ln \left(\frac{\frac{\beta}{\Delta L} L_a - (\alpha_r - \beta - \theta_a)}{\frac{\beta}{\Delta L} L_a} \right) \quad (7.20)
 \end{aligned}$$

Details of this and other mathematical calculations are attached in the Appendix 0.

Flux-linkage in region II and III can be calculated as follows:

$$\lambda(\theta) = \frac{V_s}{\omega} \theta + k$$

When $\theta = (\alpha_r - \beta - \theta_a)$, $\lambda(\theta) = \lambda_0$. The value of λ_0 is given in Equation(7.13).

$$\therefore \lambda(\theta) = L_u I_{peak} - \frac{V_s}{\omega} * (2\alpha_r - 2\theta_{dwell} - \beta - \theta) \quad (7.21)$$

And

$$\therefore d\lambda(\theta) = \frac{V_s}{\omega} \quad (7.22)$$

At the beginning of the zero volt-sec notch, flux-linkage should be equal to $\lambda_{required}$. This can be verified as follow,

When $\theta = (\alpha_r - \beta - (2 * \theta_{dwell} - \alpha_r))$,

$$\begin{aligned} \lambda(\theta) &= L_u * I_{peak} + \frac{V_s}{\omega} * (2 * \theta_{dwell} - 2 * \alpha_r + \beta + \alpha_r - \beta - 2 * \theta_{dwell} + \alpha_r), \\ \therefore \lambda(\theta) &= L_u * I_{peak} = \lambda_{required} \end{aligned}$$

7.4.2 Region II Analysis ($(\alpha_r - \beta - \theta_a) \leq \theta \leq \beta$)

Current in region II is given by,

$$I(\theta) = \frac{L_u I_{peak} - \frac{V_s}{\omega} * (2\alpha_r - 2\theta_{dwell} - \beta - \theta)}{L_a - \frac{\Delta L}{\beta} \theta} \quad (7.23)$$

Power produced in region II is given by,

$$\begin{aligned} P_2 &= \int_{\theta=(\alpha_r - \beta - \theta_a)}^{\theta=\beta} i(\theta) * d\lambda(\theta) \\ P_2 &= \int_{\theta=(\alpha_r - \beta - \theta_a)}^{\theta=\beta} \frac{L_u * I_{peak} - \frac{V_s}{\omega} * (2 * \alpha_r - 2 * \theta_{dwell} - \beta - \theta)}{L_a - \frac{\Delta L}{\beta} * \theta} * \frac{V_s}{\omega} * d\theta \end{aligned}$$

$$\begin{aligned}
P_2 &= \frac{V_s}{\omega} * \int_{\theta=(\alpha_r-\beta-\theta_a)}^{\theta=\beta} \frac{L_u * I_{peak} - \frac{V_s}{\omega} * (2 * \alpha_r - 2 * \theta_{dwell} - \beta - \theta)}{L_a - \frac{\Delta L}{\beta} * \theta} * d\theta \\
\therefore P_2 &= \frac{-V_s L_u I_{peak}}{\omega} \frac{\beta}{\Delta L} \ln \left(\frac{\frac{\beta}{\Delta L} L_a - \beta}{\frac{\beta}{\Delta L} L_a - (\alpha_r - \beta - \theta_a)} \right) - \left(\frac{V_s}{\omega} \right)^2 \frac{\beta}{\Delta L} [\theta_a - (\alpha_r - 2\beta)] \\
&\quad - \left(\frac{V_s}{\omega} \right)^2 \frac{\beta}{\Delta L} \left(\frac{\beta}{\Delta L} L_a - (2 * \alpha_r - 2 * \theta_{dwell} - \beta) \right) \ln \left(\frac{\beta - \frac{\beta}{\Delta L} L_a}{(\alpha_r - \beta - \theta_a) - \frac{\beta}{\Delta L} L_a} \right) \quad (7.24)
\end{aligned}$$

Inductance in region III and IV is constant and is given by, $L(\theta) = L_u$ i.e. value of the inductance at completely unaligned position.

7.4.3 Region III Analysis $\left(\begin{array}{l} \beta \leq \theta \leq [\alpha_r - \beta - (2 * \theta_{dwell} - \alpha_r)] \\ \beta \leq \theta \leq (2 * \alpha_r - 2 * \theta_{dwell} - \beta) \end{array} \right)$

Current in region III is given by,

$$I(\theta) = \frac{L_u I_{peak} - \frac{V_s}{\omega} * (2\alpha_r - 2\theta_{dwell} - \beta - \theta)}{L_u} \quad (7.25)$$

Power produced in the region III is given by,

$$\begin{aligned}
P_3 &= \int_{\theta=\beta}^{\theta=(2*\alpha_r-2*\theta_{dwell}-\beta)} \frac{L_u * I_{peak} - \frac{V_s}{\omega} * (2 * \alpha_r - 2 * \theta_{dwell} - \beta - \theta)}{L_u} * \frac{V_s}{\omega} * d\theta, \\
P_3 &= \frac{V_s}{\omega} * \int_{\theta=\beta}^{\theta=(2*\alpha_r-2*\theta_{dwell}-\beta)} \frac{L_u * I_{peak} - \frac{V_s}{\omega} * (2 * \alpha_r - 2 * \theta_{dwell} - \beta - \theta)}{L_u} * d\theta
\end{aligned}$$

$$\begin{aligned} \therefore P_3 = & \frac{2V_s I_{peak} (\alpha_r - \theta_{dwell} - \beta)}{\omega} - \left(\frac{V_s}{\omega} \right)^2 \frac{2}{L_u} (2^* \alpha_r - 2^* \theta_{dwell} - \beta) (\alpha_r - \theta_{dwell} - \beta) \\ & + \left(\frac{V_s}{\omega} \right)^2 \frac{1}{2L_u} \left[(2^* \alpha_r - 2^* \theta_{dwell} - \beta)^2 - \beta^2 \right] \end{aligned} \quad (7.26)$$

7.4.4 Region IV Analysis ((2*α_r - 2*θ_{dwell} - β) ≤ θ ≤ (α_r - β))

Flux linkage in region IV is given by,

$$\lambda(\theta) = \lambda_{required} = L_u * I_{peak} \quad (7.27)$$

And

$$\therefore d\lambda(\theta) = 0 \quad (7.28)$$

Current in region IV is given by,

$$I(\theta) = \frac{L_u I_{peak}}{L_u} = I_{peak} \quad (7.29)$$

Power produced in this region is zero as $d\lambda(\theta) = 0$.

$$\therefore P_4 = 0 \quad (7.30)$$

Inductance in region V and VI is given by,

$$L(\theta) = L_u + \frac{\Delta L}{\beta} * (\theta - (\alpha_r - \beta)) \quad (7.31)$$

7.4.5 Region V Analysis ((α_r - β) ≤ θ ≤ (α_r - β + θ_{commutation}))

$$\text{Flux linkage in region V is given by, } \therefore \lambda(\theta) = L_u I_{peak} + \frac{V_s}{\omega} * [\theta - (\alpha_r - \beta)] \quad (7.32)$$

$$\therefore d\lambda(\theta) = \frac{V_s}{\omega} \quad (7.33)$$

Current in region V is given by,

$$I(\theta) = \frac{L_u I_{peak} + \frac{V_s}{\omega} * [\theta - (\alpha_r - \beta)]}{L_u + \frac{\Delta L}{\beta} * (\theta - (\alpha_r - \beta))} \quad (7.34)$$

Power produced in the region V is given by,

$$\begin{aligned} P_5 &= \int_{\theta=(\alpha_r - \beta)}^{\theta=(\alpha_r - \beta + \theta_{commutation})} i(\theta) * d\lambda(\theta) \\ P_5 &= \int_{\theta=(\alpha_r - \beta)}^{\theta=(\alpha_r - \beta + \theta_{commutation})} \frac{L_u * I_{peak} + \frac{V_s}{\omega} * [\theta - (\alpha_r - \beta)]}{L_u + \frac{\Delta L}{\beta} * (\theta - (\alpha_r - \beta))} * \frac{V_s}{\omega} * d\theta \\ P_5 &= \frac{V_s}{\omega} * \int_{\theta=(\alpha_r - \beta)}^{\theta=(\alpha_r - \beta + \theta_{commutation})} \frac{L_u * I_{peak} + \frac{V_s}{\omega} * [\theta - (\alpha_r - \beta)]}{L_u + \frac{\Delta L}{\beta} * (\theta - (\alpha_r - \beta))} d\theta \end{aligned}$$

$$\therefore P_5 = \frac{V_s L_u I_{peak}}{\omega} \frac{\beta}{\Delta L} \ln \left(\frac{\frac{L_u \beta}{\Delta L} + \theta_{commutation}}{\frac{L_u \beta}{\Delta L}} \right) + \left(\frac{V_s}{\omega} \right)^2 \frac{\beta}{\Delta L} \theta_{commutation} - \left(\frac{V_s}{\omega} \frac{\beta}{\Delta L} \right)^2 L_u \ln \left(\frac{\frac{L_u \beta}{\Delta L} + \theta_{commutation}}{\frac{L_u \beta}{\Delta L}} \right) \quad (7.35)$$

7.4.6 Region VI Analysis ($(\alpha_r - \beta + \theta_{commutation}) \leq \theta \leq \alpha_r$)

From Equation(7.32), $\lambda(\theta) = L_u * I_{peak} + \frac{V_s}{\omega} * [\theta - (\alpha_r - \beta)]$

When $\theta = (\alpha_r - \beta + \theta_{commutation})$,

$$\therefore \lambda(\theta) = L_u * I_{peak} + \frac{V_s}{\omega} * \theta_{commutation} = \lambda_{peak}$$

(7.36)

i.e.

$$\lambda_{peak} = L_u * I_{peak} + \frac{V_s}{\omega} * (\theta_{dwell} - \theta_a)$$

Flux linkage in region VI is given by,

$$\lambda(\theta) = L_u I_{peak} + \frac{V_s}{\omega} * (\alpha_r - \beta + 2\theta_{commutation} - \theta)$$

(7.37)

And

$$\therefore d\lambda(\theta) = \frac{-V_s}{\omega} * d\theta$$

(7.38)

Instantaneous current in region VI is given by,

$$I(\theta) = \frac{L_u I_{peak} + \frac{V_s}{\omega} * (\alpha_r - \beta + 2\theta_{commutation} - \theta)}{L_u + \frac{\Delta L}{\beta} * (\theta - (\alpha_r - \beta))}$$

(7.39)

Power produced in the region VI is given by,

$$P_6 = \int_{\theta=(\alpha_r - \beta + \theta_{commutation})}^{\theta=\alpha_r} i(\theta) * d\lambda(\theta)$$

$$P_6 = \int_{\theta=(\alpha_r - \beta + \theta_{commutation})}^{\theta=\alpha_r} \frac{L_u * I_{peak} + \frac{V_s}{\omega} * (\alpha_r - \beta + 2 * \theta_{commutation} - \theta)}{L_u + \frac{\Delta L}{\beta} * (\theta - (\alpha_r - \beta))} * \frac{-V_s}{\omega} * d\theta$$

(7.40)

$$P_6 = \frac{-V_s}{\omega} * \int_{\theta=(\alpha_r - \beta + \theta_{commutation})}^{\theta=\alpha_r} \frac{L_u * I_{peak} + \frac{V_s}{\omega} * (\alpha_r - \beta + 2 * \theta_{commutation} - \theta)}{L_u + \frac{\Delta L}{\beta} * (\theta - (\alpha_r - \beta))} d\theta$$

$$\begin{aligned} \therefore P_6 = & \frac{-V_s L_u I_{peak}}{\omega} \frac{\beta}{\Delta L} \ln \left(\frac{\frac{\beta}{\Delta L} L_u + \beta}{\frac{\beta}{\Delta L} L_u + \theta_{commutation}} \right) + \left(\frac{V_s}{\omega} \right)^2 \frac{\beta}{\Delta L} [\beta - \theta_{commutation}] \\ & - \left(\frac{V_s}{\omega} \right)^2 \frac{\beta}{\Delta L} \left(\frac{\beta}{\Delta L} L_u + 2 * \theta_{commutation} \right) \ln \left(\frac{\frac{\beta}{\Delta L} L_u + \beta}{\frac{\beta}{\Delta L} L_u + \theta_{commutation}} \right) \end{aligned} \quad (7.41)$$

When $\theta = \alpha_r$,

$$\lambda(\theta) = L_u * I_{peak} + \frac{V_s}{\omega} * (\alpha_r - \beta + 2 * \theta_{commutation} - \alpha_r),$$

$$\lambda(\theta) = L_u * I_{peak} + \frac{V_s}{\omega} * (-\beta + 2 * \theta_{commutation}),$$

i.e.

$$\lambda(\theta) = L_u * I_{peak} + \frac{V_s}{\omega} * (2 * \theta_{dwell} - 2 * \theta_a - \beta)$$

From equation(7.17),

$$\lambda(\theta) = L_u * I_{peak} + \left[\frac{V_s}{\omega} * (2 * \theta_{commutation} - \beta - \theta) \right]$$

When $\theta = 0$,

$$\lambda(\theta) = L_u * I_{peak} + \left[\frac{V_s}{\omega} * (2 * \theta_{commutation} - \beta) \right] \quad (\text{Verification})$$

Since maximum inductance occurs when $\theta = \alpha_r$, minimum current can be calculated as follows,

$$\begin{aligned}
I(\theta) &= \frac{L_u * I_{peak} + \frac{V_s}{\omega} * (\alpha_r - \beta + 2 * \theta_{commutation} - \alpha_r)}{L_u + \frac{\Delta L}{\beta} * (\alpha_r - (\alpha_r - \beta))}, \\
\therefore I(\theta) &= \frac{L_u * I_{peak} + \frac{V_s}{\omega} * (2 * \theta_{commutation} - \beta)}{L_u + \frac{\Delta L}{\beta} * \beta}, \\
I_{min} &= \frac{L_u * I_{peak} + \frac{V_s}{\omega} * (2 * \theta_{commutation} - \beta)}{L_a},
\end{aligned} \tag{7.42}$$

$$\begin{aligned}
I_{min} &= \frac{L_u * I_{peak} + \frac{V_s}{\omega} * (2 * \theta_{commutation} - \beta)}{L_a}, \\
I_{min} &= \frac{(4.15 * 10^{-3} * 600) + \left(\frac{700}{2 * \pi * 6 * 250 / 60} \right) * \left[(2 * (31 - 22.5) - 22.5) * \left(\frac{\pi}{180} \right) \right]}{73.38 * 10^{-3}}, \\
I_{min} &= 28.10A
\end{aligned}$$

Simulation result confirms the same.

7.4.7 Analytical Results

For 8/6 SRM , total average power $P_m = \omega \frac{q}{\alpha_r} * (P_1 + P_2 + P_3 + P_4 + P_5 + P_6)$

$$\therefore P_m = \omega \frac{q}{\alpha_r} *$$

$$\left[\begin{aligned} & \frac{V_s L_u I_{peak}}{\omega} \frac{\beta}{\Delta L} \ln \left(\frac{\frac{\beta}{\Delta L} L_a - (\alpha_r - \beta - \theta_a)}{\frac{\beta}{\Delta L} L_a} \right) - \left(\frac{V_s}{\omega} \right)^2 \frac{\beta}{\Delta L} (\alpha_r - \beta - \theta_a) \\ & - \left(\frac{V_s}{\omega} \right)^2 \frac{\beta}{\Delta L} \left((\beta - 2 * \theta_{commutation}) + \frac{\beta}{\Delta L} L_a \right) \ln \left(\frac{\frac{\beta}{\Delta L} L_a - (\alpha_r - \beta - \theta_a)}{\frac{\beta}{\Delta L} L_a} \right) \\ & - \frac{V_s L_u I_{peak}}{\omega} \frac{\beta}{\Delta L} \ln \left(\frac{\frac{\beta}{\Delta L} L_a - \beta}{\frac{\beta}{\Delta L} L_a - (\alpha_r - \beta - \theta_a)} \right) - \left(\frac{V_s}{\omega} \right)^2 \frac{\beta}{\Delta L} [\theta_a - (\alpha_r - 2\beta)] \\ & - \left(\frac{V_s}{\omega} \right)^2 \frac{\beta}{\Delta L} \left(\frac{\beta}{\Delta L} L_a - (2 * \alpha_r - 2 * \theta_{dwell} - \beta) \right) \ln \left(\frac{\beta - \frac{\beta}{\Delta L} L_a}{(\alpha_r - \beta - \theta_a) - \frac{\beta}{\Delta L} L_a} \right) \\ & + \frac{2 V_s I_{peak} (\alpha_r - \theta_{dwell} - \beta)}{\omega} - \left(\frac{V_s}{\omega} \right)^2 \frac{2}{L_u} (2 * \alpha_r - 2 * \theta_{dwell} - \beta) (\alpha_r - \theta_{dwell} - \beta) \\ & + \left(\frac{V_s}{\omega} \right)^2 \frac{1}{2 L_u} [(2 * \alpha_r - 2 * \theta_{dwell} - \beta)^2 - \beta^2] \\ & + \frac{V_s L_u I_{peak}}{\omega} \frac{\beta}{\Delta L} \ln \left(\frac{\frac{L_u \beta}{\Delta L} + \theta_{commutation}}{\frac{L_u \beta}{\Delta L}} \right) + \left(\frac{V_s}{\omega} \right)^2 \frac{\beta}{\Delta L} \theta_{commutation} - \left(\frac{V_s}{\omega} \frac{\beta}{\Delta L} \right)^2 L_u \ln \left(\frac{\frac{L_u \beta}{\Delta L} + \theta_{commutation}}{\frac{L_u \beta}{\Delta L}} \right) \\ & - \frac{V_s L_u I_{peak}}{\omega} \frac{\beta}{\Delta L} \ln \left(\frac{\frac{\beta}{\Delta L} L_u + \beta}{\frac{\beta}{\Delta L} L_u + \theta_{commutation}} \right) + \left(\frac{V_s}{\omega} \right)^2 \frac{\beta}{\Delta L} [\beta - \theta_{commutation}] \\ & - \left(\frac{V_s}{\omega} \right)^2 \frac{\beta}{\Delta L} \left(\frac{\beta}{\Delta L} L_u + 2 * \theta_{commutation} \right) \ln \left(\frac{\frac{\beta}{\Delta L} L_u + \beta}{\frac{\beta}{\Delta L} L_u + \theta_{commutation}} \right) \end{aligned} \right]$$

After cancelation of terms containing $\left(\frac{V_s}{\omega}\right)^2 \frac{\beta}{\Delta L}$, we have,

$$\therefore P_m = \omega \frac{q}{\alpha_r} * \left[\begin{aligned} & \frac{V_s L_u I_{peak}}{\omega} \frac{\beta}{\Delta L} \ln \left(\frac{\frac{\beta}{\Delta L} L_a - (\alpha_r - \beta - \theta_a)}{\frac{\beta}{\Delta L} L_a} \right) - \frac{V_s L_u I_{peak}}{\omega} \frac{\beta}{\Delta L} \ln \left(\frac{\frac{\beta}{\Delta L} L_a - \beta}{\frac{\beta}{\Delta L} L_a - (\alpha_r - \beta - \theta_a)} \right) \\ & + \frac{2V_s I_{peak} (\alpha_r - \theta_{dwell} - \beta)}{\omega} + \frac{V_s L_u I_{peak}}{\omega} \frac{\beta}{\Delta L} \ln \left(\frac{\frac{L_u \beta}{\Delta L} + \theta_{commutation}}{\frac{L_u \beta}{\Delta L}} \right) \\ & - \frac{V_s L_u I_{peak}}{\omega} \frac{\beta}{\Delta L} \ln \left(\frac{\frac{\beta}{\Delta L} L_u + \beta}{\frac{\beta}{\Delta L} L_u + \theta_{commutation}} \right) + \left(\frac{V_s}{\omega} \right)^2 \frac{1}{2L_u} \left[(2^* \alpha_r - 2^* \theta_{dwell} - \beta)^2 - \beta^2 \right] \\ & - \left(\frac{V_s}{\omega} \right)^2 \frac{\beta}{\Delta L} \left((\beta - 2^* \theta_{commutation}) + \frac{\beta}{\Delta L} L_a \right) \ln \left(\frac{\frac{\beta}{\Delta L} L_a - (\alpha_r - \beta - \theta_a)}{\frac{\beta}{\Delta L} L_a} \right) \\ & - \left(\frac{V_s}{\omega} \right)^2 \frac{\beta}{\Delta L} \left(\frac{\beta}{\Delta L} L_a - (2^* \alpha_r - 2^* \theta_{dwell} - \beta) \right) \ln \left(\frac{\beta - \frac{\beta}{\Delta L} L_a}{(\alpha_r - \beta - \theta_a) - \frac{\beta}{\Delta L} L_a} \right) \\ & - \left(\frac{V_s}{\omega} \right)^2 \frac{2}{L_u} (2^* \alpha_r - 2^* \theta_{dwell} - \beta) (\alpha_r - \theta_{dwell} - \beta) - \left(\frac{V_s}{\omega} \frac{\beta}{\Delta L} \right)^2 L_u \ln \left(\frac{\frac{L_u \beta}{\Delta L} + \theta_{commutation}}{\frac{L_u \beta}{\Delta L}} \right) \\ & - \left(\frac{V_s}{\omega} \right)^2 \frac{\beta}{\Delta L} \left(\frac{\beta}{\Delta L} L_u + 2^* \theta_{commutation} \right) \ln \left(\frac{\frac{\beta}{\Delta L} L_u + \beta}{\frac{\beta}{\Delta L} L_u + \theta_{commutation}} \right) \end{aligned} \right]$$

These equations can be divided into two parts: a speed dependent part and a speed independent part.

Speed independent parts (i.e. only terms containing $1/\omega$ factor) are:

$$\begin{aligned} \therefore P_{m_speed_independent} &= \omega \frac{q}{\alpha_r} * \\ &\left\{ \begin{aligned} &\frac{V_s L_u I_{peak}}{\omega} \frac{\beta}{\Delta L} \ln \left(\frac{\frac{\beta}{\Delta L} L_a - (\alpha_r - \beta - \theta_a)}{\frac{\beta}{\Delta L} L_a} \right) - \frac{V_s L_u I_{peak}}{\omega} \frac{\beta}{\Delta L} \ln \left(\frac{\frac{\beta}{\Delta L} L_a - \beta}{\frac{\beta}{\Delta L} L_a - (\alpha_r - \beta - \theta_a)} \right) \\ &+ \frac{2V_s I_{peak} (\alpha_r - \theta_{dwell} - \beta)}{\omega} + \frac{V_s L_u I_{peak}}{\omega} \frac{\beta}{\Delta L} \ln \left(\frac{\frac{L_u \beta}{\Delta L} + \theta_{commutation}}{\frac{L_u \beta}{\Delta L}} \right) \\ &- \frac{V_s L_u I_{peak}}{\omega} \frac{\beta}{\Delta L} \ln \left(\frac{\frac{\beta}{\Delta L} L_u + \beta}{\frac{\beta}{\Delta L} L_u + \theta_{commutation}} \right) \end{aligned} \right\} \\ \\ \therefore P_{m_speed_independent} &= \frac{q}{\alpha_r} * \left\{ \begin{aligned} &V_s L_u I_{peak} \frac{\beta}{\Delta L} \left[\ln \left(\frac{\frac{\beta}{\Delta L} L_a - (\alpha_r - \beta - \theta_a)}{\frac{\beta}{\Delta L} L_a} \right) - \ln \left(\frac{\frac{\beta}{\Delta L} L_a - \beta}{\frac{\beta}{\Delta L} L_a - (\alpha_r - \beta - \theta_a)} \right) \right. \\ &\quad \left. + \ln \left(\frac{\frac{L_u \beta}{\Delta L} + \theta_{commutation}}{\frac{L_u \beta}{\Delta L}} \right) - \ln \left(\frac{\frac{\beta}{\Delta L} L_u + \beta}{\frac{\beta}{\Delta L} L_u + \theta_{commutation}} \right) \right] \\ &+ 2V_s I_{peak} (\alpha_r - \theta_{dwell} - \beta) \end{aligned} \right\} \\ \\ \therefore P_{m_speed_independent} &= \frac{q V_s I_{peak}}{\alpha_r} * \left\{ \begin{aligned} &\frac{L_u \beta}{\Delta L} \left[\ln \left(\frac{\left(\frac{\beta}{\Delta L} L_a - (\alpha_r - \beta - \theta_a) \right)^2}{\left(\frac{L_u \beta}{\Delta L} \right) \left(\frac{L_u \beta}{\Delta L} - \beta \right)} \right) + \ln \left(\frac{\left(\frac{L_u \beta}{\Delta L} + \theta_{commutation} \right)^2}{\left(\frac{L_u \beta}{\Delta L} \right) \left(\frac{L_u \beta}{\Delta L} + \beta \right)} \right) \right] \\ &+ 2(\alpha_r - \theta_{dwell} - \beta) \end{aligned} \right\} \end{aligned} \quad (7.43)$$

While the speed dependent part is:

$$\therefore P_{m_speed_dependent} = \omega \frac{q}{\alpha_r} * \left\{ \begin{aligned} & \left(\frac{V_s}{\omega} \right)^2 \frac{1}{2L_u} \left[(2*\alpha_r - 2*\theta_{dwell} - \beta)^2 - \beta^2 \right] \\ & - \left(\frac{V_s}{\omega} \right)^2 \frac{\beta}{\Delta L} \left((\beta - 2*\theta_{commutation}) + \frac{\beta}{\Delta L} L_u \right) \ln \left(\frac{\frac{\beta}{\Delta L} L_u - (\alpha_r - \beta - \theta_a)}{\frac{\beta}{\Delta L} L_u} \right) \\ & - \left(\frac{V_s}{\omega} \right)^2 \frac{\beta}{\Delta L} \left(\frac{\beta}{\Delta L} L_u - (2*\alpha_r - 2*\theta_{dwell} - \beta) \right) \ln \left(\frac{\beta - \frac{\beta}{\Delta L} L_u}{(\alpha_r - \beta - \theta_a) - \frac{\beta}{\Delta L} L_u} \right) \\ & - \left(\frac{V_s}{\omega} \right)^2 \frac{2}{L_u} (2*\alpha_r - 2*\theta_{dwell} - \beta) (\alpha_r - \theta_{dwell} - \beta) - \left(\frac{V_s}{\omega} \frac{\beta}{\Delta L} \right)^2 L_u \ln \left(\frac{\frac{L_u \beta}{\Delta L} + \theta_{commutation}}{\frac{L_u \beta}{\Delta L}} \right) \\ & - \left(\frac{V_s}{\omega} \right)^2 \frac{\beta}{\Delta L} \left(\frac{\beta}{\Delta L} L_u + 2*\theta_{commutation} \right) \ln \left(\frac{\frac{\beta}{\Delta L} L_u + \beta}{\frac{\beta}{\Delta L} L_u + \theta_{commutation}} \right) \end{aligned} \right\}$$

This can be rewritten as:

$$\therefore P_{m_speed_dependent} = \frac{q(V_s)^2}{\omega \alpha_r} * \left\{ \begin{aligned} & \frac{1}{2L_u} \left[(2\alpha_r - 2\theta_{dwell} - \beta)^2 - \beta^2 \right] \\ & - \frac{\beta}{\Delta L} \left((\beta - 2\theta_{commutation}) + \frac{\beta}{\Delta L} L_u \right) \ln \left(\frac{\frac{\beta}{\Delta L} L_a - (\alpha_r - \beta - \theta_a)}{\frac{\beta}{\Delta L} L_a} \right) \\ & - \frac{\beta}{\Delta L} \left(\frac{\beta}{\Delta L} L_a - (2\alpha_r - 2\theta_{dwell} - \beta) \right) \ln \left(\frac{\beta - \frac{\beta}{\Delta L} L_a}{(\alpha_r - \beta - \theta_a) - \frac{\beta}{\Delta L} L_a} \right) \\ & - \frac{2}{L_u} (2\alpha_r - 2\theta_{dwell} - \beta) (\alpha_r - \theta_{dwell} - \beta) - \left(\frac{\beta}{\Delta L} \right)^2 L_u \ln \left(\frac{\frac{L_u \beta}{\Delta L} + \theta_{commutation}}{\frac{L_u \beta}{\Delta L}} \right) \\ & - \frac{\beta}{\Delta L} \left(\frac{\beta}{\Delta L} L_u + 2\theta_{commutation} \right) \ln \left(\frac{\frac{\beta}{\Delta L} L_u + \beta}{\frac{\beta}{\Delta L} L_u + \theta_{commutation}} \right) \end{aligned} \right\} \quad (7.44)$$

Note that this part does not depend on the peak current requirement.

Since $\omega = \frac{2 * \pi * n * N_b}{60}$, at very high speed, i.e. as $n \rightarrow \infty$,

$$\therefore \lim_{\omega \rightarrow \infty} P_m = \frac{q V_s I_{peak}}{\alpha_r} * \left\{ \begin{aligned} & \frac{L_u \beta}{\Delta L} \left[\ln \left(\frac{\left(\frac{\beta}{\Delta L} L_a - (\alpha_r - \beta - \theta_a) \right)^2}{\left(\frac{L_a \beta}{\Delta L} \right)^2 - \frac{L_a \beta^2}{\Delta L}} \right) + \ln \left(\frac{\left(\frac{L_u \beta}{\Delta L} + \theta_{commutation} \right)^2}{\left(\frac{L_u \beta}{\Delta L} \right)^2 + \frac{L_u \beta^2}{\Delta L}} \right) \right] \\ & + 2(\alpha_r - \beta - \theta_{dwell}) \end{aligned} \right\} \quad (7.45)$$

$$\therefore \lim_{\omega \rightarrow \infty} P_m = \frac{qV_s I_{peak}}{\alpha_r} * \left\{ \frac{L_u \beta}{\Delta L} \left[\ln \left(\frac{\left(\frac{\beta}{\Delta L} L_a - (\alpha_r - \beta - \theta_{adv}) \right)^2}{L_a L_u \left(\frac{\beta}{\Delta L} \right)^2} \right) + \ln \left(\frac{\left(\frac{L_u \beta}{\Delta L} + \theta_{commutation} \right)^2}{L_a L_u \left(\frac{\beta}{\Delta L} \right)^2} \right) \right] + 2(\alpha_r - \beta - \theta_{dwell}) \right\} \quad (7.46)$$

At very high speed, the speed dependent part decreases to zero and the developed power approaches the speed independent part. Since speed dependent part does not depend on the peak current, based on output power requirement, by first calculating the speed dependent power, it is possible to calculate the peak current which will result in the desired output power.

$$P_{required} - P_{speed_dependent} = \frac{q}{\alpha_r} * \left\{ V_s L_u I_{peak} \frac{\beta}{\Delta L} \left[\ln \left(\frac{\frac{\beta}{\Delta L} L_a - (\alpha_r - \beta - \theta_a)}{\frac{\beta}{\Delta L} L_a} \right) - \ln \left(\frac{\frac{\beta}{\Delta L} L_a - \beta}{\frac{\beta}{\Delta L} L_a - (\alpha_r - \beta - \theta_a)} \right) \right] + \ln \left(\frac{\frac{L_u \beta}{\Delta L} + \theta_{commutation}}{\frac{L_u \beta}{\Delta L}} \right) - \ln \left(\frac{\frac{\beta}{\Delta L} L_u + \beta}{\frac{\beta}{\Delta L} L_u + \theta_{commutation}} \right) \right] + 2V_s I_{peak} (\alpha_r - \theta_{dwell} - \beta) \right\}$$

$$\therefore I_{peak} = \frac{\alpha_r (P_{required} - P_{speed_dependant})}{2qV_s (\alpha_r - \theta_{dwell} - \beta) + qV_s \frac{L_u \beta}{\Delta L} \left[\ln \left(\frac{\left(\frac{\beta}{\Delta L} L_a - (\alpha_r - \beta - \theta_a) \right)^2}{\left(\frac{\beta}{\Delta L} L_a \right) \left(\frac{\beta}{\Delta L} L_a - \beta \right)} \right) + \ln \left(\frac{\left(\frac{L_u \beta}{\Delta L} + \theta_{commutation} \right)^2}{\left(\frac{L_u \beta}{\Delta L} \right) \left(\frac{\beta}{\Delta L} L_u + \beta \right)} \right) \right]} \quad (7.47)$$

Using the above peak current, it is possible to produce the desired output power. How to maximize this output power? Simulation results show that for a given speed, dwell angle, and peak current set point, there is an advance angle which maximizes the output power. Because of the complex nature of the power equations, it will be tedious to find out the exact relation between the advance angle and the output power. Although, as $n \rightarrow \infty$, the advance angle which maximizes this developed power, can be derived from the speed independent part of the power equation as follows:

As $n \rightarrow \infty$, developed power approaches the value given by following equation,

$$\therefore P_m = \frac{q}{\alpha_r} * \left\{ V_s L_u I_{peak} \frac{\beta}{\Delta L} \left[\ln \left(\frac{\frac{\beta}{\Delta L} L_a - (\alpha_r - \beta - \theta_a)}{\frac{\beta}{\Delta L} L_a} \right) - \ln \left(\frac{\frac{\beta}{\Delta L} L_a - \beta}{\frac{\beta}{\Delta L} L_a - (\alpha_r - \beta - \theta_a)} \right) \right] + \ln \left(\frac{\frac{L_u \beta}{\Delta L} + \theta_{commutation}}{\frac{L_u \beta}{\Delta L}} \right) - \ln \left(\frac{\frac{\beta}{\Delta L} L_u + \beta}{\frac{\beta}{\Delta L} L_u + \theta_{commutation}} \right) \right\} + 2V_s I_{peak} (\alpha_r - \theta_{dwell} - \beta)$$

$$\therefore \frac{\partial P_m}{\partial \theta_a} = \frac{q}{\alpha_r} \frac{\partial}{\partial \theta_a} \left\{ V_s L_u I_{peak} \frac{\beta}{\Delta L} \left[\ln \left(\frac{\frac{\beta}{\Delta L} L_a - (\alpha_r - \beta - \theta_a)}{\frac{\beta}{\Delta L} L_a} \right) - \ln \left(\frac{\frac{\beta}{\Delta L} L_a - \beta}{\frac{\beta}{\Delta L} L_a - (\alpha_r - \beta - \theta_a)} \right) \right] + \ln \left(\frac{\frac{L_u \beta}{\Delta L} + \theta_{commutation}}{\frac{L_u \beta}{\Delta L}} \right) - \ln \left(\frac{\frac{\beta}{\Delta L} L_u + \beta}{\frac{\beta}{\Delta L} L_u + \theta_{commutation}} \right) \right\} + 2V_s I_{peak} (\alpha_r - \theta_{dwell} - \beta) \right\} = 0$$

$$\theta_{adv}^* = \frac{(\alpha_r - 2\beta) + \theta_{dwell}}{2} \quad (7.48)$$

Note that the advance angle which maximizes the developed power depends on the dwell angle and machine design parameters. For a dwell angle of 31°, this value evaluates to 23°. Similarly, average current can be calculated as follows,

$$I_{avg} = \frac{1}{\alpha_r} \left[\int_{\theta=0}^{\theta=(\alpha_r - \beta - \theta_a)} i_1(\theta) d\theta + \int_{\theta=(\alpha_r - \beta - \theta_a)}^{\theta=\beta} i_2(\theta) d\theta + \int_{\theta=\beta}^{\theta=(2^*\alpha_r - 2^*\theta_{dwell} - \beta)} i_3(\theta) d\theta + \int_{\theta=(2^*\alpha_r - 2^*\theta_{dwell} - \beta)}^{\theta=(\alpha_r - \beta)} i_4(\theta) d\theta + \int_{\theta=(\alpha_r - \beta)}^{\theta=(\alpha_r - \beta + \theta_{commutation})} i_5(\theta) d\theta + P_6 = \frac{-V_s}{\omega} * \int_{\theta=(\alpha_r - \beta + \theta_{commutation})}^{\theta=\alpha_r} i_6(\theta) d\theta \right]$$

Detailed mathematical calculations are attached in the Appendix 0 which shows that the average current can be written as,

$$\begin{aligned}
I_{avg} = \frac{1}{\alpha_r} & \left[\begin{aligned}
& -L_u I_{peak} \frac{\beta}{\Delta L} \ln \left(\frac{\frac{\beta L_a}{\Delta L} - (\alpha_r - \beta - \theta_a)}{\frac{\beta L_a}{\Delta L}} \right) + \frac{\beta}{\Delta L} \frac{V_s}{\omega} (\alpha_r - \beta - \theta_a) \\
& + \frac{\beta}{\Delta L} \frac{V_s}{\omega} \left(\beta - 2\theta_{commutation} + \frac{\beta}{\Delta L} L_a \right) \ln \left(\frac{\frac{\beta L_a}{\Delta L} - (\alpha_r - \beta - \theta_a)}{\frac{\beta L_a}{\Delta L}} \right) \\
& - L_u I_{peak} \frac{\beta}{\Delta L} \ln \left(\frac{\frac{\beta L_a}{\Delta L} - \beta}{\frac{\beta L_a}{\Delta L} - (\alpha_r - \beta - \theta_a)} \right) - \frac{V_s}{\omega} \frac{\beta}{\Delta L} [\theta_a - (\alpha_r - 2\beta)] \\
& - \frac{V_s}{\omega} \frac{\beta}{\Delta L} \left(\frac{\beta L_a}{\Delta L} - (2\alpha_r - 2\theta_{dwell} - \beta) \right) \ln \left(\frac{\beta - \frac{\beta L_a}{\Delta L}}{(\alpha_r - \beta - \theta_a) - \frac{\beta L_a}{\Delta L}} \right) \\
& + 2I_{peak} (\alpha_r - \theta_{dwell} - \beta) - \frac{V_s}{\omega} \frac{2}{L_u} (2\alpha_r - 2\theta_{dwell} - \beta) (\alpha_r - \theta_{dwell} - \beta) \\
& + \frac{V_s}{\omega} \frac{1}{2L_u} \left[(2\alpha_r - 2\theta_{dwell} - \beta)^2 - \beta^2 \right] + I_{peak} (2\theta_{dwell} - \alpha_r) \\
& + L_u I_{peak} \frac{\beta}{\Delta L} \ln \left(\frac{\frac{L_u \beta}{\Delta L} + \theta_{commutation}}{\frac{L_u \beta}{\Delta L}} \right) + \frac{V_s}{\omega} \frac{\beta}{\Delta L} \theta_{commutation} - \frac{V_s}{\omega} \left(\frac{\beta}{\Delta L} \right)^2 L_u \ln \left(\frac{\frac{L_u \beta}{\Delta L} + \theta_{commutation}}{\frac{L_u \beta}{\Delta L}} \right) \\
& + L_u I_{peak} \frac{\beta}{\Delta L} \ln \left(\frac{\frac{\beta L_u}{\Delta L} + \beta}{\frac{\beta L_u}{\Delta L} + \theta_{commutation}} \right) - \frac{V_s}{\omega} \frac{\beta}{\Delta L} [\beta - \theta_{commutation}] \\
& + \frac{V_s}{\omega} \frac{\beta}{\Delta L} \left(\frac{\beta}{\Delta L} L_u + 2\theta_{commutation} \right) \ln \left(\frac{\frac{\beta L_u}{\Delta L} + \beta}{\frac{\beta L_u}{\Delta L} + \theta_{commutation}} \right)
\end{aligned} \right]
\end{aligned}$$

Again this can be split into a speed dependent part and a speed independent part. The speed dependent part is:

$$I_{avg_speed_independent} = \frac{1}{\alpha_r} \left[\begin{aligned} & -L_u I_{peak} \frac{\beta}{\Delta L} \ln \left(\frac{\frac{\beta L_a}{\Delta L} - (\alpha_r - \beta - \theta_{adv})}{\frac{\beta L_a}{\Delta L}} \right) - L_u I_{peak} \frac{\beta}{\Delta L} \ln \left(\frac{\frac{\beta L_a}{\Delta L} - \beta}{\frac{\beta L_a}{\Delta L} - (\alpha_r - \beta - \theta_{adv})} \right) \\ & + 2I_{peak} (\alpha_r - \theta_{dwell} - \beta) + I_{peak} (2\theta_{dwell} - \alpha_r) \\ & + L_u I_{peak} \frac{\beta}{\Delta L} \ln \left(\frac{\frac{L_u \beta}{\Delta L} + \theta_{commutation}}{\frac{L_u \beta}{\Delta L}} \right) + L_u I_{peak} \frac{\beta}{\Delta L} \ln \left(\frac{\frac{\beta L_u}{\Delta L} + \beta}{\frac{\beta L_u}{\Delta L} + \theta_{commutation}} \right) \end{aligned} \right]$$

$$\therefore I_{avg_speed_independent} = \frac{I_{peak}}{\alpha_r} \left[\frac{L_u \beta}{\Delta L} \ln \left(\frac{\frac{\beta L_a}{\Delta L} \left(\frac{\beta L_u}{\Delta L} + \beta \right)}{\frac{L_u \beta}{\Delta L} \left(\frac{\beta L_a}{\Delta L} - \beta \right)} \right) + (\alpha_r - 2\beta) \right] \quad (7.49)$$

Note that the speed independent part is linear in the peak current and it does not depend on the choice of dwell or advance angle. This component of the average current depends on the machine design. This means that the better way to regulate output power is by changing the peak current. This results in motor current being proportional to the output power.

The speed dependent part is:

$$\begin{aligned}
I_{\text{avg_speed_dependent}} = \frac{1}{\alpha_r} & \left[\begin{aligned}
& \frac{\beta}{\Delta L} \frac{V_s}{\omega} (\alpha_r - \beta - \theta_a) - \frac{V_s}{\omega} \frac{\beta}{\Delta L} [\theta_a - (\alpha_r - 2\beta)] - \frac{V_s}{\omega} \frac{\beta}{\Delta L} [\beta - \theta_{\text{commutation}}] \\
& + \frac{\beta}{\Delta L} \frac{V_s}{\omega} \left(\beta - 2\theta_{\text{commutation}} + \frac{\beta L_a}{\Delta L} \right) \ln \left(\frac{\frac{\beta L_a}{\Delta L} - (\alpha_r - \beta - \theta_a)}{\frac{\beta L_a}{\Delta L}} \right) \\
& - \frac{V_s}{\omega} \frac{\beta}{\Delta L} \left(\frac{\beta L_a}{\Delta L} - (2\alpha_r - 2\theta_{\text{dwell}} - \beta) \right) \ln \left(\frac{\beta - \frac{\beta L_a}{\Delta L}}{(\alpha_r - \beta - \theta_a) - \frac{\beta L_a}{\Delta L}} \right) \\
& - \frac{V_s}{\omega} \frac{2}{L_u} (2\alpha_r - 2\theta_{\text{dwell}} - \beta) (\alpha_r - \theta_{\text{dwell}} - \beta) \\
& + \frac{V_s}{\omega} \frac{1}{2L_u} \left[(2\alpha_r - 2\theta_{\text{dwell}} - \beta)^2 - \beta^2 \right] \\
& + \frac{V_s}{\omega} \frac{\beta}{\Delta L} \theta_{\text{commutation}} - \frac{V_s}{\omega} \left(\frac{\beta}{\Delta L} \right)^2 L_u \ln \left(\frac{\frac{L_u \beta}{\Delta L} + \theta_{\text{commutation}}}{\frac{L_u \beta}{\Delta L}} \right) \\
& + \frac{V_s}{\omega} \frac{\beta}{\Delta L} \left(\frac{\beta}{\Delta L} L_u + 2\theta_{\text{commutation}} \right) \ln \left(\frac{\frac{\beta L_u}{\Delta L} + \beta}{\frac{\beta L_u}{\Delta L} + \theta_{\text{commutation}}} \right)
\end{aligned} \right]
\end{aligned}$$

$$\begin{aligned}
\therefore I_{avg_speed_dependent} = \frac{V_s}{\omega \alpha_r} \frac{\beta}{\Delta L} & \left[\left(\beta - 2\theta_{commutation} + \frac{\beta L_a}{\Delta L} \right) \ln \left(\frac{\frac{\beta L_a}{\Delta L} - (\alpha_r - \beta - \theta_a)}{\frac{\beta L_a}{\Delta L}} \right) \right. \\
& - \left(\frac{\beta L_a}{\Delta L} - (2\alpha_r - 2\theta_{dwell} - \beta) \right) \ln \left(\frac{\beta - \frac{\beta L_a}{\Delta L}}{(\alpha_r - \beta - \theta_a) - \frac{\beta L_a}{\Delta L}} \right) \\
& - \frac{\beta L_u}{\Delta L} \ln \left(\frac{\frac{L_u \beta}{\Delta L} + \theta_{commutation}}{\frac{L_u \beta}{\Delta L}} \right) \\
& + \left(\frac{\beta L_u}{\Delta L} + 2\theta_{commutation} \right) \ln \left(\frac{\frac{\beta L_u}{\Delta L} + \beta}{\frac{\beta L_u}{\Delta L} + \theta_{commutation}} \right) \\
& - \frac{2\Delta L}{\beta L_u} (2\alpha_r - 2\theta_{dwell} - \beta)(\alpha_r - \theta_{dwell} - \beta) \\
& \left. + \frac{\Delta L}{2\beta L_u} \left[(2\alpha_r - 2\theta_{dwell} - \beta)^2 - \beta^2 \right] + (2\alpha_r - 4\beta - 4\theta_a + 2\theta_d) \right] \\
(7.50)
\end{aligned}$$

Note that the speed dependent component of the average current is independent of the peak current. It depends linearly on the applied voltage. It also depends on the machine design parameters and control variables.

As very high speed i.e. as $n \rightarrow \infty$,

$$\lim_{\omega \rightarrow \infty} I_{avg} = \frac{I_{peak}}{\alpha_r} \left[\frac{L_u \beta}{\Delta L} \ln \left(\frac{\frac{\beta L_a}{\Delta L} \left(\frac{\beta L_u}{\Delta L} + \beta \right)}{\frac{L_u \beta}{\Delta L} \left(\frac{\beta L_a}{\Delta L} - \beta \right)} \right) + (\alpha_r - 2\beta) \right] \quad (7.51)$$

This equation can be simplified to the following form,

$$\lim_{\omega \rightarrow \infty} I_{avg} = \frac{I_{peak}}{\alpha_r} \left[2 \frac{L_u \beta}{\Delta L} \ln \left(\frac{L_a}{L_u} \right) + (\alpha_r - 2\beta) \right] \quad (7.52)$$

Note that, for a fixed machine design, at high speed, the average current only depends on the peak current and does not depend on the advance angle or the dwell angle.

At high speed, the developed power is,

$$\therefore \lim_{\omega \rightarrow \infty} P_m = \frac{q V_s I_{peak}}{\alpha_r} * \left\{ \frac{L_u \beta}{\Delta L} \left[\ln \left(\frac{\left(\frac{\beta}{\Delta L} L_a - (\alpha_r - \beta - \theta_a) \right)^2}{L_a L_u \left(\frac{\beta}{\Delta L} \right)^2} \right) + \ln \left(\frac{\left(\frac{L_u \beta}{\Delta L} + \theta_{commutation} \right)^2}{L_a L_u \left(\frac{\beta}{\Delta L} \right)^2} \right) \right] + 2(\alpha_r - \beta - \theta_{dwell}) \right\}$$

This power can be maximized using, $\theta_{adv}^* = \frac{(\alpha_r + \theta_{dwell})}{2} - \beta$

For $\theta_{dwell} = \frac{\alpha_r}{2}$, $\theta_{adv}^* = \frac{3}{4} \alpha_r - \beta$. This formula agrees with the result of linear analysis described in [13] and [78]. Number of strokes required to achieve steady state can be derived. Initially, during each cycle, since the dwell angle is more than half of the rotor pole pitch, fluxing region is going to be more than de-fluxing region. Therefore at the end of each stroke, initial flux linkage will increase by,

$$\therefore \lambda_{add} = \frac{V_s}{\omega} * (2 * \theta_{dwell} - \alpha_r),$$

Since, $\lambda_0 = L_u I_{peak} - \frac{V_s}{\omega} * (\alpha_r - \theta_{dwell} - \theta_{commutation})$,

$$\begin{aligned} \therefore strokes * \frac{V_s}{\omega} * (2 * \theta_{dwell} - \alpha_r) &= L_u * I_{peak} - \frac{V_s}{\omega} * (\theta_a + \alpha_r - 2 * \theta_{dwell}), \\ \therefore strokes &= \frac{L_u * I_{peak} - \frac{V_s}{\omega} * (\theta_a + \alpha_r - 2 * \theta_{dwell})}{\frac{V_s}{\omega} * (2 * \theta_{dwell} - \alpha_r)} \end{aligned} \quad (7.53)$$

Using above equation, based on the peak current requirement, information about the advance angle and dwell, it is possible to estimate the number strokes required to achieve steady state (number of strokes after which the current regulator will kick in).

Note that for $\theta_{dwell} = \frac{\alpha_r}{2}$, number of strokes required to achieve the desired peak current is ∞ . This means that the dwell angle has to be more than half of the rotor pole pitch in order to initiate the continuous conduction. Also note that bigger the dwell angle, lesser the number of strokes to achieve the desired peak current. As explained later, simulation results show that, in continuous conduction, the developed power depends inversely on the dwell angle. As is frequently the case, there may be tradeoffs to be made. Validation of these results is given in the next section.

7.4.8 Validation of Analytical Results

Figure 7-21 shows the simulation results of the continuous conduction type control of the flat unaligned inductance type SRM motor using linear model described in the section 7.2.1. The first part of this figure shows applied voltage (blue waveform), inductance profile (red waveform), resultant flux-linkage (magenta waveform) and

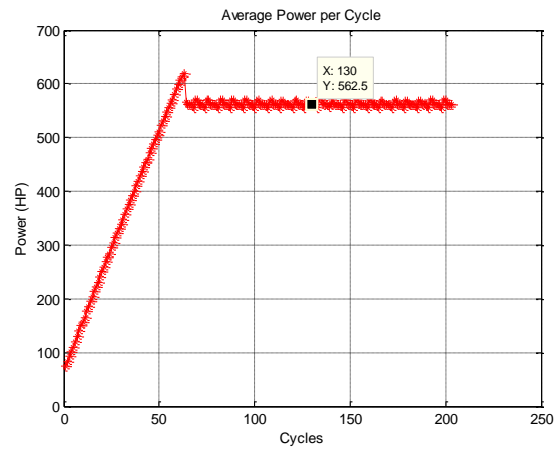
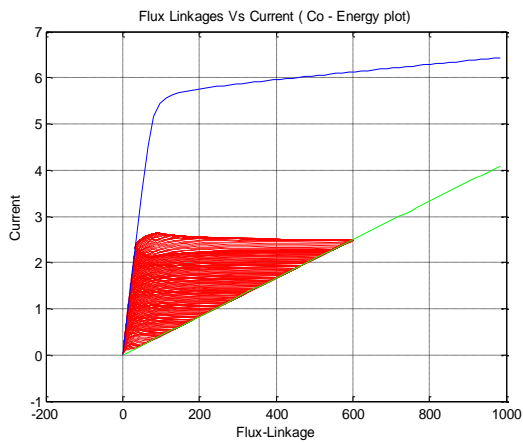
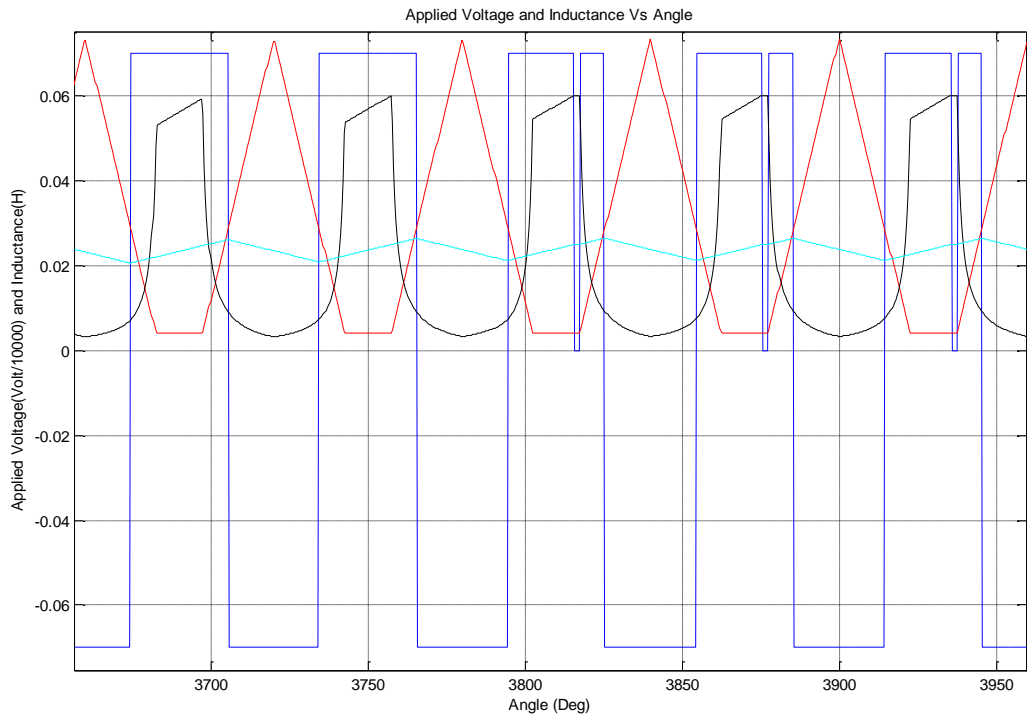


**Figure 7-21: Validation of Flat Unaligned Inductance Type SRM Motor Analysis, Speed = 6500 rpm
(n=26), Dwell = 31°, Advance Angle = 23° and Current Regulator Set Point, I_{peak} = 600A.**

resultant current (black waveform) just before and after the current regulator involvement. Note that once the desired peak current is achieved, the developed power is maintained and the growing current is stabilized. Second part of this figure is a growing flux-linkage Vs current waveform as a result of continuous conduction (co-energy plot). The third part of this figure is resultant average power. Here speed is 6500 RPM (26 time base speed), advance angle is 23° , dwell angle is 31° and the current regulator set point is 600A.

A number of simulations were carried out to validate these analytical results. Data was verified for $n = 6$ (1500 RPM) , $n = 15$ (3750 RPM) and $n = 26$ (6500 RPM) with advance angle = $15^\circ, 17^\circ, 19^\circ, 21^\circ, 23^\circ$ and 25° and current regulator set point = 600 A and 300 A, with dwell fixed at 31° . Table 7-1, Table 7-2, and Table 7-3, show comparison between the theoretical values (using formulas developed in the previous section) and simulation results (using linear model described in the section 7.2.1) for residual flux-linkage, peak flux-linkage, minimum current, average power, average current as well as the speed dependant and the speed independent split for both the average power and the average current. These tables also list the RMS current obtained from simulation.

Table 7-4 shows these values for the dwell angle of 32° . Note that as the advance angle increase, residual flux linkage, peak flux linkage, and the minimum current decreases. The average power initially increases and then it decreases as the speed dependent part of the average power becomes more negative above the “optimum” advance angle.

Table 7-1 : Flat Unaligned Inductance type SRM, Dwell = 31.

Speed = 1500 RPM , Peak Current = 600 A															
Adv. Angle	Intial Flux Linkage (Wb)		Peak Flux Linkage (Wb)		Minimum Current (A)		Average Power (HP)		Average Power (HP)		Average Current (A)		Average Current (A)		RMS Cur. (A)
	Sim. Model	Analyt. Result	Sim. Model	Analyt. Result	Sim. Model	Analyt. Result	Sim. Model	Analyt. Result	Speed Ind.	Speed Dep.	Sim. Model	Analyt. Result	Speed Ind.	Speed Dep.	
15	1.477	1.4789	3.73	3.7344	44.03	44.002	401	399.6	455.72	-56.12	200	200.23	227.49	-27.26	273.8
17	1.321	1.3233	3.575	3.5789	39.73	39.763	451.5	450.89	535.39	-84.5	195.2	195.63	227.49	-31.86	272.2
19	1.17	1.1678	3.422	3.4233	35.44	35.523	470.6	468.9	568.67	-99.77	191	191.89	227.49	-35.6	270.7
21	1.006	1.012	3.264	3.268	31.22	31.28	474.7	473.5	584.4	-111	188	188.5	227.5	-38.9	270.6
23	0.8569	0.8567	3.108	3.1122	27.05	27.043	470.6	469.52	589.14	-119.6	184.9	185.36	227.49	-42.13	270.6
25	0.6985	0.7011	2.953	2.9567	20.02	22.804	458.9	457.96	584.4	-126.4	181.7	182.18	227.49	-45.31	270

Table 7-2 : Flat Unaligned Inductance type SRM, Dwell = 31.

Speed = 3750 RPM , Peak Current = 600 A															
Adv. Angle	Intial Flux Linkage (Wb)		Peak Flux Linkage (Wb)		Minimum Current (A)		Average Power (HP)		Average Power (HP)		Average Current (A)		Average Current (A)		RMS Cur. (A)
	Sim. Model	Analyt. Result	Sim. Model	Analyt. Result	Sim. Model	Analyt. Result	Sim. Model	Analyt. Result	Speed Ind.	Speed Dep.	Sim. Model	Analyt. Result	Speed Ind.	Speed Dep.	
15	2.083	2.0856	2.985	2.9878	38.05	37.961	435.4	433.27	455.72	-22.45	216	216.58	227.49	-10.9	302.5
17	2.02	2.0233	2.922	2.9256	36.31	36.265	502.3	501.59	535.39	-33.8	214.2	214.75	227.49	-12.74	301.8
19	1.959	1.9611	2.865	2.8633	34.59	34.569	529.2	528.76	568.67	-39.91	212.7	213.25	227.49	-14.24	301.6
21	1.897	1.8989	2.801	2.8011	32.82	32.873	542.4	540.05	584.4	-44.35	211.7	211.91	227.49	-15.58	301.8
23	1.839	1.8367	2.735	2.7389	31.21	31.177	545.9	541.29	589.14	-47.85	210	210.64	227.49	-16.85	302
25	1.774	1.7744	2.678	2.6767	29.58	29.481	537.5	533.82	584.4	-50.58	209.1	209.36	227.49	-18.12	301.2
Speed = 3750 RPM , Peak Current = 300 A															
17	0.7766	0.7783	1.679	1.6806	19.39	19.298	234	233.89	267.7	-33.8	100	101	113.74	-12.74	140.8
19	0.715	0.7161	1.615	1.6183	17.59	17.602	247.3	244.43	284.33	-39.91	100	99.505	113.74	-14.24	140.3
21	0.6565	0.6539	1.555	1.5561	15.83	15.907	247.9	247.85	292.2	-44.35	98.47	98.166	113.74	-15.58	140.1
23	0.6	0.5917	1.5	1.4939	14.22	14.211	246.6	246.72	294.57	-47.85	97.2	96.893	113.74	-16.85	140.1
25	0.5313	0.5294	1.432	1.4317	12.51	12.515	243.4	241.62	292.2	-50.58	95.22	95.62	113.74	-18.12	139.8

Table 7-3 : Flat Unaligned Inductance type SRM, Dwell = 31.

Speed = 6500 RPM , Peak Current = 600 A															
Adv. Angle	Intial Flux Linkage (Wb)		Peak Flux Linkage (Wb)		Minimum Current (A)		Average Power (HP)		Average Power (HP)		Average Current (A)		Average Current (A)		RMS Cur. (A)
	Sim. Model	Analyt. Result	Sim. Model	Analyt. Result	Sim. Model	Analyt. Result	Sim. Model	Analyt. Result	Speed Ind.	Speed Dep.	Sim. Model	Analyt. Result	Speed Ind.	Speed Ind.	
15	2.261	2.2567	2.775	2.7772	36.68	36.257	445.6	442.77	455.72	-12.95	221.4	221.2	227.49	-6.29	311.7
17	2.22	2.2208	2.743	2.7413	35.53	35.278	520.5	515.89	535.39	-19.5	219.8	220.14	227.49	-7.351	312.1
19	2.18	2.1849	2.701	2.7054	34.43	34.3	550.5	545.64	568.67	-23.02	218.9	219.27	227.49	-8.215	310.5
21	2.15	2.149	2.669	2.6695	33.48	33.322	558.8	558.81	584.4	-25.58	220	218.5	227.49	-8.987	311.5
23	2.118	2.1131	2.632	2.6336	32.52	32.343	561.8	561.54	589.14	-27.6	220	217.77	227.49	-9.722	311.3
25	2.082	2.0772	2.601	2.5977	31.58	31.365	558.6	555.22	584.4	-29.18	218.3	217.03	227.49	-10.46	310.1
Speed = 6500 RPM , Peak Current = 300 A															
17	0.9799	0.9758	1.5	1.4963	18.4	18.312	250.3	248.2	267.7	-19.5	106.2	106.39	113.74	-7.351	149.5
19	0.9383	0.9399	1.464	1.4604	17.4	17.333	262.3	261.31	284.33	-23.02	105.5	105.53	113.74	-8.215	149
21	0.9128	0.904	1.422	1.4245	16.4	16.355	267.8	266.61	292.2	-25.58	105.2	104.76	113.74	-8.987	150
23	0.8679	0.8681	1.389	1.3886	15.44	15.377	269.5	266.97	294.57	-27.6	104.3	104.02	113.74	-9.722	148.9
25	0.8351	0.8322	1.352	1.3527	14.55	14.398	266	263.02	292.2	-29.18	103.2	103.29	113.74	-10.46	149.4

Table 7-4: Flat Unaligned Inductance type SRM, Dwell = 32.

Speed = 6500 RPM , Peak Current = 600 A															
Adv. Angle	Initial Flux Linkage (Wb)		Peak Flux Linkage (Wb)		Minimum Current (A)		Average Power (HP)		Average Power (HP)		Average Current (A)		Average Current (A)		RMS Cur (A)
	Sim. Model	Analyt. Result	Sim. Model	Analyt. Result	Sim. Model	Analyt. Result	Sim. Model	Analyt. Result	Speed Ind.	Speed Dep.	Sim. Model	Analyt. Result	Speed Ind.	Speed Dep.	
15	2.291	2.2926	2.794	2.7951	36.94	36.746	384.7	378.23	386.32	-8.0907	223.1	223.54	227.49	-3.9455	315.1
17	2.255	2.2567	2.759	2.7592	35.88	35.767	458.6	453.31	466.71	-13.407	222	222.5	227.49	-4.9833	314.5
19	2.218	2.2208	2.725	2.7233	34.95	34.789	491.6	484.56	500.91	-16.355	221.2	221.67	227.49	-5.8203	314.4
21	2.192	2.1849	2.685	2.6874	34.03	33.811	504	499.3	517.88	-18.577	222.3	220.93	227.49	-6.5626	316.3
23	2.153	2.149	2.656	2.6515	33.04	32.832	509.3	503.96	524.36	-20.397	220.4	220.23	227.49	-7.261	314.1
25	2.112	2.1131	2.617	2.6156	31.95	31.854	504.4	500.37	522.25	-21.88	219	219.54	227.49	-7.9513	313.9
Speed = 6500 RPM , Peak Current = 300 A															
17	1.015	1.0117	1.517	1.5142	18.91	18.801	223.1	219.95	233.36	-13.407	109.4	108.76	113.74	-4.9833	153.7
19	0.98	0.9758	1.48	1.4783	17.85	17.823	238.2	234.1	250.46	-16.355	108.1	107.92	113.74	-5.8203	152.8
21	0.9433	0.9399	1.441	1.4424	16.96	16.844	242.2	240.36	258.94	-18.577	107.2	107.18	113.74	-6.5626	152.9
23	0.9032	0.904	1.407	1.4065	15.93	15.866	244.3	241.78	262.18	-20.397	106.3	106.48	113.74	-7.261	152.4
25	0.8689	0.8681	1.372	1.3706	14.98	14.887	243.5	239.24	261.12	-21.88	106	105.79	113.74	-7.9513	152.3

Speed independent part of the average current remains constant as it does not depend on the advance angle or the dwell angle. It only depends on the peak current and machine design parameters. Negative speed dependent part increases with the advance angle. Also note that, for a given peak current, the RMS current remains constant which it does not depend on the advance angle or the dwell angle.

Figure 7-22, Figure 7-23, Figure 7-24, and Figure 7-25 show comparison between the analytical and simulation results listed in those tables. The tables and the graphs show that simulation results and theoretical values agree well with each other.

7.4.9 Controller Analysis

From previous section it is clear that by using continuous conduction, rated power can be developed at high speed without exceeding the current or the voltage rating. In order to sustain continuous conduction it is necessary that the net volt-seconds, applied to the SRM windings, be zero over each stroke.

Figure 7-26 displays the RMS current and the developed power versus advance angle for dwell angles of 30.5° , 31.5° and 32.5° . The current regulator set point is at the 500A for all data points.

Note that for the 32.5° dwell, resultant RMS current is more and the developed power is lower for any advance angle, than for the dwell angle of 31.5° . This indicates that the greatest efficiency will be achieved using a dwell that is just sufficient to initiate and sustain the continuous conduction but otherwise as small as possible.

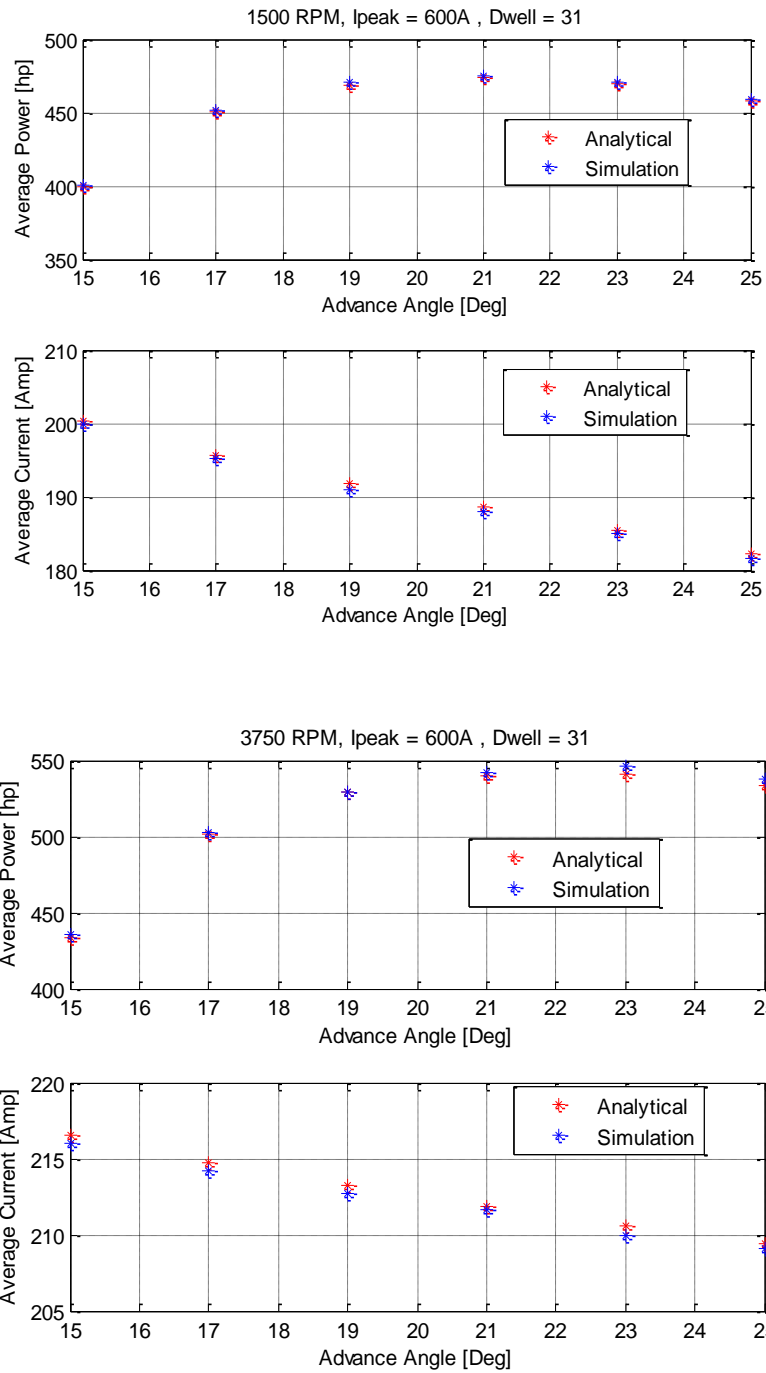


Figure 7-22 : Comparison Between Analytical and Simulation Results.

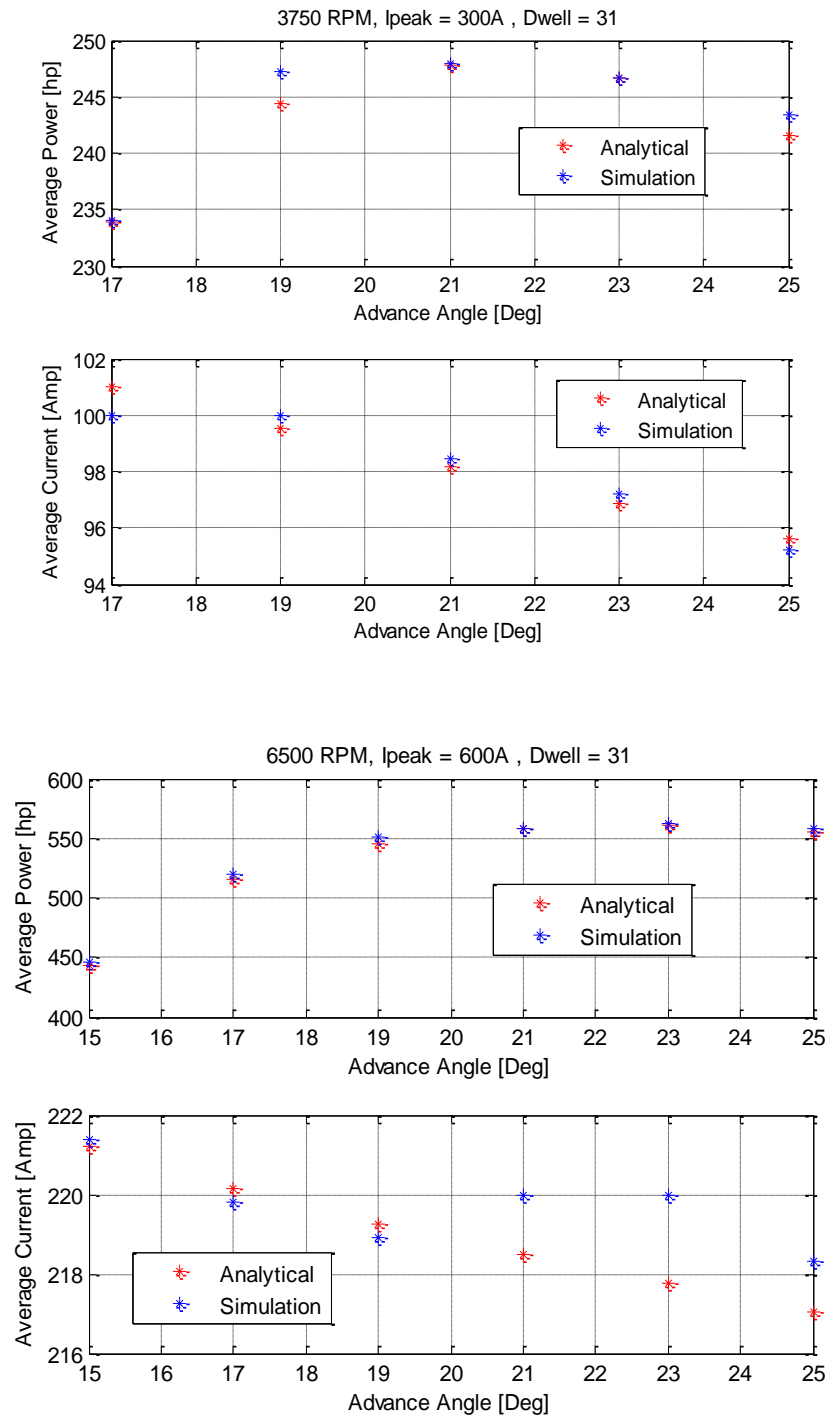


Figure 7-23 : Comparison Between Analytical and Simulation Results.

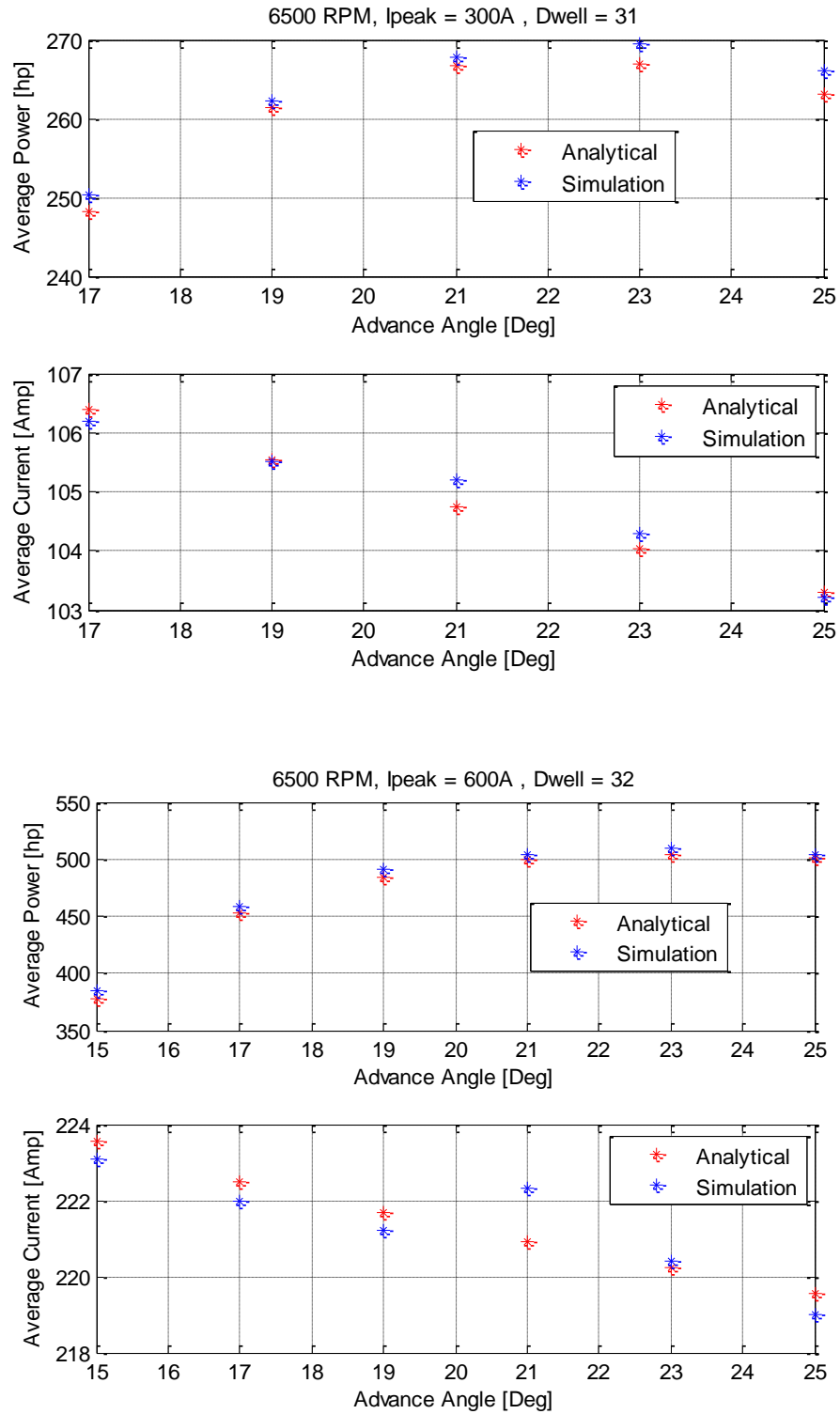


Figure 7-24 : Comparison Between Analytical and Simulation Results.

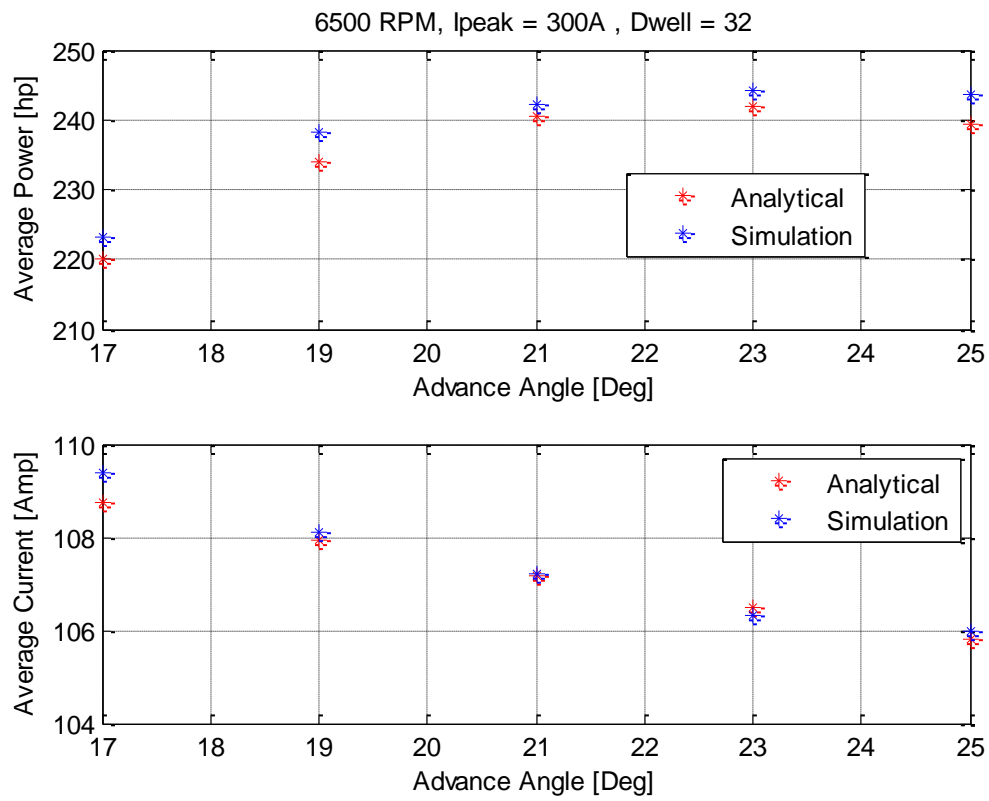


Figure 7-25 : Comparison Between Analytical and Simulation Results.

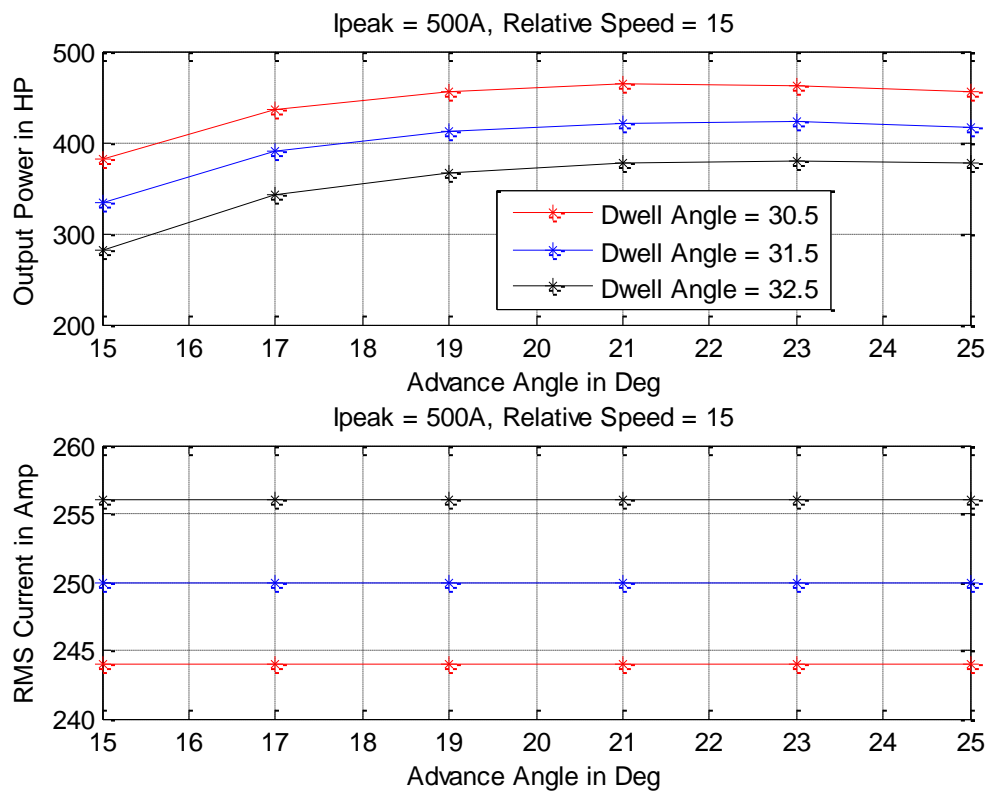


Figure 7-26 : Dwell Angle Vs Advance Angle (Speed = 3750 RPM, $I_{peak} = 500A$).

In PMSM motors, the output power is controlled by the “inverter lead angle” which is same as the advance angle. Figure 7-27 displays developed power versus advance angle for current regulator set-points of 600A, 400A and 200A with the dwell angle fixed at 31° . Plots are made for 3750 RPM ($n = 15$), and for 6500 RPM ($n = 26$). The graphs show that the current regulator set point is a more effective way of controlling output power than by varying the advance angle in high-speed SRM operation with continuous conduction. Thus the preferred way is to set the dwell at the maximum value (greater than $\alpha_r/2$) to initiate and sustain the continuous conduction, set the advance angle at the optimum value given by Equation(7.48), and adjust the current regulator set-point to control the developed output power. The dwell angle can be reduced as the current approaches the desired peak value. Table 7-5 and Table 7-6 show a simple way to develop the rated power at high speed using continuous conduction type controller. Here advance angle is set to 22.5° and the dwell angle is set to 31° for all speed ranges. Peak current regulator set point is changed to develop the rated power. Note that at high speed, peak current required to develop the rated power is much lower than the rated value of 600A. As mentioned earlier, at lower current levels, nonlinear model agrees with the linear model as saturation is minimal. In general, for the flat unaligned inductance type switched reluctance motors, when operated in continuous conduction, we have,

Residual Flux Linkage to get desired peak current:

$$\lambda_0 = L_u * I_{peak} - \frac{V_s}{\omega} * (\theta_a + \alpha_r - 2 * \theta_{dwell})$$

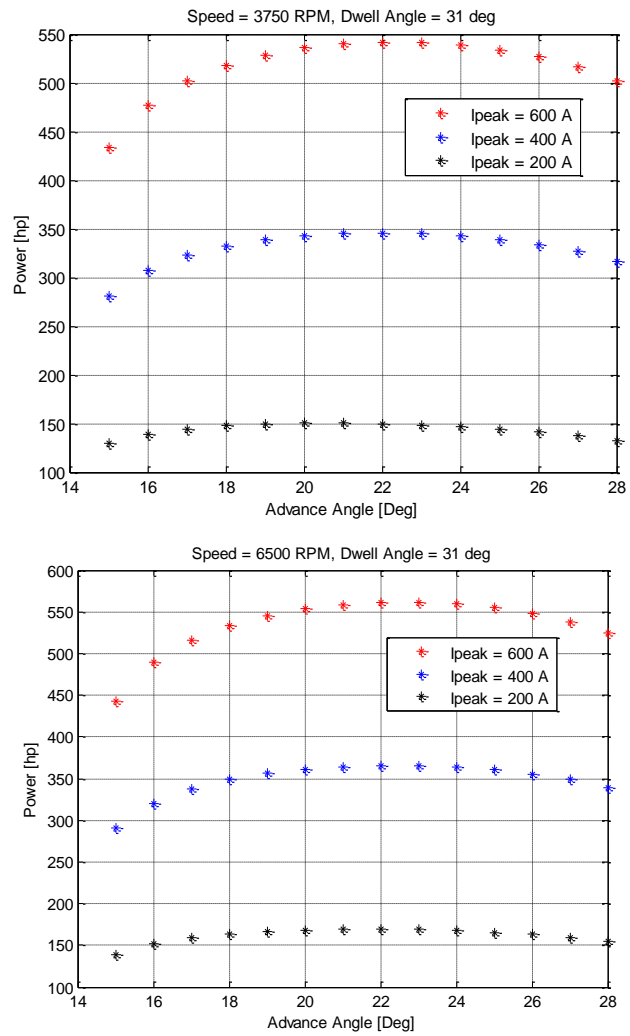


Figure 7-27: Power Control in Continuous Conduction Mode.

Table 7-5 : Peak Current Required to get Rated Power.

Relative Speed	Advance Angle	Dwell Angle	Peak current to get rated Power
6	22.5	31	445.8997
7	22.5	31	428.7797
8	22.5	31	415.9397
9	22.5	31	405.953
10	22.5	31	397.9636
15	22.5	31	373.9956
20	22.5	31	362.0116
25	22.5	31	354.8212
30	22.5	31	350.0276
100	22.5	31	333.2499

Table 7-6 : Rated Power Development at High Speed.

Advance Angle = 22.5 , Dwell Angle = 31							
Speed	Peak Current (A)	Initial Flux Linkage (Wb)	Peak Flux Linkage	Minimum Current (A)	Average Power (HP)	Average Current (A)	RMS Current (A)
6	445.8997	0.255	2.5089	9.3611	320.2902	127.4217	189.4079
7	428.7797	0.4129	2.3448	15.1629	320.4781	126.9304	186.7919
9	405.953	0.6226	2.1248	19.0774	320.8001	126.2465	183.655
11	391.4269	0.7559	1.9846	18.9621	320.8574	125.7632	181.8568
15	373.9956	0.9155	1.816	18.8462	320.8418	125.2541	180.0641
21	360.2996	1.0426	1.6847	18.8215	320.539	124.9132	178.9287
25	354.8212	1.094	1.6307	18.6945	316.9717	124.9299	178.8325
30	350.0276	1.136	1.5849	18.7403	320.6551	124.4831	177.9763
inf	326.0595	1.3531	1.3531	18.4403	320	123.6242	

Peak Flux Linkage get desired peak current:

$$\lambda_{peak} = L_u * I_{peak} + \frac{V_s}{\omega} * (\theta_{dwell} - \theta_a),$$

Minimum Current during steady state:

$$I_{min} = \frac{L_u * I_{peak} + \frac{V_s}{\omega} * (2 * \theta_{commutation} - \beta)}{L_a},$$

As $n \rightarrow \infty$,

$$I_{min} = \frac{L_u * I_{peak}}{L_a}$$

Peak Current required to produce the desired output power:

$$\therefore I_{peak} = \frac{\alpha_r (P_{required} - P_{speed_dependant})}{2qV_s (\alpha_r - \theta_{dwell} - \beta) + qV_s \frac{L_u \beta}{\Delta L} \left[\ln \left(\frac{\left(\frac{\beta}{\Delta L} L_a - (\alpha_r - \beta - \theta_a) \right)^2}{\left(\frac{\beta}{\Delta L} L_a \right) \left(\frac{\beta}{\Delta L} L_a - \beta \right)} \right) + \ln \left(\frac{\left(\frac{L_u \beta}{\Delta L} + \theta_{commutation} \right)^2}{\left(\frac{L_u \beta}{\Delta L} \right) \left(\frac{\beta}{\Delta L} L_u + \beta \right)} \right) \right]}$$

Continuous conduction is only effective after certain speed [16], [75], [13]. At medium speed, desired output power can be produced by using traditional discontinues conduction type control scheme (single pulse operation). For a given speed and advance angle, the maximum peak current that can be reached by using just the discontinuous conduction (single pulse mode) is given by the following equation,

$$I_{\max} = \left(\frac{V_s}{\omega} \theta_{adv} \right) * \frac{1}{L_u} = \frac{V_s \theta_{adv}}{\omega L_u} \quad (7.54)$$

At any given speed, if the desired output power requires a peak current (using continuous type conduction given by Equation (7.47)), which is less than the maximum current given by above Equation (7.54), then the discontinuous type control will be more advantageous to develop the required power.

Advance Angle which maximizes developed power at very high speed:

$$\theta_{adv}^* = \frac{(\alpha_r - 2\beta) + \theta_{dwell}}{2}$$

No of strokes required to achieve required peak current:

$$\therefore \text{strokes} = \frac{L_u * I_{peak} - \frac{V_s}{\omega} * (\theta_a + \alpha_r - 2 * \theta_{dwell})}{\frac{V_s}{\omega} * (2 * \theta_{dwell} - \alpha_r)}$$

Average Power:

$$\therefore P_{m_speed_independent} = \frac{q V_s I_{peak}}{\alpha_r} * \left\{ \frac{L_u \beta}{\Delta L} \left[\ln \left(\frac{\left(\frac{\beta}{\Delta L} L_a - (\alpha_r - \beta - \theta_a) \right)^2}{\left(\frac{L_a \beta}{\Delta L} \right) \left(\frac{L_a \beta}{\Delta L} - \beta \right)} \right) + \ln \left(\frac{\left(\frac{L_u \beta}{\Delta L} + \theta_{commutation} \right)^2}{\left(\frac{L_u \beta}{\Delta L} \right) \left(\frac{L_u \beta}{\Delta L} + \beta \right)} \right) \right] + 2(\alpha_r - \theta_{dwell} - \beta) \right\}$$

$$\therefore P_{m_speed_dependant} = \frac{q(V_s)^2}{\omega \alpha_r} *$$

$$\left\{ \begin{aligned} & \frac{1}{2L_u} \left[(2\alpha_r - 2\theta_{dwell} - \beta)^2 - \beta^2 \right] \\ & - \frac{\beta}{\Delta L} \left((\beta - 2\theta_{commutation}) + \frac{\beta}{\Delta L} L_a \right) \ln \left(\frac{\frac{\beta}{\Delta L} L_a - (\alpha_r - \beta - \theta_a)}{\frac{\beta}{\Delta L} L_a} \right) \\ & - \frac{\beta}{\Delta L} \left(\frac{\beta}{\Delta L} L_a - (2\alpha_r - 2\theta_{dwell} - \beta) \right) \ln \left(\frac{\beta - \frac{\beta}{\Delta L} L_a}{(\alpha_r - \beta - \theta_a) - \frac{\beta}{\Delta L} L_a} \right) \\ & - \frac{2}{L_u} (2\alpha_r - 2\theta_{dwell} - \beta) (\alpha_r - \theta_{dwell} - \beta) - \left(\frac{\beta}{\Delta L} \right)^2 L_u \ln \left(\frac{\frac{L_u \beta}{\Delta L} + \theta_{commutation}}{\frac{L_u \beta}{\Delta L}} \right) \\ & - \frac{\beta}{\Delta L} \left(\frac{\beta}{\Delta L} L_u + 2\theta_{commutation} \right) \ln \left(\frac{\frac{\beta}{\Delta L} L_u + \beta}{\frac{\beta}{\Delta L} L_u + \theta_{commutation}} \right) \end{aligned} \right\}$$

Average Current:

$$I_{avg_speed_independent} = \frac{I_{peak}}{\alpha_r} \left[\frac{L_u \beta}{\Delta L} \ln \left(\frac{\frac{\beta L_a}{\Delta L} \left(\frac{\beta L_u}{\Delta L} + \beta \right)}{\frac{L_u \beta}{\Delta L} \left(\frac{\beta L_a}{\Delta L} - \beta \right)} \right) + (\alpha_r - 2\beta) \right]$$

$$I_{avg_speed_dependent} = \frac{V_s}{\omega \alpha_r} \frac{\beta}{\Delta L} \left[\begin{aligned} & \left(\beta - 2\theta_{commutation} + \frac{\beta L_a}{\Delta L} \right) \ln \left(\frac{\frac{\beta L_a}{\Delta L} - (\alpha_r - \beta - \theta_a)}{\frac{\beta L_a}{\Delta L}} \right) \\ & - \left(\frac{\beta L_a}{\Delta L} - (2\alpha_r - 2\theta_{dwell} - \beta) \right) \ln \left(\frac{\beta - \frac{\beta L_a}{\Delta L}}{(\alpha_r - \beta - \theta_a) - \frac{\beta L_a}{\Delta L}} \right) \\ & - \frac{\beta L_u}{\Delta L} \ln \left(\frac{\frac{L_u \beta}{\Delta L} + \theta_{commutation}}{\frac{L_u \beta}{\Delta L}} \right) \\ & + \left(\frac{\beta L_u}{\Delta L} + 2\theta_{commutation} \right) \ln \left(\frac{\frac{\beta L_u}{\Delta L} + \beta}{\frac{\beta L_u}{\Delta L} + \theta_{commutation}} \right) \\ & - \frac{2\Delta L}{\beta L_u} (2\alpha_r - 2\theta_{dwell} - \beta)(\alpha_r - \theta_{dwell} - \beta) \\ & + \frac{\Delta L}{2\beta L_u} \left[(2\alpha_r - 2\theta_{dwell} - \beta)^2 - \beta^2 \right] + (2\alpha_r - 4\beta - 4\theta_a + 2\theta_d) \end{aligned} \right]$$

These equations can form the basis for a “smart” controller. Based on the speed information and the power requirement, desired peak current can be estimated by using the Equation (7.47). If this peak current is less than the current estimated by the Equation (7.54), traditional discontinuous conduction type control scheme can be used to develop the desired output power. Otherwise continuous conduction can be initiated and maintained by keeping the dwell angle as high as possible. Note that the more dwell results into faster response. Based on this dwell angle, proper advance angle (which maximizes the output power) can be selected by using the Equation (7.48). Based on the peak current requirement, dwell angle and the corresponding advance angle, number of strokes it takes to achieve the desired peak current can be estimated by using the Equation (7.53). As the developed power varies inversely with the dwell

angle (Figure 7-26), dwell angle (and the advance angle as it depends on the dwell angle) can be reduced in smaller steps. Note that the dwell angle has to be more than half of the rotor pole pitch (α_r) to sustain the continuous conduction.

Next section estimates the maximum speed at which rated power can be developed using the traditional discontinuous conduction type control scheme (CPSR estimation).

7.4.10 Constant Power Speed Ratio

CPSR is a ratio of the highest speed at which rated power can be developed to the rated base speed. With discontinuous type conduction, as speed increases, advance angle and dwell angle have to be increased. At high speed, the SRM operates in single pulse mode i.e. applied voltage is a square wave. For an 8/6 SRM motor, 30° is the highest dwell angle that can be applied which guarantees discontinuous type conduction. So the highest speed, at which rated power that can be developed, by using traditional discontinuous type conduction, can be found out by doing analysis similar to continuous conduction analysis described in Section 7.4. Assume a dwell angle is of 30° and that the motor is operating in a single pulse mode. Figure 7-28 shows resulting waveforms. Analysis similar to the previous one can be done on these waveforms to calculate the resultant power. This analysis is based on linear phase inductance waveform, although saturation can be observed for medium speeds, especially with high current values. In a single pulse mode, the developed power is given by the following equation,

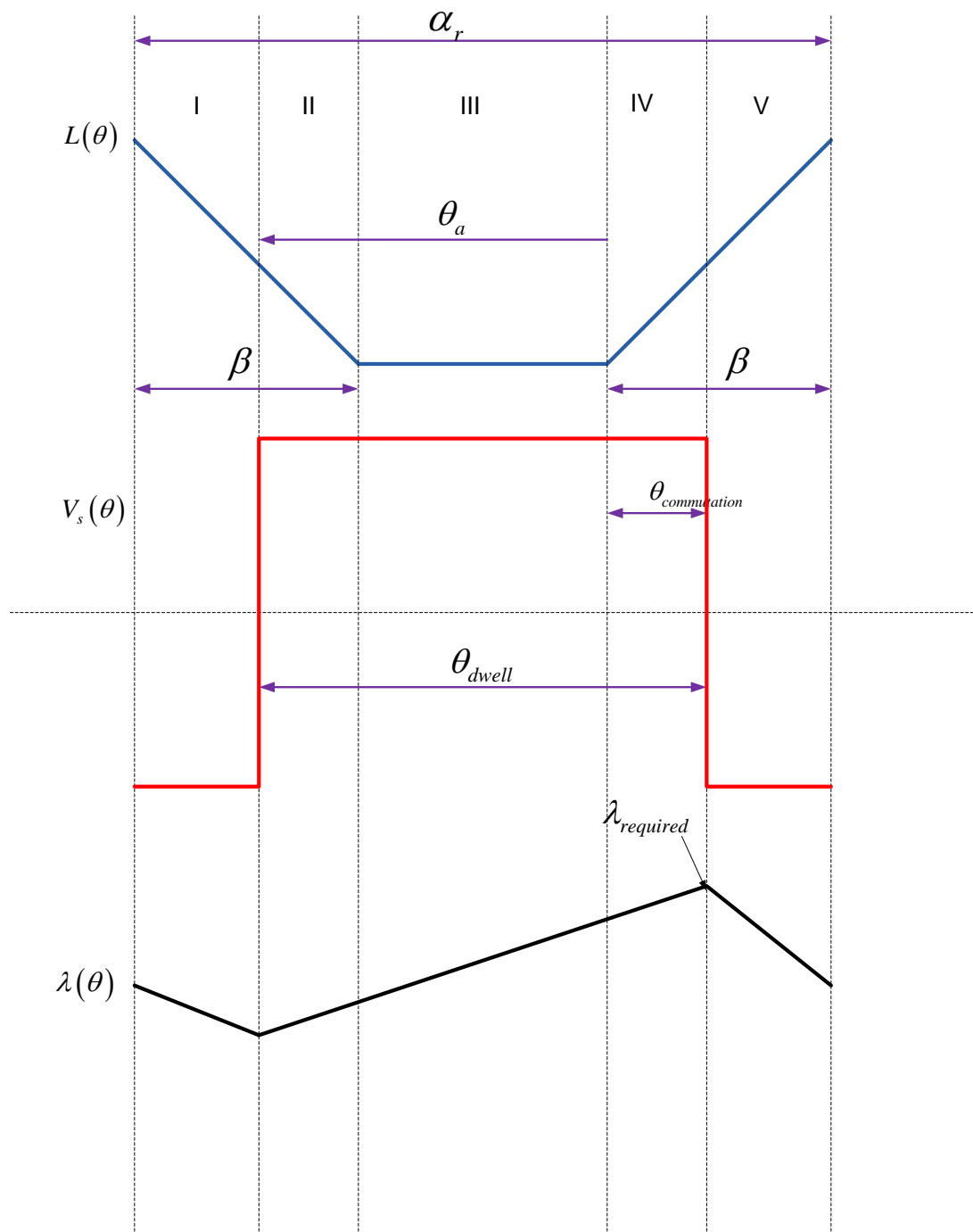


Figure 7-28 : CPSR Analysis – Flat Unaligned Inductance type SRM.

$$P_m = \left(\frac{V_s^2}{\omega} \right) \left(\frac{\beta}{\Delta L} \right) \left(\frac{q}{\alpha_r} \right) * \left\{ \begin{aligned} & - \left[\frac{\beta L_a}{\Delta L} - (\alpha_r - \beta - \theta_a) \right] \ln \left(\frac{\frac{\beta L_a}{\Delta L} - \beta}{\frac{\beta L_a}{\Delta L}} \right) \\ & - \left(\frac{\beta L_a}{\Delta L} - \beta - \theta_a \right) \ln \left(\frac{\frac{\beta L_a}{\Delta L} - \beta + \theta_{commutation}}{\frac{\beta L_a}{\Delta L} - \beta} \right) \\ & - \left(\frac{\beta L_a}{\Delta L} - \beta + 2\theta_{dwell} - \theta_a \right) \ln \left(\frac{\frac{\beta L_a}{\Delta L}}{\frac{\beta L_a}{\Delta L} - \beta + \theta_{commutation}} \right) \\ & + \frac{\Delta L}{2\beta L_u} \left((\alpha_r - \beta)^2 - \beta^2 \right) - \frac{\Delta L}{\beta L_u} (\alpha_r - \beta - \theta_a) (\alpha_r - 2\beta) \end{aligned} \right\} \quad (7.55)$$

This equation can be modified to find the maximum relative speed at which the rated power that can be developed.

$$\therefore n_{CPSR} = \left(\frac{V_s^2}{P_{rated}} \right) \left(\frac{\beta}{\Delta L} \right) \left(\frac{q}{\alpha_r} \right) \left(\frac{30}{\pi N_b} \right) * \left\{ \begin{aligned} & - \left[\frac{\beta L_a}{\Delta L} - (\alpha_r - \beta - \theta_a) \right] \ln \left(\frac{\frac{\beta L_a}{\Delta L} - \beta}{\frac{\beta L_a}{\Delta L}} \right) \\ & - \left(\frac{\beta L_a}{\Delta L} - \beta - \theta_a \right) \ln \left(\frac{\frac{\beta L_a}{\Delta L} - \beta + \theta_{commutation}}{\frac{\beta L_a}{\Delta L} - \beta} \right) \\ & - \left(\frac{\beta L_a}{\Delta L} - \beta + 2\theta_{dwell} - \theta_a \right) \ln \left(\frac{\frac{\beta L_a}{\Delta L}}{\frac{\beta L_a}{\Delta L} - \beta + \theta_{commutation}} \right) \\ & + \frac{\Delta L}{2\beta L_u} \left((\alpha_r - \beta)^2 - \beta^2 \right) - \frac{\Delta L}{\beta L_u} (\alpha_r - \beta - \theta_a) (\alpha_r - 2\beta) \end{aligned} \right\} \quad (7.56)$$

Table 7-7 shows the advance angle dependence of the CPSR. Simulation results (using a linear model described in Section 7.2.1) confirm that the values predicted by above equation are the highest speed at which rated power is produced. At relative speed of 6, with a dwell angle of 30° and advance angle of 24° , linear model simulations predicts the output power is 325 hp and the above equation predicts the highest relative speed to be 6.157. With same dwell and advance angle for a relative speed of 6.5, the linear model simulations predict the output power to be 300 hp. Note that the rated power is 320hp. Next section describes similar analysis on non-flat unaligned inductance type Switched Reluctance Motors.

7.5 Continuous Conduction Analysis - Non-Flat Unaligned Inductance

Figure 7-29 shows a different type of per phase inductance profile for a switched reluctance motor. Note that the unaligned inductance is not flat. During the unaligned region, inductance continues to decrease but at a smaller rate. Minimum value occurs at the completely unaligned position. For the example motor, value of the per phase stator winding inductance at the completely aligned position is $L_a = 0.07338$ H, inductance value at the completely unaligned position is $L_u = 0.004148$ H, and the inductance value at the on-set of alignment is $L_p = 0.00524$ H.

Table 7-7: CPSR of the Flat Unaligned Inductance type SRM with Discontinuous Conduction.

Advance Angle	CPSR	Actual Speed (RPM)
15	3.0789	769.725
16	3.4667	866.675
17	3.8469	961.725
18	4.2184	1054.6
19	4.58	1145
20	4.9298	1232.45
21	5.2658	1316.45
22	5.5851	1396.275
23	5.8839	1470.975
24	6.157	1539.25
25	6.3969	1599.225
26	6.5921	1648.025
27	6.724	1681
28	6.7592	1689.8

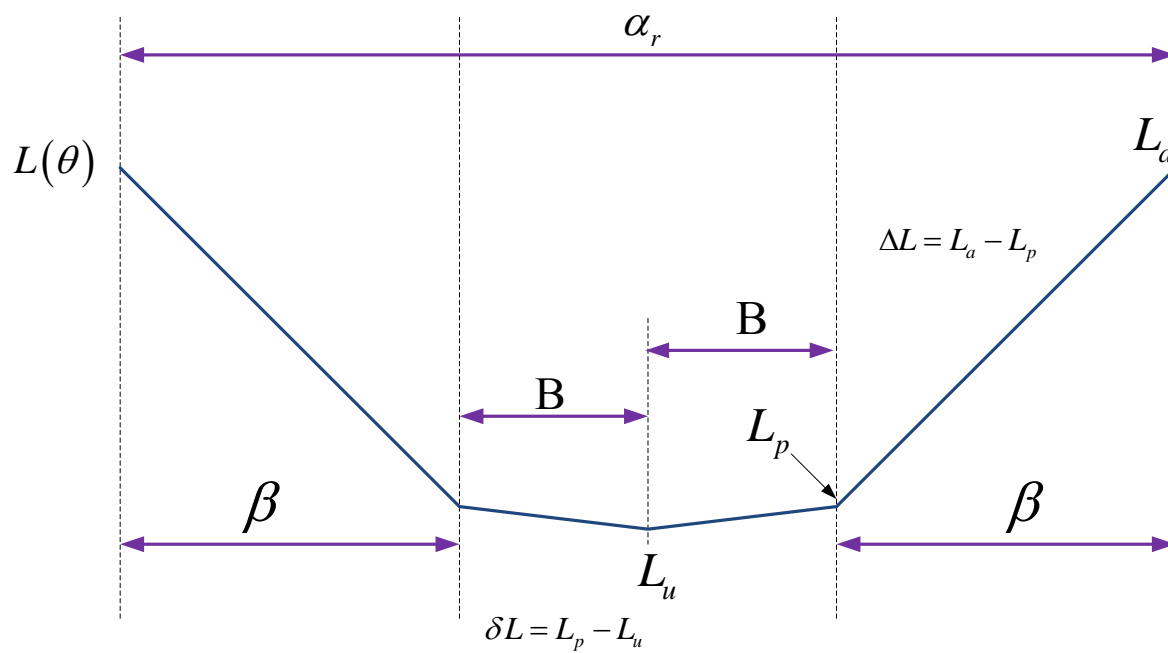


Figure 7-29 : Non-Flat Unaligned Inductance Profile.

Simulation results show that, the balancing zero volt-sec “notch” is symmetrical around this completely unaligned position.

Figure 7-30 shows the location of the zero volt-sec notch (blue waveform), resultant phase current (black waveform), resultant flux-linkage (turquoise waveform) and the per phase inductance (red waveform) profile of an 8/6 SRM motor when operated in continuous conduction mode.

For analysis purpose, these waveforms can be divided into seven regions. Based on the applied voltage waveform, the flux-linkage waveform can be derived. Based on the flux-linkage waveform and the inductance waveform, current waveform can be derived. Based on this current waveform, developed power can be estimated from the co-energy area. Figure 7-31 illustrates the same.

Simulation results suggest that the peak current is reached at the completely unaligned position (i.e. $L(\theta) = L_u$), while the minimum current occurs at the completely aligned position (i.e. $L(\theta) = L_a$). The current regulator set point is reached before the completely unaligned position ($L(\theta) = L_{required}$). This is where the zero volt-second notches starts. Past this point, current continues to increase but the increase is small.

To keep the consistency with the linear analysis described in the previous section for flat induction profile type SRM motors, current regulator set point is defined as the peak current i.e. $I_{set} = I_{peak}$ and the actual peak current is defined as I_{peak_new} .

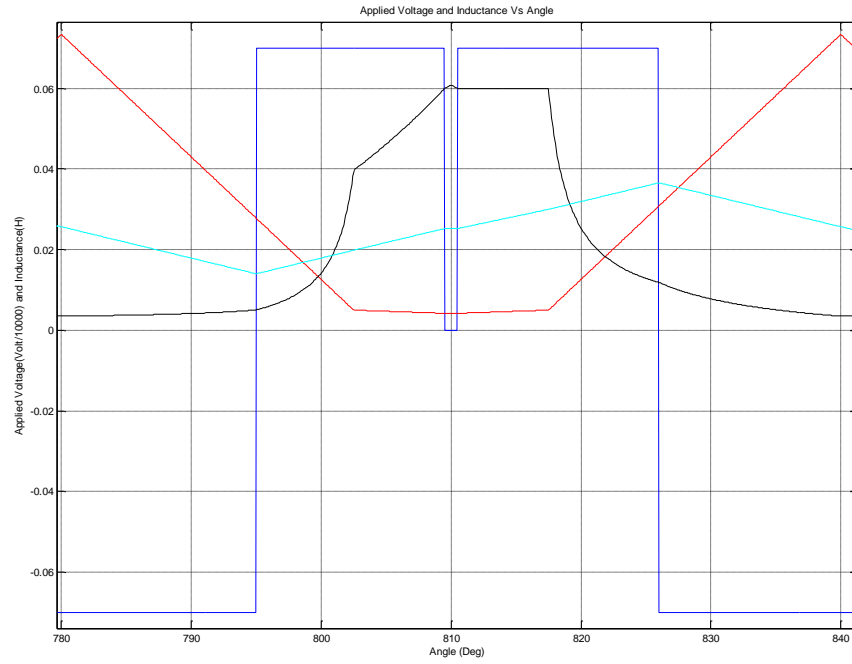


Figure 7-30 : Notch Location for Non Flat Unaligned Inductance type SRM when Operated in Continuous Conduction Mode.

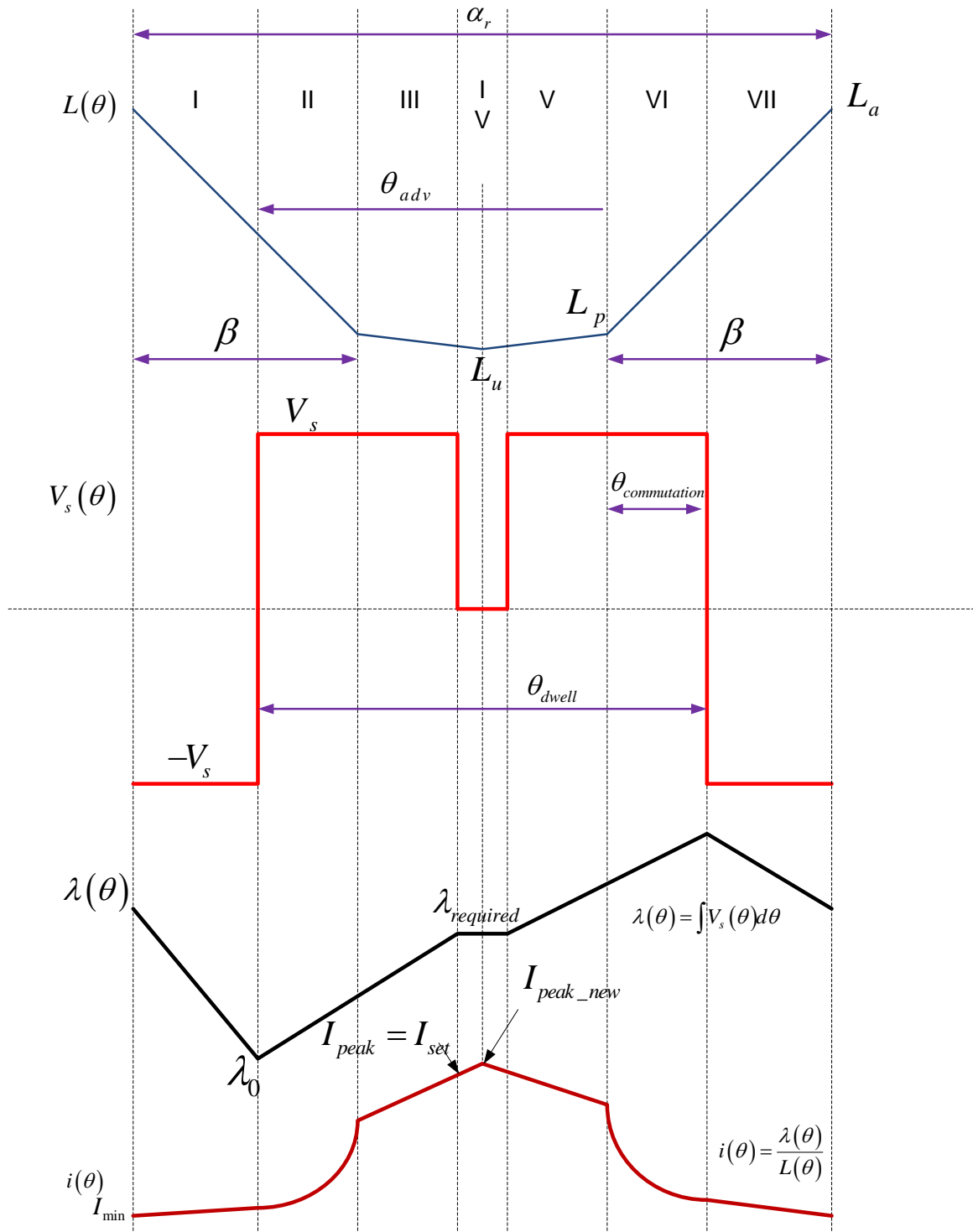


Figure 7-31 : Continuous Conduction Analysis – Non Flat Unaligned Inductance type SRM.

Now, if I_{peak} is the desired peak current set-point, the flux-linkage required to get this peak current is given by,

$$\lambda_{required} = I_{peak} * L_{required} \quad (7.57)$$

Assume that the advance angle (θ_{adv}) and the dwell angle (θ_{dwell}) are given. For an 8/6 SRM motor, the completely unaligned position will be occur at $\frac{\alpha_r}{2}^\circ$. The stabilizing zero volt-second notch will have a width of $2 * \left(\theta_{dwell} - \frac{\alpha_r}{2} \right)^\circ$. Since the current regulator set point is reached at the end of region 3, value of the phase inductance at this point can be calculated as below,

$$L(\theta) = -\frac{L_p - L_u}{\frac{\alpha_r}{2} - \beta} \theta + k, \quad i.e. \quad (7.58)$$

$$L(\theta) = L_u + \frac{\delta L}{B} \left(\frac{\alpha_r}{2} - \theta \right)$$

When⁵ $\theta = \frac{\alpha_r}{2} - \left(\theta_{dwell} - \frac{\alpha_r}{2} \right),$

⁵ $\delta L = L_p - L_u, \Delta L = L_a - L_p$

$$\begin{aligned}
L_{required} &= L_u + \frac{\delta L}{B} \left(\frac{\alpha_r}{2} - (\alpha_r - \theta_{dwell}) \right), \\
\therefore L_{required} &= L_u + \frac{\delta L}{B} \left(\theta_{dwell} - \frac{\alpha_r}{2} \right)
\end{aligned} \tag{7.59}$$

$$\therefore \lambda_{required} = I_{peak} \left[L_u + \frac{\delta L}{B} \left(\theta_{dwell} - \frac{\alpha_r}{2} \right) \right]$$

Region I ends at $(\alpha_r - \beta - \theta_{adv})^\circ$. Therefore the width of the first fluxing region can be calculated as,

$$\begin{aligned}
&= (\alpha_r - \theta_{dwell}) - (\alpha_r - \beta - \theta_{adv}), \\
&\therefore = \beta + \theta_{adv} - \theta_{dwell} \\
&\text{or} \\
&= \beta - \theta_{commutation}
\end{aligned}$$

We have, $y = mx + c \Rightarrow \lambda_{required} = \frac{V_s}{\omega} (\beta + \theta_{adv} - \theta_{dwell}) + \lambda_0$

$$\begin{aligned}
\therefore \lambda_0 &= \lambda_{required} - \frac{V_s}{\omega} (\beta + \theta_{adv} - \theta_{dwell}), \\
\therefore \lambda_0 &= \lambda_{required} - \frac{V_s}{\omega} (\beta - \theta_{commutation}) \\
\therefore \lambda_0 &= I_{peak} \left[L_u + \frac{\delta L}{B} \left(\theta_{dwell} - \frac{\alpha_r}{2} \right) \right] - \frac{V_s}{\omega} (\beta + \theta_{adv} - \theta_{dwell}),
\end{aligned} \tag{7.60}$$

This is the required value of the residual flux-linkage to achieve desired peak current set-point. Note that, at high speed, i.e.,

$$\because n \rightarrow \infty$$

$$\lambda_0 = \lambda_{required}$$

Inductance in the region I and II is given by⁶,

$$y = mx + c,$$

$$L(\theta) = \frac{-\Delta L}{\beta} * \theta + k,$$

When, $\theta = 0, L(\theta) = L_a$. When $\theta = \beta, L(\theta) = L_p$, therefore,

$$L(\theta) = \frac{\Delta L}{\beta} \left(\frac{\beta L_a}{\Delta L} - \theta \right),$$

$$L(\theta) = -\frac{\Delta L}{\beta} \theta + L_a$$
(7.61)

7.5.1 Region I Analysis ($0 \leq \theta \leq (\alpha_r - \beta - \theta_{adv})$)

Flux Linkages in the region I is given by,

$$\lambda(\theta) = -\frac{V_s}{\omega} \theta + \lambda_{required} + \frac{V_s}{\omega} (\alpha_r - 2\beta - 2\theta_{adv} + \theta_{dwell}),$$

$$\therefore \lambda(\theta) = \lambda_{required} + \frac{V_s}{\omega} (\alpha_r - 2\beta - 2\theta_{adv} + \theta_{dwell} - \theta)$$
(7.62)

And

$$\therefore d\lambda(\theta) = -\frac{V_s}{\omega} d\theta$$
(7.63)

Current in the region I is given by,

⁶ k = arbitrary constant.

$$I(\theta) = \frac{\lambda(\theta)}{L(\theta)}$$

$$\therefore I(\theta) = \frac{\lambda_{required} + \frac{V_s}{\omega}(\alpha_r - 2\beta - 2\theta_{adv} + \theta_{dwell} - \theta)}{\frac{\Delta L}{\beta} \left(\frac{\beta L_a}{\Delta L} - \theta \right)} \quad (7.64)$$

Power produced in the region I is given by,

$$\therefore P_1 = \int_{\theta=0}^{\theta=(\alpha_r - \beta - \theta_a)} i(\theta) * d\lambda(\theta)$$

$$\therefore P_1 = \int_{\theta=0}^{\theta=(\alpha_r - \beta - \theta_a)} \frac{\lambda_{required} + \frac{V_s}{\omega}(\alpha_r - 2\beta - 2\theta_{adv} + \theta_{dwell} - \theta)}{\frac{\Delta L}{\beta} \left(\frac{\beta L_a}{\Delta L} - \theta \right)} * \frac{-V_s}{\omega} d\theta$$

$$\therefore P_1 = \frac{V_s}{\omega} \frac{\beta}{\Delta L} \lambda_{required} \ln \left(\frac{\frac{\beta L_a}{\Delta L} + \beta + \theta_{adv} - \alpha_r}{\frac{\beta L_a}{\Delta L}} \right) - \left(\frac{V_s}{\omega} \right)^2 \frac{\beta}{\Delta L} (\alpha_r - \beta - \theta_{adv})$$

$$- \left(\frac{V_s}{\omega} \right)^2 \frac{\beta}{\Delta L} \left(\frac{\beta L_a}{\Delta L} + 2\beta + 2\theta_{adv} - \alpha_r - \theta_{dwell} \right) \ln \left(\frac{\frac{\beta L_a}{\Delta L} + \beta + \theta_{adv} - \alpha_r}{\frac{\beta L_a}{\Delta L}} \right) \quad (7.65)$$

Flux Linkage in the regions II and III is given by,

$$\lambda(\theta) = \lambda_{required} - \frac{V_s}{\omega} (\alpha_r - \theta_{dwell} - \theta) \quad (7.66)$$

And

$$\therefore d\lambda(\theta) = \frac{V_s}{\omega} d\theta \quad (7.67)$$

When, $\theta = (\alpha_r - \beta - \theta_{adv})$,

$$\begin{aligned}
\lambda(\theta) &= \lambda_{required} - \frac{V_s}{\omega} * (\alpha_r - \theta_{dwell} - (\alpha_r - \beta - \theta_{adv})) \\
&= \lambda_{required} - \frac{V_s}{\omega} * (-\theta_{dwell} + \beta + \theta_{adv}) \\
&= \lambda_{required} - \frac{V_s}{\omega} * (\beta - (\theta_{dwell} - \theta_{adv})) \\
&= \lambda_{required} - \frac{V_s}{\omega} * (\beta - \theta_{commutation}) = \lambda_0
\end{aligned}
\tag{Verification}$$

7.5.2 Region II Analysis ($(\alpha_r - \beta - \theta_{adv}) \leq \theta \leq \beta$)

Current in the region II is given by,

$$I(\theta) = \frac{\lambda_{required} - \frac{V_s}{\omega} (\alpha_r - \theta_{dwell} - \theta)}{\frac{\Delta L}{\beta} \left(\frac{\beta L_a}{\Delta L} - \theta \right)} \tag{7.68}$$

Power produced in region II is given by,

$$\begin{aligned}
P_2 &= \int_{\theta=(\alpha_r - \beta - \theta_{adv})}^{\theta=\beta} i(\theta) d\lambda(\theta) \\
\therefore P_2 &= \int_{\theta=(\alpha_r - \beta - \theta_{adv})}^{\theta=\beta} \frac{\lambda_{required} - \frac{V_s}{\omega} (\alpha_r - \theta_{dwell} - \theta)}{\frac{\Delta L}{\beta} \left(\frac{\beta L_a}{\Delta L} - \theta \right)} \frac{V_s}{\omega} d\theta \\
\therefore P_2 &= -\frac{V_s}{\omega} \frac{\beta}{\Delta L} \lambda_{required} \int_{\theta=(\alpha_r - \beta - \theta_{adv})}^{\theta=\beta} \frac{1}{\theta - \frac{\beta L_a}{\Delta L}} d\theta - \left(\frac{V_s}{\omega} \right)^2 \frac{\beta}{\Delta L} \int_{\theta=(\alpha_r - \beta - \theta_{adv})}^{\theta=\beta} \frac{\theta - (\alpha_r - \theta_{dwell})}{\theta - \frac{\beta L_a}{\Delta L}} d\theta
\end{aligned}$$

$$\begin{aligned} \therefore P_2 = & -\frac{V_s}{\omega} \frac{\beta}{\Delta L} \lambda_{required} \ln \left(\frac{\frac{\beta L_p}{\Delta L}}{\frac{\beta L_a}{\Delta L} + \beta + \theta_{adv} - \alpha_r} \right) + \left(\frac{V_s}{\omega} \right)^2 \frac{\beta}{\Delta L} (\alpha_r - 2\beta - \theta_{adv}) \\ & - \left(\frac{V_s}{\omega} \right)^2 \frac{\beta}{\Delta L} \left(\frac{\beta L_a}{\Delta L} + \theta_{dwell} - \alpha_r \right) \ln \left(\frac{\frac{\beta L_p}{\Delta L}}{\frac{\beta L_a}{\Delta L} + \beta + \theta_{adv} - \alpha_r} \right) \end{aligned} \quad (7.69)$$

7.5.3 Region III Analysis ($\beta \leq \theta \leq (\alpha_r - \theta_{dwell})$)

Inductance in this region and the region IV-a is given by,

$$\therefore L(\theta) = L_u + \frac{\delta L}{B} \left(\frac{\alpha_r}{2} - \theta \right) \quad (7.70)$$

Current in the region III is given by,

$$I(\theta) = \frac{\lambda_{required} - \frac{V_s}{\omega} (\alpha_r - \theta_{dwell} - \theta)}{\frac{\delta L}{B} \left(\frac{BL_u}{\delta L} + \frac{\alpha_r}{2} - \theta \right)}, \quad (7.71)$$

Power produced in the region III is given by,

$$\begin{aligned} P_3 = & \int_{\theta=\beta}^{\theta=(\alpha_r - \theta_{dwell})} \frac{\lambda_{required} - \frac{V_s}{\omega} (\alpha_r - \theta_{dwell} - \theta)}{\frac{\delta L}{B} \left(\frac{BL_u}{\delta L} + \frac{\alpha_r}{2} - \theta \right)} \frac{V_s}{\omega} d\theta, \\ \therefore P_3 = & \frac{V_s}{\omega} \int_{\theta=\beta}^{\theta=(\alpha_r - \theta_{dwell})} \frac{\lambda_{required} - \frac{V_s}{\omega} (\alpha_r - \theta_{dwell} - \theta)}{\frac{\delta L}{B} \left(\frac{BL_u}{\delta L} + \frac{\alpha_r}{2} - \theta \right)} d\theta \end{aligned}$$

$$\begin{aligned} \therefore P_3 = & -\frac{V_s}{\omega} \frac{B}{\delta L} \lambda_{required} \ln \left(\frac{\frac{BL_u}{\delta L} + \theta_{dwell} - \frac{\alpha_r}{2}}{\frac{BL_u}{\delta L} + \frac{\alpha_r}{2} - \beta} \right) - \left(\frac{V_s}{\omega} \right)^2 \frac{B}{\delta L} (\alpha_r - \theta_{dwell} - \beta) \\ & - \left(\frac{V_s}{\omega} \right)^2 \frac{B}{\delta L} \left(\frac{BL_u}{\delta L} + \theta_{dwell} - \frac{\alpha_r}{2} \right) \ln \left(\frac{\frac{BL_u}{\delta L} + \theta_{dwell} - \frac{\alpha_r}{2}}{\frac{BL_u}{\delta L} + \frac{\alpha_r}{2} - \beta} \right) \end{aligned} \quad (7.72)$$

7.5.4 Region IV-a Analysis $((\alpha_r - \theta_{dwell}) \leq \theta \leq \frac{\alpha_r}{2})$

Flux linkage in the region IV-a is given by,

$$\lambda(\theta) = \lambda_{required} \quad (7.73)$$

And

$$\therefore d\lambda(\theta) = 0 \quad (7.74)$$

Current in region IV-a is given by,

$$I(\theta) = \frac{\lambda_{required}}{L_u + \frac{\delta L}{B} \left(\frac{\alpha_r}{2} - \theta \right)} \quad (7.75)$$

At the beginning of this region current reaches the desired peak value. In this region, phase current continuous to grow. Current reaches a new peak value at the end of this section.

$$\therefore I_{peak_new} = \frac{\lambda_{required}}{L_u} = \frac{I_{peak_desired} \left[L_u + \frac{\delta L}{B} \left(\theta_{dwell} - \frac{\alpha_r}{2} \right) \right]}{L_u} \quad (7.76)$$

Power produced in this region is zero as $\frac{d\lambda}{d\theta} = 0$.

Inductance in the regions IV-b and V is given by,

$$L(\theta) = L_u + \frac{\delta L}{B} \left(\theta - \frac{\alpha_r}{2} \right) \quad (7.77)$$

When $\theta = (\alpha_r - \beta)$,

$$L(\theta) = L_u + \frac{\delta L}{B} \left((\alpha_r - \beta) - \frac{\alpha_r}{2} \right), \quad (\text{Verification})$$

$$\therefore L(\theta) = L_u + \frac{\delta L}{B} \left(\frac{\alpha_r}{2} - \beta \right) = L_p$$

7.5.5 Region IV-b Analysis ($\frac{\alpha_r}{2} \leq \theta \leq \theta_{dwell}$)

Flux linkage in the region IV-b is given by,

$$\lambda(\theta) = \lambda_{required} \quad (7.78)$$

And

$$\therefore d\lambda(\theta) = 0 \quad (7.79)$$

Current in the region IV-b is given by,

$$I(\theta) = \frac{\lambda_{required}}{L_u + \frac{\delta L}{B} \left(\theta - \frac{\alpha_r}{2} \right)} \quad (7.80)$$

Power produced in this region zero i.e. $P(\theta) = \int_{\theta=(\alpha_r-\theta_{dwell})}^{\theta_4=\theta_{dwell}} i(\theta) * d\lambda(\theta) = 0$

Flux linkage in the regions V and VI is given by,

$$\lambda(\theta) = \lambda_{required} + \frac{V_s}{\omega}(\theta - \theta_{dwell}) \quad (7.81)$$

And

$$\therefore d\lambda(\theta) = \frac{V_s}{\omega} d\theta \quad (7.82)$$

7.5.6 Region V Analysis ($\theta_{dwell} \leq \theta \leq (\alpha_r - \beta)$)

Current in the region V is given by,

$$I(\theta) = \frac{\lambda_{required} + \frac{V_s}{\omega}(\theta - \theta_{dwell})}{L_u + \frac{\delta L}{B} \left(\theta - \frac{\alpha_r}{2} \right)} \quad (7.83)$$

Power produced in the region V is given by,

$$\begin{aligned} \therefore P_5 &= \int_{\theta=\theta_{dwell}}^{\theta=(\alpha_r-\beta)} \frac{\lambda_{required} + \frac{V_s}{\omega}(\theta - \theta_{dwell})}{L_u + \frac{\delta L}{B} \left(\theta - \frac{\alpha_r}{2} \right)} \frac{V_s}{\omega} d\theta, \\ \therefore P_5 &= \frac{V_s}{\omega} \int_{\theta=\theta_{dwell}}^{\theta=(\alpha_r-\beta)} \frac{\lambda_{required} + \frac{V_s}{\omega}(\theta - \theta_{dwell})}{L_u + \frac{\delta L}{B} \left(\theta - \frac{\alpha_r}{2} \right)} d\theta, \\ \therefore P_5 &= \frac{V_s}{\omega} \frac{B}{\delta L} \lambda_{required} \int_{\theta=\theta_{dwell}}^{\theta=(\alpha_r-\beta)} \frac{1}{\theta + \frac{BL_u}{\delta L} - \frac{\alpha_r}{2}} d\theta + \left(\frac{V_s}{\omega} \right)^2 \frac{B}{\delta L} \int_{\theta=\theta_{dwell}}^{\theta=(\alpha_r-\beta)} \frac{\theta - \theta_{dwell}}{\theta + \frac{BL_u}{\delta L} - \frac{\alpha_r}{2}} d\theta \\ \therefore P_5 &= \frac{V_s}{\omega} \frac{B}{\delta L} \lambda_{required} \ln \left(\frac{\frac{BL_u}{\delta L} + \frac{\alpha_r}{2} - \beta}{\frac{BL_u}{\delta L} + \theta_{dwell} - \frac{\alpha_r}{2}} \right) + \left(\frac{V_s}{\omega} \right)^2 \frac{B}{\delta L} (\alpha_r - \beta - \theta_{dwell}) \\ &\quad - \left(\frac{V_s}{\omega} \right)^2 \frac{B}{\delta L} \left(\frac{BL_u}{\delta L} + \theta_{dwell} - \frac{\alpha_r}{2} \right) \ln \left(\frac{\frac{BL_u}{\delta L} + \frac{\alpha_r}{2} - \beta}{\frac{BL_u}{\delta L} + \theta_{dwell} - \frac{\alpha_r}{2}} \right) \end{aligned} \quad (7.84)$$

Inductance in the regions VI and VII is given by:

$$L(\theta) = \frac{\Delta L}{\beta} \left(\theta + \frac{\beta L_a}{\Delta L} - \alpha_r \right) \quad (7.85)$$

When $\theta = (\alpha_r - \beta)$,

$$\begin{aligned} L(\theta) &= L_a - \frac{\Delta L}{\beta} * (\alpha_r - (\alpha_r - \beta)) \\ &= L_a - \Delta L \quad (\text{Verification}) \\ &= L_a - (L_a - L_p) \\ &= L_p \end{aligned}$$

7.5.7 Region VI Analysis $\left(\begin{array}{l} (\alpha_r - \beta) \leq \theta \leq (\alpha_r - \beta + \theta_{commutation}) \\ (\alpha_r - \beta) \leq \theta \leq (\alpha_r - \beta + \theta_{dwell} - \theta_{adv}) \end{array} \right)$

Current in region VI is given by,

$$I(\theta) = \frac{\lambda_{required} + \frac{V_s}{\omega} (\theta - \theta_{dwell})}{\frac{\Delta L}{\beta} \left(\theta + \frac{\beta L_a}{\Delta L} - \alpha_r \right)} \quad (7.86)$$

Power produced in the region VI is given by,

$$\begin{aligned} P(\theta) &= \int_{\theta=(\alpha_r - \beta)}^{\theta=(\alpha_r - \beta + \theta_{commutation})} i(\theta) * d\lambda(\theta) \\ \therefore P_6 &= \int_{\theta=(\alpha_r - \beta)}^{\theta=(\alpha_r - \beta + \theta_{commutation})} \frac{\lambda_{required} + \frac{V_s}{\omega} (\theta - \theta_{dwell})}{\frac{\Delta L}{\beta} \left(\theta + \frac{\beta L_a}{\Delta L} - \alpha_r \right)} \frac{V_s}{\omega} d\theta \end{aligned}$$

$$\begin{aligned} \therefore P_6 = \frac{V_s}{\omega} \frac{\beta}{\Delta L} \lambda_{required} \ln \left(\frac{\frac{\beta L_p}{\Delta L} + \theta_{dwell} - \theta_{adv}}{\frac{\beta L_p}{\Delta L}} \right) + \left(\frac{V_s}{\omega} \right)^2 \frac{\beta}{\Delta L} (\theta_{dwell} - \theta_{adv}) \\ - \left(\frac{V_s}{\omega} \right)^2 \frac{\beta}{\Delta L} \left(\frac{\beta L_a}{\Delta L} + \theta_{dwell} - \alpha_r \right) \ln \left(\frac{\frac{\beta L_p}{\Delta L} + \theta_{dwell} - \theta_{adv}}{\frac{\beta L_p}{\Delta L}} \right) \end{aligned} \quad (7.87)$$

When $\theta = (\alpha_r - \beta) + \theta_{commutation}$, $\lambda(\theta) = \lambda_{peak}$

$$\begin{aligned} \therefore \lambda(\theta) &= \lambda_{required} + \frac{V_s}{\omega} ((\alpha_r - \beta) + \theta_{dwell} - \theta_{adv} - \theta_{dwell}), \\ \therefore \lambda_{peak} &= \lambda_{required} + \frac{V_s}{\omega} (\alpha_r - \beta - \theta_{adv}) \end{aligned} \quad (7.88)$$

This is the peak flux-linkage which will result into the desired peak current.

$$\begin{aligned} \therefore n \rightarrow \infty \\ \lambda_{peak} &= \lambda_{required} \end{aligned}$$

Flux-linkage in the region VII can is given by,

$$\lambda(\theta) = \lambda_{required} + \frac{V_s}{\omega} (2\alpha_r - 2\beta - 2\theta_{adv} + \theta_{dwell} - \theta) \quad (7.89)$$

And

$$\therefore d\lambda(\theta) = \frac{-V_s}{\omega} d\theta \quad (7.90)$$

7.5.8 Region VII Analysis $((\alpha_r - \beta + \theta_{commutation}) \leq \theta \leq \alpha_r)$

Current in the region VII is given by,

$$I(\theta) = \frac{\lambda_{required} + \frac{V_s}{\omega} (2\alpha_r - 2\beta - 2\theta_{adv} + \theta_{dwell} - \theta)}{\frac{\Delta L}{\beta} \left(\theta + \frac{\beta L_a}{\Delta L} - \alpha_r \right)} \quad (7.91)$$

Power produced in the region VII is given by,

$$P_7 = \int_{\theta=(\alpha_r - \beta + \theta_{commutation})}^{\theta=\alpha_r} i(\theta) * d\lambda(\theta)$$

$$\therefore P_7 = \int_{\theta=(\alpha_r - \beta + \theta_{commutation})}^{\theta=\alpha_r} \frac{\lambda_{required} + \frac{V_s}{\omega} (2\alpha_r - 2\beta - 2\theta_{adv} + \theta_{dwell} - \theta)}{\frac{\Delta L}{\beta} \left(\theta + \frac{\beta L_a}{\Delta L} - \alpha_r \right)} \frac{-V_s}{\omega} d\theta \quad (1.92)$$

$$\therefore P_7 = -\frac{V_s}{\omega} \frac{\beta}{\Delta L} \lambda_{required} \ln \left(\frac{\frac{\beta L_a}{\Delta L}}{\frac{\beta L_p}{\Delta L} + \theta_{dwell} - \theta_{adv}} \right) + \left(\frac{V_s}{\omega} \right)^2 \frac{\beta}{\Delta L} (\beta + \theta_{adv} - \theta_{dwell})$$

$$- \left(\frac{V_s}{\omega} \right)^2 \frac{\beta}{\Delta L} \left(\frac{\beta L_p}{\Delta L} + \theta_{dwell} - 2\theta_{adv} + \alpha_r - \beta \right) \ln \left(\frac{\frac{\beta L_a}{\Delta L}}{\frac{\beta L_p}{\Delta L} + \theta_{dwell} - \theta_{adv}} \right) \quad (7.93)$$

Since the maximum inductance occurs at $\theta = \alpha_r$, minimum current can be calculated as follows,

$$I_{min} = \frac{\lambda_{required} + \frac{V_s}{\omega} (2\alpha_r - 2\beta - 2\theta_{adv} + \theta_{dwell} - \alpha_r)}{\frac{\Delta L}{\beta} \left(\alpha_r + \frac{\beta L_a}{\Delta L} - \alpha_r \right)}$$

$$I_{min} = \frac{\lambda_{required} + \frac{V_s}{\omega} (\alpha_r - 2\beta - 2\theta_{adv} + \theta_{dwell})}{L_a} \quad (7.94)$$

$$\therefore n \rightarrow \infty$$

$$I_{min} = \frac{I_{peak} \left[L_u + \frac{\delta L}{B} \left(\theta_{dwell} - \frac{\alpha_r}{2} \right) \right]}{L_a} \approx \frac{I_{peak} L_u}{L_a}$$

7.5.9 Analytical Results

Average Power can be calculated as follows:

$$P_m = \omega \frac{q}{\alpha_r} \{P_1 + P_2 + P_3 + P_4 + P_5 + P_6 + P_7\}$$

Resultant average power can be split into two parts:

1. Speed independent part, and
2. Speed dependent part

$$P_{m_speed_independent} = \omega \frac{q}{\alpha_r} \left\{ \begin{aligned} & \frac{V_s}{\omega} \frac{\beta}{\Delta L} \lambda_{required} \ln \left(\frac{\frac{\beta L_a}{\Delta L} + \beta + \theta_{adv} - \alpha_r}{\frac{\beta L_a}{\Delta L}} \right) - \frac{V_s}{\omega} \frac{\beta}{\Delta L} \lambda_{required} \ln \left(\frac{\frac{\beta L_p}{\Delta L}}{\frac{\beta L_a}{\Delta L} + \beta + \theta_{adv} - \alpha_r} \right) \\ & - \frac{V_s}{\omega} \frac{B}{\delta L} \lambda_{required} \ln \left(\frac{\frac{BL_u}{\delta L} + \theta_{dwell} - \frac{\alpha_r}{2}}{\frac{BL_u}{\delta L} + \frac{\alpha_r}{2} - \beta} \right) + \frac{V_s}{\omega} \frac{B}{\delta L} \lambda_{required} \ln \left(\frac{\frac{BL_u}{\delta L} + \frac{\alpha_r}{2} - \beta}{\frac{BL_u}{\delta L} + \theta_{dwell} - \frac{\alpha_r}{2}} \right) \\ & \frac{V_s}{\omega} \frac{\beta}{\Delta L} \lambda_{required} \ln \left(\frac{\frac{\beta L_p}{\Delta L} + \theta_{dwell} - \theta_{adv}}{\frac{\beta L_p}{\Delta L}} \right) - \frac{V_s}{\omega} \frac{\beta}{\Delta L} \lambda_{required} \ln \left(\frac{\frac{\beta L_a}{\Delta L}}{\frac{\beta L_p}{\Delta L} + \theta_{dwell} - \theta_{adv}} \right) \end{aligned} \right\}$$

$$P_{m_speed_independent} = 2V_s \frac{q}{\alpha_r} I_{peak} L_{required}$$

$$\left\{ \begin{aligned} & \frac{\beta}{\Delta L} \ln \left(\frac{\beta L_a}{\Delta L} + \beta + \theta_{adv} - \alpha_r \right) + \frac{\beta}{\Delta L} \ln \left(\frac{\beta L_p}{\Delta L} + \theta_{dwell} - \theta_{adv} \right) - \frac{\beta}{\Delta L} \ln \left(\frac{\beta L_p}{\Delta L} \frac{\beta L_a}{\Delta L} \right) \\ & \frac{B}{\delta L} \ln \left(\frac{B L_u}{\delta L} + \frac{\alpha_r}{2} - \beta \right) - \frac{B}{\delta L} \ln \left(\frac{B L_u}{\delta L} + \theta_{dwell} - \frac{\alpha_r}{2} \right) \end{aligned} \right\} \quad (7.95)$$

$$P_{m_speed_dependent} = \omega \frac{q}{\alpha_r}$$

$$\left\{ \begin{aligned} & - \left(\frac{V_s}{\omega} \right)^2 \frac{\beta}{\Delta L} (\alpha_r - \beta - \theta_{adv}) + \left(\frac{V_s}{\omega} \right)^2 \frac{\beta}{\Delta L} (\alpha_r - 2\beta - \theta_{adv}) - \left(\frac{V_s}{\omega} \right)^2 \frac{B}{\delta L} (\alpha_r - \theta_{dwell} - \beta) \\ & + \left(\frac{V_s}{\omega} \right)^2 \frac{B}{\delta L} (\alpha_r - \beta - \theta_{dwell}) + \left(\frac{V_s}{\omega} \right)^2 \frac{\beta}{\Delta L} (\theta_{dwell} - \theta_{adv}) + \left(\frac{V_s}{\omega} \right)^2 \frac{\beta}{\Delta L} (\beta + \theta_{adv} - \theta_{dwell}) \\ & - \left(\frac{V_s}{\omega} \right)^2 \frac{\beta}{\Delta L} \left(\frac{\beta L_a}{\Delta L} + 2\beta + 2\theta_{adv} - \alpha_r - \theta_{dwell} \right) \ln \left(\frac{\frac{\beta L_a}{\Delta L} + \beta + \theta_{adv} - \alpha_r}{\frac{\beta L_a}{\Delta L}} \right) \\ & - \left(\frac{V_s}{\omega} \right)^2 \frac{\beta}{\Delta L} \left(\frac{\beta L_a}{\Delta L} + \theta_{dwell} - \alpha_r \right) \ln \left(\frac{\frac{\beta L_p}{\Delta L}}{\frac{\beta L_a}{\Delta L} + \beta + \theta_{adv} - \alpha_r} \right) \\ & - \left(\frac{V_s}{\omega} \right)^2 \frac{B}{\delta L} \left(\frac{B L_u}{\delta L} + \theta_{dwell} - \frac{\alpha_r}{2} \right) \ln \left(\frac{\frac{B L_u}{\delta L} + \theta_{dwell} - \frac{\alpha_r}{2}}{\frac{B L_u}{\delta L} + \frac{\alpha_r}{2} - \beta} \right) \\ & - \left(\frac{V_s}{\omega} \right)^2 \frac{B}{\delta L} \left(\frac{B L_u}{\delta L} + \theta_{dwell} - \frac{\alpha_r}{2} \right) \ln \left(\frac{\frac{B L_u}{\delta L} + \frac{\alpha_r}{2} - \beta}{\frac{B L_u}{\delta L} + \theta_{dwell} - \frac{\alpha_r}{2}} \right) \\ & - \left(\frac{V_s}{\omega} \right)^2 \frac{\beta}{\Delta L} \left(\frac{\beta L_a}{\Delta L} + \theta_{dwell} - \alpha_r \right) \ln \left(\frac{\frac{\beta L_p}{\Delta L} + \theta_{dwell} - \theta_{adv}}{\frac{\beta L_p}{\Delta L}} \right) \\ & - \left(\frac{V_s}{\omega} \right)^2 \frac{\beta}{\Delta L} \left(\frac{\beta L_p}{\Delta L} + \theta_{dwell} - 2\theta_{adv} + \alpha_r - \beta \right) \ln \left(\frac{\frac{\beta L_a}{\Delta L}}{\frac{\beta L_p}{\Delta L} + \theta_{dwell} - \theta_{adv}} \right) \end{aligned} \right\}$$

$$P_{m_speed_dependant} = -(V_s)^2 \frac{2}{\omega} \frac{\beta}{\Delta L} \frac{q}{\alpha_r} \left\{ \begin{aligned} & \left((\beta + \theta_{adv} - \theta_{dwell}) \ln \left(\frac{\beta L_a}{\Delta L} + \beta + \theta_{adv} - \alpha_r \right) \right) \\ & \left((\alpha_r + \theta_{dwell} - 2\theta_{adv} - 2\beta) \ln \left(\frac{\beta L_a}{\Delta L} \right) \right) \\ & \left((\theta_{adv} + \beta - \alpha_r) \ln \left(\frac{\beta L_p}{\Delta L} + \theta_{dwell} - \theta_{adv} \right) \right) \end{aligned} \right\} \quad (7.96)$$

As the speed increase, at very high speed ($\because n \rightarrow \infty$), speed dependant part approaches to zero and the resultant average power is nothing but the speed independent part.

$$P_m = 2V_s \frac{q}{\alpha_r} I_{peak} L_{required} \left\{ \begin{aligned} & \left[\frac{\beta}{\Delta L} \ln \left(\frac{\beta L_a}{\Delta L} + \beta + \theta_{adv} - \alpha_r \right) + \frac{\beta}{\Delta L} \ln \left(\frac{\beta L_p}{\Delta L} + \theta_{dwell} - \theta_{adv} \right) - \frac{\beta}{\Delta L} \ln \left(\frac{\beta L_p}{\Delta L} \frac{\beta L_a}{\Delta L} \right) \right] \\ & \left[\frac{B}{\delta L} \ln \left(\frac{B L_u}{\delta L} + \frac{\alpha_r}{2} - \beta \right) - \frac{B}{\delta L} \ln \left(\frac{B L_u}{\delta L} + \theta_{dwell} - \frac{\alpha_r}{2} \right) \right] \end{aligned} \right\}$$

Simulation results (shown later) suggest that this resultant average power varies significantly with an advance angle. It is possible to calculate the advance angle which maximizes this output power. Easier way to calculate the advance angle which maximizes this developed power is based speed independent part.

$$\begin{aligned} \frac{\partial P_m}{\partial \theta_{adv}} &= 0 \Rightarrow \\ 2\theta_{adv} &= \theta_{dwell} + \alpha_r - 2\beta, \end{aligned}$$

$$\begin{aligned}\therefore \theta_{adv}^* &= \frac{\theta_{dwell} + \alpha_r - 2\beta}{2} \\ \text{or} & \\ \therefore \theta_{adv}^* &= \frac{\theta_{dwell}}{2} + \frac{\alpha_r}{2} - \beta\end{aligned}\tag{7.97}$$

Note that this power maximizing advance angle only depends on the dwell angle and machine design parameters. Number of strokes required to achieve the desired peak current is calculated next. Initially during each stroke, since dwell angle is more than half of the rotor pole pitch, the fluxing region will be more than the de-fluxing region. Therefore at the end of each stroke, initial flux linkage will increase by,

$$\therefore \lambda_{add} = \frac{V_s}{\omega} * (2 * \theta_{dwell} - \alpha_r),$$

$$\text{Since } \lambda_0 = \lambda_{required} - \frac{V_s}{\omega} (\beta - (\theta_{dwell} - \theta_{adv})),$$

$$\begin{aligned}\therefore \text{strokes} \frac{V_s}{\omega} (2\theta_{dwell} - \alpha_r) &= \lambda_{required} - \frac{V_s}{\omega} (\beta - (\theta_{dwell} - \theta_{adv})), \\ \therefore \text{strokes} &= \frac{\lambda_{required} - \frac{V_s}{\omega} (\beta - (\theta_{dwell} - \theta_{adv}))}{\frac{V_s}{\omega} (2\theta_{dwell} - \alpha_r)}\end{aligned}\tag{7.98}$$

As described in the previous section, a better way to control the output power is by the peak current set-point. Developed power also depends on the advance angle and the dwell angle, but by making the output power proportional to the phase current, better partial load efficiency can be achieved (as good as the full load efficiency). The speed

dependent part of the developed average power does not depend on the peak current requirement. Therefore the peak current required to get the desired or rated power is given by,

$$I_{peak_required} = \frac{\alpha_r (P_{required} - P_{speed_dependent})}{2qV_s L_{required} \left\{ \begin{aligned} &\frac{\beta}{\Delta L} \ln \left(\frac{\beta L_a}{\Delta L} + \beta + \theta_{adv} - \alpha_r \right) + \frac{\beta}{\Delta L} \ln \left(\frac{\beta L_p}{\Delta L} + \theta_{dwell} - \theta_{adv} \right) \\ &-\frac{\beta}{\Delta L} \ln \left(\frac{\beta L_p}{\Delta L} \frac{\beta L_a}{\Delta L} \right) + \frac{B}{\delta L} \ln \left(\frac{BL_u}{\delta L} + \frac{\alpha_r}{2} - \beta \right) \\ &-\frac{B}{\delta L} \ln \left(\frac{BL_u}{\delta L} + \theta_{dwell} - \frac{\alpha_r}{2} \right) \end{aligned} \right\}} \quad (7.99)$$

The average current is given by,

$$I_{avg} = \frac{1}{\alpha_r} \left[\begin{aligned} &\int_{\theta=0}^{\theta=(\alpha_r-\beta-\theta_a)} i_1(\theta) d\theta + \int_{\theta=(\alpha_r-\beta-\theta_a)}^{\theta=\beta} i_2(\theta) d\theta + \int_{\theta=\beta}^{\theta=(\alpha_r-\theta_{dwell})} i_3(\theta) d\theta + \int_{\theta=(\alpha_r-\theta_{dwell})}^{\theta=\frac{\alpha_r}{2}} i_{4a}(\theta) d\theta \\ &\int_{\theta=\frac{\alpha_r}{2}}^{\theta=\theta_{dwell}} i_{4b}(\theta) d\theta + \int_{\theta=\theta_{dwell}}^{\theta=(\alpha_r-\beta)} i_5(\theta) d\theta + \int_{\theta=(\alpha_r-\beta)}^{\theta=(\alpha_r-\beta+\theta_{commutation})} i_6(\theta) d\theta + \int_{\theta=(\alpha_r-\beta+\theta_{commutation})}^{\theta=\alpha_r} i_7(\theta) d\theta \end{aligned} \right]$$

$$\begin{aligned}
I_{avg} &= \frac{1}{\alpha_r} \\
&\left\{ \begin{aligned}
& -\frac{\beta}{\Delta L} \lambda_{required} \ln \left(\frac{\frac{\beta L_a}{\Delta L} - \alpha_r + \beta + \theta_{adv}}{\frac{\beta L_a}{\Delta L}} \right) + \frac{V_s}{\omega} \frac{\beta}{\Delta L} [\alpha_r - \beta - \theta_{adv}] \\
& + \frac{V_s}{\omega} \frac{\beta}{\Delta L} \left(\frac{\beta L_a}{\Delta L} - \alpha_r + 2\beta + 2\theta_{adv} - \theta_{dwell} \right) \ln \left(\frac{\frac{\beta L_a}{\Delta L} - \alpha_r + \beta + \theta_{adv}}{\frac{\beta L_a}{\Delta L}} \right) \\
& - \frac{\beta}{\Delta L} \lambda_{required} \ln \left(\frac{\frac{\beta L_p}{\Delta L}}{\frac{\beta L_a}{\Delta L} - \alpha_r + \beta + \theta_{adv}} \right) - \frac{V_s}{\omega} \frac{\beta}{\Delta L} (2\beta + \theta_{adv} - \alpha_r) \\
& - \frac{V_s}{\omega} \frac{\beta}{\Delta L} \left(\frac{\beta L_a}{\Delta L} - \alpha_r + \theta_{dwell} \right) \ln \left(\frac{\frac{\beta L_p}{\Delta L}}{\frac{\beta L_a}{\Delta L} - \alpha_r + \beta + \theta_{adv}} \right) \\
& - \frac{B}{\delta L} \lambda_{required} \ln \left(\frac{\frac{BL_u}{\delta L} + \theta_{dwell} - \frac{\alpha_r}{2}}{\frac{BL_u}{\delta L} + \frac{\alpha_r}{2} - \beta} \right) - \frac{V_s}{\omega} \frac{B}{\delta L} (\alpha_r - \theta_{dwell} - \beta) \\
& - \frac{V_s}{\omega} \frac{B}{\delta L} \left(\frac{BL_u}{\delta L} + \theta_{dwell} - \frac{\alpha_r}{2} \right) \ln \left(\frac{\frac{BL_u}{\delta L} + \theta_{dwell} - \frac{\alpha_r}{2}}{\frac{BL_u}{\delta L} + \frac{\alpha_r}{2} - \beta} \right) \\
& \frac{B}{\delta L} \lambda_{required} \ln \left(\frac{\frac{BL_u}{\delta L} + \frac{\alpha_r}{2} - \beta}{\frac{BL_u}{\delta L} + \theta_{dwell} - \frac{\alpha_r}{2}} \right) + \frac{V_s}{\omega} \frac{B}{\delta L} (\alpha_r - \beta - \theta_{dwell}) \\
& - \frac{V_s}{\omega} \frac{B}{\delta L} \left(\frac{BL_u}{\delta L} + \theta_{dwell} - \frac{\alpha_r}{2} \right) \ln \left(\frac{\frac{BL_u}{\delta L} + \frac{\alpha_r}{2} - \beta}{\frac{BL_u}{\delta L} + \theta_{dwell} - \frac{\alpha_r}{2}} \right) \\
& \frac{\beta}{\Delta L} \lambda_{required} \ln \left(\frac{\frac{\beta L_p}{\Delta L} + \theta_{dwell} - \theta_{adv}}{\frac{\beta L_p}{\Delta L}} \right) + \left(\frac{V_s}{\omega} \right) \frac{\beta}{\Delta L} (\theta_{dwell} - \theta_{adv})
\end{aligned} \right\} \quad (7.100)
\end{aligned}$$

$$I_{avg_continued} = \left\{ \begin{aligned} & -\left(\frac{V_s}{\omega}\right) \frac{\beta}{\Delta L} \left(\frac{\beta L_a}{\Delta L} + \theta_{dwell} - \alpha_r \right) \ln \left(\frac{\frac{\beta L_p}{\Delta L} + \theta_{dwell} - \theta_{adv}}{\frac{\beta L_p}{\Delta L}} \right) \\ & + \frac{\beta}{\Delta L} \lambda_{required} \ln \left(\frac{\frac{\beta L_a}{\Delta L}}{\frac{\beta L_p}{\Delta L} + \theta_{dwell} - \theta_{adv}} \right) - \left(\frac{V_s}{\omega}\right) \frac{\beta}{\Delta L} (\beta + \theta_{adv} - \theta_{dwell}) \\ & + \left(\frac{V_s}{\omega}\right) \frac{\beta}{\Delta L} \left(\frac{\beta L_p}{\Delta L} + \theta_{dwell} - 2\theta_{adv} + \alpha_r - \beta \right) \ln \left(\frac{\frac{\beta L_a}{\Delta L}}{\frac{\beta L_p}{\Delta L} + \theta_{dwell} - \theta_{adv}} \right) \end{aligned} \right\}$$

The average current can also be split in two parts: a speed independent part, and a speed independent part.

$$I_{avg_speed_ind} = \frac{1}{\alpha_r} \left\{ \begin{aligned} & -\frac{\beta}{\Delta L} \lambda_{required} \ln \left(\frac{\frac{\beta L_a}{\Delta L} - \alpha_r + \beta + \theta_{adv}}{\frac{\beta L_a}{\Delta L}} \right) - \frac{\beta}{\Delta L} \lambda_{required} \ln \left(\frac{\frac{\beta L_p}{\Delta L}}{\frac{\beta L_a}{\Delta L} - \alpha_r + \beta + \theta_{adv}} \right) \\ & - \frac{B}{\delta L} \lambda_{required} \ln \left(\frac{\frac{BL_u}{\delta L} + \theta_{dwell} - \frac{\alpha_r}{2}}{\frac{BL_u}{\delta L} + \frac{\alpha_r}{2} - \beta} \right) + \frac{B}{\delta L} \lambda_{required} \ln \left(\frac{\frac{BL_u}{\delta L} + \frac{\alpha_r}{2} - \beta}{\frac{BL_u}{\delta L} + \theta_{dwell} - \frac{\alpha_r}{2}} \right) \\ & + \frac{\beta}{\Delta L} \lambda_{required} \ln \left(\frac{\frac{\beta L_p}{\Delta L} + \theta_{dwell} - \theta_{adv}}{\frac{\beta L_p}{\Delta L}} \right) + \frac{\beta}{\Delta L} \lambda_{required} \ln \left(\frac{\frac{\beta L_a}{\Delta L}}{\frac{\beta L_p}{\Delta L} + \theta_{dwell} - \theta_{adv}} \right) \\ & + 2\lambda_{required} \frac{B}{\delta L} \ln \left(\frac{\frac{BL_u}{\delta L} + \theta_{dwell} - \frac{\alpha_r}{2}}{\frac{BL_u}{\delta L}} \right) \end{aligned} \right\}$$

$$I_{avg_speed_ind} = 2 \frac{\lambda_{required}}{\alpha_r} \left\{ \frac{\beta}{\Delta L} \ln \left(\frac{L_a}{L_p} \right) + \frac{B}{\delta L} \ln \left(\frac{\frac{BL_u}{\delta L} + \frac{\alpha_r}{2} - \beta}{\frac{BL_u}{\delta L}} \right) \right\} \quad (7.101)$$

$$I_{avg_speed_ind} = 2 \frac{I_{peak} L_{required}}{\alpha_r} \left\{ \frac{\beta}{\Delta L} \ln \left(\frac{L_a}{L_p} \right) + \frac{B}{\delta L} \ln \left(\frac{\frac{BL_u}{\delta L} + \frac{\alpha_r}{2} - \beta}{\frac{BL_u}{\delta L}} \right) \right\}$$

This is the dominant part of the total average current. Note that this part does not depend on the choice of dwell angle or the advance angle. It only depends on the peak current.

$$I_{avg_speed_dependant} = \frac{1}{\alpha_r} \frac{V_s}{\omega} \frac{\beta}{\Delta L} \left\{ \begin{aligned} &2(\alpha_r + \theta_{dwell} - 2\theta_{adv} - 2\beta) \left[1 + \ln \left(\frac{\beta L_a}{\Delta L} \right) \right] \\ &+ 2 \left(\frac{\beta L_a}{\Delta L} - \alpha_r + \beta + \theta_{adv} \right) \ln \left(\frac{\beta L_a}{\Delta L} - \alpha_r + \beta + \theta_{adv} \right) \\ &- \left(\frac{\beta L_a}{\Delta L} + \frac{\beta L_p}{\Delta L} + 2\theta_{dwell} - 2\theta_{adv} - \beta \right) \ln \left(\frac{\beta L_p}{\Delta L} + \theta_{dwell} - \theta_{adv} \right) \end{aligned} \right\} \quad (7.102)$$

Simulation results suggest that the combination of the advance angle and the dwell angle which makes this speed dependant part zero, produces the maximum power per amp. In general, we have,

Required Flux Linkage to get Desired Peak Current:

$$\lambda_{required} = I_{peak} * L_{required},$$

$$\therefore \lambda_{required} = I_{peak} \left[L_u + \frac{\delta L}{B} \left(\theta_{dwell} - \frac{\alpha_r}{2} \right) \right]$$

Required Residual Flux Linkage to get desired Peak Current:

$$\lambda_0 = \lambda_{required} - \frac{V_s}{\omega} (\beta + \theta_{adv} - \theta_{dwell}),$$

Required Peak Flux Linkage to get desired Peak Current:

$$\lambda_{peak} = \lambda_{required} + \frac{V_s}{\omega} (\alpha_r - \beta - \theta_{adv})$$

Resultant Minimum Current:

$$I_{min} = \frac{\lambda_{required} + \frac{V_s}{\omega} (\alpha_r - 2\beta - 2\theta_{adv} + \theta_{dwell})}{L_a}$$

$$\therefore n \rightarrow \infty$$

$$I_{min} = \frac{I_{peak} \left[L_u + \frac{\delta L}{B} \left(\theta_{dwell} - \frac{\alpha_r}{2} \right) \right]}{L_a} \approx \frac{I_{peak} L_u}{L_a}$$

Advance Angle which maximizes the developed power at very high speed:

$$\theta_{adv}^* = \frac{\theta_{dwell}}{2} + \frac{\alpha_r}{2} - \beta$$

No of strokes required to achieve the desired peak current:

$$strokes = \frac{\lambda_{required} - \frac{V_s}{\omega} (\beta - (\theta_{dwell} - \theta_{adv}))}{\frac{V_s}{\omega} (2\theta_{dwell} - \alpha_r)}$$

Resultant Average Power:

$$P_{m_speed_independent} = 2V_s \frac{q}{\alpha_r} I_{peak} L_{required} \left\{ \begin{aligned} & \frac{\beta}{\Delta L} \ln \left(\frac{\beta L_a}{\Delta L} + \beta + \theta_{adv} - \alpha_r \right) + \frac{\beta}{\Delta L} \ln \left(\frac{\beta L_p}{\Delta L} + \theta_{dwell} - \theta_{adv} \right) - \frac{\beta}{\Delta L} \ln \left(\frac{\beta L_p}{\Delta L} \frac{\beta L_a}{\Delta L} \right) \\ & \frac{B}{\delta L} \ln \left(\frac{B L_u}{\delta L} + \frac{\alpha_r}{2} - \beta \right) - \frac{B}{\delta L} \ln \left(\frac{B L_u}{\delta L} + \theta_{dwell} - \frac{\alpha_r}{2} \right) \end{aligned} \right\}$$

$$P_{m_speed_dependant} = -(V_s)^2 \frac{2}{\omega} \frac{\beta}{\Delta L} \frac{q}{\alpha_r} \left\{ \begin{aligned} & (\beta + \theta_{adv} - \theta_{dwell}) \ln \left(\frac{\beta L_a}{\Delta L} + \beta + \theta_{adv} - \alpha_r \right) \\ & (\alpha_r + \theta_{dwell} - 2\theta_{adv} - 2\beta) \ln \left(\frac{\beta L_a}{\Delta L} \right) \\ & (\theta_{adv} + \beta - \alpha_r) \ln \left(\frac{\beta L_p}{\Delta L} + \theta_{dwell} - \theta_{adv} \right) \end{aligned} \right\}$$

Resultant Average Current:

$$I_{avg_speed_ind} = 2 \frac{\lambda_{required}}{\alpha_r}$$

$$\left\{ \frac{\beta}{\Delta L} \ln \left(\frac{L_a}{L_p} \right) + \frac{B}{\delta L} \ln \left(\frac{\frac{BL_u}{\delta L} + \frac{\alpha_r}{2} - \beta}{\frac{BL_u}{\delta L}} \right) \right\}$$

$$I_{avg_speed_dependant} = \frac{1}{\alpha_r} \frac{V_s}{\omega} \frac{\beta}{\Delta L}$$

$$\left\{ \begin{aligned} & 2(\alpha_r + \theta_{dwell} - 2\theta_{adv} - 2\beta) \left[1 + \ln \left(\frac{\beta L_a}{\Delta L} \right) \right] \\ & + 2 \left(\frac{\beta L_a}{\Delta L} - \alpha_r + \beta + \theta_{adv} \right) \ln \left(\frac{\beta L_a}{\Delta L} - \alpha_r + \beta + \theta_{adv} \right) \\ & - \left(\frac{\beta L_a}{\Delta L} + \frac{\beta L_p}{\Delta L} + 2\theta_{dwell} - 2\theta_{adv} - \beta \right) \ln \left(\frac{\beta L_p}{\Delta L} + \theta_{dwell} - \theta_{adv} \right) \end{aligned} \right\}$$

Peak Current required to get the desired Power,

$$I_{peak_required} =$$

$$\frac{\alpha_r (P_{required} - P_{speed_dependant})}{2qV_s L_{required} \left\{ \begin{aligned} & \frac{\beta}{\Delta L} \ln \left(\frac{\beta L_a}{\Delta L} + \beta + \theta_{adv} - \alpha_r \right) + \frac{\beta}{\Delta L} \ln \left(\frac{\beta L_p}{\Delta L} + \theta_{dwell} - \theta_{adv} \right) \\ & - \frac{\beta}{\Delta L} \ln \left(\frac{\beta L_p}{\Delta L} \frac{\beta L_a}{\Delta L} \right) + \frac{B}{\delta L} \ln \left(\frac{BL_u}{\delta L} + \frac{\alpha_r}{2} - \beta \right) \\ & - \frac{B}{\delta L} \ln \left(\frac{BL_u}{\delta L} + \theta_{dwell} - \frac{\alpha_r}{2} \right) \end{aligned} \right\}}$$

7.5.10 Validation of Analytical Results (Simulation Results)

A number of simulations were carried out to validate mathematical results derived in the previous section. Both the linear model (described in Section 7.2.1) and the non-linear model (described in Section 7.2.2) were used for the validation. Figure 7-32 shows the simulation results based on the linear model described in the section 7.2.1. The speed is 3750 RPM, advance angle is 23° , dwell angle is 31° and the current regulator set point is 600A. The first part of this figure shows the applied voltage (blue waveform), per phase inductance profile (red waveform), resultant flux-linkage (magenta waveform) and the resultant current (black waveform) just before and after the current regulator involvement. Note that once the desired peak current is achieved, output power is maintained and the growing current is stabilized. The second part of the figure shows a growing flux-linkage vs current plot as a result of continuous conduction (co-energy plot). The third part of the figure shows the resultant average power. During simulations, average power was calculated by using the trapezoidal method and *polyarea* function of the Matlab. Figure 7-33 shows the developed average power.

Results were verified for $n = 6$ (1500 RPM) , $n = 15$ (3750 RPM) and $n = 26$ (6500 RPM) with an advance angle = $15^\circ, 17^\circ, 19^\circ, 21^\circ, 23^\circ$ and 25° , peak current regulator set point = 600 A and 300 A, and the dwell angle fixed at 31° . Table 7-8, Table 7-9, Table 7-10, Table 7-11, and Table 7-12 show comparison between the theoretical values and the simulation results for the residual flux-linkage, peak flux-linkage, minimum current, average power and average current (with speed dependant and speed independent split). These tables also list RMS current obtained from the simulations.

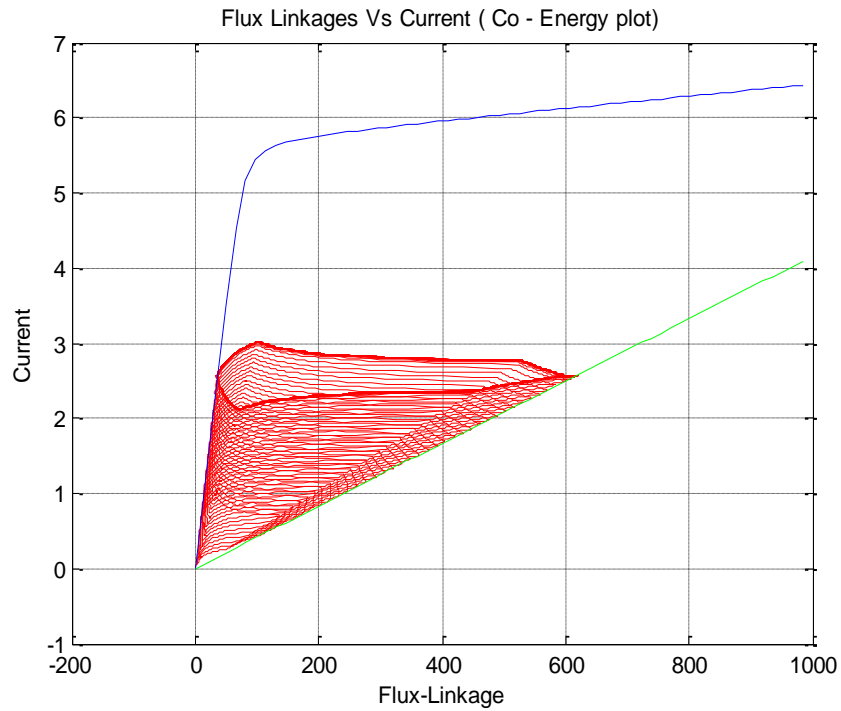
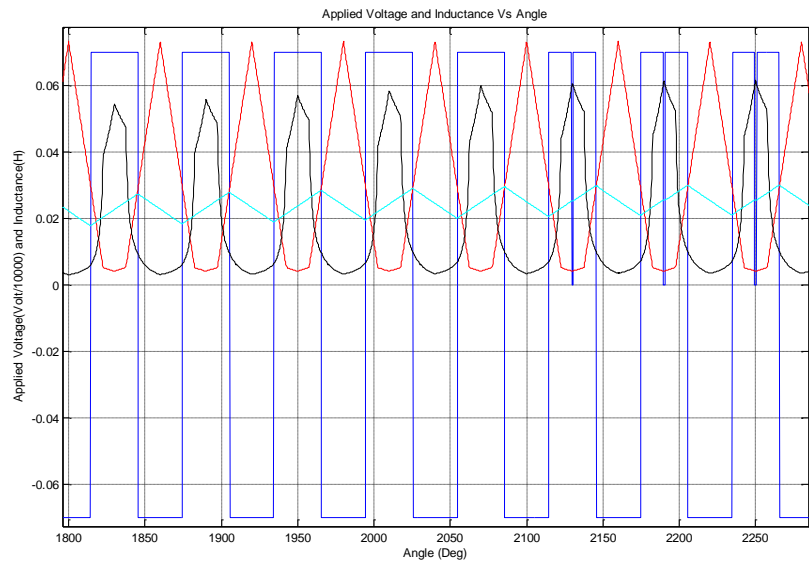


Figure 7-32: Validation of Non-flat Unaligned Inductance Type SRM Motor Analysis, Speed = 3750 rpm ($n=15$), Dwell = 31° , Advance Angle = 23° and Current Regulator Set Point, $I_{peak} = 600A$.

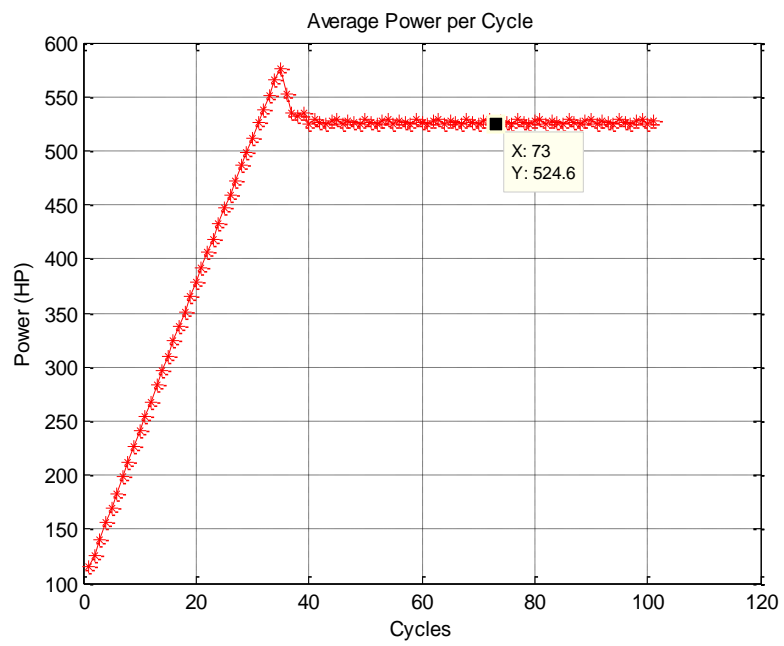


Figure 7-33 : Average Power.

Table 7-8 : Non-flat Unaligned Inductance type SRM, Dwell = 31° (Linear Model and Non Linear Model).

Speed = 1500 RPM , Peak Current = 600 A <i>Linear Model</i>															
Adv. Angle	Intial Flux Linkage (Wb)		Peak Flux Linkage (Wb)		Minimum Current (A)		Average Power (HP)		Average Power (HP)		Average Current (A)		Average Current (A)		RMS Cur.
	Sim. Result	Theor. Result	Sim. Result	Theore tical	Sim. Result	Theore tical	Sim. Result	Theore tical	Speed. Ind.	Speed Dep.	Sim. Result	Theor. Result	Speed Ind.	Speed Dep.	
15	2.0538	2.0711	4.3115	4.3266	51.905	52.073	441.68	440.01	407.49	32.525	225.97	227.13	212.6	14.527	303.71
17	1.9012	1.9155	4.1571	4.1711	47.688	47.833	499.52	499.1	476.46	22.639	221.66	222.71	212.6	10.115	302.24
19	1.7449	1.76	4.0019	4.0155	43.418	43.593	523.8	522.54	507.66	14.877	217.98	219.05	212.6	6.4516	301.3
21	1.5908	1.6044	3.8461	3.86	39.191	39.353	530.4	530.19	522.77	7.4242	214.74	215.75	212.6	3.1485	300.72
23	1.4381	1.4489	3.6926	3.7044	34.966	35.114	527.21	527.36	527.36	0	211.72	212.6	212.6	0	300.3
25	1.279	1.2933	3.5357	3.5489	30.687	30.874	516.06	515.34	522.77	-7.424	208.34	209.45	212.6	-3.149	299.37
Speed = 1500 RPM , Peak Current = 600 A <i>Non Linear Model</i>															
15	2.058	2.0711	4.3171	4.3266	53.821	52.073	615.97	440.01	407.49	32.525	318.39	227.13	212.6	14.527	378.13
17	1.9062	1.9155	4.1629	4.1711	48.926	47.833	701.48	499.1	476.46	22.639	303.52	222.71	212.6	10.115	370.79
19	1.7498	1.76	4.0076	4.0155	44.333	43.593	728.15	522.54	507.66	14.877	291.08	219.05	212.6	6.4516	365.57
21	1.5966	1.6044	3.8535	3.86	39.855	39.353	697.74	530.19	522.77	7.4242	281.42	215.75	212.6	3.1485	361.31
23	1.4443	1.4489	3.7002	3.7044	35.419	35.114	639.84	527.36	527.36	0	272.1	212.6	212.6	0	356.19
25	1.2872	1.2933	3.5458	3.5489	31.016	30.874	570.11	515.34	522.77	-7.424	261.82	209.45	212.6	-3.149	349.51

Table 7-9 : Non-flat Unaligned Inductance type SRM Dwell = 31° (Linear Model).

Speed = 3750 RPM , Peak Current = 600 A															
Adv. Angle	Initial Flux Linkage (Wb)		Peak Flux Linkage (Wb)		Minimum Current (A)		Average Power (HP)		Average Power (HP)		Average Current (A)		Average Current (A)		RMS Cur. (A)
	Sim. Result	Theor. Result	Sim. Result	Theor. Result	Sim. Result	Theor. Result	Sim. Result	Theor. Result	Speed Ind.	Speed Dep.	Sim. Result	Theor. Result	Speed Ind.	Speed Dep.	
15	2.3626	2.3744	3.2639	3.2766	41.831	41.897	422.22	420.5	407.49	13.01	217.44	218.41	212.6	5.8107	299.39
17	2.3044	2.3122	3.2048	3.2144	40.193	40.201	485.55	485.51	476.46	9.0556	215.98	216.65	212.6	4.0458	299.1
19	2.2363	2.25	3.1378	3.1522	38.415	38.505	514.92	513.61	507.66	5.9508	214.07	215.18	212.6	2.5806	298.09
21	2.1759	2.1878	3.0769	3.09	36.716	36.81	526.5	525.73	522.77	2.9697	212.91	213.86	212.6	1.2594	298.05
23	2.1166	2.1255	3.0166	3.0278	35.053	35.114	526.4	527.36	527.36	0	211.81	212.6	212.6	0	298.02
25	2.0529	2.0633	2.9539	2.9655	33.336	33.418	520.98	519.8	522.77	-2.97	210.38	211.34	212.6	-1.259	297.57
Speed = 3750 RPM , Peak Current = 300 A															
15	1.0827	1.0861	1.9833	1.9883	24.323	24.34	217.16	216.75	203.74	13.01	111.8	112.11	106.3	5.8107	151.36
17	1.0221	1.0239	1.9218	1.9261	22.646	22.645	246.77	247.28	238.23	9.0556	110.13	110.35	106.3	4.0458	150.82
19	0.9573	0.9617	1.8587	1.8639	20.912	20.949	260.49	259.78	253.83	5.9508	108.5	108.88	106.3	2.5806	150.24
21	0.8959	0.8994	1.7965	1.8017	19.218	19.253	264.46	264.35	261.38	2.9697	107.25	107.56	106.3	1.2594	150.05
23	0.8367	0.8372	1.7359	1.7394	17.551	17.557	263	263.68	263.68	0	106.14	106.3	106.3	0	150.02
25	0.7713	0.775	1.6726	1.6772	15.819	15.861	258.95	258.41	261.38	-2.97	104.71	105.04	106.3	-1.259	149.54

Table 7-10: Non-flat Unaligned Inductance type SRM Dwell = 31° (Non Linear Model).

Speed = 3750 RPM , Peak Current = 600 A															
Adv. Angle	Intial Flux Linkage (Wb)		Peak Flux Linkage (Wb)		Minimum Current (A)		Average Power (HP)		Average Power (HP)		Average Current (A)		Average Current (A)		RMS Cur.
	Sim. Result	Theor. Result	Sim. Result	Theor. Result	Sim. Result	Theor. Result	Sim. Result	Theor. Result	Speed Ind.	Speed Dep.	Sim. Result	Theor. Result	Speed Ind.	Speed Dep.	
15	2.3705	2.3744	3.2726	3.2766	42.677	41.897	467.97	420.5	407.49	13.01	273.8	218.41	212.6	5.8107	342.79
17	2.3141	2.3122	3.215	3.2144	40.964	40.201	570.65	485.51	476.46	9.0556	269.55	216.65	212.6	4.0458	340.38
19	2.2455	2.25	3.1473	3.1522	39.08	38.505	645.83	513.61	507.66	5.9508	264.75	215.18	212.6	2.5806	337.49
21	2.1856	2.1878	3.0863	3.09	37.314	36.81	678.79	525.73	522.77	2.9697	261.76	213.86	212.6	1.2594	336.66
23	2.1267	2.1255	3.0268	3.0278	35.568	35.114	660.78	527.36	527.36	0	259.13	212.6	212.6	0	336.03
25	2.0591	2.0633	2.9613	2.9655	33.734	33.418	612.52	519.8	522.77	-2.97	255.39	211.34	212.6	-1.259	333.97
Speed = 3750 RPM , Peak Current = 300 A															
15	1.0883	1.0861	1.9891	1.9883	24.495	24.34	229.01	216.75	203.74	13.01	118.41	112.11	106.3	5.8107	157.33
17	1.0275	1.0239	1.9277	1.9261	22.784	22.645	266.18	247.28	238.23	9.0556	116.16	110.35	106.3	4.0458	156.34
19	0.9636	0.9617	1.8648	1.8639	21.05	20.949	281.56	259.78	253.83	5.9508	114.51	108.88	106.3	2.5806	155.82
21	0.9019	0.8994	1.8023	1.8017	19.33	19.253	285.73	264.35	261.38	2.9697	113.17	107.56	106.3	1.2594	155.59
23	0.8427	0.8372	1.7419	1.7394	17.64	17.557	283.93	263.68	263.68	0	112.05	106.3	106.3	0	155.57
25	0.7766	0.775	1.6776	1.6772	16.141	15.861	278.61	258.41	261.38	-2.97	110.45	105.04	106.3	-1.259	154.96

Table 7-11 : Non-flat Unaligned Inductance type SRM Dwell = 31° (Linear Model).

Speed = 6500 RPM , Peak Current = 600 A															
Adv. Angle	Intial Flux Linkage (Wb)		Peak Flux Linkage (Wb)		Minimum Current (A)		Average Power (HP)		Average Power (HP)		Average Current (A)		Average Current (A)		RMS Cur. (A)
	Sim. Result	Theor. Result	Sim. Result	Theor. Result	Sim. Result	Theor. Result	Sim. Result	Theor. Result	Speed Ind.	Speed Dep.	Sim. Result	Theor. Result	Speed Ind.	Speed Dep.	
15	2.4473	2.46	2.9662	2.9805	39.043	39.027	415.28	414.99	407.49	7.5058	214.91	215.95	212.6	3.3523	298.27
17	2.4133	2.4241	2.9319	2.9446	38.038	38.049	481.24	481.68	476.46	5.2244	213.91	214.93	212.6	2.3341	297.97
19	2.3782	2.3882	2.8971	2.9087	37.072	37.071	512.09	511.09	507.66	3.4331	213.14	214.09	212.6	1.4888	297.84
21	2.3435	2.3523	2.8621	2.8728	36.108	36.092	525.01	524.48	522.77	1.7133	212.46	213.33	212.6	0.7266	297.8
23	2.3073	2.3164	2.826	2.8369	35.135	35.114	527.5	527.36	527.36	0	211.82	212.6	212.6	0	297.72
25	2.2677	2.2805	2.7868	2.801	34.105	34.135	522.21	521.05	522.77	-1.713	210.68	211.87	212.6	-0.727	297.05
Speed = 6500 RPM , Peak Current = 300 A															
15	1.171	1.1717	1.6892	1.6922	21.521	21.47	211.53	211.25	203.74	7.5058	109.5	109.65	106.3	3.3523	150.37
17	1.1341	1.1358	1.6527	1.6563	20.531	20.492	243.69	243.45	238.23	5.2244	108.45	108.63	106.3	2.3341	149.9
19	1.0966	1.0999	1.6151	1.6204	19.518	19.514	257.26	257.26	253.83	3.4331	107.42	107.79	106.3	1.4888	149.44
21	1.0609	1.064	1.5798	1.5845	18.56	18.535	263.53	263.1	261.38	1.7133	106.74	107.03	106.3	0.7266	149.38
23	1.0262	1.0281	1.5442	1.5486	17.583	17.557	263.29	263.68	263.68	0	106.02	106.3	106.3	0	149.27
25	0.9897	0.9922	1.5082	1.5127	16.603	16.578	259.68	259.67	261.38	-1.713	105.31	105.57	106.3	-0.727	149.12

Table 7-12: Non-flat Unaligned Inductance type SRM Dwell = 31° (Non Linear Model).

Speed = 6500 RPM , Peak Current = 600 A															
Adv. Angle	Intial Flux Linkage (Wb)		Peak Flux Linkage (Wb)		Minimum Current (A)		Average Power (HP)		Average Power (HP)		Average Current (A)		Average Current (A)		RMS Cur. (A)
	Sim. Result	Theor. Result	Sim. Result	Theor. Result	Sim. Result	Theor. Result	Sim. Result	Theor. Result	Speed Ind.	Speed Dep.	Sim. Result	Theor. Result	Speed Ind.	Speed Dep.	
15	2.4574	2.46	2.9771	2.9805	39.729	39.027	439.62	414.99	407.49	7.5058	265.4	215.95	212.6	3.3523	337.14
17	2.4239	2.4241	2.9429	2.9446	38.72	38.049	540.4	481.68	476.46	5.2244	262.8	214.93	212.6	2.3341	335.49
19	2.3868	2.3882	2.9061	2.9087	37.66	37.071	619.8	511.09	507.66	3.4331	260.32	214.09	212.6	1.4888	334.08
21	2.3518	2.3523	2.8704	2.8728	36.641	36.092	665.68	524.48	522.77	1.7133	258.54	213.33	212.6	0.7266	333.43
23	2.3158	2.3164	2.8353	2.8369	35.642	35.114	667.55	527.36	527.36	0	257.08	212.6	212.6	0	333.07
25	2.2809	2.2805	2.8	2.801	34.625	34.135	625.86	521.05	522.77	-1.713	255.46	211.87	212.6	-0.727	332.53
Speed = 6500 RPM , Peak Current = 300 A															
15	1.1755	1.1717	1.6941	1.6922	21.643	21.47	217.45	211.25	203.74	7.5058	115.03	109.65	106.3	3.3523	155.13
17	1.14	1.1358	1.6585	1.6563	20.65	20.492	257.73	243.45	238.23	5.2244	113.67	108.63	106.3	2.3341	154.45
19	1.1026	1.0999	1.6212	1.6204	19.63	19.514	271.09	257.26	253.83	3.4331	112.52	107.79	106.3	1.4888	153.94
21	1.0668	1.064	1.5856	1.5845	18.656	18.535	281.51	263.1	261.38	1.7133	111.81	107.03	106.3	0.7266	153.85
23	1.0318	1.0281	1.5501	1.5486	17.674	17.557	281.38	263.68	263.68	0	111.04	106.3	106.3	0	153.71
25	0.9946	0.9922	1.513	1.5127	16.658	16.578	276.95	259.67	261.38	-1.713	110.17	105.57	106.3	-0.727	153.41

Figure 7-34, Figure 7-35, and Figure 7-36 show the comparison between the simulation results (using linear and non-linear model) and the analytical values. It can be seen from the Table 7-8, Table 7-10, and Table 7-12 that for the peak current (derived in Table 7-13), the difference between resultant average power based on the linear analysis and the resultant average power based on the non-linear model simulation is less than 14%.

Table 7-13 lists the required peak current (i.e. the current regulator set point) to develop the rated power at high speed. Note that for a fixed dwell angle of 31° and a fixed advance angle of 22.5° , required peak current set point is constant. Also note that only a peak current of 364A is required to develop the rated power at high speed.

Table 7-14 shows the comparison between simulation results (based on the non-linear model) and the analytical results (based on the linear per phase inductance profile) when rated power is produced at high speed. Figure 7-37 demonstrates the same comparison.

When compared with the simulation results based on the non-linear model (Table 7-8, Table 7-10, and Table 7-12) and analytical results (based on the linear analysis), difference can be noticed. This difference is more visible for high currents. This is due the saturation.

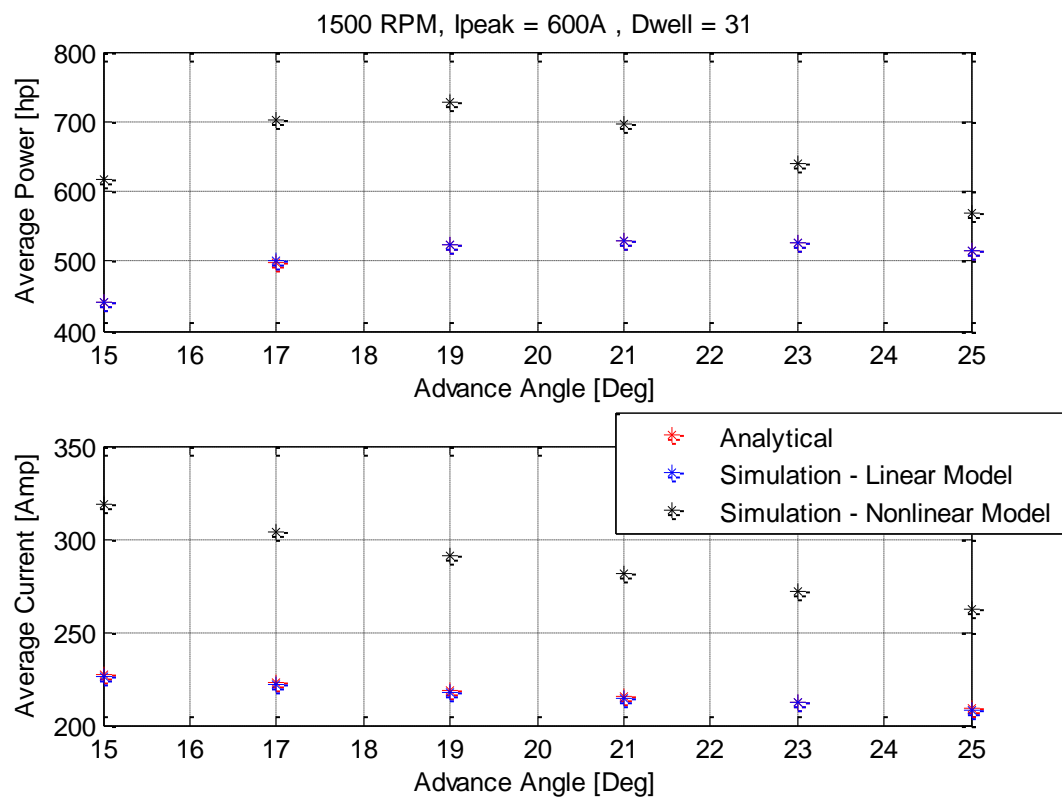


Figure 7-34: Comparison of Analytical Results with Simulation Results for a Non Flat Unaligned Inductance Profile type SRM Motor.

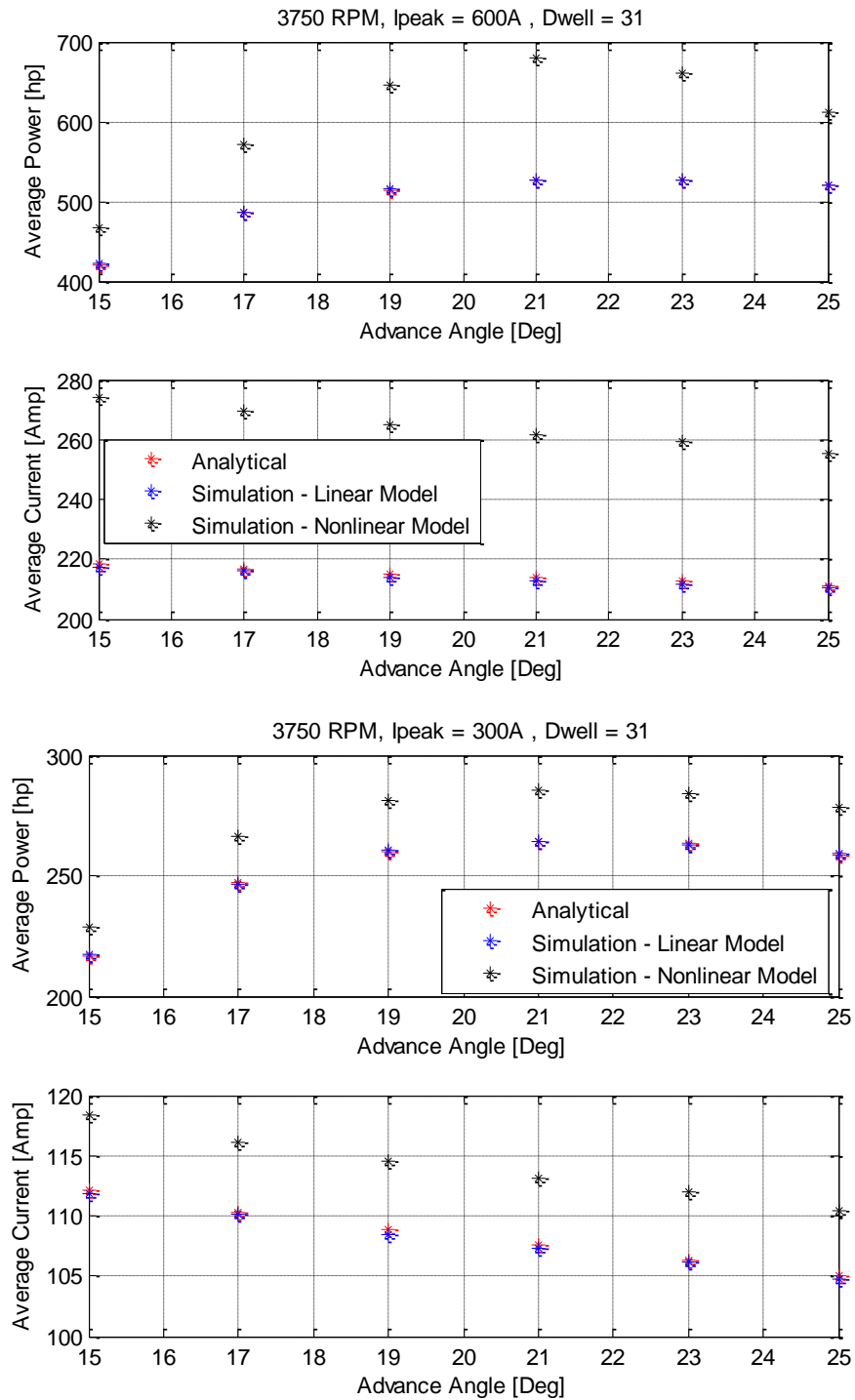


Figure 7-35 : Comparison of Analytical and Simulation Results.

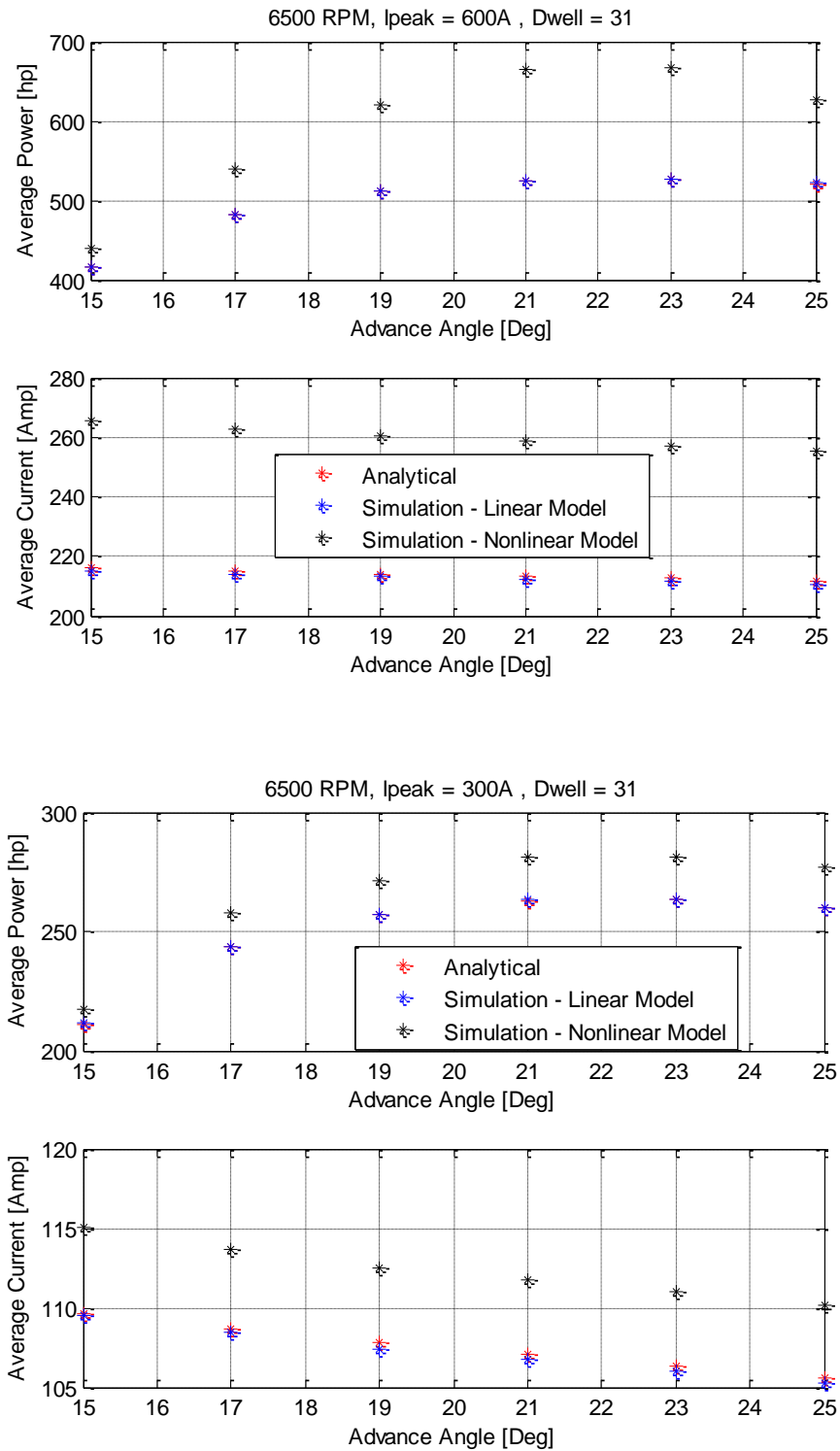


Figure 7-36 : Comparison of Analytical and Simulation Results.

Table 7-13 : Current Regulator Set Point to get Rated Power.

Relative Speed	Advance Angle	Dwell Angle	Peak current to get rated Power
6	22.5	31	362.1602
7	22.5	31	362.462
8	22.5	31	362.6884
9	22.5	31	362.8645
10	22.5	31	363.0054
15	22.5	31	363.428
20	22.5	31	363.6393
25	22.5	31	363.7661
30	22.5	31	363.8506

Table 7-14 : Rated Power at High Speed using Continuous Conduction.

Advance Angle = 22.5 , Dwell Angle = 31, I _{peak} = 364A											
Speed	Initial Flux Linkage (Wb)		Peak Flux Linkage (Wb)		Minimum Current (A)		Average Power (HP)		Average Current (A)		RSM Cur. (A)
	Theoretical I	Non linear	Theoretical I	Non linear	Theoretical I	Non linear	Theoretical I	Non linear	Theoretical I	Non linear	Non linear
6	0.4743	0.347	2.7298	2.6011	22.3622	14.2348	321.6162	356.7084	129.7583	137.9789	193.0864
7	0.6298	0.5705	2.5632	2.5025	22.2108	20.3217	321.351	365.6133	129.6466	141.1424	195.3401
8	0.7465	0.7357	2.4382	2.4262	22.0972	21.9834	321.1522	372.238	129.5629	143.6566	197.4446
9	0.8372	0.8389	2.3409	2.3405	22.0089	22.0867	320.9975	370.2463	129.4978	143.23	196.3858
10	0.9098	0.9154	2.2632	2.2651	21.9382	22.0498	320.8737	366.1549	129.4457	142.478	195.1419
15	1.1276	1.1304	2.0298	2.0306	21.7263	21.8423	320.5025	359.571	129.2894	139.8899	191.3087
20	1.2365	1.2385	1.9132	1.9133	21.6203	21.6725	320.3169	356.7916	129.2113	139.0082	190.0426
25	1.3018	1.3106	1.8432	1.8477	21.5567	21.7446	320.2055	351.8754	129.1644	139.0734	190.0257
30	1.3454	1.3505	1.7965	1.7993	21.5143	21.7161	320.1313	354.3621	129.1331	138.5515	189.3462
100	1.4978	1.5347	1.6332	1.6655	21.3659	21.8946	319.8714	342.1551	129.0238	141.2355	192.8442
inf	1.5632		1.5632		20.5761		319.76		128.9769		

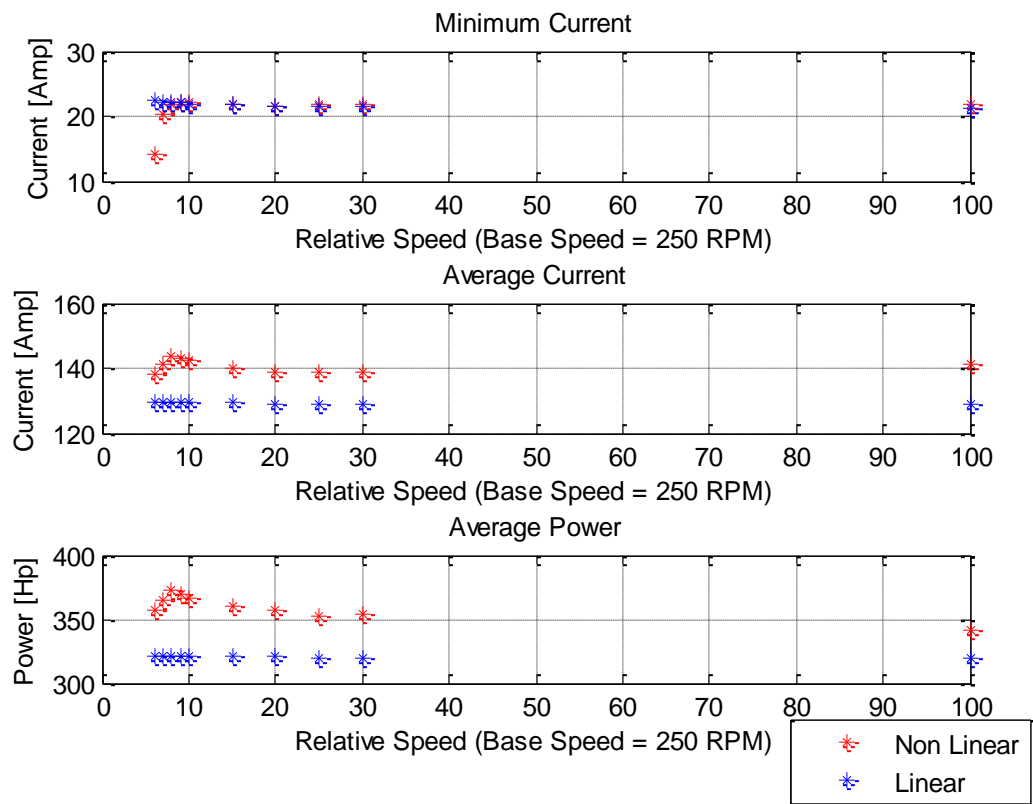


Figure 7-37 : Comparison between Non Linear and Linear Analysis for Rated Output Power.

7.5.11 Controller Analysis

Figure 7-38 displays the RMS current and the developed power versus the advance angle for dwell angles of 30.5° , 31.5° and 32.5° . The current regulator set point is fixed at the 500A. Note that for a dwell of 32.5° , more RMS current is required for any advance angle and less power is developed than a dwell angle of 31.5° . Same is true when a dwell of 31.5° is compared to a dwell of 30.5° . This indicates that the greatest efficiency can be achieved using a dwell that sufficient enough to sustain continuous conduction, but otherwise as small as possible. There is an obvious need to precisely determine the dwell as the motor may slip from continuous to discontinuous conduction with precipitous loss of the developed power if the dwell angle is reduces below 30° . Also, note that the RMS current is independent of the advance angle and depends only on the dwell angle.

While the developed power varies with the advance angle, adjustment of the advance angle is not the best way to control the developed power. The best method for power control is the current regulator set point. As shown in the Figure 7-39, output power can be efficiently controlled by changing the current regulator set point rather than changing the advance angle or the dwell angle.

Dynamic response to an increased power command can be very sluggish if the minimum dwell is used. Figure 7-40 shows the simulated response of the motor current to a step change in the current regulator set point from an initial value of 0A to 364A when operating at relative speed of 13. Simulations were carried out for a dwell of 30.5° and for a dwell of 33.5° .

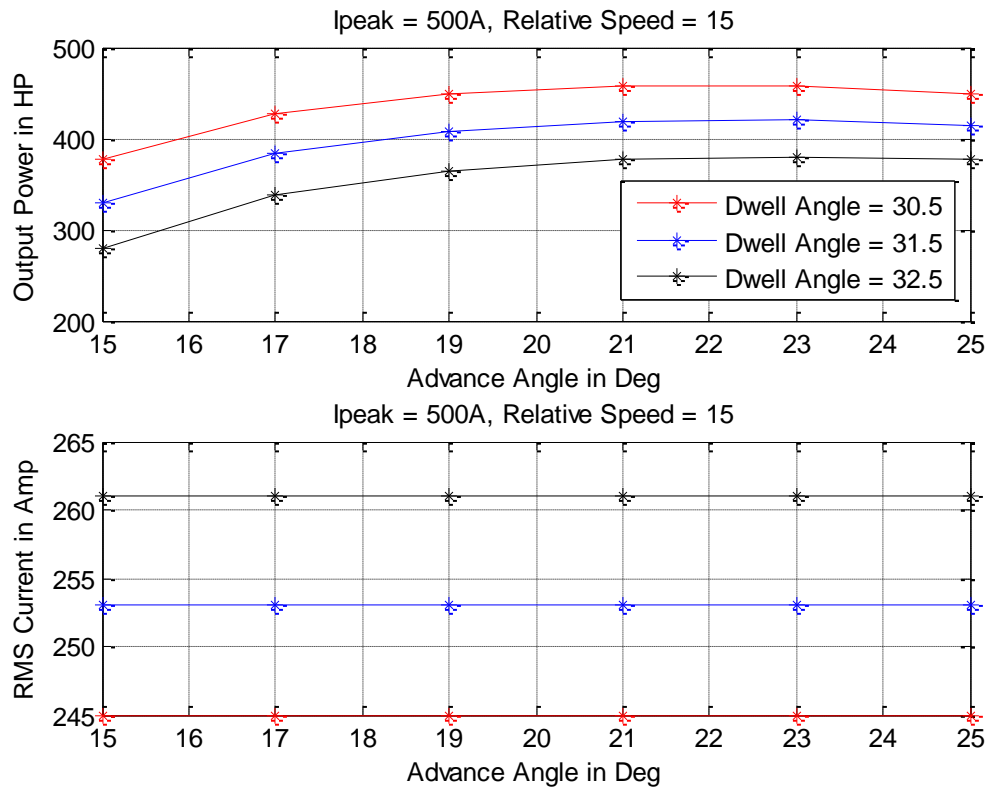


Figure 7-38: Dwell Angle Vs Advance Angle (Speed = 3750 RPM, $I_{peak} = 500A$).

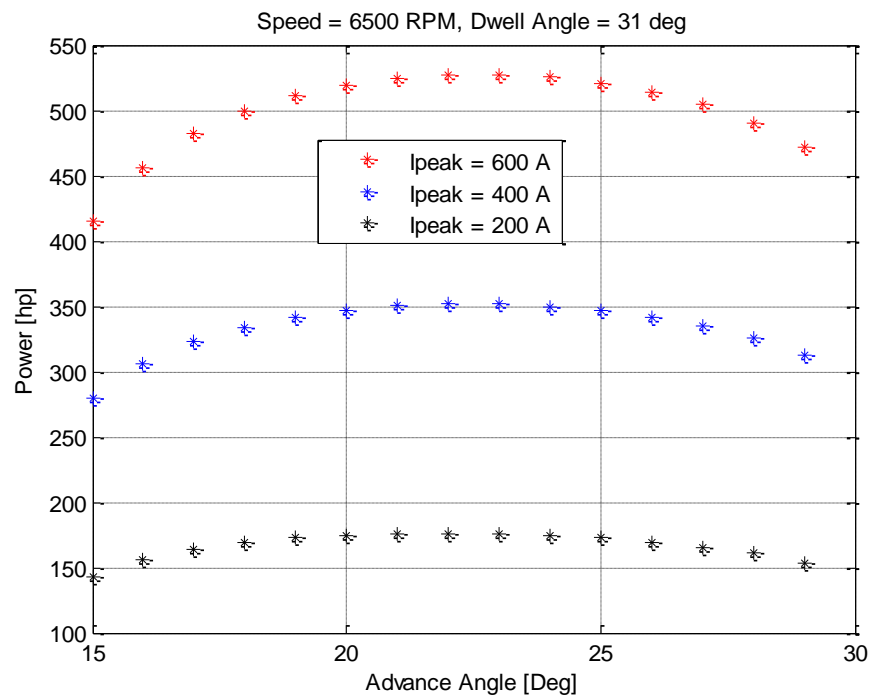
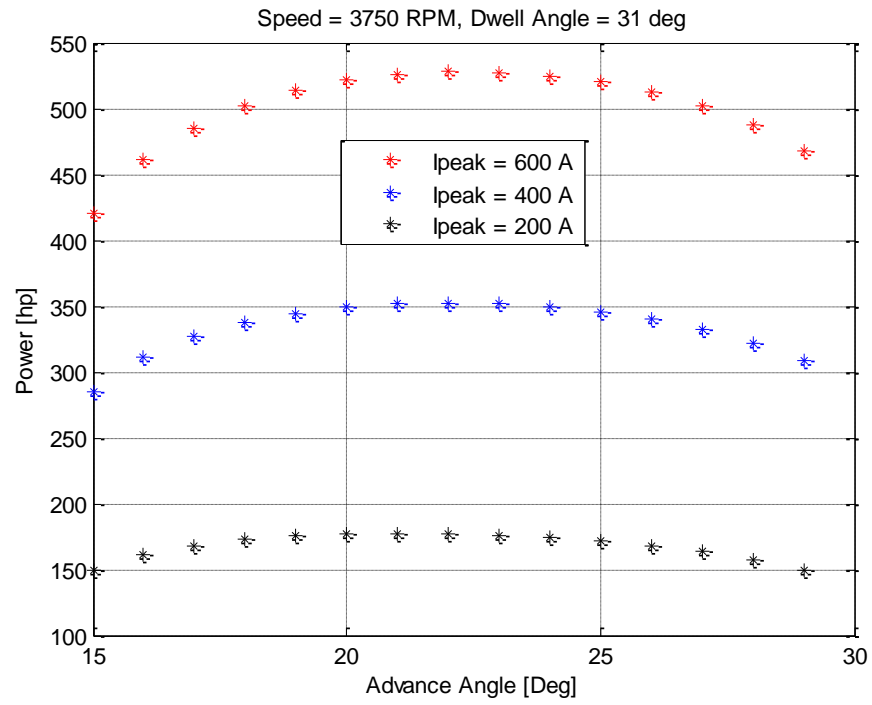
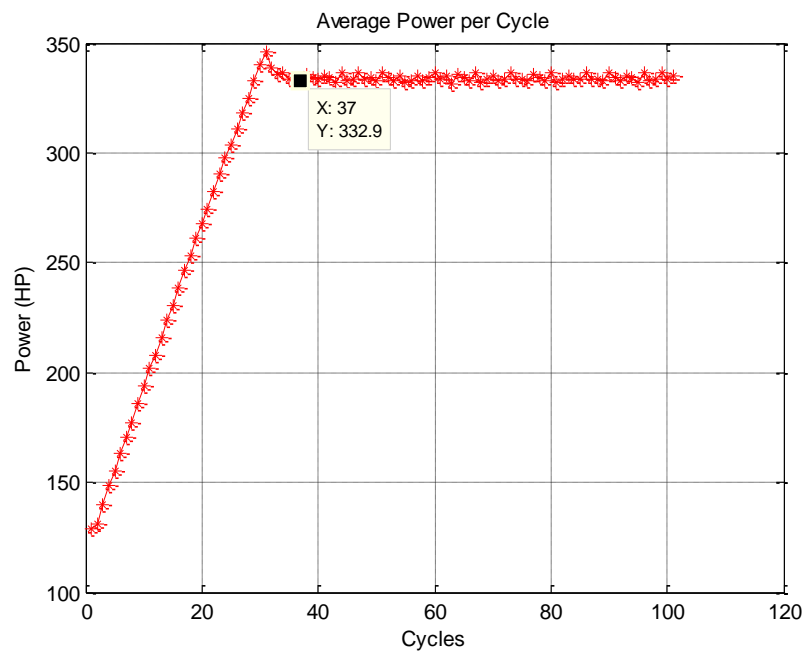
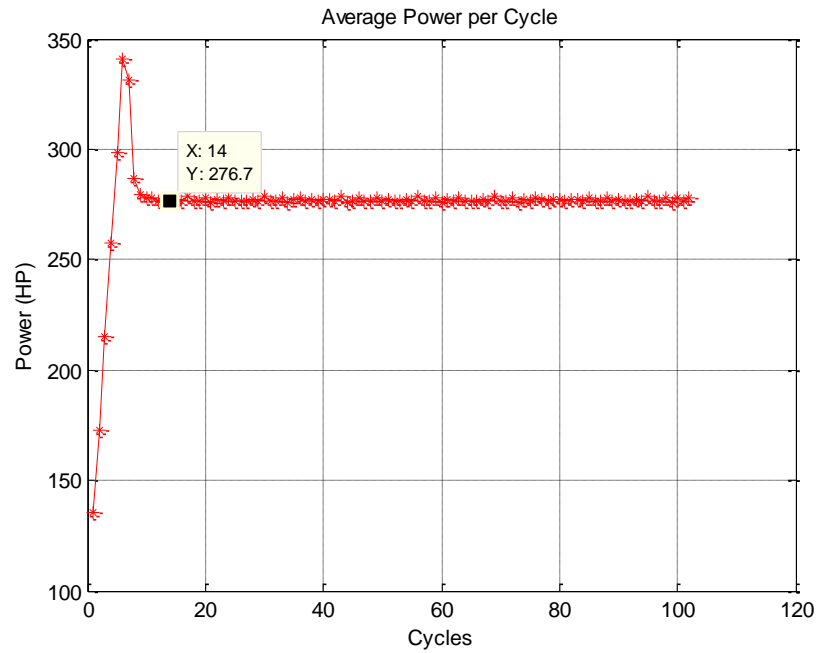


Figure 7-39 : Power Control in Continuous Conduction Mode.



**Figure 7-40 : Response to a Step Change in Current Regulator Set when Operating at 6500 RPM
with Dwell Angles of 30.25° and 31°.**

In both cases, the advance angle is 22.5° . Observe that for a dwell of 30.5° , approximately 37 cycles are required to achieve 364A but developed power is about 333Hp; while for a dwell of 33.5° , only 14 cycles are required but the output power is 276Hp. Smaller dwell yields greater steady state efficiency but it has considerably longer dynamic response time. Application requirements may dictate how to deal with a tradeoff between the speed of response and the steady state efficiency. If both are desired, a smart controller can be developed using the analytical formulas, derived in previous section. Based on the power requirement, current regulator set point can be estimated by using Equation (7.99). Initially the dwell angle can be set to the maximum possible value to get faster response. Based the dwell angle, power maximizing advance angle can be selected by using Equation (7.97). Based on this information it is possible to estimate the number of strokes it will take to achieve the steady state by using Equation (7.98). As the motor current approaches the current regulator set point, the dwell angle can be collapsed back to the minimum possible value (at least 50% of the stroke length). With the dwell, advance angle also can be changed in small increments.

7.5.12 Constant Power Speed Ratio

Linear analysis similar to the one in Section 7.4.10 can be carried out to find out the resultant output power for a non flat type SRM motor when operated in single pulse mode at speed with discontinuous type conduction. This analysis is based on the linear inductance waveform. Figure 7-41 illustrates the same. Some saturation can be observed for medium speeds, especially with the high current.

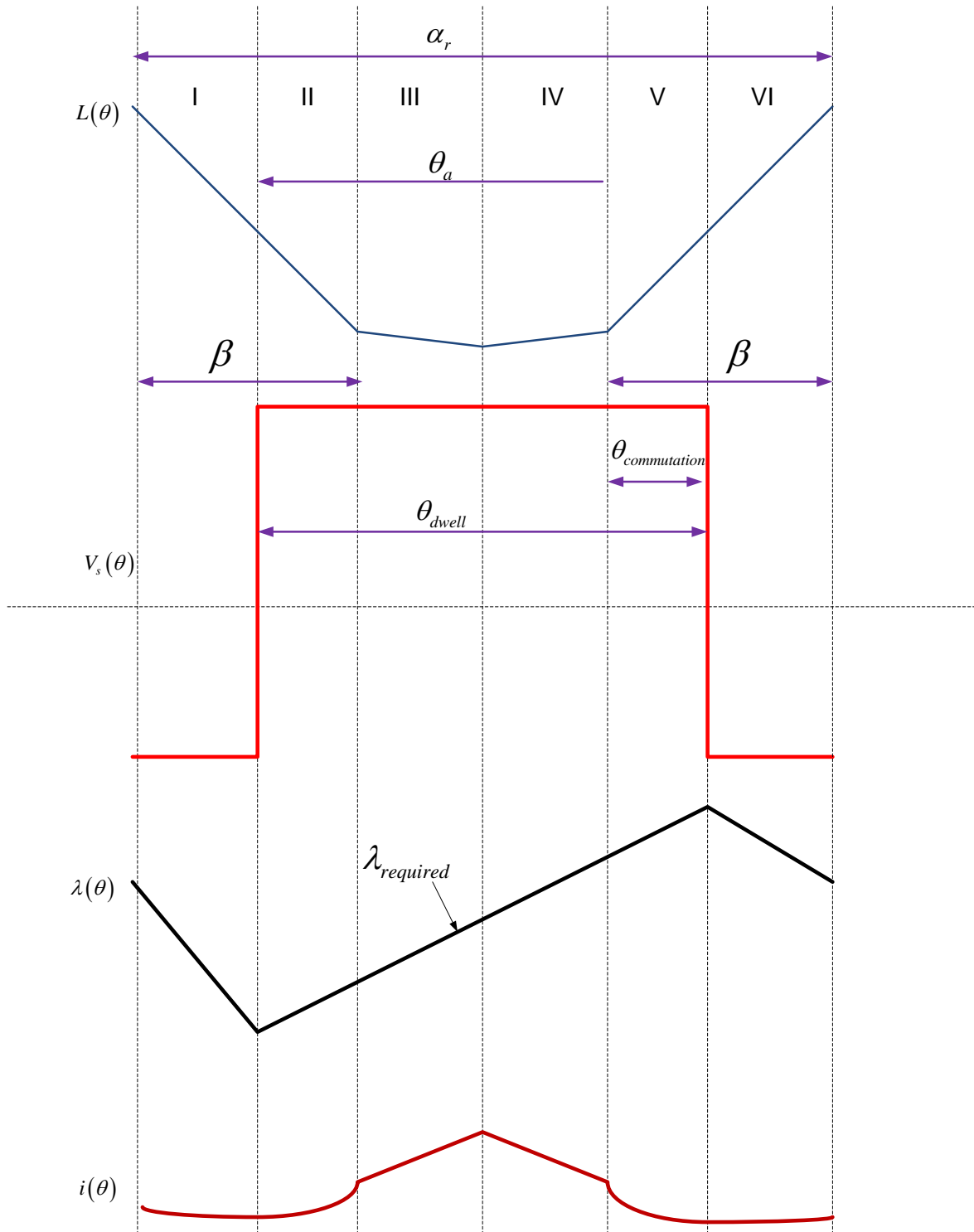


Figure 7-41: CPSR Estimation with Single Pulse High Speed Operation of the Non flat Unaligned Inductance type SRM.

But using linear analysis, it is possible to estimate the highest speed at which the rated power can be developed by using single pulse type high speed controller with discontinuous type conduction. In single pulse mode, developed power (using linear analysis) is given by the following equation,

$$P_{m_CPSR} = \omega \frac{q}{\alpha_r} \{P_1 + P_2 + P_3 + P_4 + P_5 + P_6\}$$

$$P_{m_CPSR} = \omega \frac{q}{\alpha_r} \left\{ \begin{aligned} & - \left(\frac{V_s}{\omega} \right)^2 \frac{\beta}{\Delta L} (\alpha_r - \beta - \theta_{adv}) - \left(\frac{V_s}{\omega} \right)^2 \frac{\beta}{\Delta L} \left(\frac{\beta L_a}{\Delta L} + \theta_{adv} + \beta - \alpha_r \right) \ln \left(\frac{\frac{\beta L_a}{\Delta L} + \theta_{adv} + \beta - \alpha_r}{\frac{\beta L_a}{\Delta L}} \right) \\ & - \left(\frac{V_s}{\omega} \right)^2 \frac{\beta}{\Delta L} (2\beta + \theta_{adv} - \alpha_r) - \left(\frac{V_s}{\omega} \right)^2 \frac{\beta}{\Delta L} \left(\frac{\beta L_a}{\Delta L} + \theta_{adv} + \beta - \alpha_r \right) \ln \left(\frac{\frac{\beta L_p}{\Delta L}}{\frac{\beta L_a}{\Delta L} + \beta + \theta_{adv} - \alpha_r} \right) \\ & - \left(\frac{V_s}{\omega} \right)^2 \frac{B}{\delta L} \left(\frac{\alpha_r}{2} - \beta \right) - \left(\frac{V_s}{\omega} \right)^2 \frac{B}{\delta L} \left(\frac{BL_u}{\delta L} + \theta_{adv} + \beta - \frac{\alpha_r}{2} \right) \ln \left(\frac{\frac{BL_u}{\delta L}}{\frac{BL_u}{\delta L} + \frac{\alpha_r}{2} - \beta} \right) \\ & + \left(\frac{V_s}{\omega} \right)^2 \frac{B}{\delta L} \left(\frac{\alpha_r}{2} - \beta \right) - \left(\frac{V_s}{\omega} \right)^2 \frac{B}{\delta L} \left(\frac{BL_u}{\delta L} + \frac{\alpha_r}{2} - \beta - \theta_{adv} \right) \ln \left(\frac{\frac{BL_u}{\delta L} + \frac{\alpha_r}{2} - \beta}{\frac{BL_u}{\delta L}} \right) \\ & + \left(\frac{V_s}{\omega} \right)^2 \frac{\beta}{\Delta L} (\theta_{dwell} - \theta_{adv}) - \left(\frac{V_s}{\omega} \right)^2 \frac{\beta}{\Delta L} \left(\frac{\beta L_a}{\Delta L} - \theta_{adv} - \beta \right) \ln \left(\frac{\frac{\beta L_p}{\Delta L} + \theta_{dwell} - \theta_{adv}}{\frac{\beta L_p}{\Delta L}} \right) \\ & + \left(\frac{V_s}{\omega} \right)^2 \frac{\beta}{\Delta L} (\theta_{adv} + \beta - \theta_{dwell}) - \left(\frac{V_s}{\omega} \right)^2 \frac{\beta}{\Delta L} \left(\frac{\beta L_a}{\Delta L} + 2\theta_{dwell} - \theta_{adv} - \beta \right) \ln \left(\frac{\frac{\beta L_a}{\Delta L}}{\frac{\beta L_p}{\Delta L} + \theta_{dwell} - \theta_{adv}} \right) \end{aligned} \right\}$$

(7.103)

This expression can be simplified to the following form,

$$P_{m_CPSR} = (V_s)^2 \frac{1}{\omega} \frac{q}{\alpha_r}$$

$$\left\{ \begin{aligned} & \frac{\beta}{\Delta L} \left(\frac{\beta L_a}{\Delta L} + \theta_{adv} + \beta - \alpha_r \right) \ln \left(\frac{L_a}{L_p} \right) + 2 \frac{B}{\delta L} \left(\frac{\alpha_r}{2} - \beta - \theta_{adv} \right) \ln \left(\frac{\frac{BL_u}{\delta L}}{\frac{BL_u}{\delta L} + \frac{\alpha_r}{2} - \beta} \right) \\ & - \frac{\beta}{\Delta L} \left(\frac{\beta L_a}{\Delta L} - \theta_{adv} - \beta \right) \ln \left(\frac{\frac{\beta L_p}{\Delta L} + \theta_{dwell} - \theta_{adv}}{\frac{\beta L_p}{\Delta L}} \right) \\ & - \frac{\beta}{\Delta L} \left(\frac{\beta L_a}{\Delta L} + 2\theta_{dwell} - \theta_{adv} - \beta \right) \ln \left(\frac{\frac{\beta L_a}{\Delta L}}{\frac{\beta L_p}{\Delta L} + \theta_{dwell} - \theta_{adv}} \right) \end{aligned} \right\} \quad (7.104)$$

Using this equation the highest speed is given by,

$$n_{CPSR} = (V_s)^2 \frac{1}{P_{rated}} \frac{30}{\pi} \frac{q}{\alpha_r} \frac{1}{N_b}$$

$$\left\{ \begin{aligned} & \frac{\beta}{\Delta L} \left(\frac{\beta L_a}{\Delta L} + \theta_{adv} + \beta - \alpha_r \right) \ln \left(\frac{L_a}{L_p} \right) + 2 \frac{B}{\delta L} \left(\frac{\alpha_r}{2} - \beta - \theta_{adv} \right) \ln \left(\frac{\frac{BL_u}{\delta L}}{\frac{BL_u}{\delta L} + \frac{\alpha_r}{2} - \beta} \right) \\ & - \frac{\beta}{\Delta L} \left(\frac{\beta L_a}{\Delta L} - \theta_{adv} - \beta \right) \ln \left(\frac{\frac{\beta L_p}{\Delta L} + \theta_{dwell} - \theta_{adv}}{\frac{\beta L_p}{\Delta L}} \right) \\ & - \frac{\beta}{\Delta L} \left(\frac{\beta L_a}{\Delta L} + 2\theta_{dwell} - \theta_{adv} - \beta \right) \ln \left(\frac{\frac{\beta L_a}{\Delta L}}{\frac{\beta L_p}{\Delta L} + \theta_{dwell} - \theta_{adv}} \right) \end{aligned} \right\} \quad (7.105)$$

Note that this expression assumes that there is no saturation (linear waveform) and the dwell angle is set to 30° (maximum dwell angle which avoids continuous conduction). If the base speed is assumed to be a speed at which back EMF equals applied voltage, then from expression of the back-EMF we have,

$$N_b = V_s * \frac{\beta}{\Delta L} * \frac{30}{\pi} * \frac{1}{I_{peak}} \quad (7.106)$$

Table 7-15 shows the CPSR estimation using linear model. This table also shows the CPSR using the non linear simulation model. Note that the linear model underestimates the CPSR. As described earlier, saturation can be observed at the medium speed which results in more power. Note that the dwell angle is at 30° which is not sufficient to initiate and sustain the continuous conduction. At a given speed, peak current required to develop the desired power can be calculated by using the Equation (7.99). If this current can be achieved simply by using the single pulse mode of operation, the continuous conduction can be avoided.

Table 7-15 : CPSR of the Non Flat Unaligned Inductance type SRM with Discontinuous Conduction.

Advance Angle	Dwell Angle	Maximum Relative Speed Using Linear Model	Maximum Relative Speed Using Non Linear Model
24	30	5.3872	5.9
22	30	4.8997	5.6
20	30	4.3343	5.1

8 CONCLUSION AND FUTURE WORK

8.1 Surface Permanent Magnet Synchronous Motor

Experimental results confirm that the conventional phase advancement method based high-speed controller can produce the rated power without exceeding the current limit; provided the surface PM motor has “sufficient” per phase winding inductance. This controller is based on three simple equations. In the constant torque region, required motor current can be estimated based on the torque requirement. Based on this current requirement, required voltage magnitude and phase angle can be estimated by solving a fundamental frequency model. Using this voltage magnitude, PWM modulation index can then be calculated. In this region, the supply voltage magnitude and phase angle is adjusted such that the resultant motor current is in phase with the back-EMF. This produces maximum torque-per-amp. Similarly, in the constant power region, it is possible to estimate the required motor current based on the power requirement. Based on this current requirement, required voltage phase angle can be calculated by solving a fundamental frequency model. Note that in this region, the applied voltage is a square wave and the voltage magnitude is at the rated value. In this region, the only thing that can be changed is the voltage phase angle. Hence, this method is called the phase advancement method.

The CPA method is mathematically much simpler when compared to the traditional vector control based field weakening schemes. This CPA method does not require

phase current or phase voltage measurements or any three-phase to two-phase transformations. This reduces the controller/hardware size and cost, and also increases the reliability of the controller. When using the CPA method, in the field-weakening region, the motor current decreases to a minimum value. At this speed, which is referred to as the “minimum speed”, the power factor is at unity. Also at this speed, the inverter operates in the over-modulation region. Therefore, the inverter efficiency is at its best. The magnitude of this resultant minimum current depends inversely on the maximum possible inverter output voltage. Since V_{\max} can be increased by raising the DC supply voltage, a further reduction in the motor current and inverter losses can be achieved. If the traction drive spends a significant amount of time at a certain speed, machine/control parameters can be adjusted so that this minimum speed is the same as the nominal speed of that motor. Above this minimum speed, current slowly increases to a constant value called as “characteristic current”. In theory, if this current is less than the rated current of the motor, the CPSR can be infinite when a proper control method is used. The use of fractional-slot concentrated windings increases the per phase inductance, which in turn reduces this characteristic current of the surface PM motors below the rated current.

With the constant voltage, constant power method (described in Section 2.1.1), above base speed, the stator current decreases continuously. With the constant current, constant power vector control method (described in Section 2.1.2), the stator current remains constant throughout the constant power region. In the optimum current vector control method (described in Section 2.1.3), the stator current remains constant till the

current-limit circle intersects the voltage-limit circle when the motor is above speed. After this point the stator current decreases because the d-axis component remains constant while the q-axis component decreases continuously.

During experimentation, it was possible to use a step size of 50 μ s and 9 kHz PWM switching frequency was implemented. As the PWM switching was implemented in the software itself, it is also possible to implement the PWM control in the hardware. This will further increase accuracy and reliability and will further reduce computational requirement. Since the CPA method does not work directly with the torque producing component of the phase current, it is not as accurate as the vector control method. At high speed, since the phase current approaches a constant value, partial load efficiency of surface PM motors is not as good as full load efficiency. Since the CPA method does not work directly with field weakening component of the stator current, it is difficult to comment on the possibility of rotor demagnetization. Following is a list of future work recommendations.

1. Compare the CPA method results with vector control schemes in terms of i_d - i_q components and various efficiencies, especially partial load efficiency.
2. Modify the CPA method to improve partial load efficiency.
3. Modify the CPA method to allow regenerative braking.
4. Sinusoidal PWM was implemented inside the OPAL RT software. A significant portion of computational power was used to carry out sine-triangle comparison and produce switching pattern. During experimentation, it was observed that switching becomes unstable around the modulation index of 1. Implementing

SPWM in the hardware (FPGA) will not only free up a lot of computational power, it will also increase accuracy, stability and reliability. This might also improve inverter and motor efficiency.

5. Sufficient measurements need to be carried out at different DC voltages to see the effect of a supply voltage increase on motor and inverter efficiency.
6. Study the effect of the CPA method on rotor demagnetization.

8.2 Switched Reluctance Motor

Analytical and simulation results suggest that the continuous conduction can be used to develop the rated power at high speed. Analysis of the linear magnetic model has resulted in analytical expressions relating average motor power and current to the machine and control parameters. It also resulted in analytical expressions for the residual flux linkage and peak current required to produce this desired output power. Analytical and simulation results suggest that the peak current required to develop this rated power as well as the resultant average and RMS current are well below the rated values. Analytical equations suggest that the resultant average power and current can be split into a speed dependent and independent part. The dependent part of both the average power and current approaches to zero as the speed increases.

Analytical and simulation results also suggest that it is possible to sustain the continuous conduction by using a current regulator. Analytical results (no. of strokes required to achieve steady state) suggest that by maintaining the dwell angle at more

than 50% of the stroke length, it is possible to initiate the continuous conduction. Since the fluxing region is more than the de-fluxing region, residual and peak flux-linkages grow from cycle to cycle. With the flux-linkages, phase current also grows from cycle to cycle. Once the desired peak current is reached, the current regulator imposes a zero volt-sec interval such that the resultant width of the fluxing region will be same as the de-fluxing region.

The speed independent part of the average power depends on the dwell angle, advance angle, peak current and the machine design parameters, while the speed independent part of the average current only depends on the peak current and machine design parameters. Hence, the current regulator set-point is the best way to regulate the output power rather than the advance or dwell angle. This results in the motor current being proportional to the output power.

It has been shown that the minimum dwell necessary to initiate and sustain continuous conduction, provides the maximum watts per amp control and results in minimum average current. However, it results in a slow response. The time required to achieve the steady state decreases exponentially with the increase in the dwell angle. Therefore it is possible to compromise between the speed of the response and the output efficiency.

Analytical and simulation results suggest that, for a non-flat type SRM there is a well defined combination of the advance and dwell angle which reduces the speed dependent part of both the average power and current to zero. Naturally, this

combination results into maximum efficiency as the resultant average power and current is nothing but the speed independent part. This combination (that satisfies Equation (7.97)) does not depend on the speed. Therefore, in this type of SRM motor, the dwell and the advance angle can be kept constant to this combination, and the resultant peak current required to produce the rated power will also remain constant for the entire high speed range. Simulation results also suggest that for both types of SRM motors, the resultant RMS current remains constant for a fixed dwell angle.

It has been shown that high speed continuous conduction control has the same control variables as low-speed discontinuous conduction. Based on speed information and power requirement, desired peak current can be estimated by using the Equation (7.47)/(7.99). If this peak current is less than the current estimated by Equation (7.54), the traditional discontinuous conduction type control scheme can be used to develop the desired output power. Otherwise, continuous conduction can be initiated and sustained by keeping the dwell angle constant (more than 50% of the stroke length). Based on this dwell angle, proper advance angle, which maximizes output power, can be selected by using Equation (7.48)/(7.97). By using Equation (7.53)/(7.98), it is also possible to estimate the number of strokes it will take to achieve steady state.

From analytical and simulation results, it can be seen that in continuous conduction with the current levels required to produce rated power, magnetic saturation is not a significant factor.

Following is a list of recommended future work.

1. Literature [13],[75] suggests that continuous conduction does not offer any benefits at low speed or the higher speed at which rated power can be developed using the traditional discontinuous type conduction. A smart controller, which can co-ordinate between the low and medium speed discontinuous conduction, and high speed continuous conduction needs to be developed.
2. References [76] and [16] describe a list of the machine parameters that affect the highest speed at which the rated power can be developed by using the discontinuous type single pulse operation. Similar analysis needs to be done on machine parameters that affect continuous conduction.
3. Figure 7-18 shows the effect of saturation on per phase inductance profile. Instead of using a linear inductance profile (straight lines), use of upward parabola to represent the per phase inductance profile might result in more accurate analytical expressions describing the behavior of switched reluctance motors when operated in continuous conduction.
4. Minimum dwell yields the maximum power but the slowest response. High dwell can result in faster response but low output power. If both are desired, initially the dwell angle can be kept as large as possible, and as the peak current is approached, this dwell angle can be collapsed back to the minimum possible value. This needs to be confirmed.

Bibliography

Bibliography

- [1] W. L. Soong and T. J. E. Miller, "Field Weakening Performance of Brushless Synchronous AC Motor Drives," *IEE Proceedings of the Electronic Power Application*, vol. 141, no. 6, pp. 331 - 340, November 1994.
- [2] L. H. Ward, "Volts Vs Ohms - The Speed Regulation of Electric Motors," *AIEE Transactions*, vol. 13, pp. 375 - 384, 1896.
- [3] P. L. Alger and R. E. Arndt, "The History of Induction Motors in America," *Proceedings of IEEE*, pp. 1380 - 1383, September 1976.
- [4] T. J. E. Miller, *Switched Reluctance Motors*. Oxford: Magna Physics Publishing and Clarendon Press, 1993.
- [5] P. Pillay and R. Krishnan, "Modeling, Simulation and Analysis of Permanent Magnet Motor Drives : Part I - The Permanent Magnet Synchronous Motor Drive," *IEEE Transactions on Industry Applications*, vol. 25, no. 2, pp. 265-273, March/April 1989.
- [6] P. Pillay and R. Krishnan, "Modeling, Simulation and Analysis of Permanent Magnet Motor Drives : Part II - The Brushless DC Motor Drive," *IEEE Transactions on Industry Applications*, vol. 25, no. 2, pp. 274 - 279, March / April 1989.
- [7] N. A. Patil, J. S. Lawler, and J. W. McKeever, "Determining constant power speed

- ratio of the induction motor from equivalent circuit parameters," *IEEE Southeastcon*, pp. 460 - 467 , April 2008.
- [8] T. M. Jahns, "Flux Weakening Regime Operation of an Interior Permanent Magnet Synchronous Motor Drive," *IEEE Transaction on Industry Application*, vol. 23, pp. 681 - 689, July / August 1987.
- [9] S. Morimoto, Y. Takeda, T. Hirasaka, and K. Taniguchi, "Expansion of Operating Limits for Permanent Magnet Motor by Current Vector Control Considering Inverter Capacity," *IEEE Transactions on Industrial Application*, vol. 26, pp. 866 - 871, 1990.
- [10] Cambier, "Brushless DC Motor Using Phase Timing Advancement.," 5,677,605, October 14, 1997.
- [11] S. R. MacMinn and J. W. Sember, "Control of a Switched-Reluctance Aircraft Engine Starter-Generator Over a Very Wide Speed Range," *Proceedings of Energy Conversion Engineering Conference, IECEC-89*, pp. 631 - 638, August 1989.
- [12] S. R. MacMinn and W. D. Jones, "A Very High Speed Switched-Reluctance Starter-Generator for Aircraft Engine Application," *Proceedings of IEEE National Aerospace and Electronics Conference, NAECON*, vol. 4, pp. 1758 - 1764, May 1989.
- [13] J. S. Lawler, J. M. Baily, J. W. McKeever, and P. J. Otaduy, "Impact of Continuous Conduction on the Constant Power Speed Range of the Switched Reluctance

- Motor," *IEEE International Conference on Electrical Machines and Drives*, pp. 1285 - 1292, May 2005.
- [14] R. Krishnan, *Switched Reluctance Motor Drives : Modeling, Simulation, Analysis, Design, and Applications*.: CRC Press, 2001.
- [15] T. J. E. Miller, *Switched Reluctance Motors and their Control*.: Magna Physics Publications , Oxford University Press, 1993.
- [16] M. Rekik et al., "High-Speed-Range Enhancement of Switched Reluctance Motor with Continuous Mode for Automotive Applications," *European Transactions on Electrical Power*, 2007.
- [17] T. Sebastian and G. R. Slemon, "Operating Limits of Inverter-Driven Permanent Magnet Motor Drives," *IEEE Transaction on Industry Application*, vol. IA-23, no. No. 2, pp. 327 - 333, March/April 1987.
- [18] E. Clarke, *Circuit Analysis of A-C Power Systems Vol. 1 - Symmetrical and Related Components*. New York, U.S.: John Willey and Sons, 1943.
- [19] B. K. Bose, *Power Electronics and AC Drives*. New Jersey, U.S.: Prentice - Hall, 1986.
- [20] P. C. Kraus, *Analysis of Electrical Machinery*.: McGraw - Hill, Inc., 1986.
- [21] R. H. Park, "Two - Reaction Theory of Synchronous Machines - Generalized

- Method of Analysis - Part - I," *AIEE Transaction* , vol. 48, pp. 716 - 727, July 1929.
- [22] P. Vas, *Sensorless Vector and Direct Torque Control*.: Oxford University Press, 1999.
- [23] J. S. Lai, J. M. Baily, R. W. Young, C. W. Johns, and R. A. Hawsey, "Optimum Current for a High-Speed Axial Air Gap Permanent Magnet Synchronous Motor," *IEEE - IAS Annual Meeting*, vol. Conference Records, pp. 767 - 772, 1989.
- [24] J. M. Baily, J. S. Lawler, and H. W. Blake, "Field-Weakening Schemes and Magnet-Retention Techniques for Permanent Magnet Machines," Oak Ridge National Lab., Unpublished ORNL-TM 74, 1999.
- [25] D. W. Novotny and T. A. Lipo, *Vector Control and Dynamics of AC Drives*. New York, U.S.: Oxford University Press, Inc., 1996.
- [26] F. Magnussen, P. Thelin, and C. Sadarangani, "Performance Evaluation of Permanent Magnet Synchronous Machines with Concentrated and Distributed Windings Including Effect of Field Weakening," *Proceedings of 2nd IEE International Conference on Power Electronics, Machines and, Drives*, vol. 2, pp. 679 - 685, March / April 2004.
- [27] A. M. El-Refaie, T. M. Jahns, P. J. McCleer, and J. W. McKeever, "Experimental Verification of Optimal Flux Weakening in Surface PM Machines Using Concentrated Windings," *IEEE Transaction on Industry Application* , vol. 42, no. 2,

pp. 443 - 453, March / April 2006.

- [28] S. Morimoto, Y. Takeda, and T. Hirasu, "Current Phase Control Methods for Permanent Magnet Synchronous Motors," *IEEE Transactions on Power Electronics* , vol. 5, no. 2, pp. 133 - 139, April 1990.
- [29] S. Morimoto, T. Ueno, M. Sanada, and A. Yamagiwa, "Effects and Compensation of Magnetic Saturation in Permanent Magnet Synchronous Motor Drives," *IEEE Transactions on Industry Application*, vol. 30, no. 6, pp. 59 - 64, November / December 1994.
- [30] A. Kumamoto and Y. Hirane, "A Semi-Closed Loop Torque Control of a Buried Permanent Magnet Motor Based on a New Flux-Weakening Approach," *IEEE - IAS Annual Meeting* , vol. Conference Recordings, pp. 656 - 661, 1989.
- [31] A. M. EL-Refaie, D. W. Novotny, and T. M. Jahns, "A Simple Model for Flux Weakening in Surface PM Synchronous Machines Using Back-to-Back Thyristors," *IEEE Power Electronics Letters*, vol. 2, no. 2, pp. 54-57, June 2004.
- [32] R. Monajemy and R. Krishnan, "Performance Comparison for Six-Step Voltage and Constant Back EMF Control Strategies for PMSM," *IEEE Industry Applications Conference* , vol. 1, pp. 165 - 172, 1999.
- [33] G. R. Slemon, "Achieving a Constant Power Speed Range for PM Drives," *IEEE Transactions on Industry Application*, vol. 31, no. 2, pp. 368 - 372, March / April

1995.

- [34] G. R. Slemon and X. Liu, "Modeling and Design Optimization of Permanent Magnet Machines," *Electrical Machines and Power System*, vol. 20, pp. 71 - 92, 1992.
- [35] P. L. Chapman and P. T. Krein, "Motor Re-Rating for Traction Application - Field Weakening Revisited," *Electrical Machines and Drives Conference, IEMDC*, vol. 3, pp. 1388 - 1391, June 2003.
- [36] E. Nipp, "Alternative to Field - Weakening of Surface - Mounted Permanent - Magnet Motors for Variable - Speed Drives," *IEEE Industry Applications Conference*, vol. 1, pp. 191 - 198, October 1995.
- [37] J. S. Lawler, "Control of Surface Mounted Permanent Magnet Motors with Special Application to Fractional - Slot Motors with Concentrated Windings," Oak Ridge National Laboratory, Oak Ridge, Internal ORNL/TM-2005 / 184, 2005.
- [38] T. D. Gillespie, *Fundamentals of vehicle dynamics.*, 1992.
- [39] A. M. EL-Refaie, T. M. Jahns, P. B. Reddy, and J. W. McKeever, "Modified Vector Control Algorithm for Increasing Partial-Load Efficiency of Fractional-Slot Concentrated-Winding Surface PM Machines," *IEEE Transactions on Industry Applications*, vol. 44, no. 5, pp. 1543 - 1551, September / October 2008.
- [40] P. B. Reddy and T. M. Jahns, "Impact of Winding Layer Number and Slot/Pole Combination on AC Armature Losses of Synchronous Surface PM Machines

Designed for Wide Constant-Power Speed Range Operation," *Industry Applications Society Annual Meeting*, pp. 1 - 8, October 2008.

- [41] A. M. EL-Refaie, T. M. Jahns, P. B. Reddy, and J. W. McKeever, "Modified Vector control Algorithm for Increasing Partial-Load Efficiency of Fractional-Slot Concentrated-Winding Surface PM Machines," *IEEE Transaction on Industry Applications*, vol. 44, no. 5, pp. 1543 - 1551, September / October 2008.
- [42] M. Chuntung, G. R. Slemon, and R. Bonnert, "Modeling of Iron Losses in Surface-Mounted Permanent Machine Synchronous Motors," *Industry Applications Conference*, vol. 4, pp. 2585 - 2591, 2001.
- [43] K. Atallah, D. Howe, P. H. Mellor, and D. A. Stone, "Rotor Loss in Permanent Magnet Brushless AC Machines," *International Conference on Electrical Machines and Drives*, pp. 60 - 62, May 1999.
- [44] P. H. Mellor, R. Wrobel, and N. McNeill, "Investigation of Proximity Losses for High Speed Brushless Permanent Magnet Motor," *Industry Application Conference*, vol. 3, pp. 1514 - 1518.
- [45] J. S. Lawler, J. M. Baily, and J. W. McKeever, "Minimum Current Magnitude Control of Surface PM Synchronous Machines during Constant Power Operation," *IEEE Power Electronics Letters*, vol. 3, no. 2, pp. 53 - 56, 2005.
- [46] D. A. Staton, W. L. Soong, C. Cossar, and T. E. Miller, "Unified Theory of Torque

- Production in Switched Reluctance and Synchronous Reluctance Motors," *International Conference on Electrical Machines and Drives*, pp. 67 - 72, September 1993.
- [47] C. Elmas and H. Zelaya De La Parra, "A DSP Controlled Switched Reluctance Drive System for Wide Range of Operating Speeds," *Power Electronics Specialists Conference, PESC*, vol. 2, pp. 844 -850, June - July 1992.
- [48] S. R. MacMinn and W. D. Jones, "A Very High Speed Switched-Reluctance Starter-Generator for Aircraft Engine Application," *Proceedings of IEEE National Aerospace and Electronics Conference, NAECON*, vol. 4, pp. 1758 - 1764, May 1989.
- [49] C. E. Green, "Control of Switched Reluctance Machines," B1 6,351,094, February 26, 2002.
- [50] R. C. Becerra, M. Ehsani, and T. E. Miller, "Commutation of SR Motors," *IEEE Transactions of Power Electronics*, vol. 8, no. 3, pp. 257 - 263, July 1993.
- [51] R. Krishnan, *Switched Reluctance Motor Drives : Modeling, Simulation, Analysis, Design and Applications.*: CRC Press LLC, 2001.
- [52] T. T. e. a. Borges, "Switched Reluctance Motor Drive at High Speeds, with Control of Current," *IEEE International Electrical Machines and Drives Conference Records*, pp. TB1/12.1 - TB1/12.3, May 1997.

- [53] B. C. Mecrow, "Control of a Switched Reluctance Drive," 7205694, April 17, 2007.
- [54] I. Jordison et al., "Control of a switched reluctance drive," 6972533, July 18, 2003.
- [55] M. P. Tankard, "Control Strategy for a switched Reluctance Drive Systems," 6759826, July 6, 2004.
- [56] C. E. B. Green, "Control of Switched Reluctance Machines," 6291949, September 18, 2001.
- [57] C. R. Elliott, "Hysteresis Current Controller for a Reluctance Machine," 5998945, December 7, 1999.
- [58] C. R. Elliott, "on-off controller," 5926011, July 20, 1999.
- [59] J. J. Gribble, P. C. Kjaer, and T. J. E. Miller, "Optimal Commutation in Average Torque Control of Switched Reluctance Motors," *IEE Proceedings of Electric Power Applications*, vol. 146, no. 1, pp. 2 - 10, January 1999.
- [60] I. Husain, *Electric and Hybrid Electric Vehicles Design Fundamentals*.: CRC Press.
- [61] R. B. Inderka, M. Menne, and R. W. A. A. De Doncker, "Control of Switched Reluctance Drives for Electrical Vehicle Applications," *IEEE Transactions on Industrial Electronics*, vol. 49, no. 1, pp. 48 - 53, February 2002.
- [62] P. C. Kjaer, C. Cossar, and T. J. E. Miller, "Very High Bandwidth Digital Current Controller for High-Performance Motor Drives," *Proceedings of Power Electronics*

and Variable-Speed Drives Conference, pp. 185 - 190, September 1996.

- [63] B. G. Hexamer, "Implementing of Closed-Loop Controllers for Switched Reluctance Drives on Microcontrollers and DSP Controllers," *Proceedings of EPE*, 1999.
- [64] H. Bausch, A. Grief, B. Lange, and R. Bautz, "A 50 kW / 1500 RPM Switched Reluctance Drive for an Electrical Vehicle : Current Control and Performance Characteristics," *Proceedings of International Conference on Electrical Machines*, pp. 603 - 607, August 2000.
- [65] B. K. Bose, T. J. E. Miller, P. M. Szczesny, and W. H. Bicknell, "Microcomputer Control of Switched Reluctance Motor," *IEEE Transactions on Industry Applications*, vol. IA - 22, no. 4, pp. 708 - 715, July - August 1986.
- [66] W. F. Ray, R. M. Davis, and R. J. Blake, "The Control of SR Motors," *Proceedings of the Conference on Applied Motion Control*, pp. 137 - 145, June 1986.
- [67] B. Fahimi, Y. Gao, and M. Ehsani, "On Suitability of Switched Reluctance Motor Drives for 42 Volts Super High Speed Operation: Application to Automotive Fuel Cells ," *The 27th Annual Conference of the IEEE Industrial Electronics Society*, pp. 1947 - 1951, 2001.
- [68] K. M. Rahman, B. Fahimi, G. Suresh, and M. Ehsani, "Advantages of Switched Reluctance Motor Application to EV and HEV: Design and Control Issues," *IEEE Transactions on Industry Applications*, vol. 36, no. 1, pp. 111 - 121, January /

February 2000.

- [69] I. kioskeridis and C. Mademlis, "Maximum Efficiency in Single-Pulse Controlled Switched Reluctance Motor Drives," *IEEE Transactions on Energy COntversion*, vol. 20, no. 4, pp. 809 - 817, December 2005.
- [70] J. Kim and R. Krishnan, "High Efficiency Single-Pulse Controlled Switched Reluctance Motor Drive for High Speed (48K rpm) Application: Analysis, Design, and Experimental Verification," *Industry Applications Society Annual Meeting, IAS*, pp. 1 - 8, Oct. 2008.
- [71] H. Yahia, R. Dhifaoui, and B. Multon, "Maximum Power Limits in the Field-Weakening Mode of Doubly-Salient Variable Reluctance Machines," *26th Annual Conference of the IEEE, Industrial Electronics Society, IECON*, vol. 2, pp. 783 - 788, 2000.
- [72] L. Morel, H. Fayard, R. V. Fos, A. Galindo, and G. Abba, "Study of Ultra High Speed Switched Reluctance Motor Drive," *Proceedings of Industry Applications Conference*, vol. 1, pp. 87 - 92, 2000.
- [73] V. P. Vujicic, S. N. Vukosavic, and M. B. Jovanovic, "Asymmetrical Switched Reluctance Motor for a Wide Constant Power Range," *IEEE Transactions of Energy Conversion*, vol. 21, no. 1, pp. 44 - 51, March 2006.
- [74] M. Korkosz and D. Mazur, "Operation of the Switched Reluctance Motor at

- Continuous Conduction of Phase Current," *IEEE MELECON*, pp. 1166 - 1169, May 2006.
- [75] M. Rekik et al., "Improvement in th Field-Weakening Performance of Switched Reluctance Machine with Continuous Conduction," *IET Electr. Power Appl.*, vol. 1, no. 5, pp. 785 - 792, September 2007.
- [76] S. A. Long, N. Schofield, D. Howe, M. Piron, and M. McClelland, "Design of a Switched Reluctance Machine for Extended Speed Operation," *IEEE Conference on Electrical Machines and drives*, vol. 1, pp. 235 - 240, June 2003.
- [77] P. S. Shin, P. J. Otaduy, J. W. McKeever, and D. J. Adams, "Interactive Design and Analysis Program for Switched Reluctance Motor Using an Analytical Method," *10th Biennial IEEE Conference on Electromagnetic Field Computation*, June 2002.
- [78] N. A. Patil and J. S. Lawler, "Issues in the control of the Switched Reluctance Motor During Continuous Conduction," *39th North American Power Symposium*, pp. 534-540, Sept. 2007.
- [79] T. M. Jahns, G. B. Kliman, and T. W. Neumann, "Interior Permanent Magnet Synchronous Motor for Adjustable Speed Drives," *IEEE Transactions on Industry Application*, vol. IA-22, pp. 738 - 747, July / August 1986.
- [80] R. S. Colby and D. W. Novotny, "Efficient Operation of PM Synchronous Motors," *IEEE Transactions on Industry Application*, vol. IA - 23, pp. 1048 - 1054, November

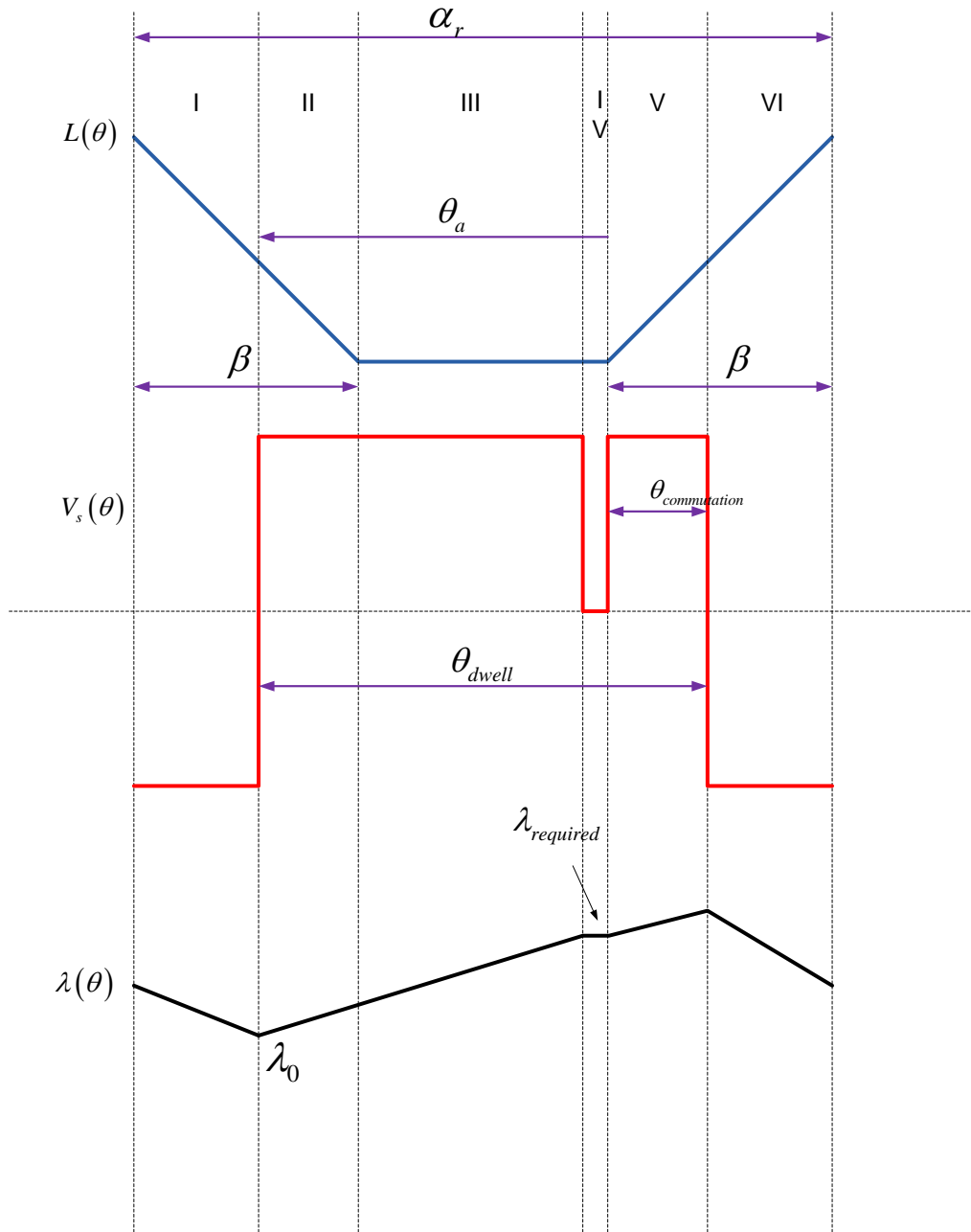
/ December 1987.

- [81] T. M. Jahns, "Motion Control with Permanent Magnet AC Machines," *Proceedings of IEEE*, vol. 82, no. 8, pp. 1241 - 1252, August 1994.
- [82] e. a. Morimoto, "Design and Control System of Inverter-Driven Permanent Magnet Synchronous Motors for High Torque Operation," *IEEE Transaction on Industry Application*, vol. 29, no. 6, pp. 1150 - 1154, Nov. / Dec. 1993.
- [83] R. Dhaouadi and N. Mohan, "Analysis of Current-Regulated Voltage-Source Inverters for Permanent Magnet Synchronous Motor Drives in Normal and Extended Speed Ranges," *IEEE Transaction on Energy Conversion*, vol. 5, no. 1, pp. 137 - 144, March 1990.
- [84] R. Krishnan and P. Pillay, "Control Characteristics and Speed Controller Design for a High Performance Permanent Magnet Synchronous Motor Drive," *IEEE Transaction on Power Electronics*, vol. 5, no. 2, pp. 151 - 159, April 1990.
- [85] R. W. DeDoncker and D. W. Novotny, "The Universal Field Oriented Controller," *Conference Recordings of IEEE - IAS*, pp. 450 - 456, October 1988.
- [86] J. S. Lawler, J. M. Baily, and J. W. McKeever, "Extended Constant Power Speed Range of the Brushless DC Motor through Dual Mode Inverter Control," Oak Ridge National Laboratory, Internal ORNL/TM-2005/184, 2005.

Appendix

Appendix : Flat Unaligned Inductance

Simulation result shows that peak of the SRM current occurs just before the on-set of alignment.



During transient state : Flux linkage starts with zero value. Since fluxing-region is greater than de-fluxing region, it does not return back to the same initial value. At what λ_0 or λ_{peak} , system achieves steady state ? One way to find this is based on peak current requirement. Let I_{peak} be the peak current required. We have,

$$\lambda_{required} = I_{peak} * L$$

Simulation results show that the peak current occurs just before the on-set of alignment. Therefore $L = L_u$. Therefore, $\lambda_{required} = I_{peak} * L_u$.

For $I_{peak} = 600A$ and $L_u = 4.15mH$, we need $\lambda_{required} = 600 * 4.15 * 10^{-3} = 2.49Wb$.

Assume, advance angle, θ_a is given.

$$\text{Notch length will be : } 2 * \left(\theta_{dwell} - \frac{\alpha_r}{2} \right) = 2 * \theta_{dwell} - \alpha_r$$

Fluxing region duration will be : $\theta_a - (2 * \theta_{dwell} - \alpha_r)$

We have,

$$\begin{aligned} y = mx + c &\Rightarrow \lambda_{required} = \frac{V_s}{\omega} * [\theta_a - (2 * \theta_{dwell} - \alpha_r)] + \lambda_0, \\ \lambda_{required} &= \frac{V_s}{\omega} * [\theta_a - (2 * \theta_{dwell} - \alpha_r)] + \lambda_0, \\ L_u * I_{peak} &= \frac{V_s}{\omega} * [\theta_a - (2 * \theta_{dwell} - \alpha_r)] + \lambda_0, \\ \lambda_0 &= L_u * I_{peak} - \frac{V_s}{\omega} * (\theta_a + \alpha_r - 2 * \theta_{dwell}) \end{aligned} \tag{1.1}$$

Above is the initial value of flux-linkage at which required current can be achieved and to return back to the same initial value, a “notch” will be required.

$$\lambda_0 = L_u * I_{peak} - \frac{V_s}{\omega} * (\theta_a + \alpha_r - 2 * \theta_{dwell}),$$

$$\lambda_0 = (4.15 * 10^{-3}) - \left(\frac{700}{2 * \pi * 6 * 250 / 60} \right) * \left[(22.5 + 60 - 62) * \left(\frac{\pi}{180} \right) \right],$$

$$\lambda_0 = 0.89$$

Simulation result confirms the same.

Inductance in region I and II is given by:

$$y = mx + c$$

$$L(\theta) = \frac{-\Delta L}{\beta} * \theta + k$$

When $\theta = 0$, $L(\theta) = L_a$

$$\therefore L(\theta) = \frac{-\Delta L}{\beta} * \theta + L_a,$$

i.e.

(1.2)

$$L(\theta) = L_a - \frac{\Delta L}{\beta} * \theta,$$

Region I Analysis ($0 \leq \theta \leq (\alpha_r - \beta - \theta_a)$)

Flux Linkage in region I is given by:

$$y = mx + c$$

$$\lambda(\theta) = \frac{-V_s}{\omega} * \theta + k$$

When $\theta = (\alpha_r - \beta - \theta_a)$, $\lambda(\theta) = \lambda_0$ The value of λ_0 is given in Equation (1.1).

Therefore,

$$\begin{aligned}\lambda_0 &= \frac{-V_s}{\omega} * (\alpha_r - \beta - \theta_a) + k \\ \therefore k &= \lambda_0 + \frac{V_s}{\omega} * (\alpha_r - \beta - \theta_a), \\ \therefore k &= L_u * I_{peak} - \frac{V_s}{\omega} * (\theta_a + \alpha_r - 2 * \theta_{dwell}) + \frac{V_s}{\omega} * (\alpha_r - \beta - \theta_a), \\ k &= L_u * I_{peak} + \left[\frac{V_s}{\omega} * (2 * \theta_{dwell} - 2\theta_a - \beta) \right] \\ \therefore \lambda(\theta) &= \frac{-V_s}{\omega} * \theta + L_u * I_{peak} + \left[\frac{V_s}{\omega} * (2 * \theta_{commutation} - \beta) \right], \\ \therefore \lambda(\theta) &= L_u * I_{peak} - \left[\frac{V_s}{\omega} * (\theta + \beta - 2 * \theta_{commutation}) \right]\end{aligned}\tag{1.3}$$

$$\therefore d\lambda(\theta) = \frac{-V_s}{\omega} * d\theta\tag{1.4}$$

Current in region I is given by,

$$\begin{aligned}I(\theta) &= \frac{\lambda(\theta)}{L(\theta)} \\ I(\theta) &= \frac{L_u * I_{peak} - \left[\frac{V_s}{\omega} * (\theta + \beta - 2 * \theta_{commutation}) \right]}{L_a - \frac{\Delta L}{\beta} * \theta}\end{aligned}\tag{1.5}$$

Power produced in region I is given by,

$$P(\theta) = \int_{\theta=0}^{\theta=(\alpha_r-\beta-\theta_a)} \lambda(\theta) * di(\theta) = \int_{\theta=0}^{\theta=(\alpha_r-\beta-\theta_a)} i(\theta) * d\lambda(\theta)$$

$$\therefore P_1 = \int_{\theta=0}^{\theta=(\alpha_r-\beta-\theta_a)} i(\theta) * d\lambda(\theta)$$

$$\therefore P_1 = \int_{\theta=0}^{\theta=(\alpha_r-\beta-\theta_a)} \frac{L_u * I_{peak} - \left[\frac{V_s}{\omega} * (\theta + \beta - 2 * \theta_{commutation}) \right] * \frac{-V_s}{\omega} * d\theta}{L_a - \frac{\Delta L}{\beta} * \theta}$$

$$\therefore P_1 = \frac{-V_s}{\omega} * \int_{\theta=0}^{\theta=(\alpha_r-\beta-\theta_a)} \frac{L_u * I_{peak} - \left[\frac{V_s}{\omega} * (\theta + \beta - 2 * \theta_{commutation}) \right] * d\theta}{L_a - \frac{\Delta L}{\beta} * \theta}$$

$$\therefore P_1 = \frac{-V_s}{\omega} * \int_{\theta=0}^{\theta=(\alpha_r-\beta-\theta_a)} \frac{L_u * I_{peak} - \left[\frac{V_s}{\omega} * (\theta + \beta - 2 * \theta_{commutation}) \right] * d\theta}{L_a - \frac{\Delta L}{\beta} * \theta}$$

$$\therefore P_1 = \frac{-V_s L_u I_{peak}}{\omega} \frac{\beta}{\Delta L} * \int_{\theta=0}^{\theta=(\alpha_r-\beta-\theta_a)} \frac{1}{\frac{\beta}{\Delta L} L_a - \theta} d\theta + \left(\frac{V_s}{\omega} \right)^2 \frac{\beta}{\Delta L} \int_{\theta=0}^{\theta=(\alpha_r-\beta-\theta_a)} \frac{\theta + (\beta - 2 * \theta_{commutation})}{\frac{\beta}{\Delta L} L_a - \theta} d\theta$$

$$\therefore P_1 = \frac{V_s L_u I_{peak}}{\omega} \frac{\beta}{\Delta L} \left[\ln \left(\frac{\beta}{\Delta L} L_a - \theta \right) \right]_{\theta=0}^{\theta=(\alpha_r-\beta-\theta_a)}$$

$$+ \left(\frac{V_s}{\omega} \right)^2 \frac{\beta}{\Delta L} \left[-\theta - \left((\beta - 2 * \theta_{commutation}) + \frac{\beta}{\Delta L} L_a \right) \ln \left(\theta - \frac{\beta}{\Delta L} L_a \right) \right]_{\theta=0}^{\theta=(\alpha_r-\beta-\theta_a)}$$

$$\begin{aligned} \therefore P_1 = & \frac{V_s L_u I_{peak}}{\omega} \frac{\beta}{\Delta L} \ln \left(\frac{\frac{\beta}{\Delta L} L_a - (\alpha_r - \beta - \theta_a)}{\frac{\beta}{\Delta L} L_a} \right) - \left(\frac{V_s}{\omega} \right)^2 \frac{\beta}{\Delta L} (\alpha_r - \beta - \theta_a) \\ & - \left(\frac{V_s}{\omega} \right)^2 \frac{\beta}{\Delta L} \left((\beta - 2 * \theta_{commutation}) + \frac{\beta}{\Delta L} L_a \right) \ln \left(\frac{\frac{\beta}{\Delta L} L_a - (\alpha_r - \beta - \theta_a)}{\frac{\beta}{\Delta L} L_a} \right) \end{aligned} \quad (1.6)$$

Flux-linkage in region II and III can be calculated as follows:

$$y = mx + c$$

$$\lambda(\theta) = \frac{V_s}{\omega} * \theta + k$$

When $\theta = (\alpha_r - \beta - \theta_a)$, $\lambda(\theta) = \lambda_0$. The value of λ_0 is given in Equation (1.1).

$$\begin{aligned} \therefore L_u * I_{peak} - \frac{V_s}{\omega} * (\theta_a + \alpha_r - 2 * \theta_{dwell}) &= \frac{V_s}{\omega} * (\alpha_r - \beta - \theta_a) + k, \\ \therefore k &= L_u * I_{peak} - \frac{V_s}{\omega} * (\theta_a + \alpha_r - 2 * \theta_{dwell}) - \frac{V_s}{\omega} * (\alpha_r - \beta - \theta_a), \\ \therefore k &= L_u * I_{peak} - \frac{V_s}{\omega} * (2 * \alpha_r - 2 * \theta_{dwell} - \beta) \end{aligned} \quad (1.7)$$

$$\begin{aligned} \therefore \lambda(\theta) &= \frac{V_s}{\omega} * \theta + L_u * I_{peak} - \frac{V_s}{\omega} * (2 * \alpha_r - 2 * \theta_{dwell} - \beta), \\ \therefore \lambda(\theta) &= L_u * I_{peak} - \frac{V_s}{\omega} * (2 * \alpha_r - 2 * \theta_{dwell} - \beta - \theta) \end{aligned}$$

At the beginning of the notch, flux-linkage should be equal to $\lambda_{required}$. This can be verified as follow,

When $\theta = (\alpha_r - \beta - (2 * \theta_{dwell} - \alpha_r))$,

$$\lambda(\theta) = L_u * I_{peak} + \frac{V_s}{\omega} * (2 * \theta_{dwell} - 2 * \alpha_r + \beta + \alpha_r - \beta - 2 * \theta_{dwell} + \alpha_r),$$

$$\therefore \lambda(\theta) = L_u * I_{peak} = \lambda_{required}$$

Region II Analysis ($(\alpha_r - \beta - \theta_a) \leq \theta \leq \beta$)

Current in region II is given by,

$$I(\theta) = \frac{\lambda(\theta)}{L(\theta)}$$

$$I(\theta) = \frac{L_u * I_{peak} - \frac{V_s}{\omega} * (2 * \alpha_r - 2 * \theta_{dwell} - \beta - \theta)}{L_a - \frac{\Delta L}{\beta} * \theta} \quad (1.8)$$

Power produced in region II is given by,

$$P_2 = \int_{\theta=(\alpha_r - \beta - \theta_a)}^{\theta=\beta} i(\theta) * d\lambda(\theta)$$

$$P_2 = \int_{\theta=(\alpha_r - \beta - \theta_a)}^{\theta=\beta} \frac{L_u * I_{peak} - \frac{V_s}{\omega} * (2 * \alpha_r - 2 * \theta_{dwell} - \beta - \theta)}{L_a - \frac{\Delta L}{\beta} * \theta} * \frac{V_s}{\omega} * d\theta$$

$$P_2 = \frac{V_s}{\omega} * \int_{\theta=(\alpha_r - \beta - \theta_a)}^{\theta=\beta} \frac{L_u * I_{peak} - \frac{V_s}{\omega} * (2 * \alpha_r - 2 * \theta_{dwell} - \beta - \theta)}{L_a - \frac{\Delta L}{\beta} * \theta} * d\theta$$

$$\begin{aligned}
\therefore P_2 &= \frac{V_s L_u * I_{peak}}{\omega} * \int_{\theta=(\alpha_r - \beta - \theta_a)}^{\theta=\beta} \frac{1}{L_a - \frac{\Delta L}{\beta} * \theta} d\theta - \left(\frac{V_s}{\omega}\right)^2 * \int_{\theta=(\alpha_r - \beta - \theta_a)}^{\theta=\beta} \frac{2 * \alpha_r - 2 * \theta_{dwell} - \beta - \theta}{L_a - \frac{\Delta L}{\beta} * \theta} d\theta \\
\therefore P_2 &= \frac{V_s L_u I_{peak}}{\omega} \frac{\beta}{\Delta L} \int_{\theta=(\alpha_r - \beta - \theta_a)}^{\theta=\beta} \frac{1}{\frac{\beta}{\Delta L} L_a - \theta} d\theta - \left(\frac{V_s}{\omega}\right)^2 \frac{\beta}{\Delta L} * \int_{\theta=(\alpha_r - \beta - \theta_a)}^{\theta=\beta} \frac{(2 * \alpha_r - 2 * \theta_{dwell} - \beta) - \theta}{\frac{\beta}{\Delta L} L_a - \theta} d\theta \\
\therefore P_2 &= \frac{-V_s L_u I_{peak}}{\omega} \frac{\beta}{\Delta L} \left[\ln \left(\frac{\beta}{\Delta L} L_a - \theta \right) \right]_{(\alpha_r - \beta - \theta_a)}^{\beta} - \left(\frac{V_s}{\omega}\right)^2 \frac{\beta}{\Delta L} [\theta]_{(\alpha_r - \beta - \theta_a)}^{\beta} \\
&\quad - \left(\frac{V_s}{\omega}\right)^2 \frac{\beta}{\Delta L} \left(\frac{\beta}{\Delta L} L_a - (2 * \alpha_r - 2 * \theta_{dwell} - \beta) \right) \left[\ln \left(\theta - \frac{\beta}{\Delta L} L_a \right) \right]_{(\alpha_r - \beta - \theta_a)}^{\beta} \\
\therefore P_2 &= \frac{-V_s L_u I_{peak}}{\omega} \frac{\beta}{\Delta L} \ln \left(\frac{\frac{\beta}{\Delta L} L_a - \beta}{\frac{\beta}{\Delta L} L_a - (\alpha_r - \beta - \theta_a)} \right) - \left(\frac{V_s}{\omega}\right)^2 \frac{\beta}{\Delta L} [\theta_a - (\alpha_r - 2\beta)] \\
&\quad - \left(\frac{V_s}{\omega}\right)^2 \frac{\beta}{\Delta L} \left(\frac{\beta}{\Delta L} L_a - (2 * \alpha_r - 2 * \theta_{dwell} - \beta) \right) \ln \left(\frac{\beta - \frac{\beta}{\Delta L} L_a}{(\alpha_r - \beta - \theta_a) - \frac{\beta}{\Delta L} L_a} \right) \quad (1.9)
\end{aligned}$$

Inductance in region III and IV is constant and is given by,

$$L(\theta) = L_u \quad (1.10)$$

$$\text{Region III Analysis (} \begin{aligned} &\beta \leq \theta \leq [\alpha_r - \beta - (2 * \theta_{dwell} - \alpha_r)] \\ &\beta \leq \theta \leq (2 * \alpha_r - 2 * \theta_{dwell} - \beta) \end{aligned})$$

Current in region III is given by,

$$I(\theta) = \frac{\lambda(\theta)}{L(\theta)}$$

$$I(\theta) = \frac{L_u * I_{peak} - \frac{V_s}{\omega} * (2 * \alpha_r - 2 * \theta_{dwell} - \beta - \theta)}{L_u} \quad (1.11)$$

Power produced in the region III is given by,

$$P_3 = \int_{\theta=\beta}^{\theta=(2*\alpha_r-2*\theta_{dwell}-\beta)} \frac{L_u * I_{peak} - \frac{V_s}{\omega} * (2 * \alpha_r - 2 * \theta_{dwell} - \beta - \theta)}{L_u} * \frac{V_s}{\omega} * d\theta,$$

$$P_3 = \frac{V_s}{\omega} * \int_{\theta=\beta}^{\theta=(2*\alpha_r-2*\theta_{dwell}-\beta)} \frac{L_u * I_{peak} - \frac{V_s}{\omega} * (2 * \alpha_r - 2 * \theta_{dwell} - \beta - \theta)}{L_u} * d\theta$$

$$P_3 = \frac{V_s I_{peak}}{\omega} \int_{\theta=\beta}^{\theta=(2*\alpha_r-2*\theta_{dwell}-\beta)} d\theta$$

$$- \left(\frac{V_s}{\omega} \right)^2 \frac{1}{L_u} (2 * \alpha_r - 2 * \theta_{dwell} - \beta) \int_{\theta=\beta}^{\theta=(2*\alpha_r-2*\theta_{dwell}-\beta)} d\theta + \left(\frac{V_s}{\omega} \right)^2 \frac{1}{L_u} \int_{\theta=\beta}^{\theta=(2*\alpha_r-2*\theta_{dwell}-\beta)} \theta d\theta$$

$$P_3 = \frac{2V_s I_{peak} (\alpha_r - \theta_{dwell} - \beta)}{\omega} - \left(\frac{V_s}{\omega} \right)^2 \frac{2}{L_u} (2 * \alpha_r - 2 * \theta_{dwell} - \beta) (\alpha_r - \theta_{dwell} - \beta)$$

$$+ \left(\frac{V_s}{\omega} \right)^2 \frac{1}{2L_u} \left[(2 * \alpha_r - 2 * \theta_{dwell} - \beta)^2 - \beta^2 \right] \quad (1.12)$$

In linear analysis, power produced in this region should be close to zero as $dL/d\theta = 0$

Region IV Analysis $((2 * \alpha_r - 2 * \theta_{dwell} - \beta) \leq \theta \leq (\alpha_r - \beta))$

Flux linkage in region IV is given by,

$$\lambda(\theta) = \lambda_{required} = L_u * I_{peak} \quad (1.13)$$

$$\therefore d\lambda(\theta) = 0$$

Current in region IV is given by,

$$\begin{aligned} I(\theta) &= \frac{\lambda(\theta)}{L(\theta)}, \\ I(\theta) &= \frac{L_u * I_{peak}}{L_u} = I_{peak}, \end{aligned} \quad (1.14)$$

Power produced in this region is zero as , $d\lambda(\theta) = 0$.

$$\therefore P_4 = 0 \quad (1.15)$$

Inductance in region V and VI is given by,

$$L(\theta) = \frac{\Delta L}{\beta} * \theta + k$$

When $\theta = (\alpha_r - \beta)$,

$$\begin{aligned} L(\theta) &= L_u, \\ \therefore L_u &= \frac{\Delta L}{\beta} * (\alpha_r - \beta) + k, \\ k &= L_u - \frac{\Delta L}{\beta} * (\alpha_r - \beta) \\ \therefore L(\theta) &= \frac{\Delta L}{\beta} * \theta + L_u - \frac{\Delta L}{\beta} * (\alpha_r - \beta), \\ \therefore L(\theta) &= L_u + \frac{\Delta L}{\beta} * (\theta - (\alpha_r - \beta)) \end{aligned} \quad (1.16)$$

Region V Analysis ($(\alpha_r - \beta) \leq \theta \leq (\alpha_r - \beta + \theta_{commutation})$)

Flux linkage in region V is given by,

$$\lambda(\theta) = \frac{V_s}{\omega} * \theta + k$$

When $\theta = (\alpha_r - \beta)$,

$$\begin{aligned} \lambda(\theta) &= \lambda_{required} = L_u * I_{peak}, \\ \therefore L_u * I_{peak} &= \frac{V_s}{\omega} * (\alpha_r - \beta) + k, \\ \therefore k &= L_u * I_{peak} - \frac{V_s}{\omega} * (\alpha_r - \beta) \\ \therefore \lambda(\theta) &= \frac{V_s}{\omega} * \theta + L_u * I_{peak} - \frac{V_s}{\omega} * (\alpha_r - \beta), \\ \therefore \lambda(\theta) &= L_u * I_{peak} + \frac{V_s}{\omega} * [\theta - (\alpha_r - \beta)] \end{aligned} \tag{1.17}$$

$$\therefore d\lambda(\theta) = \frac{V_s}{\omega}$$

Current in region V is given by,

$$\begin{aligned} I(\theta) &= \frac{\lambda(\theta)}{L(\theta)}, \\ I(\theta) &= \frac{L_u * I_{peak} + \frac{V_s}{\omega} * [\theta - (\alpha_r - \beta)]}{L_u + \frac{\Delta L}{\beta} * (\theta - (\alpha_r - \beta))} \end{aligned} \tag{1.18}$$

Power produced in the region V is given by,

$$P_5 = \int_{\theta=(\alpha_r-\beta)}^{\theta=(\alpha_r-\beta+\theta_{commutation})} i(\theta) * d\lambda(\theta)$$

$$P_5 = \int_{\theta=(\alpha_r-\beta)}^{\theta=(\alpha_r-\beta+\theta_{commutation})} \frac{L_u * I_{peak} + \frac{V_s}{\omega} * [\theta - (\alpha_r - \beta)]}{L_u + \frac{\Delta L}{\beta} * (\theta - (\alpha_r - \beta))} * \frac{V_s}{\omega} * d\theta$$

$$P_5 = \frac{V_s}{\omega} * \int_{\theta=(\alpha_r-\beta)}^{\theta=(\alpha_r-\beta+\theta_{commutation})} \frac{L_u * I_{peak} + \frac{V_s}{\omega} * [\theta - (\alpha_r - \beta)]}{L_u + \frac{\Delta L}{\beta} * (\theta - (\alpha_r - \beta))} d\theta$$

$$P_5 = \frac{V_s L_u I_{peak}}{\omega} \frac{\beta}{\Delta L} * \int_{\theta=(\alpha_r-\beta)}^{\theta=(\alpha_r-\beta+\theta_{commutation})} \frac{1}{\frac{L_u \beta}{\Delta L} - (\alpha_r - \beta) + \theta} d\theta$$

$$+ \left(\frac{V_s}{\omega} \right)^2 \frac{\beta}{\Delta L} \int_{\theta=(\alpha_r-\beta)}^{\theta=(\alpha_r-\beta+\theta_{commutation})} \frac{\theta - (\alpha_r - \beta)}{\frac{L_u \beta}{\Delta L} - (\alpha_r - \beta) + \theta} d\theta$$

$$P_5 = \frac{V_s L_u I_{peak}}{\omega} \frac{\beta}{\Delta L} \ln \left(\frac{L_u \beta}{\Delta L} - (\alpha_r - \beta) + \theta \right) \Big|_{\theta=(\alpha_r-\beta)}^{\theta=(\alpha_r-\beta+\theta_{commutation})} + \left(\frac{V_s}{\omega} \right)^2 \frac{\beta}{\Delta L} [\theta]_{\theta=(\alpha_r-\beta)}^{\theta=(\alpha_r-\beta+\theta_{commutation})}$$

$$- \left(\frac{V_s}{\omega} \right)^2 \frac{\beta}{\Delta L} \left((\alpha_r - \beta) + \frac{L_u \beta}{\Delta L} - (\alpha_r - \beta) \right) \left[\ln \left(\frac{L_u \beta}{\Delta L} - (\alpha_r - \beta) + \theta \right) \right]_{\theta=(\alpha_r-\beta)}^{\theta=(\alpha_r-\beta+\theta_{commutation})}$$

$$P_5 = \frac{V_s L_u I_{peak}}{\omega} \frac{\beta}{\Delta L} \ln \left(\frac{\frac{L_u \beta}{\Delta L} + \theta_{commutation}}{\frac{L_u \beta}{\Delta L}} \right) + \left(\frac{V_s}{\omega} \right)^2 \frac{\beta}{\Delta L} \theta_{commutation} - \left(\frac{V_s}{\omega} \frac{\beta}{\Delta L} \right)^2 L_u \ln \left(\frac{\frac{L_u \beta}{\Delta L} + \theta_{commutation}}{\frac{L_u \beta}{\Delta L}} \right)$$

(1.19)

Region VI Analysis ($(\alpha_r - \beta + \theta_{commutation}) \leq \theta \leq \alpha_r$)

From Equation (1.17),

$$\lambda(\theta) = L_u * I_{peak} + \frac{V_s}{\omega} * [\theta - (\alpha_r - \beta)]$$

When $\theta = (\alpha_r - \beta + \theta_{commutation})$,

$$\begin{aligned} \lambda(\theta) &= L_u * I_{peak} + \frac{V_s}{\omega} * [(\alpha_r - \beta + \theta_{commutation}) - (\alpha_r - \beta)], \\ \therefore \lambda(\theta) &= L_u * I_{peak} + \frac{V_s}{\omega} * \theta_{commutation} = \lambda_{peak} \end{aligned} \quad (1.20)$$

i.e.

$$\lambda_{peak} = L_u * I_{peak} + \frac{V_s}{\omega} * (\theta_{dwell} - \theta_a)$$

Flux linkage in region VI is given by,

$$\lambda(\theta) = \frac{-V_s}{\omega} * \theta + k$$

When, $\theta = (\alpha_r - \beta + \theta_{commutation})$,

$$\begin{aligned} \lambda_{peak} &= \frac{-V_s}{\omega} * (\alpha_r - \beta + \theta_{commutation}) + k, \\ \therefore k &= \lambda_{peak} + \frac{V_s}{\omega} * (\alpha_r - \beta + \theta_{commutation}), \\ \therefore k &= L_u * I_{peak} + \frac{V_s}{\omega} * \theta_{commutation} + \frac{V_s}{\omega} * (\alpha_r - \beta + \theta_{commutation}), \\ \therefore k &= L_u * I_{peak} + \frac{V_s}{\omega} * (\alpha_r - \beta + 2 * \theta_{commutation}), \\ \therefore \lambda(\theta) &= \frac{-V_s}{\omega} * \theta + L_u * I_{peak} + \frac{V_s}{\omega} * (\alpha_r - \beta + 2 * \theta_{commutation}), \\ \lambda(\theta) &= L_u * I_{peak} + \frac{V_s}{\omega} * (\alpha_r - \beta + 2 * \theta_{commutation} - \theta), \end{aligned} \quad (1.21)$$

$$\therefore d\lambda(\theta) = \frac{-V_s}{\omega} * d\theta$$

Instantaneous current in region VI is given by,

$$I(\theta) = \frac{\lambda(\theta)}{L(\theta)},$$

$$I(\theta) = \frac{L_u * I_{peak} + \frac{V_s}{\omega} * (\alpha_r - \beta + 2 * \theta_{commutation} - \theta)}{L_u + \frac{\Delta L}{\beta} * (\theta - (\alpha_r - \beta))} \quad (1.22)$$

Power produced in the region VI is given by,

$$P_6 = \int_{\theta=(\alpha_r - \beta + \theta_{commutation})}^{\theta=\alpha_r} i(\theta) * d\lambda(\theta)$$

$$P_6 = \int_{\theta=(\alpha_r - \beta + \theta_{commutation})}^{\theta=\alpha_r} \frac{L_u * I_{peak} + \frac{V_s}{\omega} * (\alpha_r - \beta + 2 * \theta_{commutation} - \theta)}{L_u + \frac{\Delta L}{\beta} * (\theta - (\alpha_r - \beta))} * \frac{-V_s}{\omega} * d\theta$$

$$P_6 = \frac{-V_s}{\omega} * \int_{\theta=(\alpha_r - \beta + \theta_{commutation})}^{\theta=\alpha_r} \frac{L_u * I_{peak} + \frac{V_s}{\omega} * (\alpha_r - \beta + 2 * \theta_{commutation} - \theta)}{L_u + \frac{\Delta L}{\beta} * (\theta - (\alpha_r - \beta))} d\theta$$

$$P_6 = \frac{-V_s L_u I_{peak}}{\omega} \frac{\beta}{\Delta L} \int_{\theta=(\alpha_r - \beta + \theta_{commutation})}^{\theta=\alpha_r} \frac{1}{\frac{\beta}{\Delta L} L_u - (\alpha_r - \beta) + \theta} d\theta$$

$$- \left(\frac{V_s}{\omega} \right)^2 \frac{\beta}{\Delta L} \int_{\theta=(\alpha_r - \beta + \theta_{commutation})}^{\theta=\alpha_r} \frac{(\alpha_r - \beta + 2 * \theta_{commutation}) - \theta}{\frac{\beta}{\Delta L} L_u - (\alpha_r - \beta) + \theta} d\theta$$

$$P_6 = \frac{-V_s L_u I_{peak}}{\omega} \frac{\beta}{\Delta L} \ln \left(\frac{\beta}{\Delta L} L_u - (\alpha_r - \beta) + \theta \right)_{(\alpha_r - \beta + \theta_{commutation})}^{\alpha_r} + \left(\frac{V_s}{\omega} \right)^2 \frac{\beta}{\Delta L} [\theta]_{(\alpha_r - \beta + \theta_{commutation})}^{\alpha_r} \\ - \left(\frac{V_s}{\omega} \right)^2 \frac{\beta}{\Delta L} \left((\alpha_r - \beta + 2 * \theta_{commutation}) + \frac{\beta}{\Delta L} L_u - (\alpha_r - \beta) \right) \left[\ln \left(\frac{\beta}{\Delta L} L_u - (\alpha_r - \beta) + \theta \right) \right]_{(\alpha_r - \beta + \theta_{commutation})}^{\alpha_r}$$

$$P_6 = \frac{-V_s L_u I_{peak}}{\omega} \frac{\beta}{\Delta L} \ln \left(\frac{\frac{\beta}{\Delta L} L_u + \beta}{\frac{\beta}{\Delta L} L_u + \theta_{commutation}} \right) + \left(\frac{V_s}{\omega} \right)^2 \frac{\beta}{\Delta L} [\beta - \theta_{commutation}] \\ - \left(\frac{V_s}{\omega} \right)^2 \frac{\beta}{\Delta L} \left(\frac{\beta}{\Delta L} L_u + 2 * \theta_{commutation} \right) \ln \left(\frac{\frac{\beta}{\Delta L} L_u + \beta}{\frac{\beta}{\Delta L} L_u + \theta_{commutation}} \right)$$

When $\theta = \alpha_r$,

$$\lambda(\theta) = L_u * I_{peak} + \frac{V_s}{\omega} * (\alpha_r - \beta + 2 * \theta_{commutation} - \alpha_r),$$

$$\lambda(\theta) = L_u * I_{peak} + \frac{V_s}{\omega} * (-\beta + 2 * \theta_{commutation}),$$

i.e.

$$\lambda(\theta) = L_u * I_{peak} + \frac{V_s}{\omega} * (2 * \theta_{commutation} - \beta)$$

$$\lambda(\theta) = L_u * I_{peak} + \left[\frac{V_s}{\omega} * (2 * \theta_{commutation} - \beta - \theta) \right]$$

When $\theta = 0$,

$$\lambda(\theta) = L_u * I_{peak} + \left[\frac{V_s}{\omega} * (2 * \theta_{commutation} - \beta) \right] \quad \text{(Verification)}$$

When $\theta = \alpha_r$,

$$I(\theta) = \frac{L_u * I_{peak} + \frac{V_s}{\omega} * (\alpha_r - \beta + 2 * \theta_{commutation} - \alpha_r)}{L_u + \frac{\Delta L}{\beta} * (\alpha_r - (\alpha_r - \beta))},$$

$$\therefore I(\theta) = \frac{L_u * I_{peak} + \frac{V_s}{\omega} * (2 * \theta_{commutation} - \beta)}{L_u + \frac{\Delta L}{\beta} * \beta}, \quad (1.23)$$

$$I_{min} = \frac{L_u * I_{peak} + \frac{V_s}{\omega} * (2 * \theta_{commutation} - \beta)}{L_a},$$

$$\lambda_{peak} = L_u * I_{peak} + \frac{V_s}{\omega} * (\theta_{dwell} - \theta_a),$$

$$\lambda_{peak} = (4.15 * 10^{-3} * 600) + \left(\frac{700}{2 * \pi * 6 * 250/60} \right) * \left[(31 - 22.5) * \left(\frac{\pi}{180} \right) \right],$$

$$\lambda_{peak} = 3.1511$$

Simulation result confirms the same.

$$I_{min} = \frac{L_u * I_{peak} + \frac{V_s}{\omega} * (2 * \theta_{commutation} - \beta)}{L_a},$$

$$I_{min} = \frac{(4.15 * 10^{-3} * 600) + \left(\frac{700}{2 * \pi * 6 * 250/60} \right) * \left[(2 * (31 - 22.5) - 22.5) * \left(\frac{\pi}{180} \right) \right]}{73.38 * 10^{-3}},$$

$$I_{min} = 28.10A$$

Simulation result confirms the same.

For 8/6 SRM , total average power =

$$P_m = \omega \frac{q}{\alpha_r} * (P_1 + P_2 + P_3 + P_4 + P_5 + P_6)$$

$$\therefore P_m = \omega \frac{q}{\alpha_r} *$$

$$\left[\begin{aligned} & \frac{V_s L_u I_{peak}}{\omega} \frac{\beta}{\Delta L} \ln \left(\frac{\frac{\beta}{\Delta L} L_a - (\alpha_r - \beta - \theta_a)}{\frac{\beta}{\Delta L} L_a} \right) - \left(\frac{V_s}{\omega} \right)^2 \frac{\beta}{\Delta L} (\alpha_r - \beta - \theta_a) \\ & - \left(\frac{V_s}{\omega} \right)^2 \frac{\beta}{\Delta L} \left((\beta - 2 * \theta_{commutation}) + \frac{\beta}{\Delta L} L_a \right) \ln \left(\frac{\frac{\beta}{\Delta L} L_a - (\alpha_r - \beta - \theta_a)}{\frac{\beta}{\Delta L} L_a} \right) \\ & - \frac{V_s L_u I_{peak}}{\omega} \frac{\beta}{\Delta L} \ln \left(\frac{\frac{\beta}{\Delta L} L_a - \beta}{\frac{\beta}{\Delta L} L_a - (\alpha_r - \beta - \theta_a)} \right) - \left(\frac{V_s}{\omega} \right)^2 \frac{\beta}{\Delta L} [\theta_a - (\alpha_r - 2\beta)] \\ & - \left(\frac{V_s}{\omega} \right)^2 \frac{\beta}{\Delta L} \left(\frac{\beta}{\Delta L} L_a - (2 * \alpha_r - 2 * \theta_{dwell} - \beta) \right) \ln \left(\frac{\beta - \frac{\beta}{\Delta L} L_a}{(\alpha_r - \beta - \theta_a) - \frac{\beta}{\Delta L} L_a} \right) \\ & + \frac{2 V_s I_{peak} (\alpha_r - \theta_{dwell} - \beta)}{\omega} - \left(\frac{V_s}{\omega} \right)^2 \frac{2}{L_u} (2 * \alpha_r - 2 * \theta_{dwell} - \beta) (\alpha_r - \theta_{dwell} - \beta) \\ & + \left(\frac{V_s}{\omega} \right)^2 \frac{1}{2 L_u} [(2 * \alpha_r - 2 * \theta_{dwell} - \beta)^2 - \beta^2] \\ & + \frac{V_s L_u I_{peak}}{\omega} \frac{\beta}{\Delta L} \ln \left(\frac{\frac{L_u \beta}{\Delta L} + \theta_{commutation}}{\frac{L_u \beta}{\Delta L}} \right) + \left(\frac{V_s}{\omega} \right)^2 \frac{\beta}{\Delta L} \theta_{commutation} - \left(\frac{V_s}{\omega} \frac{\beta}{\Delta L} \right)^2 L_u \ln \left(\frac{\frac{L_u \beta}{\Delta L} + \theta_{commutation}}{\frac{L_u \beta}{\Delta L}} \right) \\ & - \frac{V_s L_u I_{peak}}{\omega} \frac{\beta}{\Delta L} \ln \left(\frac{\frac{\beta}{\Delta L} L_u + \beta}{\frac{\beta}{\Delta L} L_u + \theta_{commutation}} \right) + \left(\frac{V_s}{\omega} \right)^2 \frac{\beta}{\Delta L} [\beta - \theta_{commutation}] \\ & - \left(\frac{V_s}{\omega} \right)^2 \frac{\beta}{\Delta L} \left(\frac{\beta}{\Delta L} L_u + 2 * \theta_{commutation} \right) \ln \left(\frac{\frac{\beta}{\Delta L} L_u + \beta}{\frac{\beta}{\Delta L} L_u + \theta_{commutation}} \right) \end{aligned} \right]$$

After cancelations of terms containing $\left(\frac{V_s}{\omega}\right)^2 \frac{\beta}{\Delta L}$, we have,

$$\begin{aligned} \therefore P_m = \omega \frac{q}{\alpha_r} * \\ \left[\begin{aligned} & \frac{V_s L_u I_{peak}}{\omega} \frac{\beta}{\Delta L} \ln \left(\frac{\frac{\beta}{\Delta L} L_a - (\alpha_r - \beta - \theta_a)}{\frac{\beta}{\Delta L} L_a} \right) - \frac{V_s L_u I_{peak}}{\omega} \frac{\beta}{\Delta L} \ln \left(\frac{\frac{\beta}{\Delta L} L_a - \beta}{\frac{\beta}{\Delta L} L_a - (\alpha_r - \beta - \theta_a)} \right) \\ & + \frac{2V_s I_{peak} (\alpha_r - \theta_{dwell} - \beta)}{\omega} + \frac{V_s L_u I_{peak}}{\omega} \frac{\beta}{\Delta L} \ln \left(\frac{\frac{L_u \beta}{\Delta L} + \theta_{commutation}}{\frac{L_u \beta}{\Delta L}} \right) \\ & - \frac{V_s L_u I_{peak}}{\omega} \frac{\beta}{\Delta L} \ln \left(\frac{\frac{\beta}{\Delta L} L_u + \beta}{\frac{\beta}{\Delta L} L_u + \theta_{commutation}} \right) + \left(\frac{V_s}{\omega} \right)^2 \frac{1}{2L_u} \left[(2^* \alpha_r - 2^* \theta_{dwell} - \beta)^2 - \beta^2 \right] \\ & - \left(\frac{V_s}{\omega} \right)^2 \frac{\beta}{\Delta L} \left((\beta - 2^* \theta_{commutation}) + \frac{\beta}{\Delta L} L_a \right) \ln \left(\frac{\frac{\beta}{\Delta L} L_a - (\alpha_r - \beta - \theta_a)}{\frac{\beta}{\Delta L} L_a} \right) \\ & - \left(\frac{V_s}{\omega} \right)^2 \frac{\beta}{\Delta L} \left(\frac{\beta}{\Delta L} L_a - (2^* \alpha_r - 2^* \theta_{dwell} - \beta) \right) \ln \left(\frac{\beta - \frac{\beta}{\Delta L} L_a}{(\alpha_r - \beta - \theta_a) - \frac{\beta}{\Delta L} L_a} \right) \\ & - \left(\frac{V_s}{\omega} \right)^2 \frac{2}{L_u} (2^* \alpha_r - 2^* \theta_{dwell} - \beta) (\alpha_r - \theta_{dwell} - \beta) - \left(\frac{V_s}{\omega} \frac{\beta}{\Delta L} \right)^2 L_u \ln \left(\frac{\frac{L_u \beta}{\Delta L} + \theta_{commutation}}{\frac{L_u \beta}{\Delta L}} \right) \\ & - \left(\frac{V_s}{\omega} \right)^2 \frac{\beta}{\Delta L} \left(\frac{\beta}{\Delta L} L_u + 2^* \theta_{commutation} \right) \ln \left(\frac{\frac{\beta}{\Delta L} L_u + \beta}{\frac{\beta}{\Delta L} L_u + \theta_{commutation}} \right) \end{aligned} \right] \end{aligned}$$

These equations can be divided into two parts : speed dependant and speed independent .

Speed Independent Part (i.e. only terms containing $1/\omega$) :

$$\begin{aligned} \therefore P_{m_speed_independent} &= \omega \frac{q}{\alpha_r} * \\ &\left\{ \begin{aligned} &\frac{V_s L_u I_{peak}}{\omega} \frac{\beta}{\Delta L} \ln \left(\frac{\frac{\beta}{\Delta L} L_a - (\alpha_r - \beta - \theta_a)}{\frac{\beta}{\Delta L} L_a} \right) - \frac{V_s L_u I_{peak}}{\omega} \frac{\beta}{\Delta L} \ln \left(\frac{\frac{\beta}{\Delta L} L_a - \beta}{\frac{\beta}{\Delta L} L_a - (\alpha_r - \beta - \theta_a)} \right) \\ &+ \frac{2V_s I_{peak} (\alpha_r - \theta_{dwell} - \beta)}{\omega} + \frac{V_s L_u I_{peak}}{\omega} \frac{\beta}{\Delta L} \ln \left(\frac{\frac{L_u \beta}{\Delta L} + \theta_{commutation}}{\frac{L_u \beta}{\Delta L}} \right) \\ &- \frac{V_s L_u I_{peak}}{\omega} \frac{\beta}{\Delta L} \ln \left(\frac{\frac{\beta}{\Delta L} L_u + \beta}{\frac{\beta}{\Delta L} L_u + \theta_{commutation}} \right) \end{aligned} \right\} \\ \\ \therefore P_{m_speed_independent} &= \frac{q}{\alpha_r} * \left\{ \begin{aligned} &\frac{V_s L_u I_{peak}}{\Delta L} \left[\ln \left(\frac{\frac{\beta}{\Delta L} L_a - (\alpha_r - \beta - \theta_a)}{\frac{\beta}{\Delta L} L_a} \right) - \ln \left(\frac{\frac{\beta}{\Delta L} L_a - \beta}{\frac{\beta}{\Delta L} L_a - (\alpha_r - \beta - \theta_a)} \right) \right] \\ &+ \ln \left(\frac{\frac{L_u \beta}{\Delta L} + \theta_{commutation}}{\frac{L_u \beta}{\Delta L}} \right) - \ln \left(\frac{\frac{\beta}{\Delta L} L_u + \beta}{\frac{\beta}{\Delta L} L_u + \theta_{commutation}} \right) \\ &+ 2V_s I_{peak} (\alpha_r - \theta_{dwell} - \beta) \end{aligned} \right\} \end{aligned}$$

$$\therefore P_{m_speed_independent} = \frac{qV_s I_{peak}}{\alpha_r} * \left\{ \frac{L_u \beta}{\Delta L} \ln \left[\frac{\left(\frac{\beta}{\Delta L} L_a - (\alpha_r - \beta - \theta_a) \right)^2}{\left(\frac{L_a \beta}{\Delta L} \right) \left(\frac{L_a \beta}{\Delta L} - \beta \right)} \right] + \ln \left[\frac{\left(\frac{L_u \beta}{\Delta L} + \theta_{commutation} \right)^2}{\left(\frac{L_u \beta}{\Delta L} \right) \left(\frac{L_u \beta}{\Delta L} + \beta \right)} \right] \right\} + 2(\alpha_r - \theta_{dwell} - \beta)$$

For $\theta_{dwell} = 31, \theta_{adv} = 22.5$, this evaluates to be : 588.8495 HP

Note that this part depends on machine parameters, applied voltage, peak current, advance angle and dwell angle.

Speed Dependant Part :

$$\therefore P_{m_speed_dependant} = \omega \frac{q}{\alpha_r} * \left\{ \begin{aligned} & \left(\frac{V_s}{\omega} \right)^2 \frac{1}{2L_u} \left[(2 * \alpha_r - 2 * \theta_{dwell} - \beta)^2 - \beta^2 \right] \\ & - \left(\frac{V_s}{\omega} \right)^2 \frac{\beta}{\Delta L} \left((\beta - 2 * \theta_{commutation}) + \frac{\beta}{\Delta L} L_a \right) \ln \left(\frac{\frac{\beta}{\Delta L} L_a - (\alpha_r - \beta - \theta_a)}{\frac{\beta}{\Delta L} L_a} \right) \\ & - \left(\frac{V_s}{\omega} \right)^2 \frac{\beta}{\Delta L} \left(\frac{\beta}{\Delta L} L_a - (2 * \alpha_r - 2 * \theta_{dwell} - \beta) \right) \ln \left(\frac{\beta - \frac{\beta}{\Delta L} L_a}{(\alpha_r - \beta - \theta_a) - \frac{\beta}{\Delta L} L_a} \right) \\ & - \left(\frac{V_s}{\omega} \right)^2 \frac{2}{L_u} (2 * \alpha_r - 2 * \theta_{dwell} - \beta) (\alpha_r - \theta_{dwell} - \beta) - \left(\frac{V_s}{\omega} \frac{\beta}{\Delta L} \right)^2 L_u \ln \left(\frac{\frac{L_u \beta}{\Delta L} + \theta_{commutation}}{\frac{L_u \beta}{\Delta L}} \right) \\ & - \left(\frac{V_s}{\omega} \right)^2 \frac{\beta}{\Delta L} \left(\frac{\beta}{\Delta L} L_u + 2 * \theta_{commutation} \right) \ln \left(\frac{\frac{\beta}{\Delta L} L_u + \beta}{\frac{\beta}{\Delta L} L_u + \theta_{commutation}} \right) \end{aligned} \right\}$$

This can be rewritten as:

$$\therefore P_{m_speed_dependant} = \frac{q(V_s)^2}{\omega \alpha_r} * \left\{ \begin{aligned} & \frac{1}{2L_u} \left[(2\alpha_r - 2\theta_{dwell} - \beta)^2 - \beta^2 \right] \\ & - \frac{\beta}{\Delta L} \left((\beta - 2\theta_{commutation}) + \frac{\beta}{\Delta L} L_u \right) \ln \left(\frac{\frac{\beta}{\Delta L} L_u - (\alpha_r - \beta - \theta_a)}{\frac{\beta}{\Delta L} L_u} \right) \\ & - \frac{\beta}{\Delta L} \left(\frac{\beta}{\Delta L} L_u - (2\alpha_r - 2\theta_{dwell} - \beta) \right) \ln \left(\frac{\beta - \frac{\beta}{\Delta L} L_u}{(\alpha_r - \beta - \theta_a) - \frac{\beta}{\Delta L} L_u} \right) \\ & - \frac{2}{L_u} (2\alpha_r - 2\theta_{dwell} - \beta)(\alpha_r - \theta_{dwell} - \beta) - \left(\frac{\beta}{\Delta L} \right)^2 L_u \ln \left(\frac{\frac{L_u \beta}{\Delta L} + \theta_{commutation}}{\frac{L_u \beta}{\Delta L}} \right) \\ & - \frac{\beta}{\Delta L} \left(\frac{\beta}{\Delta L} L_u + 2\theta_{commutation} \right) \ln \left(\frac{\frac{\beta}{\Delta L} L_u + \beta}{\frac{\beta}{\Delta L} L_u + \theta_{commutation}} \right) \end{aligned} \right\}$$

Note that this part does not depend on peak current requirement.

Since $\omega = \frac{2 * \pi * n * N_b}{60}$, at higher speeds, i.e. as $n \rightarrow \infty$,

$$\therefore \lim_{\omega \rightarrow \infty} P_m = \frac{q V_s I_{peak}}{\alpha_r} * \left\{ \begin{aligned} & \frac{L_u \beta}{\Delta L} \left[\ln \left(\frac{\left(\frac{\beta}{\Delta L} L_u - (\alpha_r - \beta - \theta_a) \right)^2}{\left(\frac{L_u \beta}{\Delta L} \right)^2 - \frac{L_u \beta^2}{\Delta L}} \right) + \ln \left(\frac{\left(\frac{L_u \beta}{\Delta L} + \theta_{commutation} \right)^2}{\left(\frac{L_u \beta}{\Delta L} \right)^2 + \frac{L_u \beta^2}{\Delta L}} \right) \right] \\ & + 2(\alpha_r - \beta - \theta_{dwell}) \end{aligned} \right\}$$

Based on power requirement, by first calculating speed dependant power which is independent of the peak current, it is possible to calculate peak current requirement.

i.e.

$$P_{required} - P_{speed_dependant} = \frac{q}{\alpha_r} * \left\{ V_s L_u I_{peak} \frac{\beta}{\Delta L} \left[\ln \left(\frac{\frac{\beta}{\Delta L} L_a - (\alpha_r - \beta - \theta_a)}{\frac{\beta}{\Delta L} L_a} \right) - \ln \left(\frac{\frac{\beta}{\Delta L} L_a - \beta}{\frac{\beta}{\Delta L} L_a - (\alpha_r - \beta - \theta_a)} \right) + \ln \left(\frac{\frac{L_u \beta}{\Delta L} + \theta_{commutation}}{\frac{L_u \beta}{\Delta L}} \right) - \ln \left(\frac{\frac{\beta}{\Delta L} L_u + \beta}{\frac{\beta}{\Delta L} L_u + \theta_{commutation}} \right) \right] + 2V_s I_{peak} (\alpha_r - \theta_{dwell} - \beta) \right\}$$

$$\therefore I_{peak} = \frac{\alpha_r (P_{required} - P_{speed_dependant})}{2qV_s (\alpha_r - \theta_{dwell} - \beta) + qV_s \frac{L_u \beta}{\Delta L} \left[\ln \left(\frac{\left(\frac{\beta}{\Delta L} L_a - (\alpha_r - \beta - \theta_a) \right)^2}{\left(\frac{\beta}{\Delta L} L_a \right) \left(\frac{\beta}{\Delta L} L_a - \beta \right)} \right) + \ln \left(\frac{\left(\frac{L_u \beta}{\Delta L} + \theta_{commutation} \right)^2}{\left(\frac{L_u \beta}{\Delta L} \right) \left(\frac{\beta}{\Delta L} L_u + \beta \right)} \right) \right]}$$

As $n \rightarrow \infty$, the advance angle which maximizes the developed power, can be find out.

As $n \rightarrow \infty$, developed power approaches value given by following equation,

$$\therefore P_m = \frac{q}{\alpha_r} * \left\{ V_s L_u I_{peak} \frac{\beta}{\Delta L} \left[\ln \left(\frac{\frac{\beta}{\Delta L} L_a - (\alpha_r - \beta - \theta_a)}{\frac{\beta}{\Delta L} L_a} \right) - \ln \left(\frac{\frac{\beta}{\Delta L} L_a - \beta}{\frac{\beta}{\Delta L} L_a - (\alpha_r - \beta - \theta_a)} \right) \right] \right. \\ \left. + \ln \left(\frac{\frac{L_u \beta}{\Delta L} + \theta_{commutation}}{\frac{L_u \beta}{\Delta L}} \right) - \ln \left(\frac{\frac{\beta}{\Delta L} L_u + \beta}{\frac{\beta}{\Delta L} L_u + \theta_{commutation}} \right) \right] \\ \left. + 2V_s I_{peak} (\alpha_r - \theta_{dwell} - \beta) \right\}$$

$$\therefore \frac{\partial P_m}{\partial \theta_a} = \frac{q}{\alpha_r} \frac{\partial}{\partial \theta_a} \left\{ V_s L_u I_{peak} \frac{\beta}{\Delta L} \left[\ln \left(\frac{\frac{\beta}{\Delta L} L_a - (\alpha_r - \beta - \theta_a)}{\frac{\beta}{\Delta L} L_a} \right) - \ln \left(\frac{\frac{\beta}{\Delta L} L_a - \beta}{\frac{\beta}{\Delta L} L_a - (\alpha_r - \beta - \theta_a)} \right) \right] \right. \\ \left. + \ln \left(\frac{\frac{L_u \beta}{\Delta L} + \theta_{commutation}}{\frac{L_u \beta}{\Delta L}} \right) - \ln \left(\frac{\frac{\beta}{\Delta L} L_u + \beta}{\frac{\beta}{\Delta L} L_u + \theta_{commutation}} \right) \right] \\ \left. + 2V_s I_{peak} (\alpha_r - \theta_{dwell} - \beta) \right\} = 0$$

$$\therefore \frac{\partial}{\partial \theta_a} \left\{ \left[\ln \left(\frac{\beta}{\Delta L} L_a - (\alpha_r - \beta - \theta_a) \right) + \ln \left(\frac{\beta}{\Delta L} L_a - (\alpha_r - \beta - \theta_a) \right) \right] \right. \\ \left. + \ln \left(\frac{L_u \beta}{\Delta L} + \theta_{commutation} \right) + \ln \left(\frac{\beta}{\Delta L} L_u + \theta_{commutation} \right) \right\} = 0$$

$$\therefore \frac{\partial}{\partial \theta_a} \left[2 \ln \left(\left(\frac{\beta}{\Delta L} L_a - \alpha_r + \beta \right) + \theta_a \right) + 2 \ln \left(\frac{\beta}{\Delta L} L_u + \theta_{commutation} \right) \right] = 0,$$

$$\therefore \frac{\partial}{\partial \theta_a} \left[2 \ln \left(\left(\frac{\beta}{\Delta L} L_a - \alpha_r + \beta \right) + \theta_a \right) + 2 \ln \left(\left(\frac{\beta}{\Delta L} L_u + \theta_{dwell} \right) - \theta_a \right) \right] = 0,$$

$$\therefore \frac{2}{\theta_a + \left(\frac{\beta}{\Delta L} L_a - \alpha_r + \beta \right)} - \frac{2}{\left(\frac{\beta}{\Delta L} L_u + \theta_{dwell} \right) - \theta_a} = 0,$$

$$\therefore \frac{1}{\theta_a + \left(\frac{\beta}{\Delta L} L_a - \alpha_r + \beta \right)} + \frac{1}{\theta_a - \left(\frac{\beta}{\Delta L} L_u + \theta_{dwell} \right)} = 0,$$

$$\therefore \theta_a - \left(\frac{\beta}{\Delta L} L_u + \theta_{dwell} \right) + \theta_a + \left(\frac{\beta}{\Delta L} L_a - \alpha_r + \beta \right) = 0,$$

$$\therefore 2\theta_a - \theta_{dwell} - \alpha_r + \beta + \beta \frac{L_a - L_u}{\Delta L} = 0,$$

$$\therefore L_a - L_u = \Delta L,$$

$$\therefore 2\theta_a - \theta_{dwell} - \alpha_r + 2\beta = 0$$

i.e.

$$\theta_a^* = \frac{(\alpha_r - 2\beta) + \theta_{dwell}}{2}$$

Average current can be calculated as follows:

$$I_{avg} = \frac{1}{\alpha_r} \left[\int_{\theta=0}^{\theta=(\alpha_r-\beta-\theta_a)} i_1(\theta) d\theta + \int_{\theta=(\alpha_r-\beta-\theta_a)}^{\theta=\beta} i_2(\theta) d\theta + \int_{\theta=\beta}^{\theta=(2^*\alpha_r-2^*\theta_{dwell}-\beta)} i_3(\theta) d\theta + \int_{\theta=(2^*\alpha_r-2^*\theta_{dwell}-\beta)}^{\theta=(\alpha_r-\beta)} i_4(\theta) d\theta + \int_{\theta=(\alpha_r-\beta)}^{\theta=(\alpha_r-\beta+\theta_{commutation})} i_5(\theta) d\theta + P_6 = \frac{-V_s}{\omega} * \int_{\theta=(\alpha_r-\beta+\theta_{commutation})}^{\theta=\alpha_r} i_6(\theta) d\theta \right]$$

$$\therefore I_1 = \int_{\theta=0}^{\theta=(\alpha_r-\beta-\theta_a)} i(\theta) d\theta$$

$$\therefore I_1 = \int_{\theta=0}^{\theta=(\alpha_r-\beta-\theta_a)} \frac{L_u I_{peak} - \left[\frac{V_s}{\omega} (\theta + \beta - 2\theta_{commutation}) \right]}{L_a - \frac{\Delta L}{\beta} * \theta} d\theta$$

$$\therefore I_1 = \int_{\theta=0}^{\theta=(\alpha_r-\beta-\theta_a)} \frac{L_u I_{peak} - \left[\frac{V_s}{\omega} (\theta + \beta - 2\theta_{commutation}) \right]}{L_a - \frac{\Delta L}{\beta} \theta} d\theta$$

$$\therefore I_1 = L_u I_{peak} \frac{\beta}{\Delta L} \int_{\theta=0}^{\theta=(\alpha_r - \beta - \theta_a)} \frac{1}{\frac{\beta}{\Delta L} L_a - \theta} d\theta - \frac{\beta}{\Delta L} \frac{V_s}{\omega} \int_{\theta=0}^{\theta=(\alpha_r - \beta - \theta_a)} \frac{\theta + \beta - 2\theta_{commutation}}{\frac{\beta}{\Delta L} L_a - \theta} d\theta$$

$$\begin{aligned} \therefore I_1 &= -L_u I_{peak} \frac{\beta}{\Delta L} \ln \left(\frac{\beta}{\Delta L} L_a - \theta \right) \Big|_{\theta=0}^{\theta=(\alpha_r - \beta - \theta_a)} + \frac{\beta}{\Delta L} \frac{V_s}{\omega} [\theta]_{\theta=0}^{\theta=(\alpha_r - \beta - \theta_a)} \\ &+ \frac{\beta}{\Delta L} \frac{V_s}{\omega} \left(\beta - 2\theta_{commutation} + \frac{\beta}{\Delta L} L_a \right) \ln \left(\theta - \frac{\beta}{\Delta L} L_a \right) \Big|_{\theta=0}^{\theta=(\alpha_r - \beta - \theta_a)} \\ \therefore I_1 &= -L_u I_{peak} \frac{\beta}{\Delta L} \ln \left(\frac{\frac{\beta L_a}{\Delta L} - (\alpha_r - \beta - \theta_a)}{\frac{\beta L_a}{\Delta L}} \right) + \frac{\beta}{\Delta L} \frac{V_s}{\omega} (\alpha_r - \beta - \theta_a) \\ &+ \frac{\beta}{\Delta L} \frac{V_s}{\omega} \left(\beta - 2\theta_{commutation} + \frac{\beta}{\Delta L} L_a \right) \ln \left(\frac{\frac{\beta L_a}{\Delta L} - (\alpha_r - \beta - \theta_a)}{\frac{\beta L_a}{\Delta L}} \right) \end{aligned}$$

$$\begin{aligned} \therefore I_2 &= -L_u I_{peak} \frac{\beta}{\Delta L} \ln \left(\frac{\frac{\beta L_a}{\Delta L} - \beta}{\frac{\beta L_a}{\Delta L} - (\alpha_r - \beta - \theta_a)} \right) - \frac{V_s}{\omega} \frac{\beta}{\Delta L} [\theta_a - (\alpha_r - 2\beta)] \\ &- \frac{V_s}{\omega} \frac{\beta}{\Delta L} \left(\frac{\beta L_a}{\Delta L} - (2\alpha_r - 2\theta_{dwell} - \beta) \right) \ln \left(\frac{\beta - \frac{\beta L_a}{\Delta L}}{(\alpha_r - \beta - \theta_a) - \frac{\beta L_a}{\Delta L}} \right) \end{aligned}$$

$$\begin{aligned} I_3 &= 2I_{peak} (\alpha_r - \theta_{dwell} - \beta) - \frac{V_s}{\omega} \frac{2}{L_u} (2\alpha_r - 2\theta_{dwell} - \beta) (\alpha_r - \theta_{dwell} - \beta) \\ &+ \frac{V_s}{\omega} \frac{1}{2L_u} \left[(2\alpha_r - 2\theta_{dwell} - \beta)^2 - \beta^2 \right] \end{aligned}$$

$$I_4 = \int_{\theta=(2\alpha_r-2\theta_{dwell}-\beta)}^{\theta=(\alpha_r-\beta)} I_{peak} d\theta$$

$$\therefore I_4 = I_{peak} [\theta]_{\theta=(2\alpha_r-2\theta_{dwell}-\beta)}^{\theta=(\alpha_r-\beta)}$$

$$\therefore I_4 = I_{peak} (\alpha_r - \beta - 2\alpha_r + 2\theta_{dwell} + \beta)$$

$$\therefore I_4 = I_{peak} (2\theta_{dwell} - \alpha_r)$$

$$I_5 = L_u I_{peak} \frac{\beta}{\Delta L} \ln \left(\frac{\frac{L_u \beta}{\Delta L} + \theta_{commutation}}{\frac{L_u \beta}{\Delta L}} \right) + \frac{V_s}{\omega} \frac{\beta}{\Delta L} \theta_{commutation} - \frac{V_s}{\omega} \left(\frac{\beta}{\Delta L} \right)^2 L_u \ln \left(\frac{\frac{L_u \beta}{\Delta L} + \theta_{commutation}}{\frac{L_u \beta}{\Delta L}} \right)$$

$$I_6 = L_u I_{peak} \frac{\beta}{\Delta L} \ln \left(\frac{\frac{\beta L_u}{\Delta L} + \beta}{\frac{\beta L_u}{\Delta L} + \theta_{commutation}} \right) - \frac{V_s}{\omega} \frac{\beta}{\Delta L} [\beta - \theta_{commutation}]$$

$$+ \frac{V_s}{\omega} \frac{\beta}{\Delta L} \left(\frac{\beta}{\Delta L} L_u + 2\theta_{commutation} \right) \ln \left(\frac{\frac{\beta L_u}{\Delta L} + \beta}{\frac{\beta L_u}{\Delta L} + \theta_{commutation}} \right)$$

$$\begin{aligned}
I_{avg} = \frac{1}{\alpha_r} & \left[\begin{aligned}
& -L_u I_{peak} \frac{\beta}{\Delta L} \ln \left(\frac{\frac{\beta L_a}{\Delta L} - (\alpha_r - \beta - \theta_a)}{\frac{\beta L_a}{\Delta L}} \right) + \frac{\beta}{\Delta L} \frac{V_s}{\omega} (\alpha_r - \beta - \theta_a) \\
& + \frac{\beta}{\Delta L} \frac{V_s}{\omega} \left(\beta - 2\theta_{commutation} + \frac{\beta}{\Delta L} L_a \right) \ln \left(\frac{\frac{\beta L_a}{\Delta L} - (\alpha_r - \beta - \theta_a)}{\frac{\beta L_a}{\Delta L}} \right) \\
& -L_u I_{peak} \frac{\beta}{\Delta L} \ln \left(\frac{\frac{\beta L_a}{\Delta L} - \beta}{\frac{\beta L_a}{\Delta L} - (\alpha_r - \beta - \theta_a)} \right) - \frac{V_s}{\omega} \frac{\beta}{\Delta L} [\theta_a - (\alpha_r - 2\beta)] \\
& - \frac{V_s}{\omega} \frac{\beta}{\Delta L} \left(\frac{\beta L_a}{\Delta L} - (2\alpha_r - 2\theta_{dwell} - \beta) \right) \ln \left(\frac{\beta - \frac{\beta L_a}{\Delta L}}{(\alpha_r - \beta - \theta_a) - \frac{\beta L_a}{\Delta L}} \right) \\
& + 2I_{peak} (\alpha_r - \theta_{dwell} - \beta) - \frac{V_s}{\omega} \frac{2}{L_u} (2\alpha_r - 2\theta_{dwell} - \beta) (\alpha_r - \theta_{dwell} - \beta) \\
& + \frac{V_s}{\omega} \frac{1}{2L_u} \left[(2\alpha_r - 2\theta_{dwell} - \beta)^2 - \beta^2 \right] + I_{peak} (2\theta_{dwell} - \alpha_r) \\
& + L_u I_{peak} \frac{\beta}{\Delta L} \ln \left(\frac{\frac{L_u \beta}{\Delta L} + \theta_{commutation}}{\frac{L_u \beta}{\Delta L}} \right) + \frac{V_s}{\omega} \frac{\beta}{\Delta L} \theta_{commutation} - \frac{V_s}{\omega} \left(\frac{\beta}{\Delta L} \right)^2 L_u \ln \left(\frac{\frac{L_u \beta}{\Delta L} + \theta_{commutation}}{\frac{L_u \beta}{\Delta L}} \right) \\
& + L_u I_{peak} \frac{\beta}{\Delta L} \ln \left(\frac{\frac{\beta L_u}{\Delta L} + \beta}{\frac{\beta L_u}{\Delta L} + \theta_{commutation}} \right) - \frac{V_s}{\omega} \frac{\beta}{\Delta L} [\beta - \theta_{commutation}] \\
& + \frac{V_s}{\omega} \frac{\beta}{\Delta L} \left(\frac{\beta}{\Delta L} L_u + 2\theta_{commutation} \right) \ln \left(\frac{\frac{\beta L_u}{\Delta L} + \beta}{\frac{\beta L_u}{\Delta L} + \theta_{commutation}} \right)
\end{aligned} \right]
\end{aligned}$$

Again this can be split into Speed Dependent part and Speed Independent part.

$$I_{avg_speed_independent} = \frac{1}{\alpha_r} \left[\begin{aligned} & -L_u I_{peak} \frac{\beta}{\Delta L} \ln \left(\frac{\frac{\beta L_a}{\Delta L} - (\alpha_r - \beta - \theta_a)}{\frac{\beta L_a}{\Delta L}} \right) - L_u I_{peak} \frac{\beta}{\Delta L} \ln \left(\frac{\frac{\beta L_a}{\Delta L} - \beta}{\frac{\beta L_a}{\Delta L} - (\alpha_r - \beta - \theta_a)} \right) \\ & + 2I_{peak} (\alpha_r - \theta_{dwell} - \beta) + I_{peak} (2\theta_{dwell} - \alpha_r) \\ & + L_u I_{peak} \frac{\beta}{\Delta L} \ln \left(\frac{\frac{L_u \beta}{\Delta L} + \theta_{commutation}}{\frac{L_u \beta}{\Delta L}} \right) + L_u I_{peak} \frac{\beta}{\Delta L} \ln \left(\frac{\frac{\beta L_u}{\Delta L} + \beta}{\frac{\beta L_u}{\Delta L} + \theta_{commutation}} \right) \end{aligned} \right]$$

$$I_{avg_speed_independent} = \frac{I_{peak}}{\alpha_r} \left[\frac{L_u \beta}{\Delta L} \ln \left(\frac{\frac{\beta L_a}{\Delta L} \left(\frac{\beta L_u}{\Delta L} + \beta \right)}{\frac{L_u \beta}{\Delta L} \left(\frac{\beta L_a}{\Delta L} - \beta \right)} \right) + (\alpha_r - 2\beta) \right]$$

$$\begin{aligned}
I_{\text{avg_speed_dependent}} = \frac{1}{\alpha_r} & \left[\begin{aligned}
& \frac{\beta}{\Delta L} \frac{V_s}{\omega} (\alpha_r - \beta - \theta_a) - \frac{V_s}{\omega} \frac{\beta}{\Delta L} [\theta_a - (\alpha_r - 2\beta)] - \frac{V_s}{\omega} \frac{\beta}{\Delta L} [\beta - \theta_{\text{commutation}}] \\
& + \frac{\beta}{\Delta L} \frac{V_s}{\omega} \left(\beta - 2\theta_{\text{commutation}} + \frac{\beta L_a}{\Delta L} \right) \ln \left(\frac{\frac{\beta L_a}{\Delta L} - (\alpha_r - \beta - \theta_a)}{\frac{\beta L_a}{\Delta L}} \right) \\
& - \frac{V_s}{\omega} \frac{\beta}{\Delta L} \left(\frac{\beta L_a}{\Delta L} - (2\alpha_r - 2\theta_{\text{dwell}} - \beta) \right) \ln \left(\frac{\beta - \frac{\beta L_a}{\Delta L}}{(\alpha_r - \beta - \theta_a) - \frac{\beta L_a}{\Delta L}} \right) \\
& - \frac{V_s}{\omega} \frac{2}{L_u} (2\alpha_r - 2\theta_{\text{dwell}} - \beta) (\alpha_r - \theta_{\text{dwell}} - \beta) \\
& + \frac{V_s}{\omega} \frac{1}{2L_u} \left[(2\alpha_r - 2\theta_{\text{dwell}} - \beta)^2 - \beta^2 \right] \\
& + \frac{V_s}{\omega} \frac{\beta}{\Delta L} \theta_{\text{commutation}} - \frac{V_s}{\omega} \left(\frac{\beta}{\Delta L} \right)^2 L_u \ln \left(\frac{\frac{L_u \beta}{\Delta L} + \theta_{\text{commutation}}}{\frac{L_u \beta}{\Delta L}} \right) \\
& + \frac{V_s}{\omega} \frac{\beta}{\Delta L} \left(\frac{\beta}{\Delta L} L_u + 2\theta_{\text{commutation}} \right) \ln \left(\frac{\frac{\beta L_u}{\Delta L} + \beta}{\frac{\beta L_u}{\Delta L} + \theta_{\text{commutation}}} \right)
\end{aligned} \right]
\end{aligned}$$

$$I_{avg_speed_dependent} = \frac{V_s}{\omega \alpha_r} \frac{\beta}{\Delta L} \left[\begin{aligned} & \left(\beta - 2\theta_{commutation} + \frac{\beta L_a}{\Delta L} \right) \ln \left(\frac{\frac{\beta L_a}{\Delta L} - (\alpha_r - \beta - \theta_a)}{\frac{\beta L_a}{\Delta L}} \right) \\ & - \left(\frac{\beta L_a}{\Delta L} - (2\alpha_r - 2\theta_{dwell} - \beta) \right) \ln \left(\frac{\beta - \frac{\beta L_a}{\Delta L}}{(\alpha_r - \beta - \theta_a) - \frac{\beta L_a}{\Delta L}} \right) \\ & - \frac{\beta L_u}{\Delta L} \ln \left(\frac{\frac{L_u \beta}{\Delta L} + \theta_{commutation}}{\frac{L_u \beta}{\Delta L}} \right) \\ & + \left(\frac{\beta L_u}{\Delta L} + 2\theta_{commutation} \right) \ln \left(\frac{\frac{\beta L_u}{\Delta L} + \beta}{\frac{\beta L_u}{\Delta L} + \theta_{commutation}} \right) \\ & - \frac{2\Delta L}{\beta L_u} (2\alpha_r - 2\theta_{dwell} - \beta)(\alpha_r - \theta_{dwell} - \beta) \\ & + \frac{\Delta L}{2\beta L_u} \left[(2\alpha_r - 2\theta_{dwell} - \beta)^2 - \beta^2 \right] + (2\alpha_r - 4\beta - 4\theta_a + 2\theta_d) \end{aligned} \right]$$

As speed increases, i.e. $n \rightarrow \infty$,

$$\lim_{\omega \rightarrow \infty} I_{avg} = \frac{I_{peak}}{\alpha_r} \left[\frac{L_u \beta}{\Delta L} \ln \left(\frac{\frac{\beta L_a}{\Delta L} \left(\frac{\beta L_u}{\Delta L} + \beta \right)}{\frac{L_u \beta}{\Delta L} \left(\frac{\beta L_a}{\Delta L} - \beta \right)} \right) + (\alpha_r - 2\beta) \right]$$

And developed power,

$$\therefore \lim_{\omega \rightarrow \infty} P_m = \frac{q V_s I_{peak}}{\alpha_r} * \left\{ \frac{L_u \beta}{\Delta L} \left[\ln \left(\frac{\left(\frac{\beta}{\Delta L} L_a - (\alpha_r - \beta - \theta_a) \right)^2}{\left(\frac{L_u \beta}{\Delta L} \right)^2 - \frac{L_u \beta^2}{\Delta L}} \right) + \ln \left(\frac{\left(\frac{L_u \beta}{\Delta L} + \theta_{commutation} \right)^2}{\left(\frac{L_u \beta}{\Delta L} \right)^2 + \frac{L_u \beta^2}{\Delta L}} \right) \right] \right. \\ \left. + 2(\alpha_r - \beta - \theta_{dwell}) \right\}$$

This power can be optimized using, $\theta_a^* = \frac{(\alpha_r - 2\beta) + \theta_{dwell}}{2}$.

Vita

Niranjan Anandrao Patil was raised in Shirala (Maharashtra, India). He graduated from PVP Institute of Technology with honors, in year 2000 and received a B.Eng. in Instrumentation and Control. He then worked for an automation firm as a Project Engineer (Distributed Control Systems) for two years. There, he worked on three projects involving automation of metal and chemical industries.

He joined the University of Tennessee, Knoxville in year 2002 and received a M.S. in Electrical Engineering in December 2004. During his M.S., he worked at Office of Information and Technology as Graduate Assistant. In 2005, he started his Ph.D. During his Ph.D., he worked with National Transportation Research Center as a Research Assistant. He also received a Teaching Assistantship from the ECE department.

In 2008, he worked part-time for MESA Inc. in Knoxville, TN as an Electrical Engineer. There, he was responsible for electrical distribution analysis. His professional interest includes process instrumentation and control; electrical drives and control; power system analysis and control. He is currently working as Drives and Power System Engineer with GE Industrial Automation division. He is a member of ISA and IEEE.